AN INVESTIGATION INTO THE IMPACT OF HVDC SCHEMES ON ESKOM HV NETWORK'S TRANSIENT STABILITY

KAMATI N.I. MBANGULA

IN FULFILMENT OF MASTER OF SCIENCE DEGREE IN ENGINEERING

COLLEGE OF AGRICULTURE, ENGINEERING AND SCIENCE

UNIVERSITY OF KWAZULU-NATAL

October 2015

Supervisor: Dr I.E. Davidson (UKZN)

Co-supervisor: Dr R. Tiako (UKZN)

Industrial Mentor: Mr N. Parus (Eskom)

EXAMINER'S COPY

DECLARATION 1 – PLAGIARISM

I, Kamati N.I. Mbangula declare that:

1. The research reported in this dissertation, except where otherwise indicated, is my original research.
2. This dissertation has not been submitted for any degree or examination at any other university.
3. This dissertation does not contain other persons' data, pictures, graphs or other information, unless specifically acknowledged as being sourced from other persons.
4. This dissertation does not contain other persons' writing, unless specifically acknowledged as being sourced from other researchers. Where other written sources have been quoted, then:
    a. Their words have been re-written but the general information attributed to them has been referenced
    b. Where their exact words have been used, then their writing has been placed in italics and inside quotation marks, and referenced.
5. This dissertation does not contain text, graphics or tables copied and pasted from the Internet, unless specifically acknowledged, and the source being detailed in the dissertation and in the References sections.

Signed:

Mr Kamati N.I. Mbangula

Date:

As the candidate's Supervisor I agree/do not agree to the submission of this dissertation.

Signed:

Dr I.E. Davidson

Date:

ACKNOWLEDGMENTS

First and foremost I would like to thank the Almighty God for giving me strength, knowledge, patience, the will to learn and keeping me in good health throughout the duration of my studies, and thus making it possible for me to carry out this research investigation.

Secondly, I would like to thank my project supervisor DR Innocent Davidson for suggesting this research topic to me and for the continuous professional and fatherly support, encouragement and guidance that he has provided me with throughout the duration of my studies.

I would like to express my sincere gratitude to my co-supervisor DR Remy Tiako, for making time to review, critic, correct and provide advice on how I should carry out my research work.

I would further like to thank my industrial mentor Mr Nishanth Parus for the technical support that he has provided me with, for providing me with the much needed Eskom network information, for assisting me in identifying a focus area for my research work and for reviewing my work.

I would like to thank my family, friends and colleagues for their continuous support and wise words of encouragement.

I would like to express my sincere gratitude towards Eskom for providing me with financial support and for affording me the rare opportunity to study towards my MSc degree under the Eskom Power Plant Engineers Institute (EPPEI) program.

Kamati N.I. Mbangula

October, 2015

ABSTRACT

Compared to high voltage alternating current (HVAC) lines, the response of HVDC schemes to system faults is faster and more controllable, thus making it more tolerable to system faults. Due to the inherent advantages of HVDC schemes over HVAC lines when it comes to bulk power transmission over long distances, it has become a common practice for power utilities to integrate HVDC schemes into their networks. The main objective of this research is to investigate the impacts that HVDC schemes may have on the transient rotor angle and voltage stability of Eskom's main transmission system (MTS) network. Three test systems were used to carry out this research, namely: a two machines infinite busbar network (test network 1), a 30 machine 24 busbar network (test network 2) and Eskom's MTS network (test network 3), with the emphasis being on test network 3. HVDC schemes may be used to improve the system synchronizing torque by making use of robust, fast, state-of-the-art control techniques with good communication systems, for DC power modulation at the converters. The HVDC controllers are used for temporary increment or decrement of DC power during system faults and transient periods. This restores the balance between the acceleration power gained by the generator during the fault and the system retarding power applied onto the generator. Previous research shows that the ability of a HVDC scheme to improve the transient stability of an AC system largely depends on the pre-disturbance conditions of the network and the robustness of the HVDC scheme controllers used. In this study, carried out using the DIgSILENT PowerFactory software tool, HVDC schemes of various configurations have been integrated at strategic locations of Eskom's MTS network and time-domain dynamic simulation studies were carried out to determine how the HVDC scheme affects the network transient stability. This was done by assessing the obtained results on system fault levels, critical fault clearing times (CCTs), minimum and maximum voltage violations and thermal limit violations, against the requirements as stipulated in the South African Grid Code-The Network version. It was found that the integration of the LCC-HVDC scheme causes an improvement in the CCT of the generators, which indicates an improvement of machine transient rotor angle stability. In terms of transient rotor angle stability, the integration of the LCC-HVDC scheme meets the South African Grid Code (SAGC) requirements. The HVDC scheme does not have a significant impact on the network fault levels.

DECLARATION 2 - PUBLICATIONS

The following publications emanated from this research investigation, namely:

1. K.N.I. Mbangula and I.E. Davidson, "Improving Power System Stability of South Africa's HVAC Network Using Strategic Placement of HVDC Links." Paper accepted for presentation at the CIGRE International Symposium on Development of Electricity Infrastructure in Sub-Saharan Africa, Cape Town, 2015.

2. K.N.I. Mbangula, I. E. Davidson and R. Tiako, "Power System Transient Stability Analysis and Stability Improvement of a Large Multi-Machine HVAC Network using HVDC Technologies" in 23rd Southern African Universities Power Engineering Conference, Johannesburg, 2015.

3. K.N.I. Mbangula and I.E. Davidson, "Power System Modelling and Fault Analysis of a HVAC Transmission Line using DIgSILENT PowerFactory Software". Paper presented at the 1st Eskom-EPPEI Students Conference, Midrand, 2014.

Signed:

Kamati N.I. Mbangula

TABLE OF CONTENTS

LIST OF FIGURES

FIGURE PAGE NUMBER

LIST OF TABLES

TABLE PAGE NUMBER

LIST OF ABBREVIATIONS

CCT: Critical Fault Clearing Time

CIGRE: International Council for Large Electric Systems

DIgSILENT: Digital Simulation and Electrical Network Calculation Program

DSL: DIgSILENT Simulation Language

EHV: Extra High Voltage

EMT: Electromagnetic Transient Simulation Tool Bar

FACTS: Flexible AC Transmission Systems

FCT: Fault Clearing Time

FRT: Fault Recovery Time

HVDC: High Voltage Direct Current

HVAC: High Voltage Alternating Current

HMI: Hybrid Multi-Infeed

IGBT: Insulated Gate Bi-Polar Transistor

IEEE: Institute of Electrical and Electronic Engineers

LCC: Line Commutated Current Source Converter

MMC: Modular Multi-Level Converter

MTS: Main Transmission system

PWM: Pulse Width Modulation

RTDS: Real Time Digital Simulator

SPWM: Sinusoidal Pulse Width Modulation

SIL: Surge Impedance Loading

SAGC: South African Grid Code

UHV: Ultra High Voltage

VSC: Voltage Source Converter

WAMS: Wide Area Measurement Systems

CHAPTER 1: INTRODUCTION

1.1 Background

The electric power system serves to generate, transport and distribute electrical energy to consumers in an efficient, economic and reliable manner. It is made up of generating stations, transmission lines and distribution networks. Eskom is South Africa's dominant electric power utility and one of the largest electricity suppliers in Africa. Eskom is a vertically intergraded company licensed to generate, transmit and distribute electricity. Eskom supplies power to its local consumers and exports power to its neighbours namely: Namibia, Swaziland, Lesotho and Botswana. Eskom also imports electric power from Mozambique. The demand on Eskom's network exceeds the supply from time to time and this compels the utility into taking measures such as load shedding in order to maintain a balance of generation and the load demand on the system. This enables the stability of the network and therefore ensuring that the system remains secure and reliable most of the time.

As part of its mitigation strategy against overload of the grid, Eskom decided to invest in new power generation and transmission infrastructure [1]. As a result, the Medupi Greenfield coal-fired base load power station in the Limpopo province of South Africa is under construction. With an expected total installed generation capacity of 4764 MW to be spread between six generating units after completion. Synchronization of the first generating unit (unit 6) of Medupi power station onto the grid was done on 15th February 2015. Transmission lines carry electric power over long distances from generating stations to load centres. It is planned that electric power from Medupi power station will be delivered to the load centres in the central power grid of South Africa, with parallel 765 kV and 400 kV HVAC lines. It is also planned that in future, two additional coal-fired base load power stations under the project names Coal 2 and Coal3 power stations will be built in the vicinity of Medupi and Matimba power stations. When Coal 2 and Coal 3 power stations become operational, it is planned that an HVDC scheme will be required to assist with the transmission of base load electric power and more importantly to assist with maintaining the (N-2) and (N-3) transmission contingency scenarios for the parallel 400 kV and 765 kV AC lines. These power lines will form part of the Limpopo-West power transmission corridor.

Various measures can be taken to enhance the stability of an electrical network. These measures can either be taken at generator level, network level (transmission system) or at load level. The use of Flexible AC Transmission Systems (FACTS) devices are some of the measures used to prevent or mitigate against instability at network level [2, 3]. HVDC transmission schemes are now widely regarded as alternatives to HVAC schemes for long distance transmission [4]. Like most power utilities, Eskom utilises the current installed Cahora-Bassa HVDC transmission scheme for bulk power transfer over a long distance and does not make optimal usage of the HVDC scheme as a measure of enhancing power system stability besides its primary functions of bulk power transmission over long distances, interconnection of asynchronous systems and decoupling of electrical networks to avoid cascading of faults. The following provide a background and motivation for this research investigation:

- The construction of the base load power stations in the Limpopo province warrants new transmission infrastructure for bulk power transfer from the power stations to the load centres. Provision has been made for the possibility of using a LCC-HVDC scheme in parallel with the HVAC lines, to transmit bulk power from the power stations to the load centres. It is however not known to what extent this planned HVDC scheme will affect the transient stability of the machines (generators) in close proximity of the Limpopo-West power transmission corridor, as well as the transient voltage stability at the sending end and receiving end busbars of the transmission lines.
- All power systems are unique in terms of infrastructure and network topology. Very few published studies have been done on how HVDC transmission schemes might affect the transient stability of Eskom's network. An investigation therefore needs to be carried out, taking the unique features of South Africa's electrical grid into consideration.
- It was observed from literature that not much emphasis was placed on the comparative analysis of different scenarios for imbedding HVDC schemes in a power system, and their impacts on system transient stability. It is planned that in this research, a comparative analysis will be done for various system operation scenarios that include HVDC schemes.

In this research therefore, an in-depth investigation was proposed to evaluate the impacts that HVDC transmission schemes might have on the transient stability of large

AC networks such as that of Eskom. Using DIgSILENT PowerFactory simulation software tool, the research is carried out on three test networks, namely: a two machine infinite bus system, a 30 machine 24 busbar system and Eskom's MTS network.

1.2 Research Objectives

The objective of this research investigation is to determine the impacts that HVDC schemes might have on the transient rotor angle and voltage stability of a large electrical network, such as that of Eskom. This will be achieved by:

- Developing a suitable research methodology, that would yield accurate results in analysing the transient rotor angle stability of a large multi-machine AC network.
- Successfully modelling and testing the HVDC schemes to be used in the study.
- Modelling the planned power stations and transmission lines (HVAC and HVDC) onto Eskom's MTS network.
- Carrying out transient rotor angle stability analysis on the generators of the existing and planned power stations in the Northern grid of Eskom's MTS network.
- Determining the best network configuration and system operation scenarios for a large electrical network with HVDC transmission schemes integrated into it, for transient stability improvement.

1.3 Significance of the Study

This research investigation seeks to provide network planners of large power utilities with a better understanding of the possible impacts that HVDC schemes may have on the transient stability of the overall network. It is possible that a parallel HVDC scheme may have a negative impact on the system transient rotor angle stability, if the converter controllers are not optimally configured to improve the system stability[5]. The outcome of the research would be used by power utilities such as Eskom to make optimal usage of HVDC schemes by using it to enhance the power system stability. This will ensure that the system maintains a high stability limit at all times, which contributes to a more secure and reliable electrical network.

The installation of new power system components, in particular HDVC transmission schemes is costly and requires a careful comparison of the competing decision criteria. The decision criteria usually includes the cost of installation of the HVDC scheme, the potential economic gain on the power market, the possible political and bureaucratic

challenges, and a measure of the technical performance of the power grid during transients or other disturbances in the system. The results of this study can assist electric power utilities in the decision making process of installation of new HVDC transmission schemes.

1.4 Project Scope, Limitations and Delimitations

This research project is limited to Eskom's MTS network only, even though medium voltage and low voltage DC transmission and distribution lines may have an impact on the transient stability of the network. The focus area of this research is the Northern transmission grid of Eskom's MTS network.

This research is limited to transient rotor angle and voltage stability analysis of the network using software simulation tools only. The research will also be limited to the modelling capabilities of the available software (DIgSILENT PowerFactory), such as the ability to model different types of loads and the level at which the software can be used to create the common and composite models required for generator and HVDC converter controllers.

1.5 Dissertation Layout

Chapter 2: This chapter presents the fundamental concepts of power system stability and the different methods used to assess, analyse and improve the transient stability of an electric power system. The principles of operation and control of HVDC systems are presented. A review and scrutiny of previous work done by other researchers on the subject of using HVDC schemes to improve power systems stability is presented.

Chapter 3: This chapter presents the research methodology used to carry out the investigation and gives a detailed description of the test networks used to carry out the research.

Chapter 4: The composite models of the HVDC schemes used in this research are presented in this chapter. The results obtained from testing the response of the HVDC systems for various faults and to step changes in the reference parameters of the converter controllers are presented and explained. The work done under this chapter was to ensure that the HVDC schemes used in this investigation have been modelled correctly and that their operation is stable.

Chapter 5: This chapter presents the analysis done on the small (two machine infinite bus) and medium sized (30 machine 24 bus) networks. The obtained results are presented and brief explanations of the results are given.

Chapter 6: This chapter presents the analysis done on the larger Eskom MTS network. The obtained results for this network are presented and brief explanations of the results are given.

Chapter 7: This chapter summarizes and explains the overall findings of the research project. Detailed explanations are given and comparisons are made between the results obtained from the various test networks.

Chapter 8: This chapter presents the conclusions drawn from the discussions of the results and gives recommendations on how the proposed project should be implemented. Suggestions and recommendations on further research that needs to be carried out on this subject in future are also given.

CHAPTER 2: LITERATURE REVIEW

2.1 Modern Power Systems

The first complete power system (comprising a generator, cable, fuse, meter and loads) was built by Thomas Edison, the historic Pearl Street Station in New York city which began operation in September 1881. This was a DC system consisting of a steam engine driven DC generator, supplying power to 59 customers within an area roughly 1.5 km in radius [6]. The first limiting factors encountered on such systems were voltage drop and resistance losses on the low voltage DC distribution circuits. The solution to these problems came with the introduction of the AC generators and transformers [7]. As shown in figure 2.1, the modern power system is a complex network that consists of distributed generation sources, renewable energy sources, power electronics based reactive power compensation devices, smart grid technologies, HVAC and HVDC technology based power transmission schemes. Previous studies shows that compared to HVAC transmission lines, the response of HVDC systems to faults is quicker and more controllable, therefore making HVDC lines more tolerable to faults.

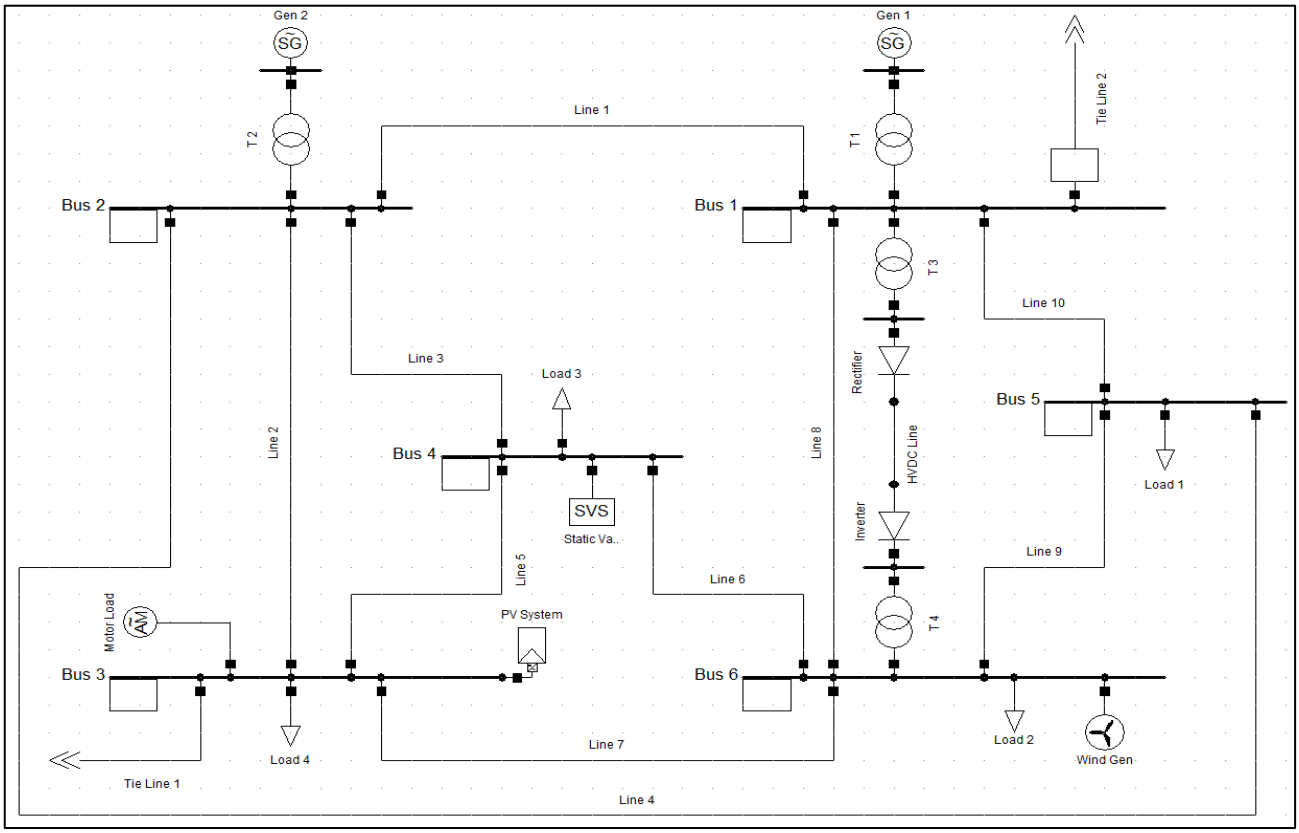

Figure 2.1: Typical Modern Power System Structure

2.2 Power System Stability

Successful operation of the power system depends largely on the engineer's ability to provide reliable and uninterrupted services to the loads. Ideally, the reliability of the power system implies that the loads must be supplied at constant voltage and frequency at all times. In practice this means that both voltage and frequency must be held within close tolerances so that the consumer's equipment may operate satisfactory. This means that the power system operator must maintain a very high standard of continuous electrical service. The first requirement of reliable service is to keep the synchronous generators running in parallel and within adequate capacity to meet the load demand with few interruptions over an extended period of time. If at any time a generator loses synchronism with the rest of the system, significant voltage and current fluctuations may occur, therefore lowering the standard of electrical service and affecting the power system reliability [8].

Power system stability has been recognised as an important problem for secure power system operation. Security of a power system refers to the degree of risk in its ability to survive imminent disturbances (contingencies) without interruption of customer service [9]. Reliability is the overall objective in power system design and operation. To be reliable, the system must be secure most of the time. To be secure, the system must be stable but must also be secure against other contingencies that would not be classified as stability problems. It is therefore important to ensure that the electric power system is stable at all times in order to allow for maximum power flow and the generation of voltage at system frequency and at the same phase angle for all the generators in the network [10].

2.2.1 Definition of Power System Stability

Power system stability is the ability of an electric power system, for a given initial operating condition, to regain a state of operating equilibrium after being subjected to a physical disturbance, with most system variables bounded so that practically the entire system remains intact [9]. The stability of an electric network can be classified into three main categories, namely: Steady state, small-disturbance (dynamic) and large-disturbance (transient) stability. Steady state stability relates to the response of a synchronous machine to a gradually increasing load. Small-signal stability refers to the ability of the power system, when operating under given load conditions, to retain

synchronism when subjected to small disturbances. Transient stability refers to the response of synchronous machines to large disturbances [6, 11]. Large-disturbance and small-disturbance stability of a power system may further be classified as: rotor angle stability, frequency stability or voltage stability. Voltage stability refers to the ability of a power system to maintain steady voltages at all system buses after being subjected to a disturbance from a given initial operating condition. It depends on the ability to maintain or restore equilibrium between load demand and load supply from the power system. An example of instability that may result occurs in the form of a progressive fall or rise of voltage at some buses in the system, this is also referred to as voltage collapse. Static analysis of voltage stability involves the use of P-V and Q-V curves to investigate the maximum active and reactive power that can be transmitted through a transmission line to a load considering the voltage level of the load bus. Transient voltage stability of an electric power system can be analysed by carrying out transient dynamic simulations by introducing a severe fault in the system and observing whether the different busbar voltages are within the acceptable busbar voltage limits.

[9]. Frequency stability refers to the ability of a power system to maintain a steady frequency following a severe system upset resulting in significant imbalance between generation and load. Instability that may result occurs in the form of sustained frequency swings leading to tripping of generating units and/or loads [9]. Transient rotor angle and busbar voltage stability is of interest in this research.

2.2.2 Transient Rotor Angle Stability

Transient rotor angle stability is the ability of synchronous machines of an interconnected power system to remain in synchronism after being subjected to a severe disturbance, such as a short circuit on a transmission line. It depends on the ability to maintain or restore equilibrium between electromagnetic torque and mechanical torque of each synchronous machine in the system. The resulting system response involves large excursions of generator rotor angles and is influenced by the nonlinear power-angle relationship. Instability that may result occurs in the form of increasing angular swings of some generators leading to their loss of synchronism with other generators. If one generator temporarily runs faster than another, the angular position of its rotor relative to that of the slower machine will advance. The resulting angular difference transfers part of the load from the slow machine to the fast machine, depending on the power-angle relationship. This tends to reduce the speed difference and hence the

angular separation. The power-angle relationship is highly nonlinear. Beyond a certain limit, an increase in angular separation is accompanied by a decrease in power transfer such that the angular separation is increased further. Instability results if the system cannot absorb the kinetic energy corresponding to these rotor speed differences. Transient stability depends on both the initial operating state of the system and the severity of the disturbance. The time frame of interest in transient stability studies is usually 3 to 5 seconds following the disturbance [6, 9, 11].

Some of the common causes of transient stability problems in HVAC systems are:

Low machine inertia

Synchronous machines with low inertia values are prone to transient instability because they will accelerate much faster when the power system is subjected to a large disturbance.

Low power system impedance

Low system impedance minimizes the power transfer capability of the transmission lines, which affects the flow of synchronising power need by the generators to maintain synchronism and this may lead to transient stability problems.

Unreliable or slow protection systems

If the power system protection system does not clear the fault and isolate the faulted part fast enough, the fault will persists on the system and this leads to long fault durations which increases the severity of the fault and may cause transient stability problems in the system.

High system loading

Overload of the system leads to high generator loading. The loading of the generator determines the internal voltages of the generator and the phase angle between the internal voltage and terminal voltage of the machine, and this angle determines the power output of the machine. High system loading may therefore cause transient stability problems.

2.2.3 Swing Equation and Power Angle Characteristics

The angular momentum and inertia constant play an important role in determining the transient stability of a synchronous machine. Under steady state conditions, the corresponding input power (P_i) of the input torque provided by the prime mover at the generator shaft is equal to the output electromagnetic power (P_e), with the armature resistance neglected. Thus we have:

$$P_i - P_e = 0 \tag{2-1}$$

If a departure from steady state occurs, such as a change in load or a major fault, the power in, is no longer equal to the power out. Thus an acceleration torque comes into play. If P_a is the corresponding acceleration power, then:

$$\frac{2H}{\omega}\frac{d^2\delta}{dt^2} = \frac{H}{\pi f}\frac{d^2\delta}{dt^2} = P_i - P_e = P_a\ p.u. \tag{2-2}$$

Where H is the per unit inertia constant, δ is the power angle in electrical radians and ω = 2πf, is the radian frequency in electrical radians/s.

Equation (2-2) is called the swing equation. To investigate the stability of the machine or the stability of a particular power system after a disturbance, it is necessary to solve the dynamic equation describing the angle δ immediately, following an imbalance or disturbance to the system. A plot of δ (t) is known as the swing curve [12].

The internal power developed by a round rotor lossless synchronous machine in steady-state is equal to the output power of the machine, and is given by [7]:

$$P_e = P_d = \frac{|E_g||V_t|}{X_s}\sin\delta\ \ W/phase \tag{2-3}$$

Where:

δ = is the electrical power angle, which is the angle by which E_g (machine internal voltage) leads V_t (machine terminal voltage)

P_e = internal power developed

P_d = output power generated

Equation 2-3 is said to be a representation of the power-angle characteristics of a synchronous machine and it shows that the internal power developed by a synchronous machine is proportional to sinδ. The power-angle characteristics of a salient pole machine depends on the direct and quadrature axis reactance X_d and X_q [7]. The per-phase power delivered by a salient-pole rotor synchronous machine as a function of the power angle δ is therefore given by:

$$P_d = \frac{|E_g||V_t|}{X_d}\sin\delta + \frac{|V_t|^2}{2}\left(\frac{1}{X_q} - \frac{1}{X_d}\right)\sin 2\delta \ \ W/phase \qquad (2\text{-}4)$$

From equation (2-4) it can be seen that the resulting power developed by a salient pole rotor synchronous machine is a sum of two power components. This is the power due to field excitation (the first term) and the power due to saliency (the second term). When X_d=X_q, the machine has no saliency and the second term reduces to zero.

2.2.4 Methods of Assessing and Analysing Transient Stability

Following a large-disturbance or fault in a power system, the transient stability analysis and assessment of the power systems involves a study of non-linear differential equations. The obtained solution of the non-linear swing equation allows for the power systems engineer to determine the stability or instability of the electric network [8].

Various methods have been developed and used to determine the stability of a power system. The two main methods used for power system transient stability assessment are the traditional time-domain numerical integration method and the direct or energy function methods. Due to non-linearity of the differential equations, the solving process is tedious and complicated and therefore in the time domain approach, methods of numerical integration are applied to the swing equation in order to examine the power system stability [13].Various numerical integration methods are used to solve ordinary non-linear differential equations. Examples of such methods of numerical integration are the Euler method, modified Euler method, Runge-Kutta (R-K) method, second-order R-K method, fourth-order R-K method and Gill's version of fourth order R-K method (R-K-G) [6]. According to Maria et.al [14], one of the advantages of the time-domain simulation method is its unlimited modelling capabilities. The time-domain approach is directly applicable to any level of detail of power system models, all the information of state variables during transients, as well as steady-state operations are available and the simulation results can be interpreted directly by the system operators [13]. The time

domain simulation method has two main disadvantages. It is inherently slow because of the step by step integration process involved in solving the non-linear differential equations. The other short coming is that it only yields a yes or no type of answer on the stability problem, without any identification on the degree of stability of the system. The lack of sensitivity information on the power system's degree of stability therefore has to be compensated by many stability runs in order to derive and determine the stability limits of the system. This trial and error process requires much central processing unit (CPU) time and is therefore not suitable for online transient stability assessment [14].

An alternative approach to transient stability analysis is the direct or energy function method. In contrast to the time-domain methods, the direct methods determine the degree of system stability based on energy functions, without explicitly integrating differential equations describing the post-fault system [13, 15]. The time domain simulation approach is normally used as the benchmark for transient stability analysis because it is considered to give the most accurate assessment, even though it has a major disadvantage of the large computational burden of the numerical integration in the post-fault period. On the other hand, while requiring much less computations and computational time, the accuracy in stability assessment of the direct methods is questionable and inferior to the time domain approach.

2.2.5 Critical Fault Clearing Time (CCT)

In order to remove a faulted element from the power system, a protective relay system is required to detect that a fault has occurred on the power system and to initiate the opening of circuit breakers which will isolate the faulted element from the system. The total fault-clearing time is therefore made up of the relaying time and the circuit breaker-interrupting time. The relay time is the time from the initiation of the short-circuit current to the initiation of the trip signal to the circuit breaker. The interrupting time is the time from the initiation of the trip signal to the interruption of the current through the breaker. On high voltage (HV) and extra high voltage (EHV) transmission systems, the normal relay time ranges from 15 to 30 ms and this is 1 to 2 cycles. The normal circuit breaker-interrupting times ranges from 30 to 70 ms, which is 2 to 4 cycles [6]. The total maximum normal fault clearing time is therefore 100 ms. The critical clearing rotor angle is that angle for which the system is at the edge of instability [8]. If the switching and protection system does not clear the fault in time before the

critical clearing angle is reached, the power system goes into an unstable state. The critical fault clearing time (CCT) corresponds to the critical angle and it is defined as the maximum time between the initiation and the isolation of a system fault such that the power system remains transiently stable [11].

2.2.6 Methods of Improving Transient Stability

Most of the methods used for enhancing power system transient stability make use of Flexible AC Transmission Systems (FACTS). FACTS make use of power-electronics based controllers to regulate power flow and transmission voltages and to mitigate against disturbances. The two main objectives of FACTS are to increase the useable power transfer capacity of transmission lines and to control power flow over designated routes of transmission lines [16]. A review on the effect of different FACTS controllers on power system stability was carried out in [16]. The impacts of the different controllers were expressed in terms of CCTs. The controller parameters were selected with only consideration of maximizing the CCT, and the CCTs obtained for different controllers were compared. From the comparison, it was found that, in terms of improving CCT, the STATCOM performs much better than the SVC. The TCSC is more effective than the shunt controllers, as it offers greater controllability of the power flow in the line. It was also found that the UPFC is by far the best controller as it provides independent control over the bus voltage and the line active and reactive power flow. A new power-electronics controller technology that emerged is the Insulated Gate Bi-Polar Transistor (IGBT) based power electronic controller. The IGBT with an anti-parallel diode connected across it has bi-directional current carrying capabilities and therefore makes the converter to possess current bi-directional characteristics. The converter makes use of the pulse width modulation (PWM) techniques to control active and reactive power output as well as harmonic distortions. The PWM control techniques are based on the switching frequency. The overall objectives of the methods used to improve transient stability is to try and achieve one or more of the following effects on the power system [6].

- Reduction in the disturbing influence by minimizing the fault severity and duration
- Increase of the restoring system synchronizing torque
- Reduction of the accelerating torque through control of the input mechanical power
- Reduction of the accelerating torque by applying artificial load

2.3 HVDC Technologies and Principles of Operation

The original motivation for the development of DC technology was transmission efficiency, as the power loss of a DC line is lower than that of a corresponding AC line of the same power rating. This however required the use of HVDC, and therefore the development of conversion switches capable of withstanding high voltages. HVDC links are built for different purposes and therefore, the specific factors to be taken into account in their economic evaluation will largely depend on the purpose of the particular HVDC link [4]. There are three main types of HVDC converter technologies that are mostly used in modern HVDC transmission schemes, namely: Line Commutated Current Source Converter (LCC-HVDC), Self-Commutated Voltage Source Converter (VSC-HVDC) and the modern Modular Multi-Level Converters (MMC). In this research, the classical LCC-HVDC and VSC-HVDC technologies are going to be studied. HVDC is widely regarded as being advantageous over HVAC for long distance power transmission. Table 2.1 shows a technical comparison between HVDC and HVAC, and summarizes some of the advantages and disadvantages that HVDC has over HVAC.

Table 2.1: Advantages and Disadvantages of HVDC [17].

Advantages	**Disadvantages**
Greater power per conductor	Converters are expensive
Simpler and cheaper line construction for lines of same transfer capacity as HVAC lines	Converters require much reactive power
Ground return can be used	Converters generate harmonics
No charging current	Converters require filters for harmonics
Line power factor always unity hence reactive power compensation is not needed	Multi-terminal or network operation is more challenging to implement
Synchronous operation not required	
Distance not limited by stability	
Low short circuit current on DC line	
Line power is easily controlled	
No skin effect	
Needed for under water cables > 50 km	

2.3.1 HVDC Scheme Configurations

There are three basic HVDC scheme configurations, namely; point-to-point, back-to-back and multi-terminal configuration.

Point-to-point

The most basic HVDC scheme is a point-to-point interconnection that consists of two converter stations, whereby one converter operates as a rectifier and the other converter operates as an inverter. Such converters are connected by overhead lines, land or sea cables or a combination of these. As shown in figure 2.2, a point-to-point HVDC scheme can be implemented as a monopole with either a metallic or earth return, as a bi-pole with earth or metallic return, or as a balanced monopole with no return. Earth electrodes are required to operate the HVDC scheme with an earth return[6].

Back-to-back

Two asynchronous AC systems can be connected with a back-to-back HVDC scheme. In a back-to back scheme, the two converters are located at the same place. Therefore, there are no transmission lines or transmission cables needed to connect the two converters. With this configuration, line losses do not need to be considered in the design, and direct voltage can be kept low, and thus simplifying equipment design. There is no need for DC side switchgear, and both the rectifier and inverter valves may be housed in the same building [18].

Multi-terminal

As shown in figure 2.2, a multi-terminal HVDC scheme consists of three or more converter stations interconnected by overhead lines or cables. The converter stations are the same as those in a point-to-point configuration, but are provided with equipment to connect and control the operation of multiple converters on a common DC network. All converters in a multi-terminal configuration have to operate at a common DC voltage polarity and voltage level. The direct current ratings of the converters can differ [4].

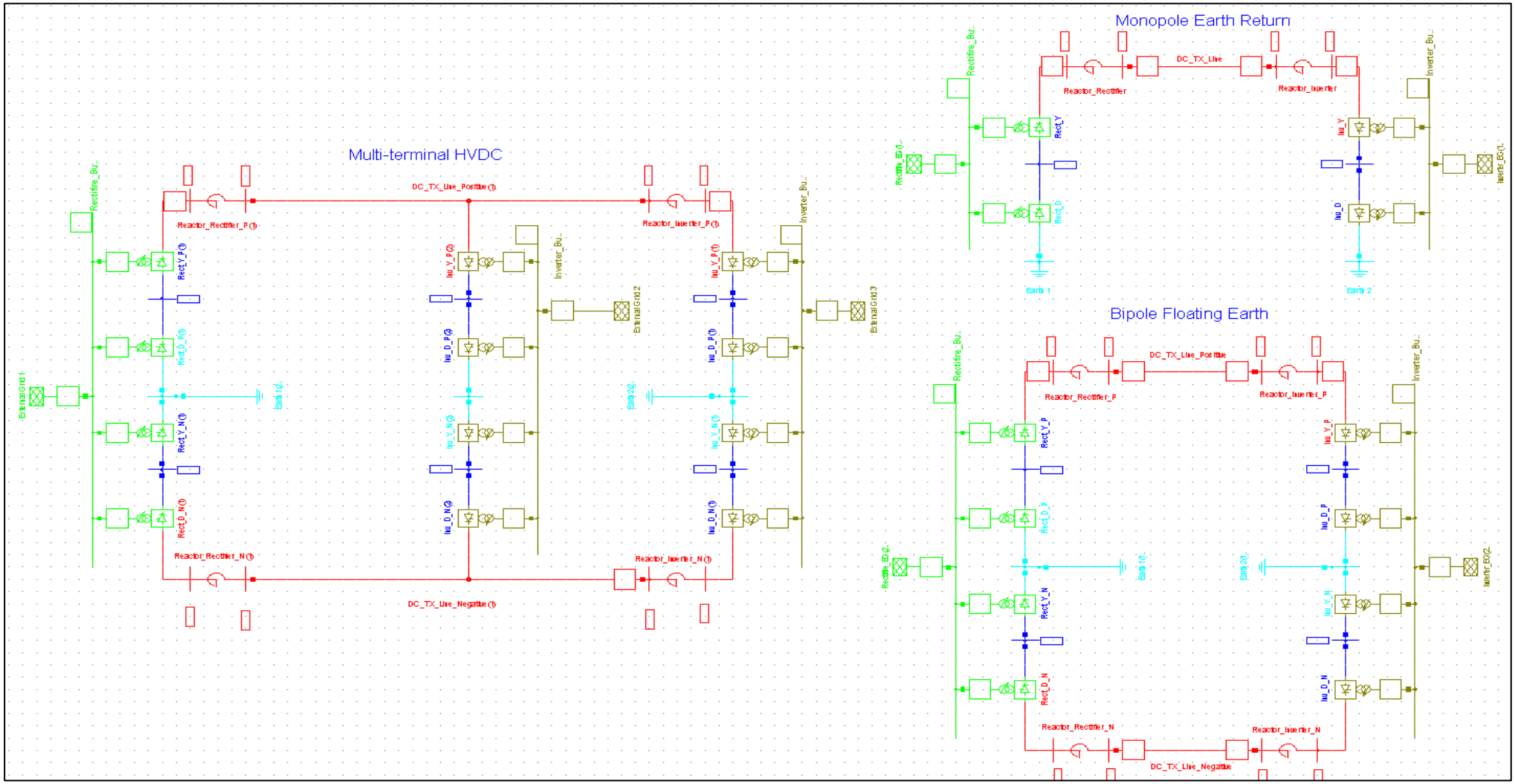

Figure 2.2: HVDC Scheme Configurations

2.3.2 LCC-HVDC Station Layout and Operation

The design and layout of a HVDC converter station depends largely on the following important factors: the configuration of the DC system (monopole, bi-pole etc.), reactive power compensation requirements and AC filtering requirements. A typical HVDC scheme is made up of the following main elements: AC lines, AC switch yard (containing reactive power compensation shunt capacitors and harmonic filters), converter transformers, valve hall, a DC switch yard (containing smoothing reactors), and DC lines [6].

The classical HVDC transmission system employs line-commutated current source converters (CSC) which makes use of thyristor valves as controlled switching elements used for the power conversion process as shown in figure 2.3. The basic building blocks of these thyristor valves is the three-phase full wave bridge which is also referred to as a six-pulse bridge because of the six commutations per period [19]. Commutation is the transfer of DC between valves on the same side of the bridge [4]. In order to meet the required DC voltage and eliminate some of the harmonics, the DC terminals of two six-pulse bridges with AC voltage sources phase displaced by 30^{o} are connected in series. These types of converters are known as twelve-pulse converters. The converter transformers are used to bring the AC source voltage to the rated voltage of the converter. The 30^{o} phase displacement is achieved by feeding one bridge through a converter transformer with a star-connected secondary and feeding the other converter through a transformer with a delta-connected secondary [4].

LCC-HVDC converters require a strong synchronous AC voltage source for them to operate. LCC-HVDC converters can only operate with the AC current lagging the voltage, the power conversion process therefore demands a large amount of reactive power. The extra reactive power is supplied from the AC filters, shunt and or series capacitor banks. The purpose of the smoothing reactor in the DC switchyard is to reduce the rate of rise of DC flowing during a disturbance. This helps to reduce the number of commutation failures following a reduction in AC voltage [20].

2.3.3 VSC-HVDC Station Layout and Operation

Most of the elements in a VSC-HVDC converter station are similar to those in a LCC-HVDC converter station. The main difference is the equipment specifications and ratings. The transmission circuits of VSC-HVDC usually consists of a bi-polar two wire

HVDC system, with converters connected pole-to-pole. DC capacitors are used to provide a stiff voltage sources and a low-inductance path for the turn off switching currents as well as to provide energy storage. These DC capacitors are grounded at their electrical centre point to establish an earth reference potential for the transmission system and therefore there is no earth return operation [20]. The AC filters in a VSC-HVDC station have much smaller rating and they are not required for reactive power compensation.

Unlike LCC-HVDC, VSC-HVDC uses insulated gate bi-polar transistors (IGBTs) as controlled switching elements. The IGBTs have the ability to self-commutate and they are operated with an anti-parallel diode to ensure bi-directional conduction of current [21]. A two level voltage source converter can be controlled by using one of the following pulse width modulation (PWM) techniques: Selective harmonic elimination PWM, carrier based PWM and space vector PWM. The aim of all the mentioned modulation techniques is to create a train of voltage or current pulses, with the same fundamental as the carrier signal, these pulses are then used as the gating signals for the switching elements (valves). The carrier based sinusoidal pulse width modulation (SPWM) technique is attractive in many applications because of its simplicity to implement practically and its ability to suppress harmonics effectively [21]. Unlike LCCs, VSCs have no reactive power demand, they have control over their reactive power and therefore they are able to regulate AC system voltage [20].

2.3.4 LCC-HVDC and VSC-HVDC Control

One of the main advantages that HVDC has over HVAC it's the ability to control various electrical quantities simultaneously. HVDC control systems are generally used to archive the following objectives [18, 20]:

- To control basic system quantities such as DC line current, DC voltage, and transmitted active power and converter reactive power accurately and with adequate speed.
- To maintain adequate commutation margin in inverter operation so that the valves can recover their forward blocking capability after conduction, before their voltage polarity reverses.
- To control high level quantities such as frequency in isolated mode or provide power oscillation damping to stabilize the network.

- To compensate for loss of a pole, generator, or an AC transmission circuit, by adjusting the power rapidly.
- To make sure that the system remains in a stable mode of operation with reliable commutation, when the system is subjected to perturbations.
- To minimize the losses of the system and reduce amount of reactive power needed for converter operation.

2.3.4.1 LCC-HVDC Control

HVDC control systems are made up of two basic sub-systems, namely: converter firing angle control and pole power control. The LCC-HVDC control system consists of the following four main functions: Voltage Dependent Current Order Limiter (VDCOL), Current Control Amplifier (CCA), Phase Locked Oscillator (PLO) and Gate Control (GC). A detailed explanation of the LCC-HVDC scheme control and the implementation of each of the mentioned control system functions is given in appendix D. HVDC converters contain a closed loop current controller which receives a measure of the DC current and generates the firing angle in order to control the converter valves. Normally the rectifier controls the DC current by comparing it to a reference current and the inverter controls the DC voltage by controlling the firing angle, since the DC voltage is a function of the firing angle [22].

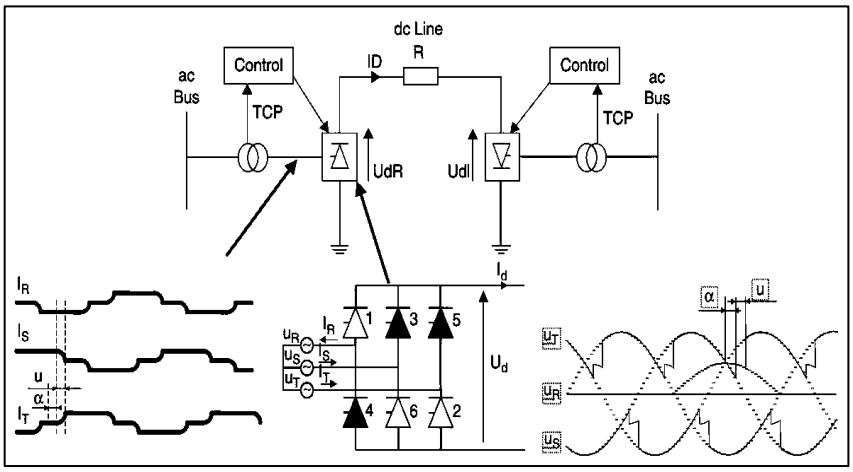

Figure 2.3: General LCC-HVDC Configuration and Control [20]

Some of the key HVDC system variables, as seen from figures 2.3 and 2.4 are:

V_{ac} = voltage at the AC busbar

I_{ac} = AC current flowing into or out of the converter transformer

P = active power flow

U_d = DC voltage

I_d = DC current

α = firing angle of the converter

γ = extinction angle of the converter

C = shunt capacitance at the AC busbar

Only three variables in an HVDC system can be controlled directly: the firing angle α, the converter transformer ratio 1: T (tap position) and the shunt capacitance C. A change in α modifies U_d and therefore I_d [18].

For LCC-HVDC, one terminal sets the DC voltage level while the other terminal regulates the DC current by controlling its output voltage relative to that maintained by the voltage setting terminal. Large changes can be made in the DC current value and hence the DC power by making small changes to the firing angle. This is because of the low resistance of the DC line. For LCC-HVDC, two main techniques are used to control the system variables. The first method is by changing the delay angle α, in order to change the ratio between the DC voltage and the AC voltage. The second technique is by using the load tap changers (LTC) of the converter transformers to change the AC voltage at both line terminals. The LTC is used at the rectifier terminal to keep the firing angle within its steady-state range of values of (13^o-18^o), and at the inverter to keep the extinction angle within the desired range of (17^o-20^o). Changing the firing angle is considered to be the faster method of control [18, 20]. It is important to keep the firing and extinction angles of the converters within the stated desired ranges during steady state operation of the converter. This is so because it is desired that both the rectifier and inverter maintain a high power factor as possible. A high power factor operation of the converters minimizes the reactive power compensation needed by the AC system and increases the capacity of active power that can be processed by the converters and converter transformers, which allows for a high active power transmission capacity of the DC link. For the rectifier to operate at a high power factor, it should have a small firing angle delay and for the inverter to operate at a high power factor should to have a small leading extinction angle. However, in real operations, there is a minimum constraint on the rectifier firing angle delay of 5 degrees, in 50 Hz systems. The firing angle is usually set to be greater than the minimum firing angle and normal operation uses a firing angle of 13-18 degrees to leave a certain margin. This margin is provided

to ensure that the valves have adequate positive voltage before commutation to provide sufficient energy to the firing generation circuit. Similarly, the inverters also need adequate time to complete commutation under positive valve voltage after firing.

2.3.4.2 VSC-HVDC Control

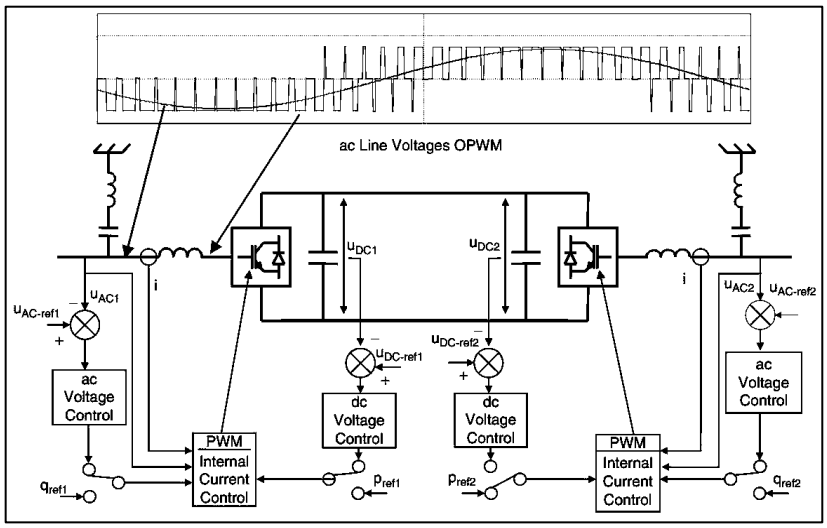

Figure 2.4: General VSC-HVDC Configuration and Control [20]

Figure 2.4 shows the configuration and control system of a typical VSC-HVDC system. Each VSC station has two degrees of control freedom. One degree of freedom is used to control the reactive power and the other degree is used to control the DC voltage which in turn controls the active power. VSC stations allow for fully independent control of active and reactive power, depending on the operating design limits of the converters. There should always be a balance of the active power flowing through the DC link, considering the transmission losses to be negligible. In order to achieve this, one converter (normally the rectifier) is set to control active power and the inverter controls the DC voltage which also regulates the active power flow, therefore ensuring a balanced power flow through the DC transmission system [23]. In order to minimise damage that may be caused by faults on the control system, the VSC-HVDC employs a control system structure made up of different layers.

Yuan and Wang [24] proposes a VSC-HVDC control system structure divided into the following five layers: DC system control layer, pole control layer, converters control layer, valves control layers and separate control layer. The layers exhibit a top-down communication process, whereby, the top layers order the lower layers to execute a

particular instruction. The lower layers have direct control over the devices and objects in the system.

By applying the power angle relationship presented in equation (2-3) to the HVAC-HVDC system, it can be observed that varying the phase angle of the converter AC voltage with respect to that of the grid has a large influence on the active power, but negligible influence on the reactive power, since this phase angle is usually small. If the converter voltage leads the system voltage, active power is injected into the AC system, if the converter voltage lags the system voltage, the converter then acts as a rectifier and active power is absorbed by the converter from the grid and transmitted via the HVDC link. This technique is used to control the active power of the VSC-HVDC scheme. This therefore makes the active and reactive power control of the VSC independent from each other. There is continuous control of the converter active power, whereby, the rectifier is set in active power control mode and the inverter is set to control the DC voltage, which in turn controls the DC power transmitted. This is done to ensure that there is always an active power balance between the active power processed at the rectifier and the active power received at the inverter.

The magnitude of the converter voltage with respect to that of the system voltage has a large influence on reactive power but negligible impact on the active power. When the converter voltage magnitude is larger than the system voltage magnitude, reactive power is injected into the AC system and when it is smaller, reactive power is absorbed by the converter. This technique is used for reactive power control of the VSC, and this therefore means that VSC do not have reactive power demand problems. Control of the reactive power at the converter is essential in the sense that it can be used for reactive power compensation for voltage regulation at the AC busbars, when the system is subjected to a fault.

This particular control principle is similar to that of a SVC. The active power transfer by a VSC-HVDC link can therefore be changed rapidly without altering the reactive power exchange of the DC link with the AC network [18, 20, 24].

2.3.5 Technical Comparison of VSC-HVDC to LCC-HVDC

Table 2.2 summarizes a comparison of the technical characteristics of LCC-HVDC and VSC-HVDC technologies.

Table 2.2: Technical Comparison of LCC-HVDC and VSC-HVDC [18, 25]

Attributes	**LCC-HVDC**	**VSC-HVDC**
Converter technology	Thyristor valve, Grid-commutation, CSC	Transistor valve, (IGBTs) self-commutation, VSC
Max. converter rating at present	6400MW, ±800kV (overhead line)	1200MW, ±320kV (cable)
Typical delivery time	36 months	24 months
Reactive power demand	50% of active power transferred	No reactive power demand
Reactive power compensation and control	Discontinuous control (switch shunt banks)	Continuous control (converter In-build PWM)
Independent control of active and reactive power	No	Yes
Typical system losses	2.5-4.5 %	4-6 %
Multi-terminal configuration	Complex, limited to 3 terminals	Simple, no limitations
Scheduled maintenance	Typically < 1 %	Typically < 0.5 %
Commutation Failures	Suffers commutation failures	Does not suffer commutation failures
Station footprint	Relatively large	Relatively small
Response to system faults	Relatively slow	Relatively fast

2.4 Using HVDC to Improve System Transient Stability

Power system stability enhancement is an interesting and complex subject, and many methods of enhancing network transient stability have been proposed by various researchers. Inherently, FACTS devices such as SVCs, STATCOMs, TCSC and UPFCs are used to improve transient stability of an AC network [26-29]. With HVDC now widely regarded as an alternative to HVAC for bulk power transmission over long distances, previous investigations carried out on the subject shows that it is feasible for power system dynamics, especially the transient stability of parallel AC-DC systems to be improved by making optimal usage of the controllability and temporary overload capability of HVDC converters. Earlier studies have been carried out whereby different techniques and methods have been developed to prove the feasibility of this hypothesis [5, 30-38].

Machida [30] presents the fundamental concepts used in the design of the method used to control HVDC power flow for power system stability improvement. In order for a generator to remain in step with the rest of the generators after being subjected to a system fault, there needs to be a balance between the acceleration power gained by the generator during the fault and the retarding power of the system applied onto the generator during the transient period, after the fault has been cleared. The method presented in [30] employs a strategy whereby rapid control of the HVDC converters is used for temporary increment of DC power during the fault and transient period after fault clearance. The temporary increase in DC power adds to the retarding torque of the of the generator, which allows for the total retarding energy to be greater than or equal to the total acceleration energy, which then prevents the generator from going out of step. The DC power increment required for stable operation of the generator depends on the severity of the transient experienced by the generators and AC lines.

Hammad [5] carried out an investigation on the effects of parallel HVDC systems on transient stability of the AC network. It was found that HVDC schemes in parallel with HVAC lines may deprive the AC system of the needed synchronizing torque during disturbances and may cause system instability if conventional control strategies are used for DC power modulation instead of making use of advanced, robust, fast, state of the art control techniques. These advanced large-signal stabilizing control techniques can be developed to produce large system synchronizing and damping torques in the AC system and therefore improving transient stability of the AC system. Such advanced control techniques optimizes the temporary overload capability of the HVDC converters.

An alternative and effective method of using HVDC for power system transient stability improvement is by simultaneous AC-DC power transmission through a transmission line. In a simultaneous AC-DC scheme, a line is used to transport both three-phase AC and DC power at the same time. Part of the transmitted AC power is converted into DC at the rectifier side and injected into the neutral point of zig-zag connected secondary windings of the sending end transformer. The injected current is distributed equally among the three windings of the transformer and transmitted to the receiving end transformer. The current is then converted back to AC by the inverter at the receiving end of the line. The zig-zag connection is used to avoid the saturation of the transformer core due to the flow of the DC component of the current. Just like in parallel AC-DC

schemes, fast control of converters for modulation of the transmitted DC power is used to produce a retarding torque and improve the total system synchronizing torque, and therefore bringing back the generators to their nominal speeds and improving first swing stability of the generators in the system [39-41].

Recent studies have been carried out on test networks and existing grids to demonstrate the ability of HVDC schemes to improve system stability. Fuchs et.al [42] demonstrated the feasibility to stabilize large power systems using VSC-HVDC links. Based on global power system measurements or Wide Area Measurement Systems (WAMS), a model predictive control (MPC) scheme that manipulates the power injections of the HVDC links to damp oscillations in the AC system was developed. Similar studies were carried out in [43, 44]. Machowski et.al [45] proposes to apply a WAMS-based MPC scheme to a multi-terminal HVDC network. The supplementary control scheme which uses a fast communication platform to transmit the relevant information needed for the controls is used to modulate the active and reactive power at the DC terminals of the network. By so doing, the supplementary controller is used to damp power swings in the AC system and thus improving the transient stability of the AC power system. The MPC grid controller explicitly accounts for constraints and the expected future behaviour of the system. Fuchs et.al tested the MPC-based grid controller on a large model of the European Network of Transmission Systems Operators for Electricity (ENTSO-E) system and a suitable dynamic model of the relevant HVDC dynamics. The proposed control objective measures the instantaneous relative frequency error between the system generators. This enables the use of the adjustment of the HVDC injections purely for power oscillation damping. Different stress (fault) scenarios were simulated to test and compare the local damping control and the global MPC-based grid controller. The power system was modelled in MATLAB and PowerFactory software. The simulated stress scenarios were: loss of an AC link, loss of a large power plant and loss of a large load in the European system. The system variables of interest were: average frequency, frequency deviation and active power flow in the line. It was found that with the global MPC-based grid controller, the installed HVDC links effectively damp the oscillations and guide the system to a new stable equilibrium point (SEP).

Huang and Krishnaswamy [46] proposes a new control mechanism to augment the power system's rotor angle stability. An HVDC model that considers physical constraints on tap changing, reactive power limits etc. was used to carry out the

analysis. Huang and Krishnaswamy [46] states that, when reactive power injection at the AC terminals of the converter is assumed, a DC link can operate under different control modes and these control modes change when certain variables hits their limits. It is further claimed that during a transient disturbance, the DC power can be ramped down rapidly to reduce the generation/load imbalance of the AC system on both sides of the converter. In some situations, it may be necessary to ramp up the DC power to assist system stability by taking advantage of the short-term over load capability of the HVDC system. Due to the fact that the power flow through a HVDC link can be highly controllable, the HVDC link can be used to strengthen the power system stability. The study was carried out on the P.M. Anderson 9-bus system. Three control scenarios were simulated under a ground fault condition induced on one of the AC links. In the first case the HVDC link maintains the same control as in the normal state in which the post-fault HVDC power flow settings remain the same as before. In the other two cases, two stabilizing controls, the P and PI controllers are used to alter power flow settings in the HVDC link, therefore stabilizing the system. It was found that when the PI controller was used, the rotor angles of all three generators in the network are very close to each other and this means that the stability of the system was enhanced. The PI controller was also found to be more effective compared to the P controller.

Wang et.al [47] proposes a control strategy that employs a LCC-HVDC line together with a modal control PID designed rectifier current regulator (RCR) to perform the control and compensation of the active and reactive power generated by induction generators in four parallel operated offshore wind power generation farms. It was found that the LCC-HVDC scheme together with its controls provides fast reactive power compensation, fast control of active power delivered by the HVDC link to the substation Inverter, as well as minimizing the voltage drop at the Inverter substation busbar.

Liu and Chen [48] presents an improved Hybrid Multi-Infeed (HMI)-HVDC system model imbedded in a large AC system to prove that the required reactive power load value as well as the electrical distance of the tie line between the HVDC links has an influence on the transient voltage stability of the system. The HMI-HVDC links consist of a LCC-HVDC link and a VSC-HVDC link. The grid configuration is based on a possible future structure of the western Danish power system which was modelled in RTDS. In the report, a voltage adjustment method is proposed to improve the transient

voltage stability of the network. According to Liu [48], these claims are substantiated by the fact that assuming a constant load at each bus, as the distance of the tie line becomes longer, its equivalent impedance also increases and less power is transmitted by the line and consequently the voltage drop at the buses will be more severe under fault conditions. In a case were reactive power loads are adopted at a certain busbar which is supplied by the VSC-HVDC link, the AC transmission line and the tie line connecting the two HVDC links, there is an increased need of reactive power at the busbar if the fault occurs on the AC transmission line. If this need is unsupported during transient conditions it will lead to transient voltage instability of the system. Studies carried out in [48-51] shows that a HVDC link operated with an improved VSC-HVDC control mechanism stabilizes the busbar voltages after the system has been subjected to a fault. It was further found in [48] that an increase in reactive power value of the loads and an increase in length of the tie line connecting the two HVDC links have a negative effect on transient voltage stability.

The main objective of the work done in [52] was to determine the optimum location for a new HVDC link placement for system performance enhancement during transients, in a meshed AC system. The analysis was done using a model of the central European power grid. The achievable performance is compared to an economic measure given by the length of the evaluated HVDC link. A new control method whose outcome of optimization depends on the dynamic state of the system and recomputed at sampling rate of 50Hz, was proposed to improve on the Model Predictive Control (MPC) method. According to [52] the function used in the MPC method is only known point wise and cannot be used as a general grid performance measure. To overcome this limitation, the problem can be formulated in continuous time using linear matrix inequalities. A closed loop performance measure J, was found to be the best achievable power system performance measure for the worst expected initial disturbance. The value of J differed depending on the selected HVDC location. The smaller the value of J, the better the HVDC location is suited for power systems control. The computation of the grid performance measure is performed as an equivalent semi-definite program. The trajectories of the generator rotor angles relative to their centre of inertia for different choices of HVDC link placements were observed. HVDC links were then placed on the central European system to determine the optimal placement of the HVDC link according to the performance measure J. It was found that the damping of generator

rotor angle oscillations increases with an increase in the number of HVDC links chosen to minimize the value of the performance measure J. It was further found that that the best placement was obtained with a rather short line in southern France. This means that the longest line does not necessarily give the best placement, nor does the shortest line.

The study in [53] focuses on transient stability enhancement of a multi-machine AC power system by controlling power injected into the power system by an HVDC scheme. It also extends earlier work to include variation of reactive power following transient commands of AC active power, to enhance transient performance of the power system. Comparisons were made for similar systems equipped with optimized Static VAr Compensators (SVCs) to demonstrate that modulation of active power injection in accordance with the proposed strategy is an effective tool for damping power system machine rotor angle swings. Hammons et.al [53] makes use of the high controllability of the HVDC link to enhance system stability. A multi-machine transient stability simulation program called STAB was developed. Using the proposed regulation and control algorithms, simulations were performed to illustrate the efficiency of these algorithms. A CIGRE 7-machine system was used as a test system for time domain simulations. Damping of rotor angle swing following a 3-phase short-circuit on a transmission line was compared for different system operation scenarios. Comparisons were made for the following operation scenarios: no HVDC power control, only active power HVDC link control, active power HVDC link control together with its associated transient reactive power, and using SVC instead of HVDC for power control and system stability enhancement. From the obtained simulation results it was found that; in general, there was significant rotor angle oscillation damping due to HVDC control, particularly for faults close to the HVDC converter. It was also observed that critical fault clearing times (CCT) were up to 10%-20% longer with HVDC control compared with using SVCs under similar system conditions. In [53] it is stated that the practical effectiveness of the proposed strategy is dependent on the conditions of the particular system under study.

Dorn et.al [54] carried out a review on HVDC technologies operation principles, applications and the ability to solve system stability and reliability problems. Various HVDC projects across the world were discussed. Based on existing literature it was found that innovative solutions involving power electronics with both HVDC and FACTS solutions have the potential to deal with the various power systems challenges.

According to Dorn [54], HVDC is an important measure of protection against cascading faults that may lead to a massive spread of black outs since it acts as a firewall of the network. An example of a DC line fault clearance with HVDC classic was presented. The example is illustrated by the Thailand-Malaysia classic HVDC (300kV) link [54]. Comparisons were made between detailed field measurements of the DC current and voltage at the rectifier side of the HVDC link and results obtained from simulating a similar fault on the HVDC line. From the measurement results and the results obtained via simulations it was concluded that the modular multi-level full bridge (MMC Full Bridge, HVDC Plus) solution for HVDC transmission offers significant benefits with regard to fast DC line fault clearing, with a strategy similar to the proven HVDC classic. Therefore it was concluded that when HVDC is equipped with the latest technology of MMC Full Bridge, it can be regarded as the optimum solution for point-to-point DC transmissions and radial systems.

Upgrading of HVAC transmission lines to HVDC lines to allow for higher power transfer capabilities is an interesting and well established research subject, with previous and ongoing research continuing to discover new and improved methods of optimally upgrading and converting HVAC lines into HVDC schemes [55-60]. Using a case study of South Africa's electric network, Naidoo et.al [57] presents an investigation into the upgrading of the existing HVAC power transmission circuits of South Africa's MTS, for higher power transfer capabilities, using HVDC. The proposed method uses one phase of the AC conventional line as the positive pole, another phase as the negative pole and the remaining third phase to be periodically swapped between positive and negative poles. This HVDC line configuration yields almost 2.5 times the power transfer capability of the conventional HVAC line. From this research it was found that for HVAC lines where the thermal capacity is close to surge impedance loading, no additional benefits would arise from converting them to HVDC lines. Similarly, for those lines that have higher capabilities for surge impedance loading but of small bundle configuration, the employment of FACTS technology would be more cost effective. For those circuits having greater conductor bundle configurations, the gap between thermal capacity and surge impedance loading is the largest and in these cases, the upgrade of HVAC lines to HVDC would have the most benefits. It was therefore concluded that it is feasible to convert an existing HVAC line to a HVDC line that has a higher power transfer capability compared to that of the HVAC line being converted.

Investigating the impacts of HVDC schemes on machine rotor angle transient stability is the main objective of this research. From the literature reviewed thus far, the main observations made are summarized as follows:

- The fundamental principle used for improvement of machine rotor angle transient stability of a network by making use of a HVDC scheme, is by using the HVDC scheme to modulate the DC power transferred during the fault and transient periods, thereby allowing the DC power to have a positive contribution to the system synchronizing torque applied to the generators and thus preventing the generators from going out of step.
- HVDC schemes in parallel to HVAC lines may have a negative impact on the system synchronising torque, therefore increasing the risk of system instability, if slow and outdated ineffective methods of converter DC power control are used. Modern, fast, state of the art control techniques that make use of very good measurement and communication systems are therefore required to allow the HVDC scheme to effectively and optimally contribute large amounts of system synchronizing and damping torque. For this reason, compared to LCC-HVCD, VSC-HVDC schemes are expected to be more effective in improving the system transient stability.
- Some researchers made use of the rate of power oscillations and rotor angle damping as the criteria and measure of machine transient rotor angle stability, rather than using the more accurate and well established method of analysing the duration of the CCT, as a measure of machine rotor angle transient stability.
- It was observed that most of the investigations done on this subject were carried out on small simplified test networks (i.e. single machine infinite bus system, two machine infinite bus system, four machine two area system, CIGRE 7-machine system and the P.M. Anderson 9-bus system). Very few studies were carried out on network models of existing power grids. This is an indication that due to the iterative and time consuming process of carrying out transient stability studies, carrying out these studies on large multi-machine systems of existing power grids can be a challenging task that requires a very good research methodology in order to yield realistic and accurate results.

- It was further observed that not much emphasis was placed on the optimal location, network configuration and operation scenario of an HVDC scheme in the power grid for system stability enhancement.
- Considering the fact that each power system is unique in structure and system operation conditions. Many of the researchers concur that the effectiveness of any proposed power transmission and control scheme for network stability improvement largely depends on the structure and pre-fault conditions of the network on which the scheme is being applied to.

In this research, due to its higher accuracy compared to the energy function method, the classical time-domain numerical integration method will be used to assess the transient stability of the machines.

In this study, the HVDC scheme will be used to improve the system synchronizing torque by making use of its temporary overload capability and its ability of fast modulation of DC power flowing through it during the fault and post-fault periods. This may be achieved by making use of a robust control system that detects a change in the AC system conditions and then uses that change as a control signal to adequately adjust the transient state DC power and thus preventing the system generators from going out of step.

Based on the above mentioned observations made from the literature reviewed, it is planned that in this research, an improved methodology of assessing transient rotor angle stability of a large multi-machine network will be used to carry out the investigation. The methodology includes a detailed procedure of identifying the critical machines in the network, determining the CCT of the network and assessing the obtained CCT against the grid code requirements of that particular network.

While acknowledging the fact the HVDC transmission is usually warranted by new large scale power generation projects, this research further aims at complementing the existing knowledge of the optimal location at which an HVDC scheme should be placed in a large multi-machine power grid for system transient rotor angle stability improvement. This includes determining the most effective HVAC-HVDC network topologies. Examples of possible network configurations and scenarios to be studied are: Placing an HVDC scheme in parallel to existing HVAC lines, converting/replacing an existing HVAC line into a HVDC scheme, analyzing the impact of the HVDC line

length on the machine transient rotor angle stability, analyzing the impact of the magnitude of the steady state power transmitted via the DC link on the system transient rotor angle stability.

It should be noted that this research does not attempt to enhance converter control theory or to develop a new HVDC converter control method, but rather it makes use of existing converter controller models to investigate the possible impacts that an HVDC scheme may have on the transient rotor angle and busbar voltage stability of a large multi-machine network such as that of Eskom.

CHAPTER 3: RESEARCH METHODOLOGY

3.1 Research Instruments

DIgSILENT's PowerFactory software tool was used to carry out network modelling and simulations for this research project. PowerFactory provides two flexible and powerful simulation tool bars that are used for power system stability analysis and electromagnetic transient simulations. These are the high precision time-domain RMS and EMT simulation tool bars.

3.2 Research Procedure

Due to numerous repetitions of various steps in the power systems transient stability problem solving process, it can be said that this process resembles an iterative design procedure. The main activities that were undertaken to carry out this research are:

- Study organization
- Time domain simulations and outputs
- Results analysis
- Specification of new test cases, operation scenarios and remedial measures

In solving the power system transient stability problem, the main activities as well as a number of other steps which are required to accurately determine the stability level of the power system have to be repeated until satisfactory results have been obtained. In this research the four main activities for stability analysis and assessment have been implemented as explained in the following sub-sections.

3.2.1 Study Organization

This activity sets out to organise and manage the entire process of carrying out the transient stability study. The steps taken under this activity are as follows:

- A comprehensive literature review was carried out to get broader knowledge and clear understanding of the transient stability subject, the development of HVDC technologies and implementation and principles of operation of different HVDC control schemes. A review of literature was carried out on previous works done by

other researchers on the subject of investigating the impacts of HVDC transmission schemes on the power system stability.

- Based on information from the reviewed literature and after various consultations with industry experts (Eskom), a focus area was identified and the project research scope was identified.
- After clearly defining the research scope and focus area, the next step was to identify the system conditions and contingencies that are considered to be critical in terms of power system transient stability.
- The power system element models and controller models suitable for carrying out this research were identified and tuned to suit the network conditions.

The main deliverable of the study organization activity is the case list of pre-determined critical system conditions. These critical conditions were further analysed using time-domain software simulations. The critical case list serves as a guide in carrying out the research. Some of the power system conditions included in the critical case list are: the system power generation level, system loading level, system reactive power compensation, generator controls, load models, fault types, fault location, fault duration, fault impedance and the switching events.

3.2.2 Time-Domain Simulations and Outputs

Under this activity, time-domain simulations were carried out on the network using DIgSILENT PowerFactory software to analyse the system critical conditions and determine the power system stability level. The DIgSILENT PowerFactory RMS tool bar makes use of the time-domain numerical integration methods integrated into it to solve the load flow solution of the network and asses the transient rotor angle stability of the network generators. The steps taken to carry out this activity are as follows:

- Define the variables to be analysed.
- Run a load flow to determine the system's pre-disturbance conditions.
- Determine the lines and generators with the largest impact of system stability when tripped.
- Implement a disturbance in the system at the most critical location.
- Run a simulation to carry out the transient state analysis of the network
- The results obtained from the simulation are displayed either in graphical and/or tabular form.

- For graphical presentation of the results, and for good comparison, various types of plots are generated from the obtained results. These plots included plotting an individual variable against time, plotting multiple variables against time on the same graph and cross plotting of variables.

3.2.3 Analysis of Results

The following steps were taken to analyse the obtained results:

- From the obtained graphs, observe the behaviour of variables of interest to determine whether the machine losses synchronism or not
- To determine the critical fault clearing time of the machine, change the fault duration (increase or decrease) until the machine goes out of step
- Assess the obtained CCT against South Africa's grid code requirements
- Compare obtained CCT with CCT obtained for other operation scenarios
- Draw a conclusion on the transient stability level of the network

3.2.4 Specifying new Test Cases and Operation Scenarios

After the CCT has been determined for a particular scenario, the network configuration is changed to create a new operation scenario. This is done by taking some elements in the network out of service or integrating new elements into the network. This is done without changing the fault location and fault conditions, except for the fault duration. The CCT of the generators, under the new system operation conditions is then determined and compared to the CCT obtained for other operation scenarios. The details of the different study cases, operation scenarios and remedial measures are given in section 3.3.

3.3 Test Networks

Three networks were used to carry out this research. A two machine infinite busbar network (test network 1), a30 machine 24 busbar network (test network 2), and Eskom's MTS network (test network 3). The equipment ratings and parameters of the network element models are presented in appendix A.

3.3.1 Test Network 1

Network 1 consists of two synchronous generators connected by two long (350 km) HVAC transmission lines to an external grid that represents an infinite bus relative to the synchronous machines. This network was used to test, configure and tune the

settings of the HVDC schemes in order to allow the HVDC switching devices (valves) to operate and to allow the HVDC controllers to be initialised before a transient state simulation could be performed. The network was also used to determine the network conditions under which the HVDC schemes operate most effectively and to observe how the HVDC schemes affect the transient stability of the machines in the small power system.

3.3.2 Test Network 2

Network 2 consists of 30 synchronous generators and 24 busbars. The machines are grouped into four main areas and these areas are interconnected by long HVAC transmission lines. This network was used to test the project research methodology and to determine the transient rotor angle stability of the most critical (weak) machine in a medium sized multi-machine power system, as well as to observe how the integration of an HVDC scheme in this network affects the transient stability of the critical machine.

3.3.3 Test Network 3

Network 3 is the MTS network of the South African power grid. Network 3's schematic diagram is shown in appendix C. Please note that not all the stations are visible in the schematic diagram as some stations were modelled on separate grids. The MTS network includes all the major power stations in South Africa, the main transmission lines and substations with voltage ratings of 275 kV and above. A detailed model of Eskom's MTS network was used as the base study case for this project. The Northern power grid, which is mainly in the Limpopo and North-West provinces of South Africa, was chosen as the focus area on which to carry out the transient stability analysis of the network. The focus area consists of existing, under construction and planned power stations, substations and transmission lines. There are two existing power stations (Matimba and Medupi) and two planned power stations (Coal 2 and Coal3) in the Northern grid. Matimba power station is located in the north eastern part of Limpopo province. Adjacent to Matimba power station is Medupi power station whose construction commenced in 2012 and is expected to be completed in 2017. Synchronisation of the first generating unit (unit 6) of Medupi power station onto the grid was done on 15th February 2015. It is planned that two other coal fired power stations to be funded by prospective independent power producers (IPP's), under the project names Coal 2 and Coal 3, will be constructed in the vicinity of Medupi and Matimba power stations, and

will be commissioned in the near future. It is planned that a LCC-HVDC scheme that consists of a rectifier station, a single HVDC transmission line and two split inverters (multi-terminal) will be used to help evacuate bulk power from the generation sources to the load centre. The rectifier station is to be located near Masa substation which is in Lephalale. One inverter station will be located near Etna substation while the other inverter station will be located near Jupiter substation. The project is known as the Limpopo-West HVDC scheme. The initial specifications of the proposed LCC-HVDC scheme, which are subject to change, depending on the final outcomes of the feasibility and geo-technical studies, are as follows:

- Two bipolar schemes utilising a single HVDC line (+&- poles)
- Proposed rectifiers are to be located at Masa substation
- Proposed two inverter injection sites (i.e. split inverters/multi-terminal)
- Inverter stations are to be located near Jupiter and Etna substations
- Proposed 4000 MW per bi-pole (i.e. 2000 MW per pole)
- ± 600kV or 500 kV nominal system operating voltage, line length is 600 km

It is important to note that the HVDC scheme is designed to use the earth as the return path of the current. The location of the HVDC converters therefore largely depends on the site that is most suitable for installation of earth electrodes (EE). The sites identified as most suitable for earth electrodes is the vicinity of Masa substation in Lephalale, for the rectifier station and the vicinities of Etna and Jupiter substations in the Gauteng area, for the inverter stations. The HVDC scheme is intended to be routed via Selemo substation, near Pochefstroom. In this research, an assumption is made that the transmission station at Medupi substation is also suitable for installation of earth electrodes, and therefore, a rectifier station can be built in that vicinity. This assumption is made to make it possible to analyse various other network configuration scenarios. It is expected that the proposed scheme will operate at full load in the year 2030. This research is being carried out on the envisioned 2021 electrical grid, so it is be assumed that only half of the expected power will be transmitted via the HVDC scheme during 2021 i.e. 2000 MW per bi-pole. For simplicity and for the purpose of this research, the LCC-HVDC schemes will be modelled as two separate bipolar schemes delivering power from Masa substation to Enta and Jupiter substations, thus avoiding the multi-terminal configuration. The overview diagram of Network 3 is shown in figures 5.1 and C1. The overview diagram of the proposed HVDC scheme is shown in figure C2.

CHAPTER 4: HVDC SCHEME MODELS AND TESTING

4.1 LCC-HVDC Model

4.1.1 Schematic Diagram

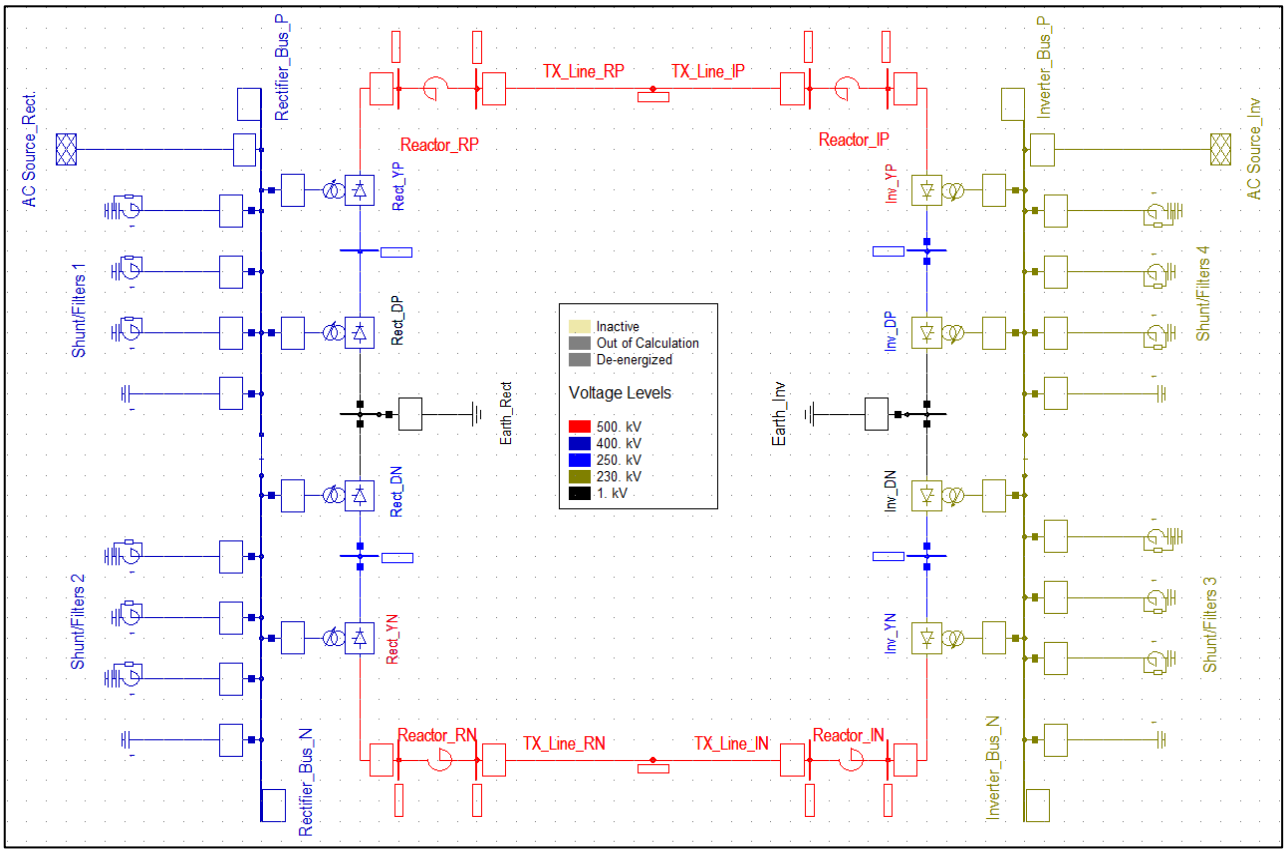

Figure 4.1: LCC-HVDC Model Schematic Diagram

The schematic diagram of the LCC-HVDC scheme model used in this project is shown in figure 4.1. The HVDC scheme is based on the CIGRE HVDC benchmark model [61, 62], and it is implemented in the DIgSILENT PowerFactory environment. From figure 4.1 it can be observed that the modelled LCC-HVDC scheme has a point-to-point, bipolar with floating earth configuration. Each pole has two units of six pulse thyristor switched rectifiers and two units of six pulse thyristor switched inverters, resulting into twelve pulse converters. The AC power sources of the converters are modelled as a 400 kV external grid supplying the rectifier side and a 230 kV external grid at the inverter side absorbing the transmitted power. A summary of the ratings of the main elements of the HVDC scheme is given in table 4.1. The element ratings can be changed to suit the network in which the HVDC scheme is being utilized.

Table 4.1: LCC-HVDC Scheme Element Ratings

Converters			
Rectifier		**Inverter**	
Rated AC voltage	375 kV	Rated AC voltage	210 kV
Rated DC voltage	250 kV	Rated DC voltage	250 kV
Rated DC current	2 kA	Rated DC current	2 kA
Rated power	600 MW	Rated power	600 MW
Control mode	Current	Control mode	voltage
Current set point	2 kA	Voltage set point	-1 p.u.
Firing angle	15 degrees	Extinction angle	20 degrees
Rectifier Transformer		**Inverter Transformer**	
Min. turns ratio	0.7	Min. turns ratio	0.9
Max. turns ratio	1.4	Max. turns ratio	1.3
Tap control mode	Alpha-control	Tap control mode	Gamma-control
DC Line			
Rated voltage		500 kV	
Rated current		2.5 kA	
Length		600 km	
Smoothing reactor		650 mH	

4.1.2 LCC-HVDC Controller Models

User defined block definitions of the rectifier and inverter controllers were used to build the composite model of the HVDC scheme. The user defined block definitions are made up of reference blocks and a control algorithm code written in DIgSILENT Simulation Language (DSL). The user defined block definitions were then converted into DSL models which are also referred to as common models in PowerFactory. The common models are used as building blocks that fill the different slots that make up the composite HVDC model.

For the LCC-HVDC scheme shown in figure 4.1, the rectifier and inverter uses the same controller model. The negative pole and positive pole of the HVDC scheme uses the same HVDC composite model, with the only difference being a change of polarity (+ or -) made to the pole parameter of the voltage dependant current order limiter (VDCL) in order to distinguish between the two poles. The common (DSL) models for

the positive pole are shown in figure 4.2. The letter P at the end of the name of each common model denotes the positive pole, the letter R denotes rectifier and the letter I denotes inverter. The composite model for a single pole of the HVDC scheme is shown in figure 4.3.

	Name	Type	Out of Service	Object modified	Object modified by
▶ dsl	Inverter_Ctrl_P	LCC-HVDC Controller	☐	2015/06/11 12:1	user
dsl	Min_Gamma_I_P	Min	☐	2015/06/11 12:0	user
dsl	Min_Gamma_R_P	Min	☐	2015/06/11 04:0	user
dsl	Power_Ctrl_P	HVDC Power Controll	☐	2015/06/11 11:3	user
dsl	Rectifier_Ctrl_P	LCC-HVDC Controller	☐	2015/09/21 09:5	user
dsl	VDCL_IP	VDCOL	☐	2015/06/11 12:2	user
dsl	VDCL_RP	VDCOL	☐	2015/06/11 12:2	user
PLL	PLL_I_P		☐	2015/06/11 12:4	user
PLL	PLL_R_P		☐	2015/06/11 12:4	user

Figure 4.2: Positive Pole Common Models

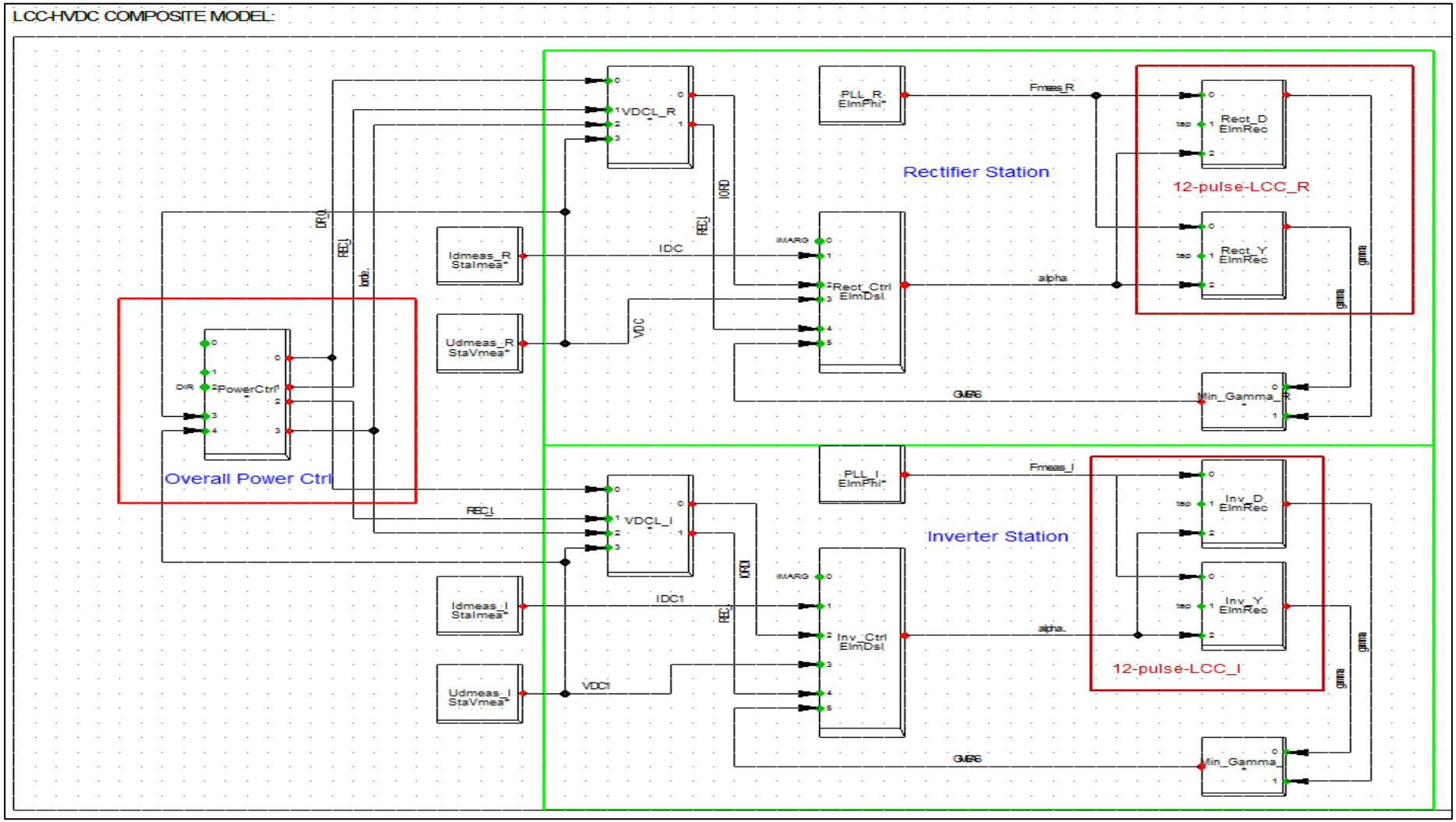

Figure 4.3: LCC-HVDC Composite Model

From figure 4.3 it can be observed that the HVDC composite model is made up several slots. It can also be seen that the rectifier station and the inverter stations are made up of the same types of slots. The function of each slot in the composite model is explained briefly as follows:

Rect/Inv slot:

The rectifier and inverter slots are used to insert the rectifier and inverter elements into the composite model.

Rect_Ctrl/Inv_Ctrl slot:

The rectifier and inverter controllers are used to regulate the DC current and voltage. This is done by controlling the firing and extinction angles to the pre-set values, thereby controlling the winding ratios of the rectifier and inverter commutation transformers. By regulating the DC current and voltage of the line, the converter controllers allow for a constant value of the desired active power to be transmitted though the line.

PLL_R/PLL_I slot:

The phase lock loops (PLL) are used to measure the frequency of the voltage on the AC busbars, both on the rectifier and inverter sides of the HVDC scheme.

VDCL_R/VDCL_I slot:

The voltage dependant current order limiters (VDCL) are used to change the magnitude of the DC current order when there is a significant drop in the DC line voltage, which may be caused by a fault in the AC or DC system. The current order is usually reduced to a value equal to the current order minus the margin current.

Idmeas_R/Udmeas_R slot:

The current and voltage measurement elements are used to take measurements of the DC line current and voltage at the rectifier and inverter sides of the line.

Overall Power_Ctrl slot:

The power controller is used to regulate the amount of power that flows through the DC line by controlling the interaction between the HVDC scheme and the AC grid.

4.1.3 LCC-HVDC Model Response Test

In order to determine whether the modelled LCC-HVDC scheme is stable in its operation, it is essential to observe the response of the HVDC scheme to a step change in its control parameters and to faults in the AC grid. The simulations were carried out using the time-domain electromagnetic transient (EMT) simulation tool bar in PowerFactory software. The graphs present the obtained results of signal and variable responses of the positive pole controller models only. Since the positive and negative poles use the same controller models, it is assumed that the negative pole signals and variables will have a similar response. The plotted rectifier and inverter controller signals can be traced and seen in the HVDC composite model shown in figure 4.3.

4.1.3.1 Step Change Response

A parameter event for a step change in the reference DC voltage of the inverter controller was defined. The reference DC voltage changed from the initially defined value of 1.15 p.u. to a new value of 0.98 p.u., at 1 second. The response of the measured DC voltage to the step change of the reference voltage is shown in figure 4.4.

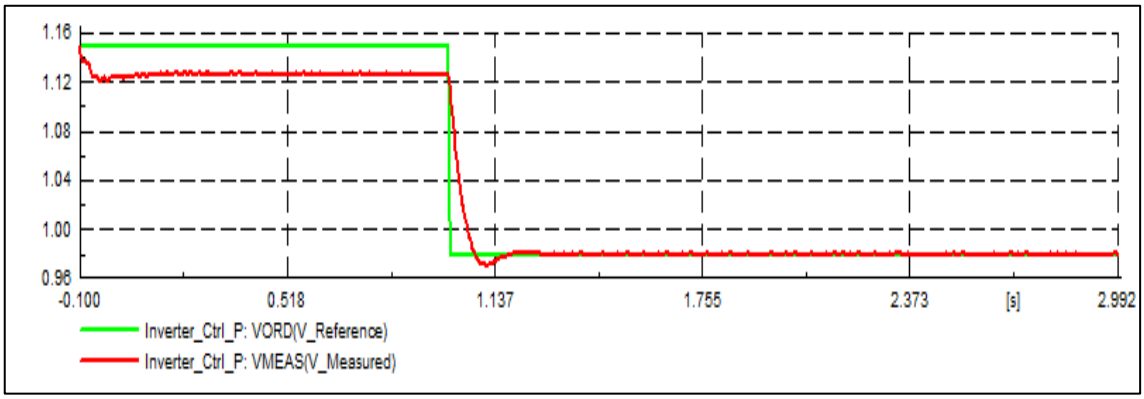

Figure 4.4: Measured DC Voltage Response to DC Voltage Reference Step Change

Figure 4.4 illustrates the step change response test of the HVDC scheme. Step change response testing is a fundamental method used for the verification of the stability of a system. From figure 4.4 it can be seen that when a step change is applied to the DC reference voltage, the measured DC voltage follows the response of the reference voltage and it is regulated to the new reference voltage value. This is an indication of stable operation of the HVDC scheme controllers.

4.1.3.2 Response to Fault on Rectifier Station AC Busbar

To further observe the operation of the controller models and to observe how the reference parameters regulate the measured variables, a three-phase fault, with a fault impedance of 50 ohms and fault duration of 500 ms was simulated on the AC busbar on the rectifier side of the HVDC scheme. The obtained results are presented in figures 4.5 to 4.9.

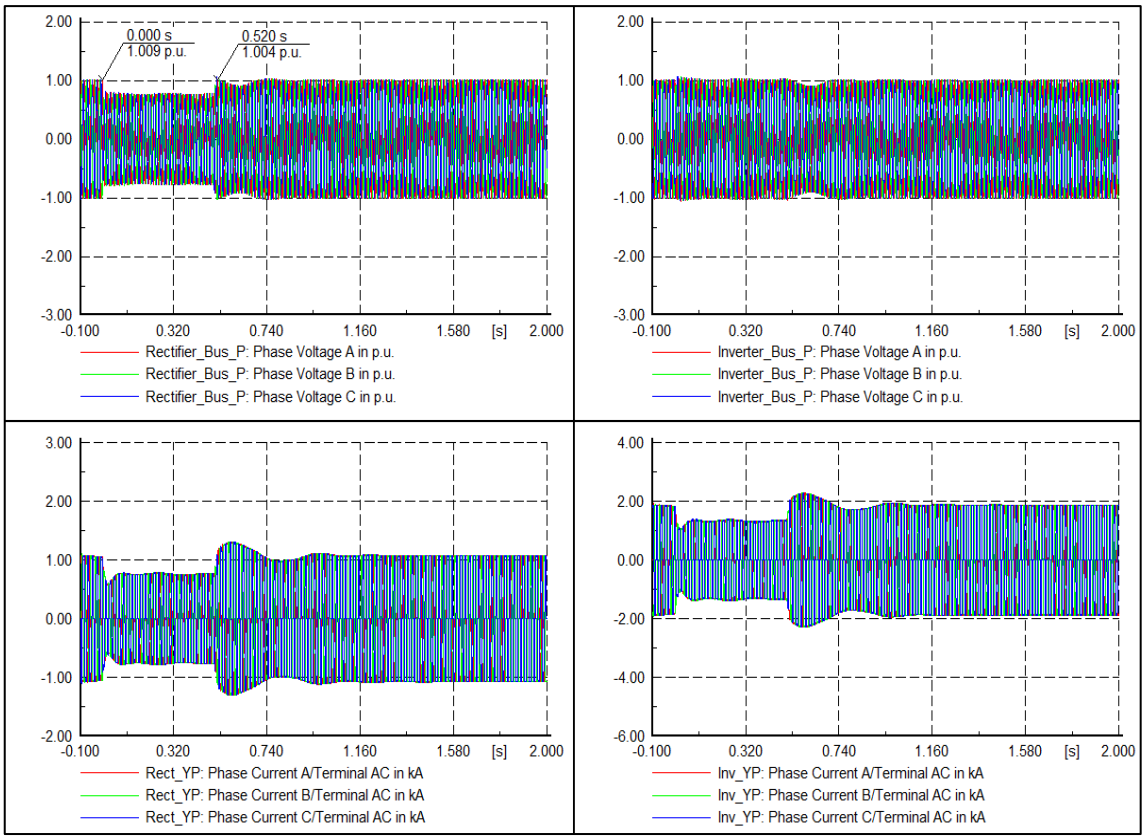

Figure 4.5: AC Voltage and Current Waveforms

Figure 4.5 presents the response of the rectifier and inverter AC busbars phase voltages and the converter AC currents, for a fault at the rectifier AC busbar. It can be observed that before the fault, the AC voltages and currents maintain their steady state values, during the fault there is a small decrease in the voltage and current magnitudes, except for the inverter busbar voltage that maintains its steady state voltage magnitude, after the fault has been successfully cleared, the AC voltages and currents return to their steady state values. No commutation failure response is observed in the current waveforms.

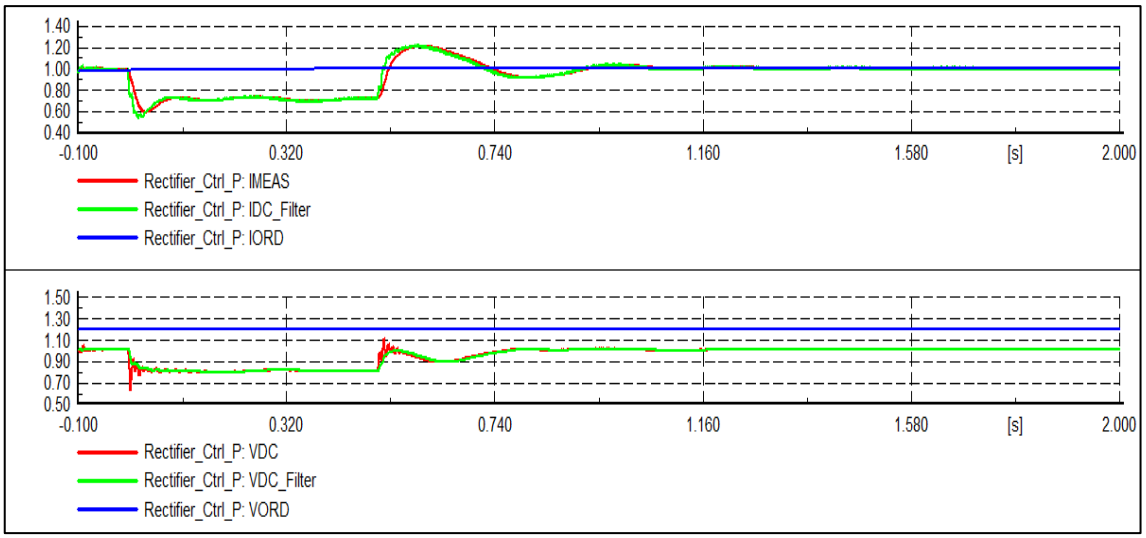

Figure 4.6: Rectifier DC Current and Voltage Control

Figure 4.6 shows the response of the DC current and voltage measured at the rectifier side DC busbar. It can be seen that the filtered voltage and current curves are smoother than the measured curves. It can also be observed that the voltages and currents are regulated back to their steady state values by the reference voltages and currents, after successful clearance of the fault.

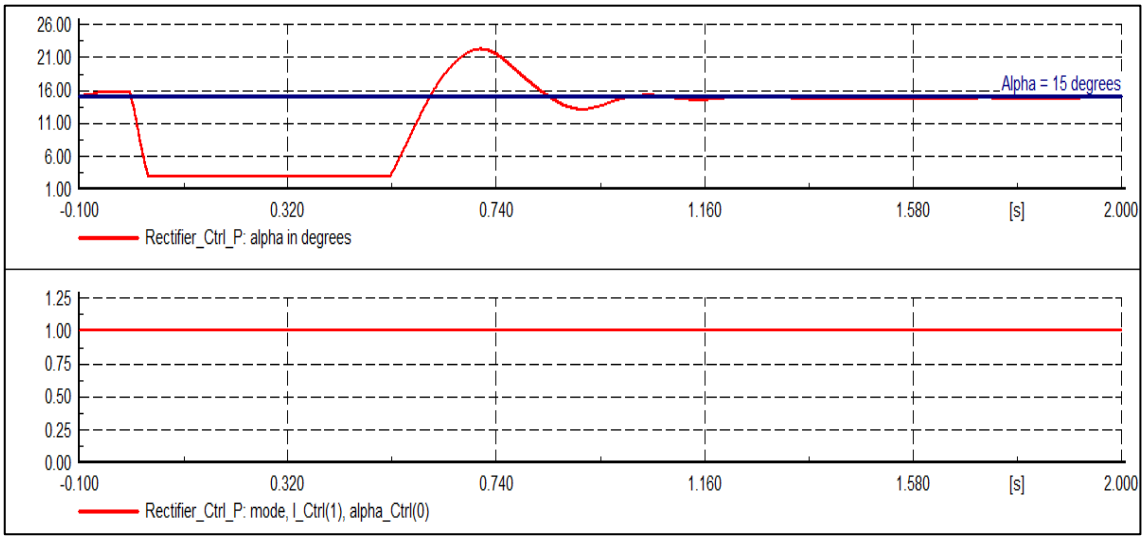

Figure 4.7: Rectifier Firing Angle Control and Mode Selection

From figure 4.7 it can be seen that the rectifier firing angle is regulated back to its nominal value of 15 degrees after the fault has been cleared. It can further be observed that for a fault on the rectifier side AC busbar, the rectifier remains in current control mode before, during and post-fault.

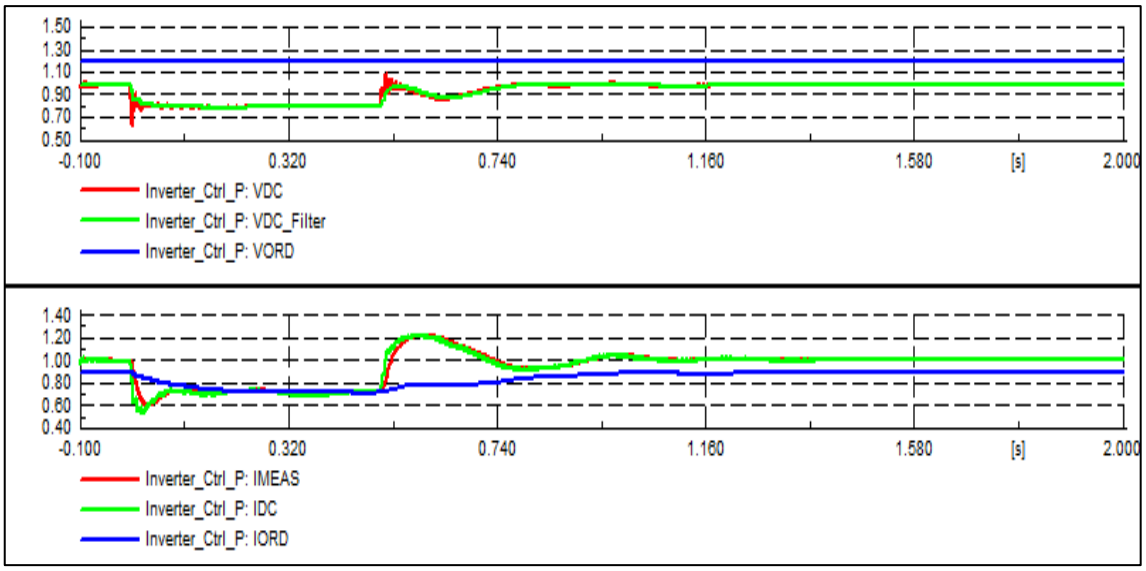

Figure 4.8: Inverter DC Current and Voltage Control

The response of the DC voltage and current measured at the inverter DC busbar is shown in figure 4.8. It can be observed that the inverter controller successfully regulates the DC line current and voltage after the fault has been cleared.

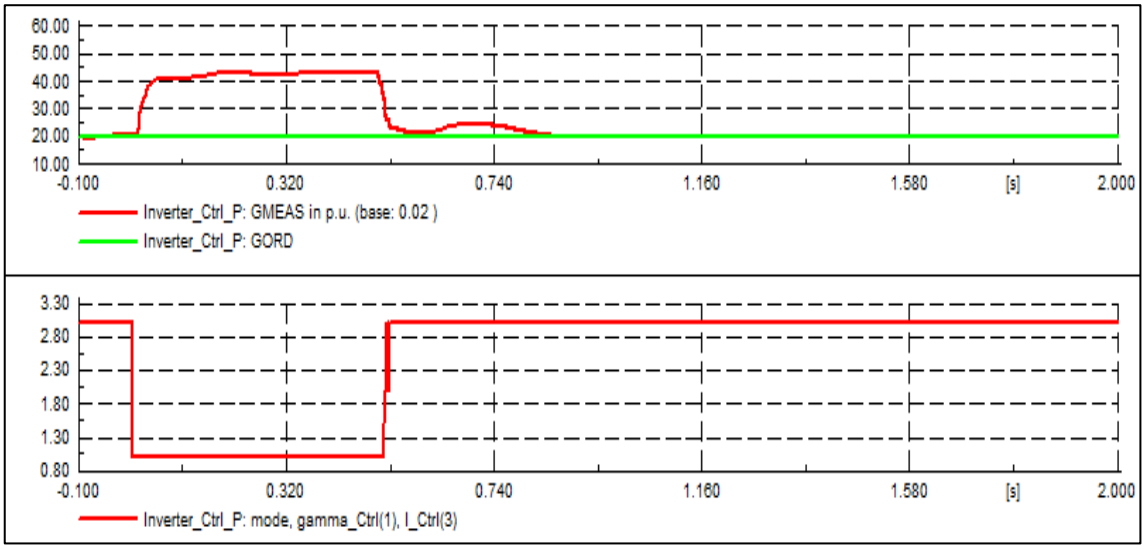

Figure 4.9: Inverter Extinction Angle Control and Mode Selection

From figure 4.9 it can be seen that the inverter extinction angle is successfully regulated back to its nominal value of 20 degrees after the fault has been cleared. Looking at the inverter control mode selection graph in figure 4.9, it can be seen that before the fault, the inverter is in current control mode, which allows for the inverter side voltage to be regulated to its pre-disturbance value, during the fault, the inverter switches to extinction angle control mode and after successful clearance of the fault, the inverter switches back to current control mode as expected.

4.1.3.3 Response to Fault on Inverter Station AC Busbar

To observe the operation of the converter controllers and the response of the controlled variables to a fault on the inverter AC busbar, a three-phase fault, with a fault impedance of 50 ohms and fault duration of 500 ms was simulated on the AC busbar on the inverter side of the HVDC scheme. The obtained results are presented in figures 4.10 to 4.14.

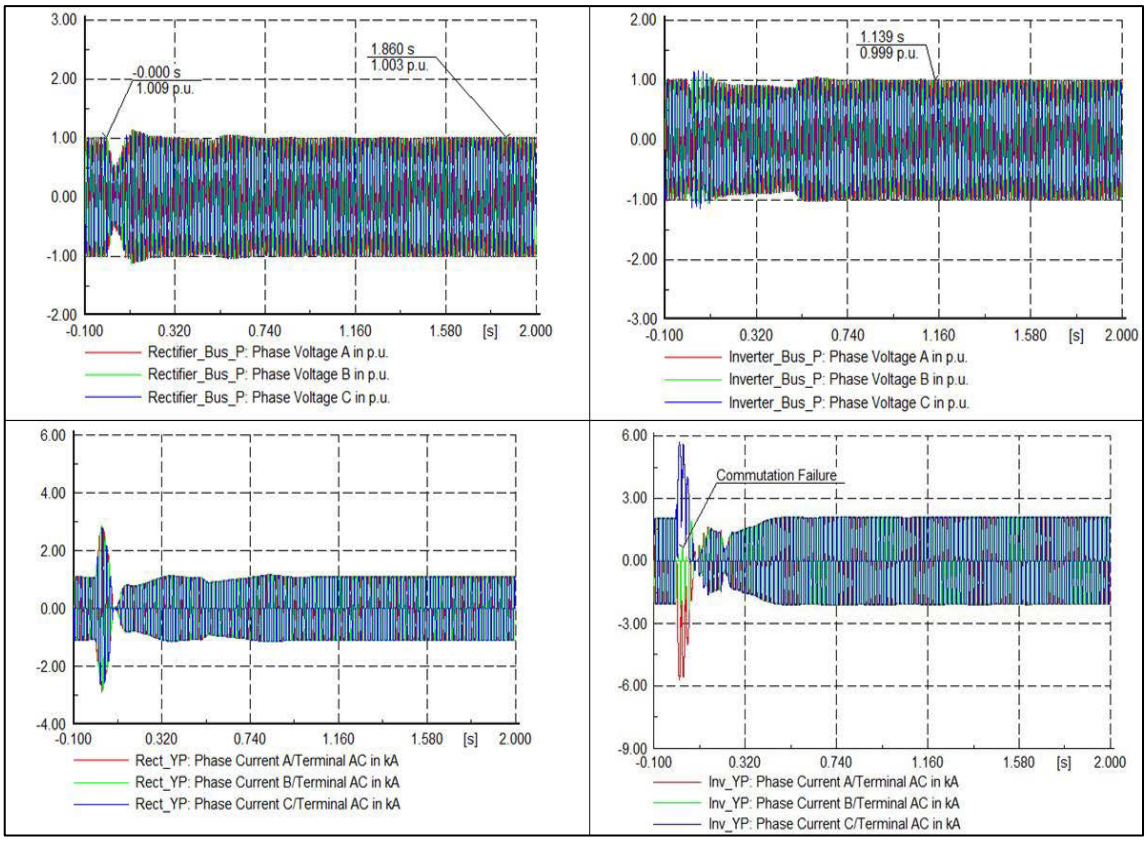

Figure 4.10: AC Voltage and Current Waveforms

Figure 4.10 presents the response of the AC busbar phase voltages and the converter AC currents, for a fault at the inverter station AC busbar. It can be seen that both the inverter and rectifier side voltages and currents are affected by this fault. The voltage and current values however return to their steady state magnitudes after the fault has been cleared, which is an indication of stable operation of the converters. From the graph showing the AC phase currents flowing through the inverter, it can be seen that the observed fault causes commutation failure at the inverter, which prevents the current from being transferred from one conducting valve to the other.

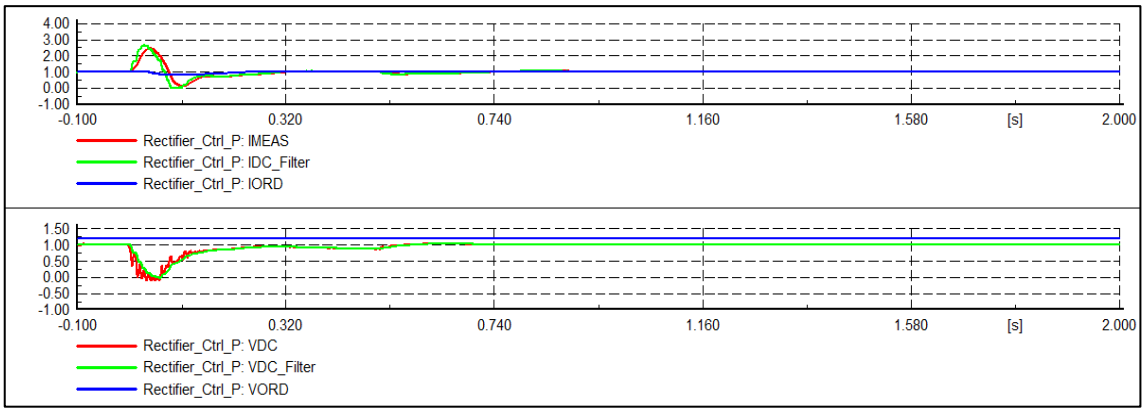

Figure 4.11: Rectifier DC Current and Voltage Control

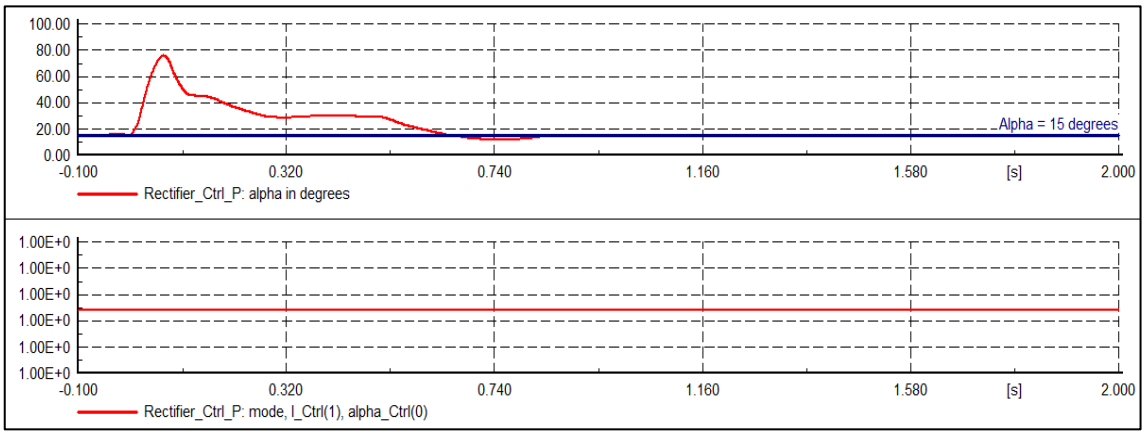

Figure 4.12: Rectifier Firing Angle Control and Mode Selection

Figures 4.11 and 4.12 show the response of the rectifier DC voltage and current, and the firing angle response to a three-phase fault on the inverter AC busbar. It can be seen that the rectifier voltage, current and the firing angle are successfully regulated to their pre-disturbance values, after the fault has been cleared. It can further be observed that the rectifier remains in current control mode for the entire duration of the simulation.

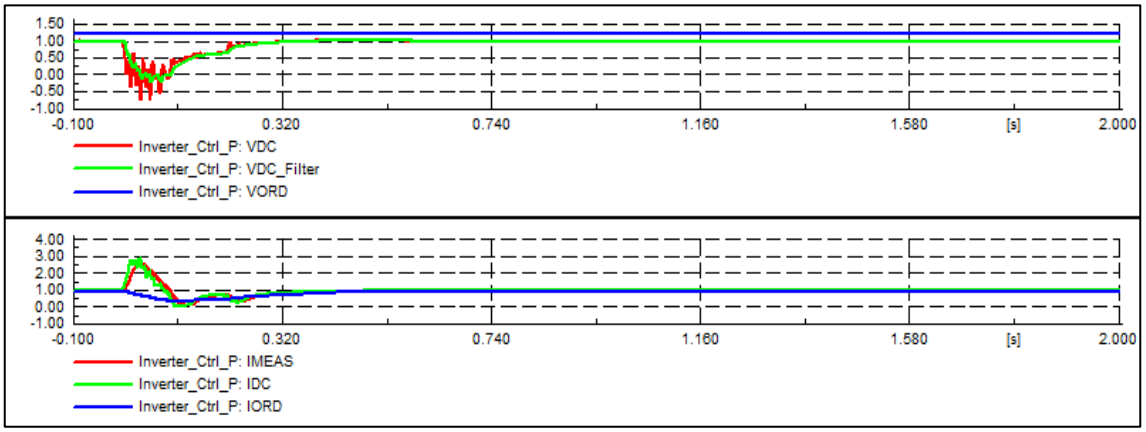

Figure 4.13: Inverter DC Voltage and Current Control

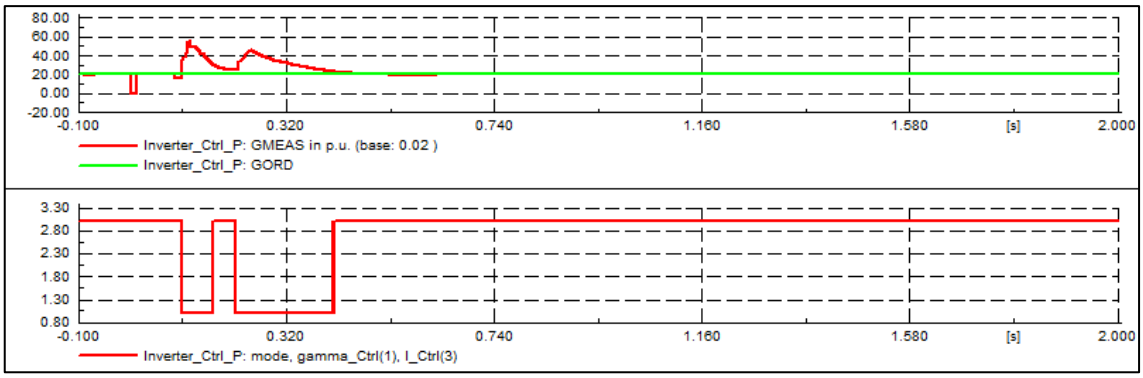

Figure 4.14: Inverter Extinction Angle and Mode Selection Control

Figures 4.13 and 4.14 show the response of the inverter DC voltage and current, the inverter extinction angle response, as well as the inverter control mode selection. It can be seen that the voltage, current and the extinction angle are successfully regulated back to their steady state values after the fault has been cleared successfully. From the mode selection graph it can be seen that, initially the inverter is in current control mode, during the fault the inverter switches to gamma control and then back to current control for a few milliseconds, after which it again switches back to gamma control, and then finally switches back to current control mode after the fault has been cleared. From the analysis done on the obtained results, it can be concluded that the LCC-HVDC scheme has been modelled correctly. The operation of the HVDC scheme is stable, the PLL, VDCL, rectifier controller and inverter controller models are operating correctly, as expected.

4.2 VSC-HVDC Model

The schematic diagram of the VSC-HVDC model used in this project is presented in figure 4.15. The converters of this VSC-HVDC scheme use controller models which were developed by DIgSILENT. From the diagram it can be observed that the scheme has a bi-polar configuration, with the converter on either side of the scheme controlling both the positive and negative poles. The VSC converters used in this HVDC model use IGBT based valves for switching. The ratings of the converters and the harmonic filters were configured in such a way that they suit the operation conditions of the network in which the HVDC scheme is to be implemented. Two transformers were used to transform the grid voltage to the rated AC voltage of the converters and vice-versa. A summary of the ratings, parameters and set points of the elements of the VSC-HVDC scheme is presented in table 4.2.

4.2.1 Schematic Diagram

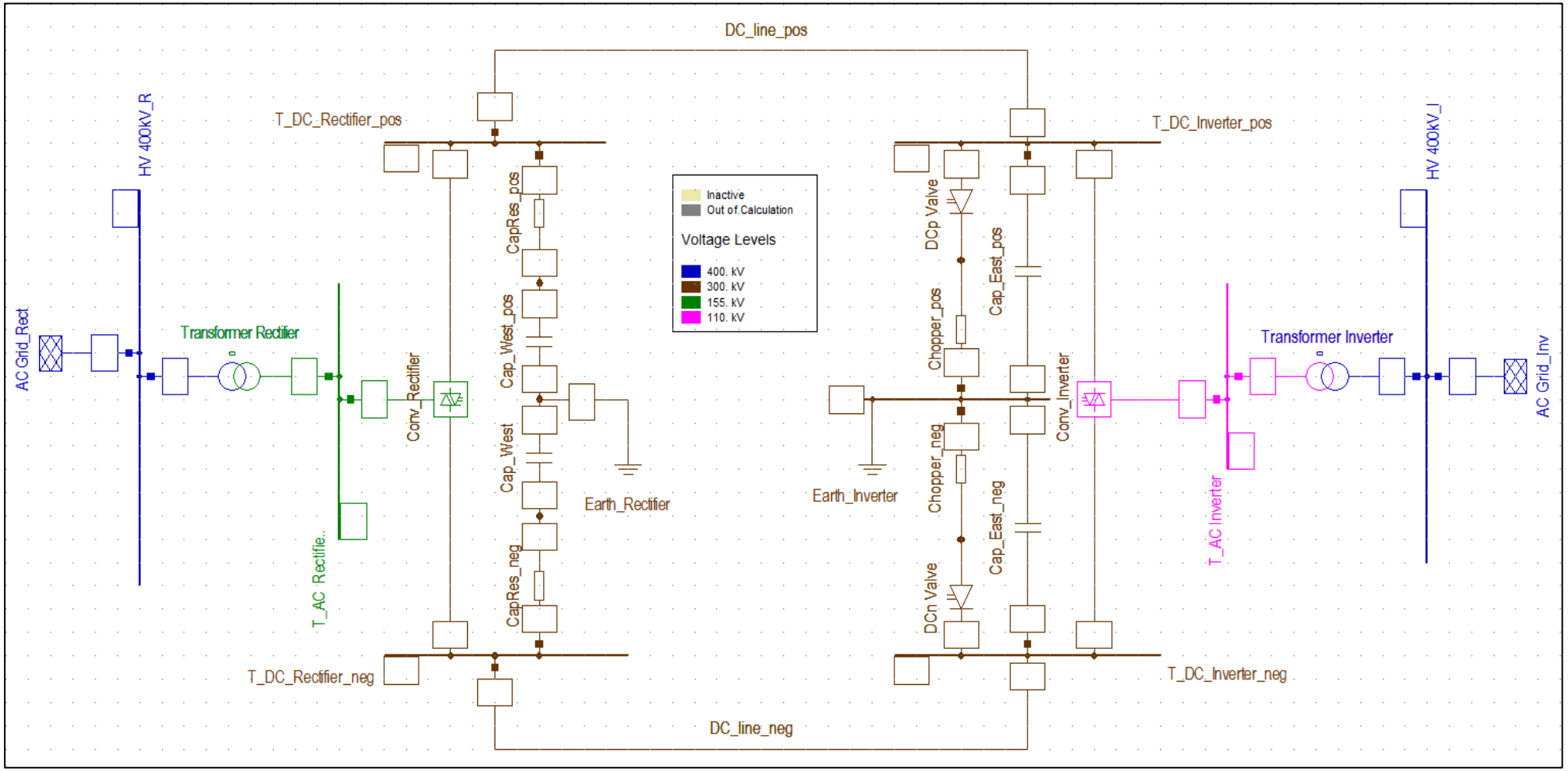

Figure 4.15: VSC-HVDC Model

Table 4.2: VSC-HVDC Scheme Element Ratings

Converters			
VSC-Rectifier		**VSC-Inverter**	
Rated AC voltage	155 kV	Rated AC voltage	110 kV
Rated DC voltage per pole	300 kV	Rated DC voltage per pole	300 kV
Rated power	900 MVA	Rated power	900 MVA
Control mode	P-Q	Control mode	DC voltage
Active Power set point per pole	300 MW	Voltage set point	-1 p.u.
Modulation	Sinusoidal PWM	Modulation	Sinusoidal PWM
DC Line			
Rated voltage		300 kV	
Rated current		1.3 kA	
Length		400 km	

4.2.2 VSC Controller Models

Unlike in the LCC-HVDC scheme, the controller model used for the rectifier slightly differs from the one used at the inverter of the VSC-HVDC scheme. The composite models of the rectifier and inverter controllers are shown in figures 4.16 and 4.17. The functions of the different slots are similar to those of the LCC-HVDC scheme, with the main difference being the operations and functions of the controllers.

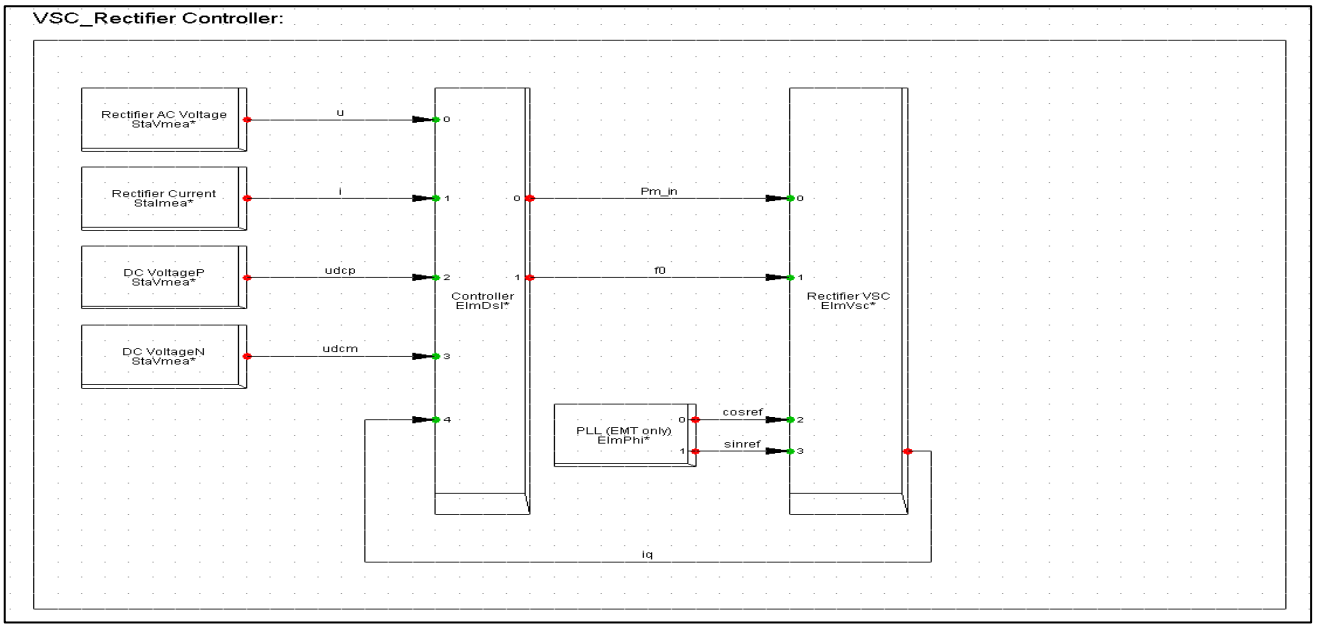

Figure 4.16: Rectifier Controller Composite Model

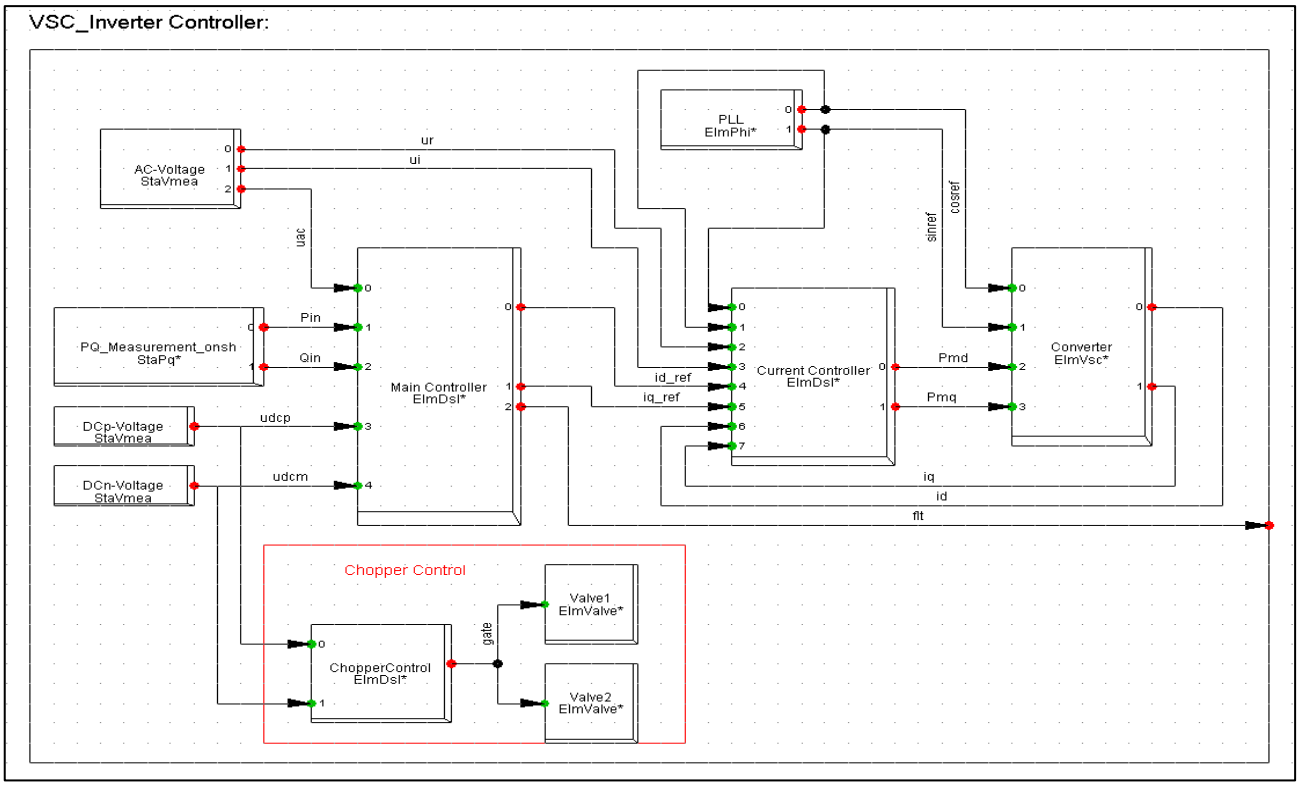

Figure 4.17: Inverter Controller Composite Model

4.2.3 VSC-HVDC Model Response Test

In order to verify the stability of the modelled VSC-HVDC scheme, various tests have been carried out on the HVDC scheme and the response of the variables and parameters of interest have been observed. Like with the LCC-HVDC scheme, the two tests that were carried out on the VSC-HVDC scheme are: the step change response test and the response to a fault in the AC grid. The obtained results are presented in figures 4.18 to 4.21.

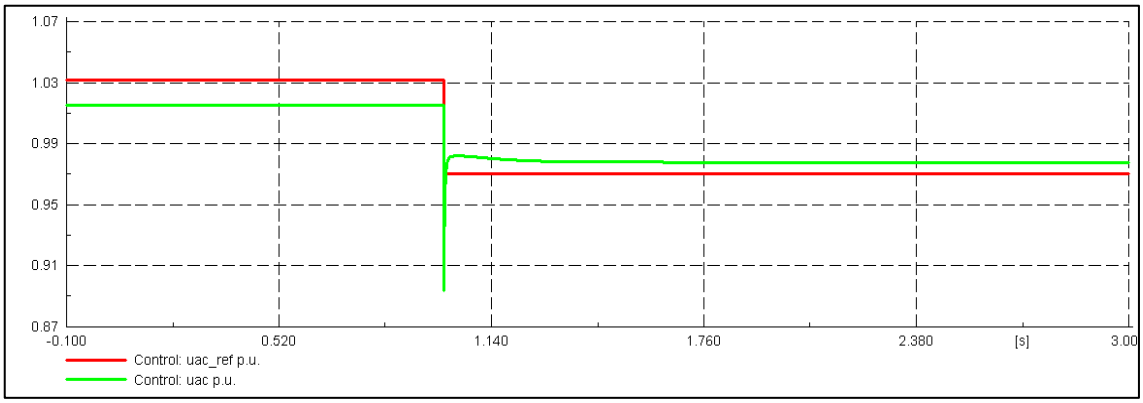

Figure 4.18: AC Reference Voltage Step Change Response

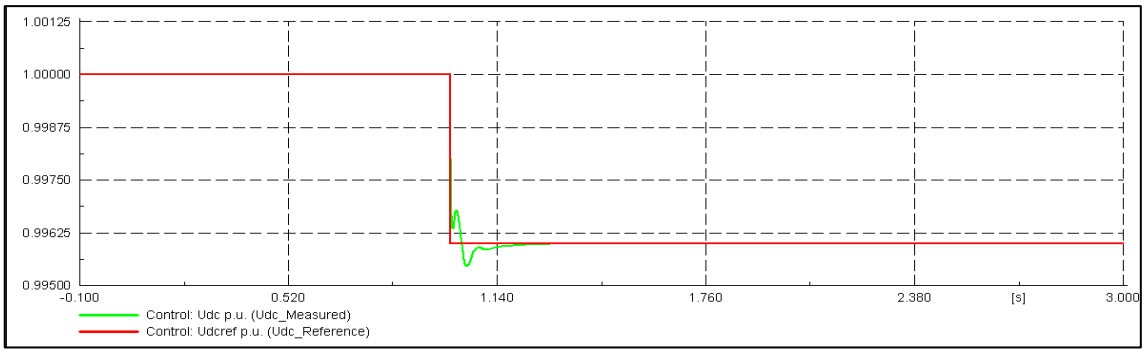

Figure 4.19: DC Reference Voltage Step Change Response

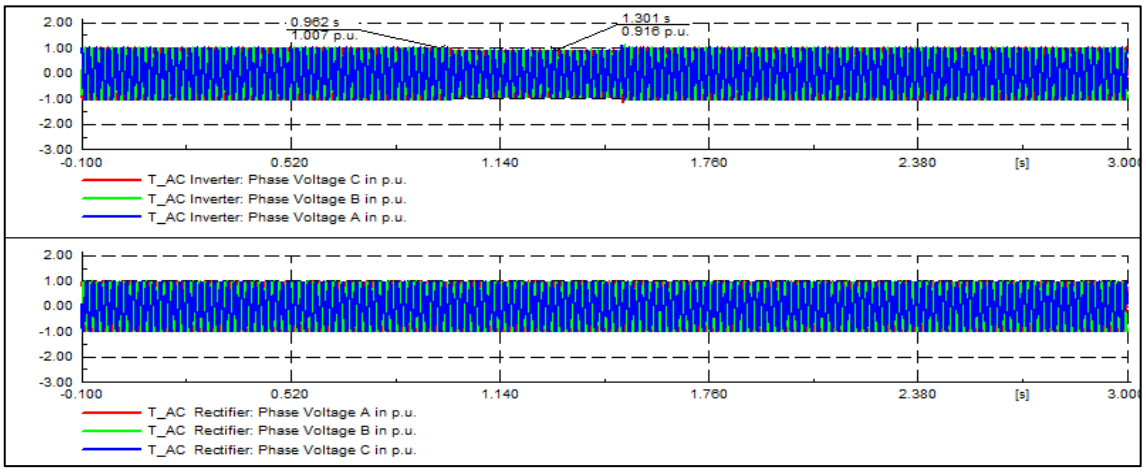

Figure 4.20: AC Busbar Voltage Response to Fault on Inverter Busbar

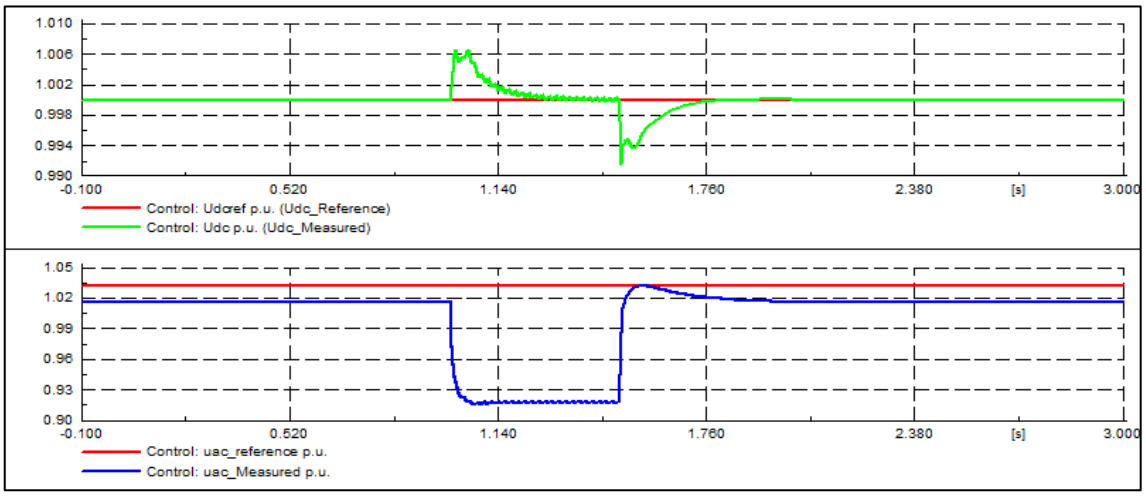

Figure 4.21: Inverter DC and AC Voltage Control

Figures 4.18 to 4.21 presents the results obtained for the step change response and AC grid fault tests done on the VSC-HVDC scheme. Two parameter events were simulated to instantly change the values of the AC and DC reference voltages from their pre-set

values to 0.97 p.u. at 1 second. A three-phase fault with a fault impedance of 10 ohms and fault duration of 500 ms was simulated on the inverter AC busbar. From figures 4.18 and 4.19 it can be observed that when the step change occurs, the measured AC and DC voltages follow the response of the reference voltages. The measured voltages are regulated to the new values of the reference voltages. From figure 4.20 it can be seen that the fault on the inverter AC busbar has a negligible impact on the AC voltage of the inverter busbar and no effect on the rectifier AC busbar voltage. Figure 4.21 shows how the measured AC and DC voltages respond to a fault on the inverter side AC busbar and how the reference AC and DC voltages regulate the measured values. It can be observed that before the fault, the measured DC voltage is equal to the reference DC voltage, during the fault, the DC reference remains constant and the measured voltage undergoes some oscillations. After the fault has been cleared successfully, the measured voltage is regulated back to its steady state value. From figure 4.21 it can be seen that the measured AC voltage follows a similar response, whereby after the fault has been cleared, the measured voltage is regulated back to its pre-disturbance value.

From the analysis done on the obtained results, it can be concluded that the VSC-HVDC scheme has been modelled correctly, the converter controllers are operating as expected, and the overall operation of the VSC-HVDC scheme is stable.

CHAPTER 5: NETWORKS 1 AND 2 ANALYSIS

5.1 Test Network 1

Network 1 is used to investigate the effects of an HVDC scheme in parallel with HVAC lines on transient rotor angle stability of the generators in a small AC grid. Network 1 consists of two synchronous generators connected to an external grid by two long HVAC transmission lines (two machine infinite busbar system). The external grid represents an infinite busbar relative to the synchronous machines. The equipment parameters, ratings and the composite model of the generator type used in this research is presented in appendix A.

5.1.1 Mathematical Analysis

The fundamental principle of using a parallel HVDC scheme to improve machine transient rotor angle stability was presented by Machida [30]. Transient rotor angle stability of an AC system can be improved by employing rapid control of the converters, for DC power modulation during the transient period, after the system has been subjected to a severe fault. The HVDC control system is required to have the ability to detect the AC system conditions during the transient period, and to make use of the AC voltage drop caused by a fault in the AC system to derive a change in the DC current control signal, and then add this control signal to the limited current reference of the converter. Alternatively, the control signal can be derived from the speed deviation signal of the generator using a controller (PI or PD). The control signal is then used to increase or decrease the converter DC reference current, and thus in turn controls the DC power flowing through the HVDC link during the transient period. The DC power is expected to return to its steady state value after successful power modulation. This helps with improving the system synchronizing torque. The schematic diagram of Network 1 is shown in figure 5.4 (scenario C). The simplified power-angle characteristics of the generators in the parallel AC-DC system of Network 1 is shown in figure 5.1. For simplicity of the analysis, the two parallel generators (G1 and G2) are assumed to be a single machine with an apparent power rating equal to the sum of the power ratings of the two machines.

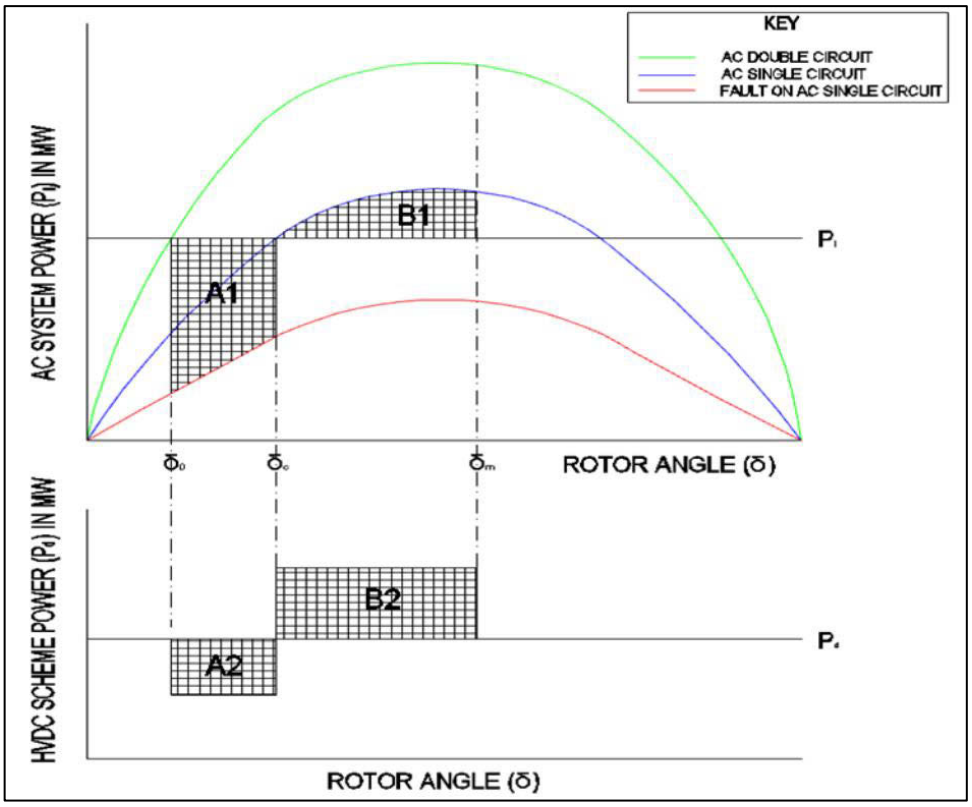

Figure 5.1: Simplified Power-Angle Characteristics of Network 1

The simulation results of the actual power-angle characteristics of the first swing of Gen1 for stable and unstable conditions are shown in figure 5.3. The analysis is done for a scenario where a sever three-phase short circuit occurs on one of the parallel AC lines (Line2) in Network 1. The meaning of each symbol is explained as follows:

δ_0 = Steady-state rotor angle

δ_c = Rotor angle when AC fault is cleared

δ_m = Maximum rotor angle at which the transient stability power limit is reached

P_M = Input mechanical power

P_i = AC system steady state power

P_d = HVDC scheme steady state power

P_i' = AC system transient power

P_g' = Generator transient power output

P_d' = DC power transferred via the HVDC link during the transient period

A_1 = Acceleration energy of the generator caused by the decrement of AC power transferred due to the fault

A_2 = Decrement of the DC steady state power P_d caused by the fault (causing generator acceleration)

B_1 = Retarding energy of the generator

B_2 = Increment of the DC power during and after the fault has been cleared (causing the generator to retard)

In order to ensure that the total acceleration area A_1+$A_2$is not larger than the total retarding area B_1+B_2 (A_1+$A_2 \leq B_1$+B_2), which would cause the generator to continue accelerating and go out of step, it is important that fast and robust control of the converters is employed to increase the DC power being transferred via the DC link during the transient period. This acts as a counter measure to the net acceleration energy absorbed by the generator during the fault, and therefore prevents the step out of the generator and thus improving transient rotor angle stability of the machine. The DC power is increased by B_2 as specified by equation (5-1).

$$B_2 = (A_1 + A_2) - B_1 \tag{5-1}$$

Taking all the pre-fault and transient state powers of the system into consideration, equation (5-1) can be re-written in integral form as:

$$\int_{\delta_c}^{\delta_m}(P'_d - P_d)d\delta = \int_{\delta_0}^{\delta_c}[(P_i - P'_i) + (P_d - P'_d)]\,d\delta - \int_{\delta_c}^{\delta_m}(P'_i - P_i)d\delta \tag{5-2}$$

During steady state, the system is at an equilibrium point of operation and ideally the input mechanical power is equal to the generator output power i.e. $P_M = P_g$. During the transient state the total generator output power is the sum of the transient AC power and the transient DC power, i.e. $P'_g = P'_d + P'_i$. Using these relationships, equation (5-2) can be re-written as:

$$\int_{\delta_c}^{\delta_m}(P'_d d\delta = \int_{\delta_0}^{\delta_m} P_M\, d\delta - \int_{\delta_0}^{\delta_c} P'_g d\delta + \int_{\delta_c}^{\delta_m} P'_i d\delta \tag{5-3}$$

Solving for the DC power flowing through the HVDC scheme during the transient period (P'_d), from equation (5-3) it is found that:

$$P'_d \cong P_M \frac{\delta_m - \delta_0}{\delta_m - \delta_c} - \frac{1}{\delta_m - \delta_c}\left(\int_{\delta_0}^{\delta_c} P'_g d\delta + \int_{\delta_c}^{\delta_m} P'_i d\delta\right) \tag{5-4}$$

With P_d' known, both the steady state and transient state DC power of the HVDC link is known at a particular time instant, therefore, the increment in DC power required to keep the generator in synchronism is known and is given by: $\Delta P_d = P_d' - P_d$. For simplification of analysis, it is assumed that the input mechanical power is constant. From equation (5-4) it can be seen that the required increment in DC power to prevent the machine from going out of step is dependent on the values of the generator output power and the power flowing in the AC lines during the transient period.

5.1.2 Simulation Results

A solid three-phase short circuit fault was simulated at the end of one of the parallel HVAC lines (line 2) of Network 1, for different network configurations. The CCT of the generators was then determined under the different network operation scenarios. This was done to observe how the imbedded HVDC schemes impacts the transient rotor angle stability of the network. The four simulated scenarios are:

a) Two machine infinite busbar system (TMIB) with two AC lines
b) Two machine infinite busbar system with an additional HVAC line in parallel
c) Two machine infinite busbar system with a LCC-HVDC scheme in parallel
d) Two machine infinite busbar system with a VSC-HVDC scheme in parallel

The schematic diagrams for scenarios A, B and D are shown in appendix C.

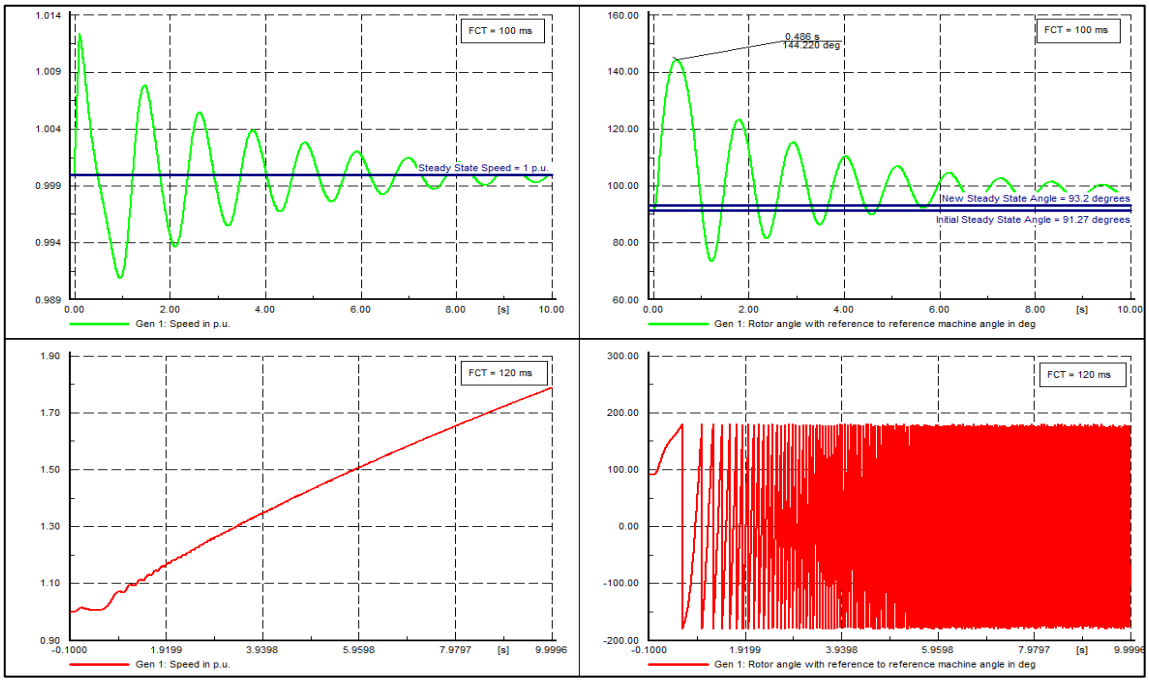

Figure 5.2: TMIB System Results (Scenario A)

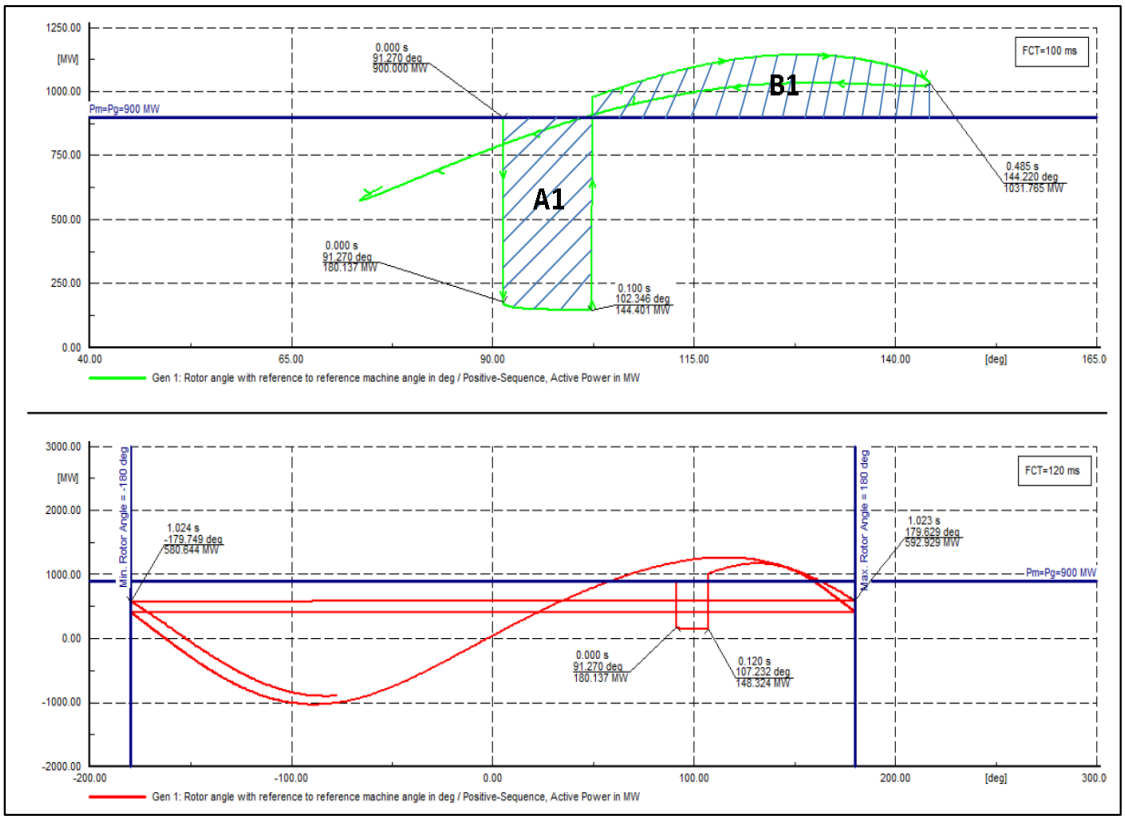

Figure 5.3: TMIB System Power-Angle Characteristics Results (Scenario A)

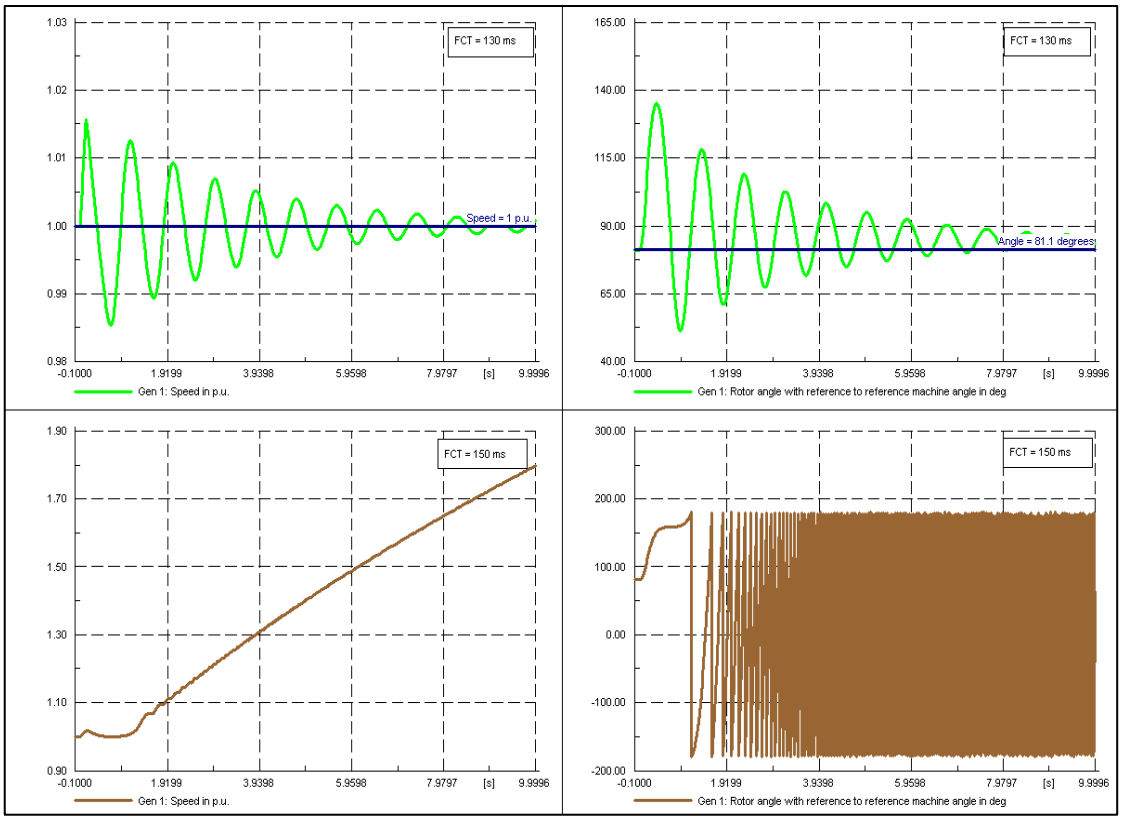

Figure 5.4: TMIB System with additional HVAC Line in Parallel Results (Scenario B)

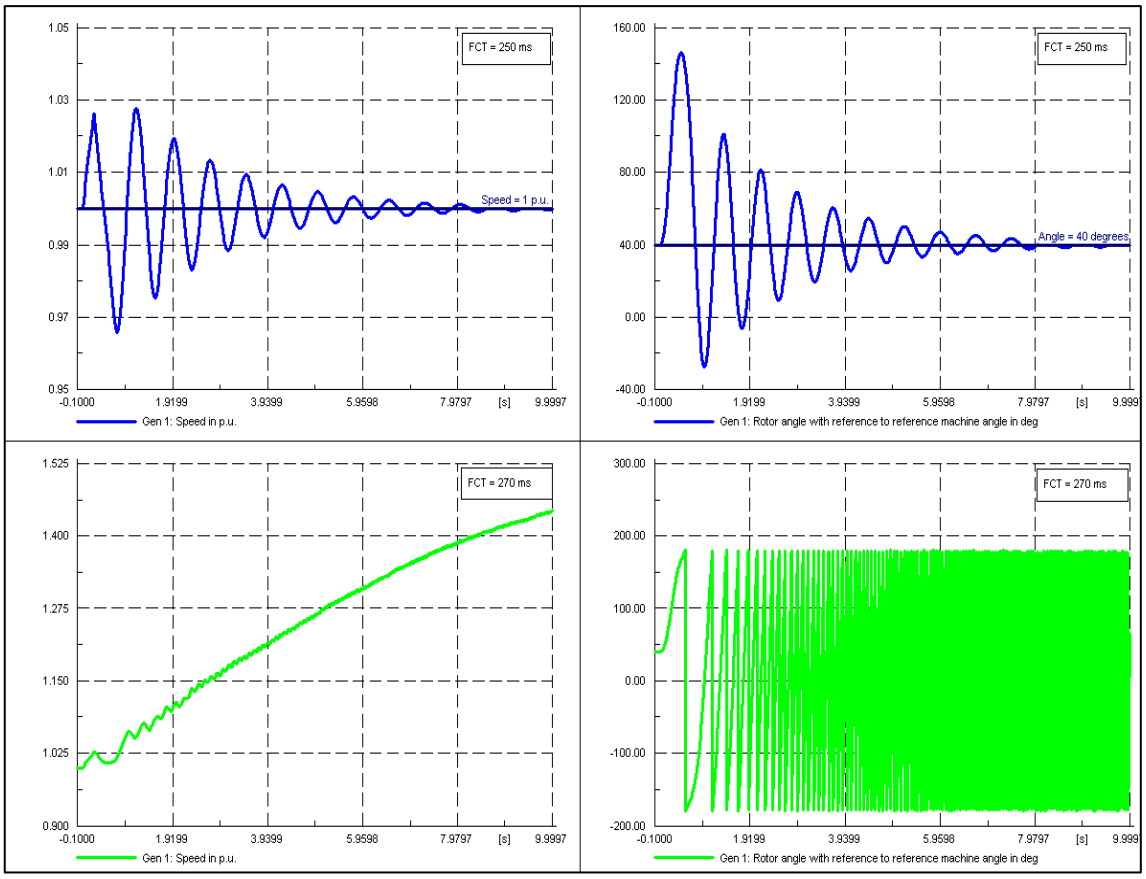

Figure 5.5: TMIB System with LCC_HVDC in Parallel Results (Scenario C)

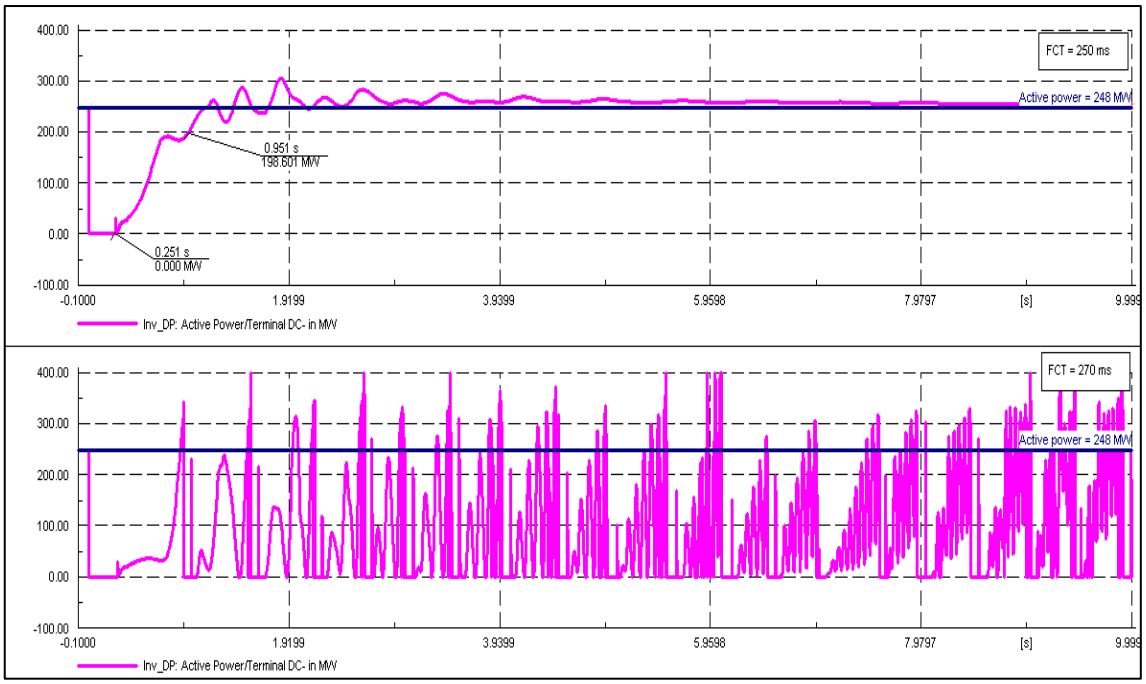

Figure 5.6: LCC-Inverter DC Power (Scenario C)

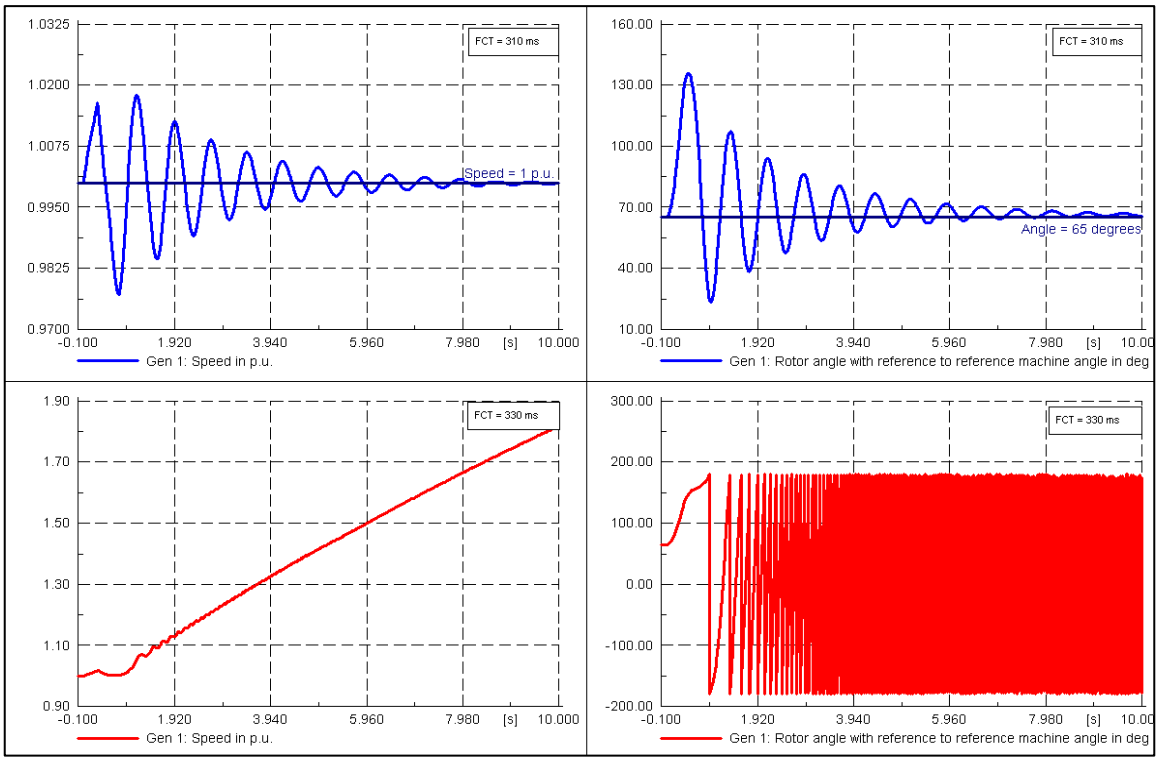

Figure 5.7: TMIB System with VSC-HVDC in Parallel (Scenario D)

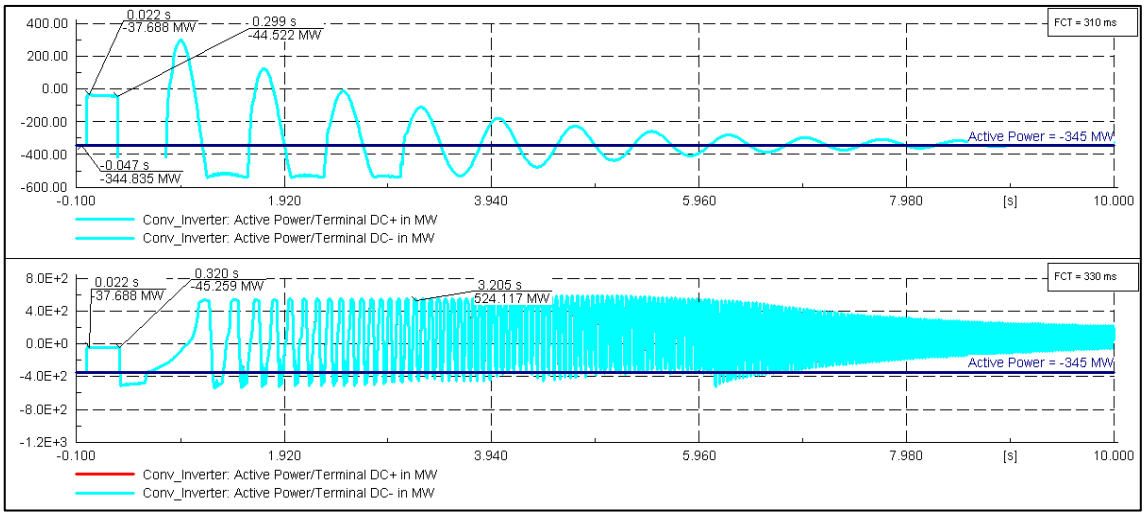

Figure 5.8: VSC-Inverter DC Power (Scenario D)

Figures 5.2 to 5.8 presents the response of the active power, rotor speed and rotor angle of the synchronous generator (Gen 1) and the converter DC power response to the disturbance in Network 1. The machine power-angle characteristics, speed and rotor angle response is analysed in order to determine the CCT of the machine under the different network configurations. From figure 5.2 it can be seen that when the generator is connected to the infinite busbar by two HVAC lines only, the CCT is 100 ms.

Figure 5.3 presents the power-angle characteristics of Gen 1 during stable and unstable operation conditions. The machine power-angle characteristics are governed by equation (2-4). From the graph showing the results when the fault is cleared at 100 ms, it can be seen that the steady state rotor angle δ_0=91.27 and the input mechanical power P_M is equal to the steady state generator output power $P_g = 900$ MW, which is also equal to the AC system power P_i in this scenario. When the fault occurs at zero seconds, P_i instantly drops to 160 MW, which is less than P_M. Due to the high machine inertia, the rotor angle does not change instantly when the fault occurs at zero seconds. Because P_i is less than P_M during the fault duration, there is a net acceleration torque which causes the rotor angle to increase to $\delta_c = 102$ degress where the fault is cleared at 100 ms. The net acceleration power of the rotor is governed by the swing equation (2-2). After the fault has been cleared successfully, P_i instantly increases to 977 MW, which is greater than P_M, and the rotor therefore experiences a net retarding torque which causes the rotor velocity to start decreasing. Because at this instant the rotor velocity of the machine is still higher than that of the reference machine, the machine rotor angle continues to increase until all the acceleration energy gained by the rotor during the fault is expended. The rotor then reaches the maximum angle of $\delta_m = 144$ degrees. The value of δ_m can also be seen in figure 5.2. The rotor will then continue to swing until the machine settles at the new equilibrium point where δ_0=93.2 degrees as shown in figures 5.2 and 5.3. The result showing the simulation for an extended period of 50 seconds, to determine the exact point at which the rotor settles, is shown in figure B2 in appendix B. From figure 5.3 it can be seen that the acceleration energy area A1 is approximately equal to the retarding energy area B1. It can therefore be concluded that, under the simulated network conditions and the simulated fault duration of 100 ms, the machine is transiently stable.

From the graph showing the simulation results for a fault duration of 120 ms, it can be seen that after the fault is cleared at 120 ms, the rotor angle swings to a maximum value of 180 degrees. At this point P_i remains less than P_M and there continues to be a net acceleration torque acting on the rotor and this causes the rotor to continue accelerating until it goes out of step due to pole slip. This action can also be seen from the rotor speed and rotor angle graphs in figure 5.2. It can therefore be concluded that for operation scenario A the CCT of Gen 1 is 100 ms.

From figure 5.4 it can be seen that the CCT improves from 100 ms to 130 ms when an additional HVAC line is placed in parallel to the two HVAC lines. When the third HVAC line is replaced with the LCC-HVDC scheme that was presented in chapter 4, the CCT improves from 130 ms to 250 ms, as shown in figure 5.5. The response of the transferred DC power flowing through the LCC-HVDC inverter is shown in figure 5.6. It can be seen that for a FCT of 250 ms (stable operation), the DC power collapses to zero MW due to commutation failure of the converter valves during the fault duration, and then recovers after the fault has been cleared. The DC power fault recovery time (FRT) is the time from the instant the fault has been cleared to the time the DC power is restored to 80% of its steady state value. From figure 5.6 it can be seen that the FRC is approximately 700 ms during stable operation of the generators and the LCC-HVDC scheme. It can further be observed that during the transient period after the fault has been cleared, the DC power remains greater than its pre-fault value. This is the DC power P_d' required to improve the system synchronising torque and thus it helps to maintain the machine transient stability. This action of the converters allows for an increase in the total power transferred during the transient period and therefore adds to the retarding power needed to counterbalance the acceleration power gained by the generator during the fault duration. The temporary overload capability of the converters therefore contributes to the synchronizing torque of the generator and thus improves the generator's CCT.

Figure 5.7 shows that the CCT of the generator improves from 250 ms to 310 ms when the LCC-HVDC scheme is replaced with a VSC-HVDC scheme. From figure 5.8 it can be observed that for stable operation (FCT of 310 ms), the DC power flowing through the inverter does not collapse to zero during the fault period. It can also be seen that the DC power of the VSC-inverter is instantly restored to 80% of its pre-fault value after the fault has been cleared. This is an indication that the response of the VSC controllers is faster, compared to those of the LCC controllers. This means that the retarding power contributed by the VSC-HVDC system is greater than that contributed by the LCC-HVDC system during the transient period. The transient stability of Gen 1 is enhanced more when the VSC-HVDC scheme is connected in parallel to the HVAC lines.

Overall, it has been observed that the two HVDC schemes improve the transient stability of Gen 1 by absorbing part of the excess power supplied by the generators

during the fault and transient periods, and therefore contributing to the system retarding power which allows the generators to maintain a stable state operation.

From the obtained results, it can be concluded that the parallel VSC-HVDC scheme improves the transient rotor angle stability of the generator more compared to the LCC-HVC scheme. This is so because compared to the LCC-HVDC scheme, the VSC-HVDC scheme has the ability to improve the system synchronizing power more during and after the fault has been cleared. When a HVDC scheme is placed in parallel with HVAC transmission lines, and the converter controllers are set such that the amount of DC power flowing through the converters is well regulated in a way that the DC power contributes to the total retarding power of the system, the HVDC scheme can be used to improve the system CCT. The schematic diagram of the TMIB system with LCC-HVDC in parallel is shown in figure 5.9. The network configurations for the other network operation scenarios are presented in appendix C.

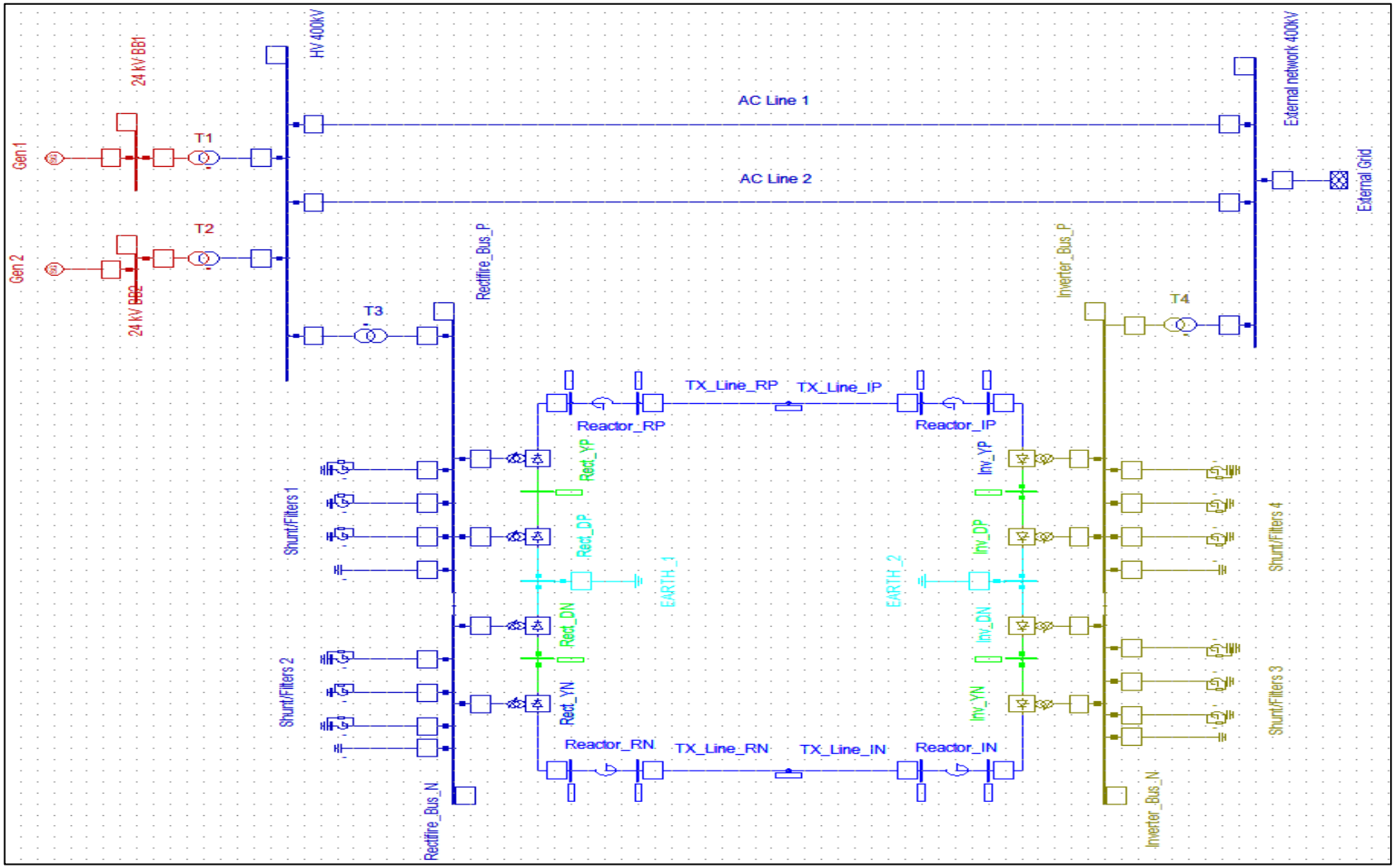

Figure 5.9: TMIB System with LCC-HVDC in Parallel

5.2 Test Network 2

In order to test the effectiveness and applicability of the research methodology described in chapter 3, on a large multi-machine electric power system, the methodology is applied to test Network 2. Network 2 is made up of four main areas (zones), namely: area North-West (NW), North-East (NE), South-West (SW) and South-East (SE). Figure 5.10 depicts the over view diagram of Network 2. It can be seen that the four areas are interconnected by HVAC lines. Areas South-West, North-West and North-East are closely interconnected by short HVAC lines, whereas area South-East is loosely connected to the rest of the network with long HVAC lines. The power interchange between areas North-East and South-East is controlled by means of a power-flow controller. All the generators in Network 2 are equipped with IEEE based PSSs, AVRs and turbine governor models which are presented in appendix A.

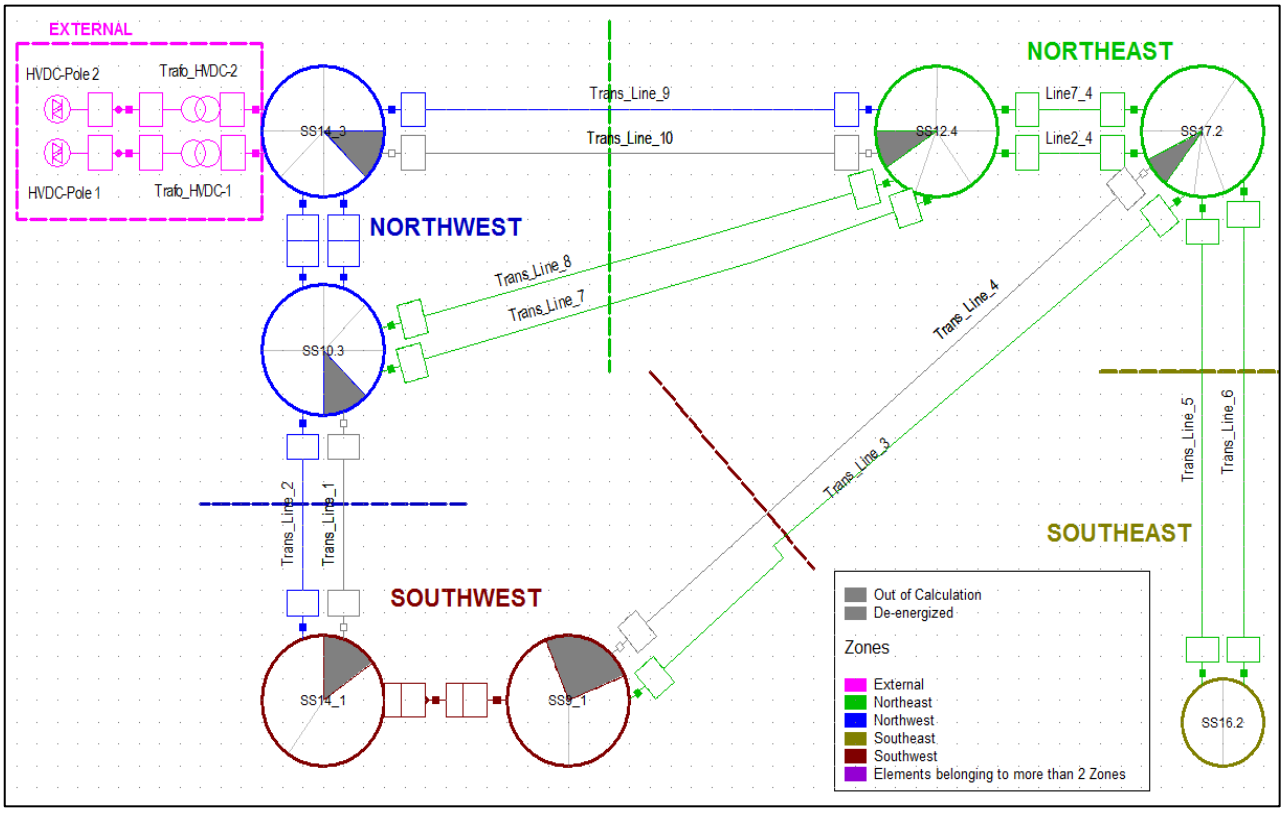

Figure 5.10: Overview Diagram of Test Network 2

For a clear view of the elements in each area of the grid, see the grid schematic diagram in figure C6 of appendix C. The HVAC transmission lines have a nominal voltage rating of 400 kV and 230 kV and the HVDC scheme is rated at 345 kV. The ratings and parameters of the elements in Network 2 are presented in appendix A.

5.2.1 Steady State Analysis

The network pre-disturbance conditions are analysed to determine the weakest or critical machines in the network, as well as the most sever fault locations in the network. The network steady state conditions are evaluated by running load flow and RMS simulations without any fault being induced in the network. For power flow analysis, the DIgSILENT PowerFactory software makes use of the Newton-Raphson method of numerical integration. The network steady state analysis is done to specify the critical cases on the basis of the generators in the network that have the largest rotor angles with reference to the reference machine angle, and the transmission lines in the network that have the highest loading. The steady state analysis of the network forms part of the study organization activity. The deliverable of this activity is a case list of the critical system conditions, which are examined in more detail through transient state time-domain simulations. The following variables of interest have been defined for all the machines in the network:

- Generator rotor angle with reference to reference machine angle in degrees
- Generator speed in p.u.
- Generator active power in MW

For steady state analysis of the network, all the generators and loads were placed into service. In order to get the true state of system stability, the transient stability analysis of the network should be done based on the worst case scenario. The worst case scenario is considered to be when the AC system is weakest. Some reactive power compensation devices such as SVC's, reactors and shunt capacitors were placed out of service. This was done to weaken the network by minimizing reactive power compensation. Some parallel transmission lines were taken out of service in order to increase the total effective transmission network reactance and therefore reducing the maximum power transfer capabilities of the transmission lines. This worsens the system transient stability by reducing the system post fault synchronizing power.

Fault levels are used as indicators of network strength. High fault levels indicate a strong network and low fault levels indicate a weak network. The generator connected to the busbar with the highest fault level is usually considered to be the reference machine of the network. The reference busbar has the ability to effectively maintain its voltage after being subjected to a severe system fault and therefore minimizing power

swings during and after a transient. The rotor angles of the rest of the generators in the network are measured with reference to the rotor position of the reference machine. Generator NW_G6 was chosen as the reference machine of Network 2. The machines with the high rotor angles with reference to the reference machine angle are considered to be weak. The steady state values of the rotor angles of all the machines in the network were plotted to determine the weakest and strongest generators in each of the four areas of the network. The obtained results are further verified with transient state simulations. The stability of the machines identified as the least stable in each area of the network is then analysed. In order to determine the worst case operation scenario of the network, the rotor angles of the machines were measured under the following network operational conditions:

- Generator AVRs and PSS in service and all transmission lines in service
- Generator AVRs and PSS out of service and all transmission lines in service
- Generator AVRs and PSS in service and lines L_1, L_6 and L_10 out of service
- Generator AVRs and PSS out of service, lines L_1, L_4 and L_10 out of service
- Generator AVRs and PSS out of service, lines L_1, L_4 and L_10 out of service

Lines 1, 4, 6 and 10 are one of the parallel lines interconnecting the four areas of the network. The machine AVRs and PSS were taken out of service in order to observe what effects they have on the machine rotor angle during steady state operation of the network. The obtained results are presented in figures 5.11 to 5.15.

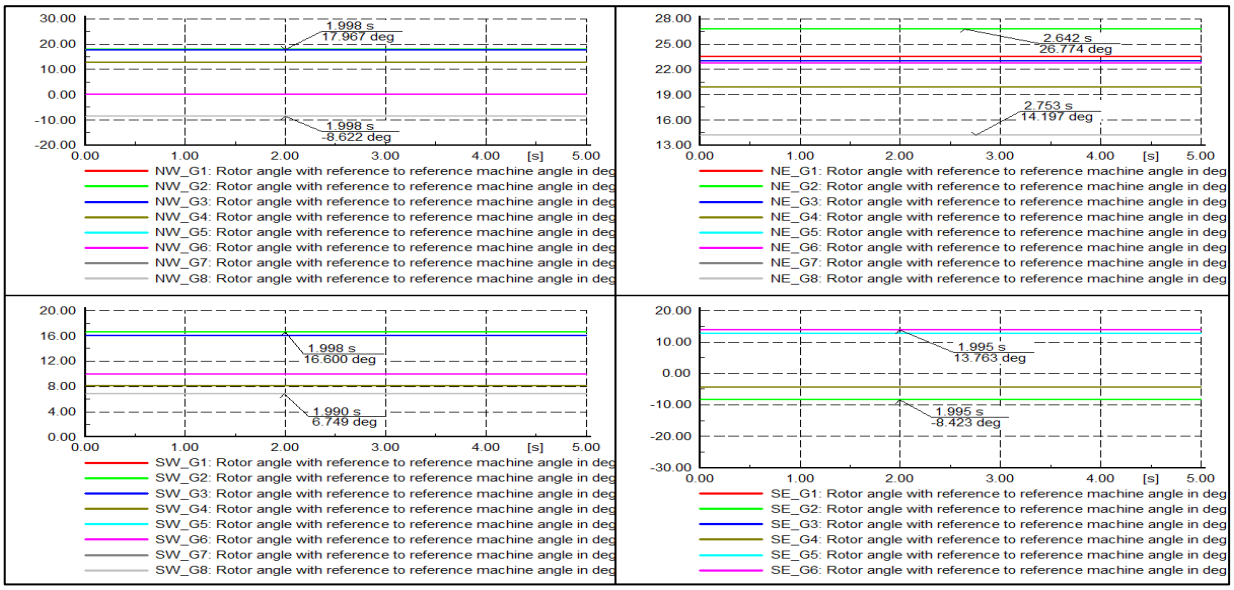

Figure 5.11: PSS and AVRs in Service and All Lines in Service

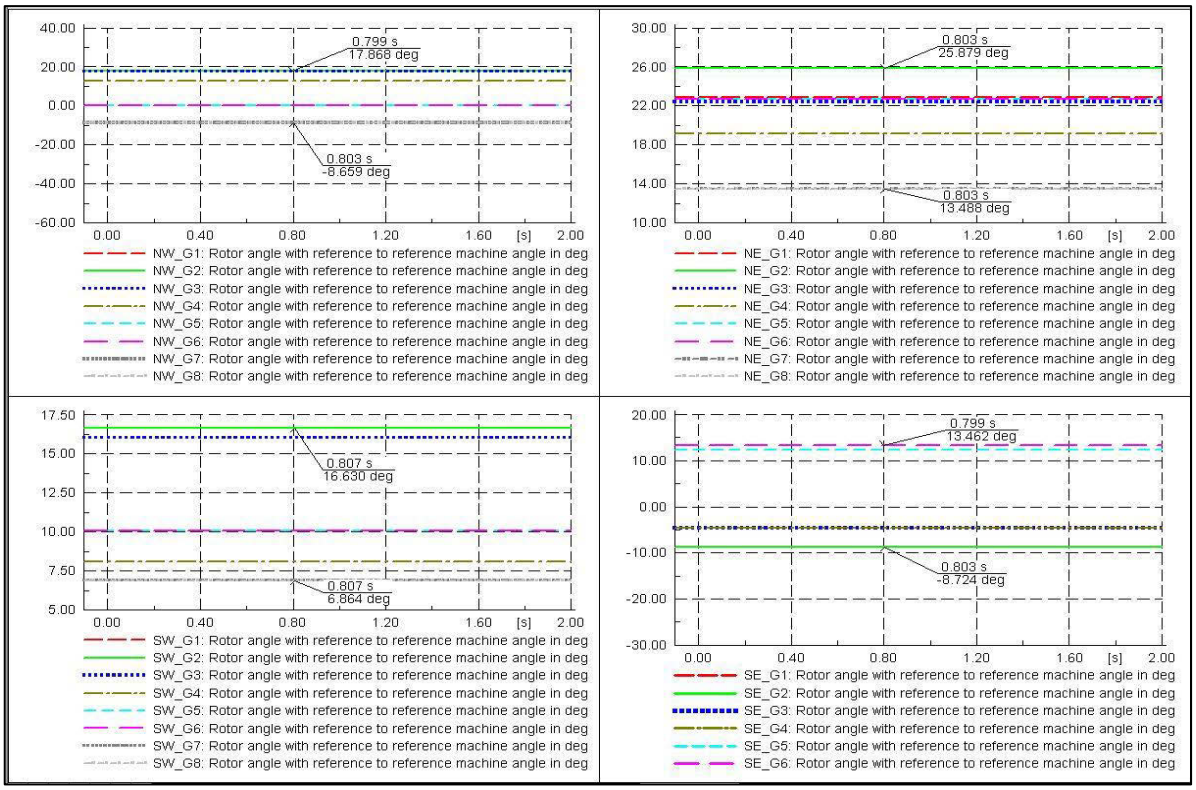

Figure 5.12: PSS and AVRs out of Service and All Lines in Service

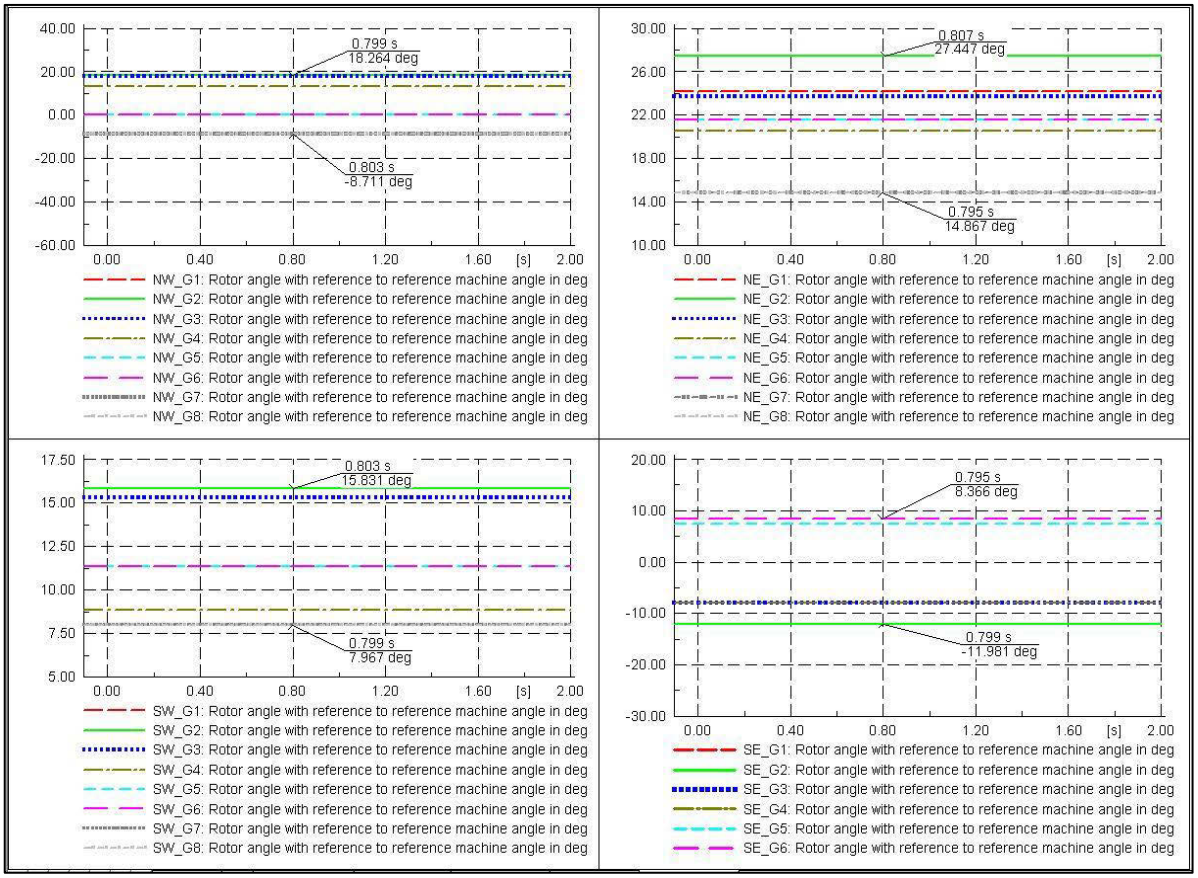

Figure 5.13: PSS and AVRs in Service and L1, L4 and L10 out of Service

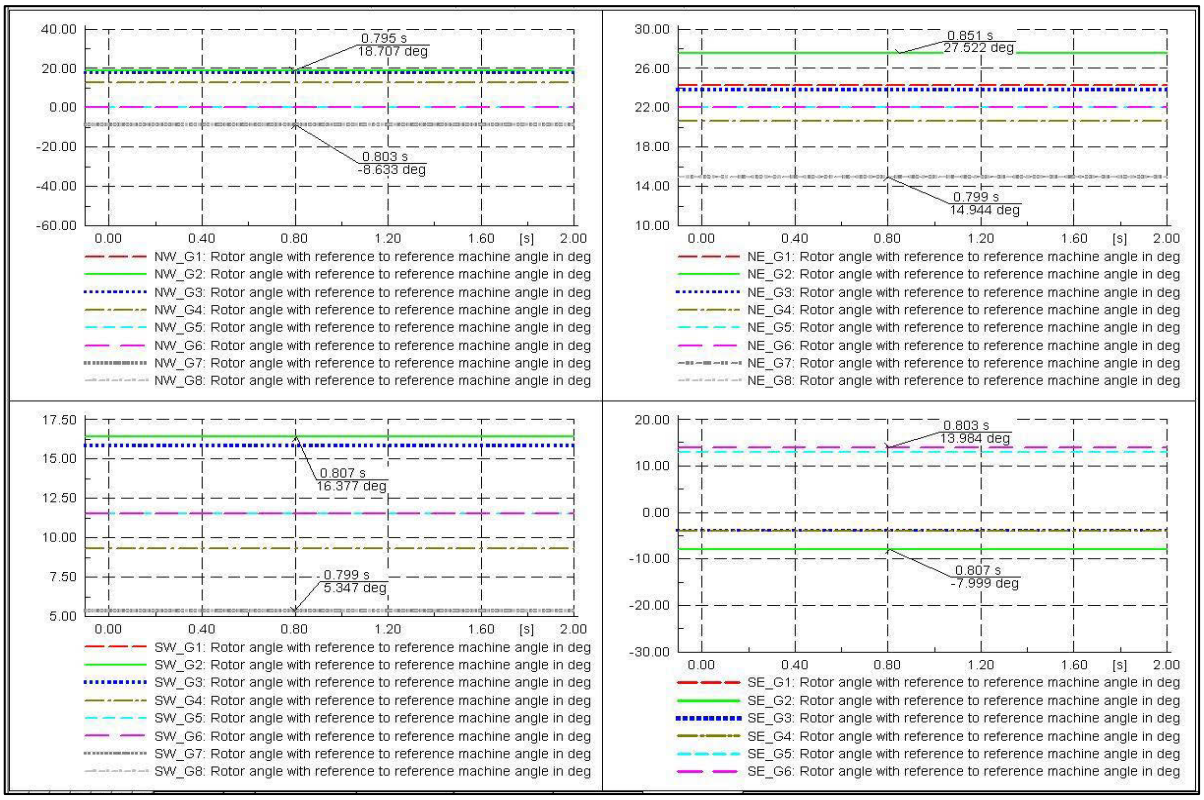

Figure 5.14: PSS and AVRs out of Service and L1, L4 and L10 out of Service

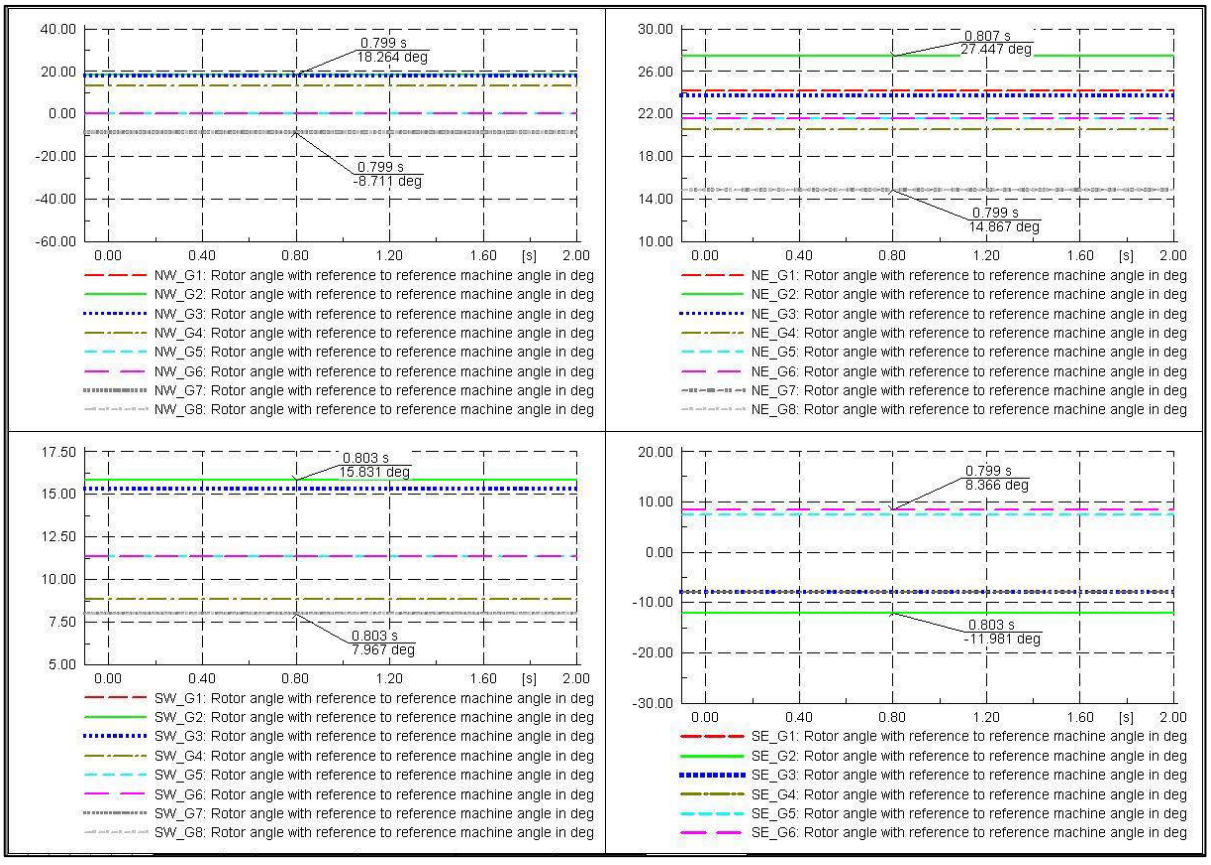

Figure 5.15: PSS and AVRs out of Service and L1, L6 and L10 out of Service

The results presented in figures 5.11 to 5.15 show the impact of the machine PSS and AVR on the rotor angle response of the machines. Some of the main HVAC transmission lines were taken out of service in order to observe the impact of system impedance on the transient stability of the machines. This was done to determine the most critical conditions of the network, under which the transient stability study should be carried out.

Comparing figures 5.11 and 5.12 it can be seen that there is not much of a difference in the machine rotor angle values when the PSS and AVRs are in service and when they are taken out of service during steady state operation. This shows that the PSS and AVRs have very little effect on the machine rotor angle during steady state operation of the system. Comparing figures 5.11 and 5.13, it can be observed that generally the rotor angle values of the machines increases when some of the lines are taken out of service. From figures 5.14 and 5.15, it can been observed that the rotor angle values of the machines are slightly higher when line 4 is taken out of service compared to when line 6 is taken out of service. Generally, the machines in area North-East have higher rotor angle values compared to the machines in the other areas of the network. From these results it can be concluded that the worst case operation scenario of Network 2 would be when transmission lines, L1, L4 and L10 are out of services.

5.2.2 Transmission Line and Generator Loading

It is important to identify the critical generators and lines in the network. According to Nayak [63], the power transmission capacity of a High Voltage (HV) line is limited by two main factors: the thermal capacity of the line, which is the ultimate capacity of the line and corresponds to the line's capability to withstand heat generated during line losses, and the surge impedance loading (SIL) of the line, which corresponds to the transmission line stability limit. For an Extra High Voltage AC (EHVAC) line, the efficiency of power transmission capacity is below its thermal limit and restricted by angular and voltage stability limits, which restricts the line load ability up to its Surge Impedance Loading (SIL) level. SIL is the MW loading of an EHV transmission line at which natural reactive power balance occurs [63]. AC Transmission lines produce reactive power depending on their voltage level and capacitance, and they consume reactive power to support the magnetic field. A load flow simulation was run to determine the highest loaded lines and generators. Results were obtained for the five highest loaded transmission lines in the network and the highest loaded generator in

each area of the network. The results are presented in table 5.1. From the results it can be concluded that the most critical line fault would be a fault on line 3_4, while the most critical generator busbar fault would be a fault on BB1 on which NW_G4 is connected.

Table 5.1: Transmission Line and Generator Loading

Element Loadings			
Transmission Lines	Percentage Loading	Generators	Percentage Loading
Line 3_4	108.8 %	NE_G4	89.81 %
Line 6_3	74.80 %	NW_G4	92.51 %
Line 6_4	75.58 %	SE_G3	88.20 %
Line 4_3	79.69 %	SW_G2	61.72 %
Line 3_3	78.05%		

5.2.3 Critical Case List and Simulation Events

The aim of the study organization activity which was carried out in sub-sections 5.2.1 to 5.2.2 is to come up with a case list of the critical system conditions, as well as the system fault and switching events under which transient stability analysis of the network should be carried out. The critical case list of Network 2 is presented in table 5.2.

Table 5.2: Network 2 Critical Case List and Switching Events

Pre-fault System Conditions	
Generator Controls	PSS and AVR in service
System Loading	Full load
System Generation	All generators in service
Power Compensation	Some FACTS devices out of service
Lines out of Service	Line_1, Line_4 and Line_10
Load Models	Voltage dependent
Fault Condition 1	
Fault Type	Solid three-phase short circuit
Initial Fault Duration	100 milliseconds
Fault Location	End (99%) of line 3_4

Fault Impedance	0 ohms
Fault Condition 2	
Fault Type	Solid three-phase short circuit
Initial Fault Duration	100 milliseconds
Fault Location	Area North-West BB1 (NW_G4 BB)
Fault Impedance	0 ohms
Switching Events	
Fault Occurring Time	0 seconds
Fault Clearing Time	100 milliseconds
Switching Type	Fault clearing event or opening of the line circuit breakers

5.2.4 Transient State Analysis

In order to observe and analyse the rotor angle response of the machines in the network when subjected to a disturbance, the critical case list was used as a guide to simulate a solid 3-phase short circuit fault on transmission line L3_4. From the obtained results it was observed that all the generators remain in a stable operation state for a maximum fault duration of 380 ms. For fault clearing times longer than 380 ms, some of the generators in the network go out of step due to pole slip. The simulation results for a fault duration of 380 ms are shown in figures 5.16 and 5.17.

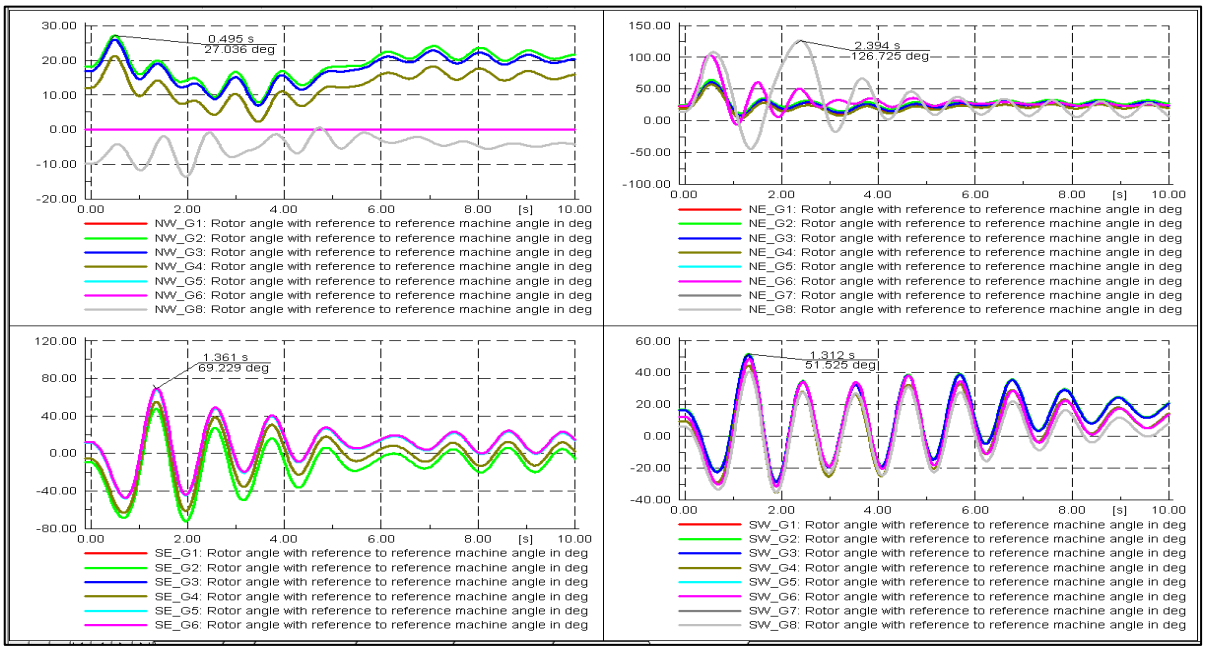

Figure 5.16: Generator Rotor Angles in Degrees

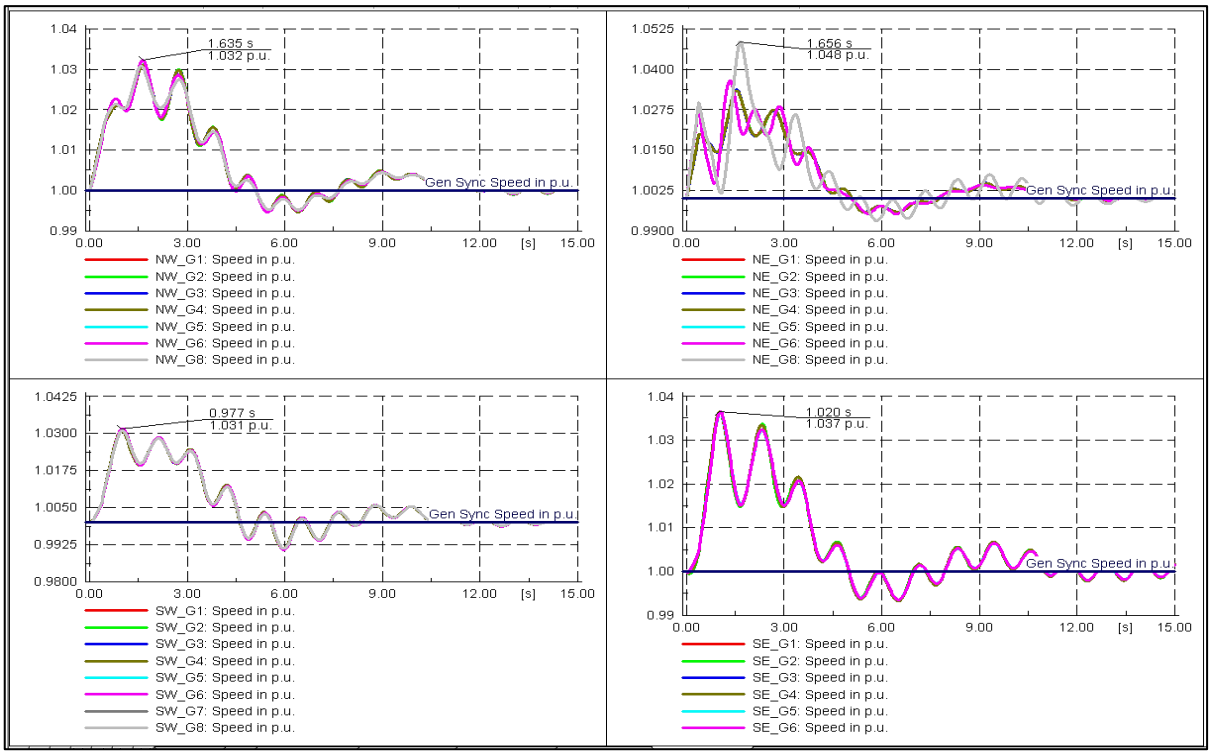

Figure 5.17: Generator Speed in p.u.

Figures 5.16 and 5.17 illustrate the response of the rotor angle and rotor speed of all the generators in network 2 when subjected to a solid three-phase short circuit on line L3_4. From figure 5.16 it can be seen that generator NE_G8 experiences the highest rotor angle swing with a peak value of 127 degrees in area NE, after the fault has been cleared. In area NW, generator NW_G2 has the highest rotor angle value of 27.0 degrees. In area SE, the response of all the machine rotor angles follow a similar pattern and generator SE_G6 has the highest rotor angle value of 69.2 degrees. The response of the rotor angles of all the machines in area SW also follow a similar pattern to each other, with generator SW_G3 having the highest rotor angle value of 51.5 degrees. The rotor angle value of NW_G6 is zero degrees. This is so because, NW_G6 was chosen as the reference machine of the network. After the fault has been cleared, the rotor angles of all the machines in the network eventually return to their steady state values. This is an indication of transient rotor angle stability of the machines. From figure 5.17 it can be observed that the speeds of the different generators in the network have a similar response whereby when the fault occurs, the rotor speed undergoes a steep rise, after the fault has been successfully cleared, the rotor speed begins to oscillate and the amplitudes of oscillations are damped out with an increase in time. The oscillations eventually die out and the rotor speed returns to the steady state value of 1 p.u. NE_G8

experiences the highest rotor speed of 1.048 p.u. From these results, it can be concluded that the critical generators in each area of the network are: NE_G8, SE_G6, NW_G2 and SW_G5. The transient rotor angle stability of these generators will be assessed.

5.2.5 Analysing Generator Critical Fault Clearing Times

The critical fault clearing times (CCT) of the critical machines in the network will be determined. The first step will be to determine the CCT of the entire network by running a critical fault screening script.

5.2.5.1 Critical Fault Screening Script (CFSS)

The CFSS was developed by DIgSILENT. It monitors all the active generators in the system for loss of synchronism and then calculates the longest fault duration at which the system remains in a stable state of operation. The result obtained after running the script for a fault on line L3_4 is shown in figure 5.18.

```
Calculation of Initial Conditions  Run Simulation
30 synchronous generators being monitored for loss of synchronism.
-------------------------------------------------------------------
Starting Calculation for Line  Line3_4  at  99 %
Iteration    0 for clearing time 0.0500 s.
Iteration    0 for clearing time 1.0000 s.
Iteration    1 for clearing time 0.5250 s.
Iteration    2 for clearing time 0.2875 s.
Iteration    3 for clearing time 0.4063 s.
Iteration    4 for clearing time 0.4656 s.
Iteration    5 for clearing time 0.4359 s.
Iteration    6 for clearing time 0.4211 s.
Iteration    7 for clearing time 0.4137 s.
Critical Fault Clearing Time after   7  iterations:  0.4063 s


Critical Fault Clearing Times at  99 per cent
---------------------------------------------
Line3_4 tcrit=  0.406 s
---------------------------------------------
DIgSI/info - (t=02:000 s) DPL program 'Critical Fault Screening' successfully executed
```

Figure 5.18: CCT obtained using Critical Fault Screening Script

From figure 5.18 it can be seen that the CCT time for clearing a solid three-phase fault at the end of line L3_4 is 406 ms. The CCTs of the generators identified as the weakest in each area of the network are going to be determined and the average CCT will be compared to the network CCT obtained using the CFSS.

5.2.5.2 CCT of Generator NE_G8

The various steps outlined in the methodology for time-domain simulations and results outputs were taken systematically to obtain the results of the response of the rotor angle,

rotor speed and the power-angle characteristics of generator NE_G8, when subjected to fault condition 1. The obtained results are presented in figures 5.19 to 5.21.

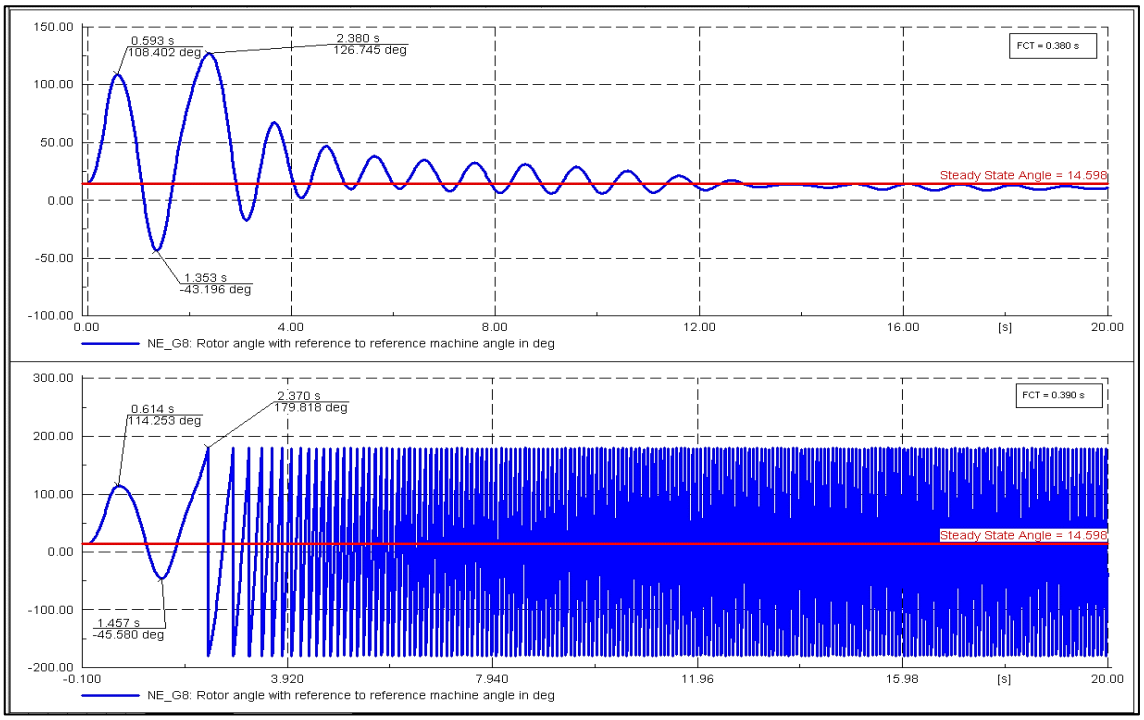

Figure 5.19: NE_G8 Rotor Angle

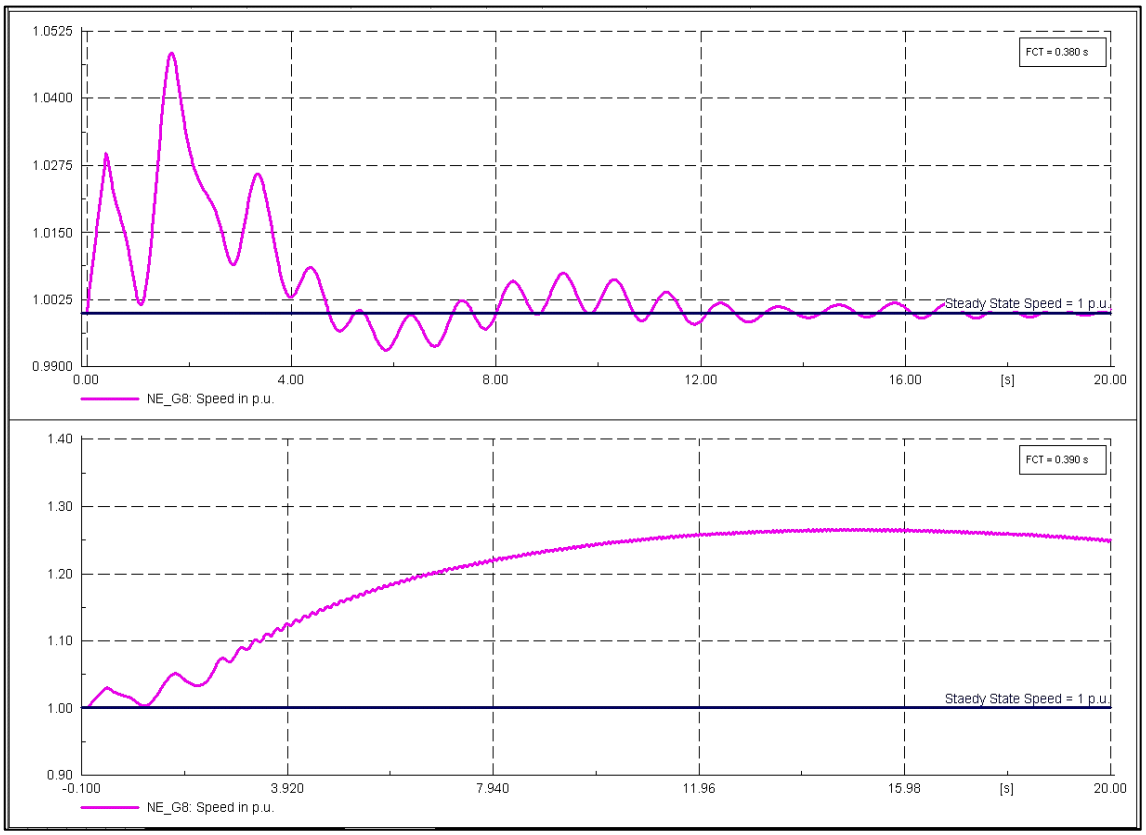

Figure 5.20: NE_G8 Rotor Speed

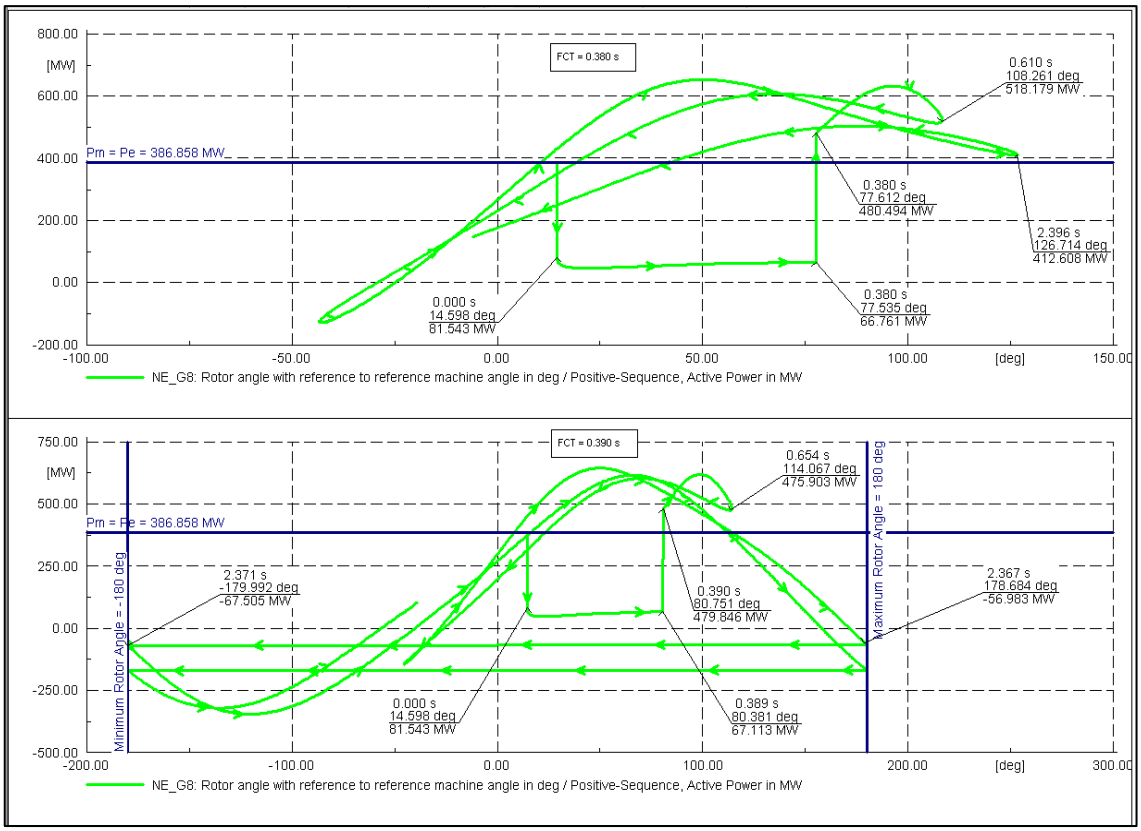

Figure 5.21: NE_G8 Power-Angle Characteristics

Figures 5.19 to 5.21 presents a comparison of the response of the variables of interest when the three-phase fault on L3_4 is cleared at 380 ms and 390 ms. From figure 5.19 it can be seen that for a fault duration of 380 ms, the machine rotor angle undergoes some oscillations after the fault is cleared, the amplitudes of the oscillations are damped with an increase in time and they eventually die out and the rotor angle returns to its steady state value. This is an indication that the machine has settled at a new stable equilibrium point of operation. For a fault duration of 390 ms, the rotor angle oscillates between the maximum and minimum values of 179 degrees and -179 degrees indefinitely. This is an indication that the machine has lost synchronism due to pole slip.

Figure 5.20 shows the response of the machine rotor speed with a change in time. It can be observed that for a fault duration of 380 ms, the rotor speed undergoes some oscillations after the fault is cleared. The speed then begins to drop until it eventually returns to the steady state value of 1 p.u. In contrast, when the fault is cleared at 390 ms, the machine rotor speed continues to increase indefinitely and this is an indication of loss of synchronism of the machine due to pole slip.

Two graphs illustrating the power-angle characteristics of generator NE_G8 are shown in figure 5.21. The operation points of the machine are shown in the form of labels showing the time, active power and rotor angle.

For a fault duration of 380 ms, the initial steady state rotor angle is 14.6 degrees and the input mechanical power is equal to the generated output electrical power of 387 MW. In order to simplify the analysis, the input mechanical power is assumed to be constant for the duration of the simulation. When the fault occurs at zero seconds, the operating point suddenly shifts to (14.6 degrees, 81.5 MW). At this point the rotor angle remains the same due to the large inertia of the machine which does not allow the rotor position to change instantly. The input mechanical power is greater than the output electrical power at this point and this causes a net acceleration power. The rotor accelerates and causes the rotor speed to be greater than the reference machine rotor speed and this in turn causes the machine rotor angle with reference to the reference machine angle to increase to 77.6 degrees, which is the fault clearing angle. After the fault has been cleared at 380 ms, the operating point instantly shifts to (77.6 degrees, 481 MW). At this operating point the output electrical power is greater than the input mechanical power and therefore, there is a net decelerating power which causes the rotor to retard by transferring all the kinetic energy gained during acceleration back into the network. Because at this point the rotor speed is still greater than that of the reference machine, the rotor angle continues to increase until the maximum rotor angle at the operating point (108 degrees, 518 MW) is reached when all the kinetic energy gained during the acceleration period is expended and the rotor speed is now equal to that of the reference machine. Since the output electrical power is still greater than the input mechanical power at this point, there is a net deceleration power which causes the rotor to continue retarding. This causes the rotor speed to fall below the speed of the reference machine, hence causing a decrease in the machine rotor angle. The rotor angle continues to decrease until it reaches the minimum value of -45.3 degrees to complete the first swing.

During the second swing, the rotor angle reaches a maximum value of 127 degrees at a power output value of 413 MW. The power at this operating point remains greater than the input mechanical power, therefore the rotor continues to retard. The maximum rotor angle values of the subsequent swings remain less than 127 degrees and it continues to decrease. This means that the rotor angle will continue to oscillate about a new stable

equilibrium point (SEP) with a continued rotor angle oscillation damping until it eventually settles at a new steady state value. This response indicates that the machine remains transiently stable for a fault duration of 380 ms.

From figure 5.21 it can be observed that for a fault duration of 390 ms, the rotor angle response is similar to the first swing response of the rotor when the fault was cleared at 380 ms. During the second swing however, the rotor angle increases to an extent that the maximum operating point of the machine has a large rotor angle value and the output electrical power is less than the input mechanical power. This means that there is a net acceleration power which causes the rotor to continue accelerating and this causes the rotor angle to continue increasing until the maximum rotor angle limit of 180 degrees is reached. The rotor angle then continues to oscillate indefinitely between the maximum and minimum rotor angle values of 180 and -180 degrees. This is an indication that the generator lost synchronism due to pole slip. From the analysis done on the obtained results it can be concluded that the CCT for NE_G8 to remain in synchronism with the rest of the generators is 380 ms.

5.2.5.3 CCT of Generator NW_G2

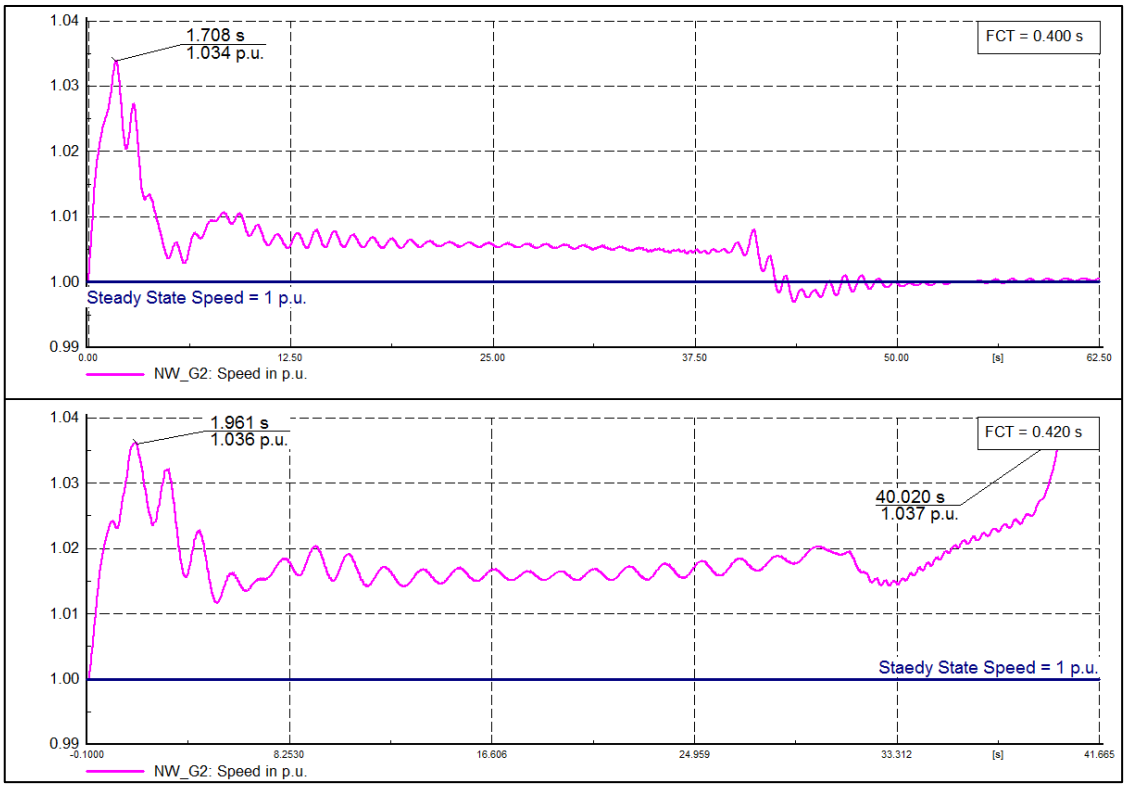

Figure 5.22: NW_G2 Rotor Speed

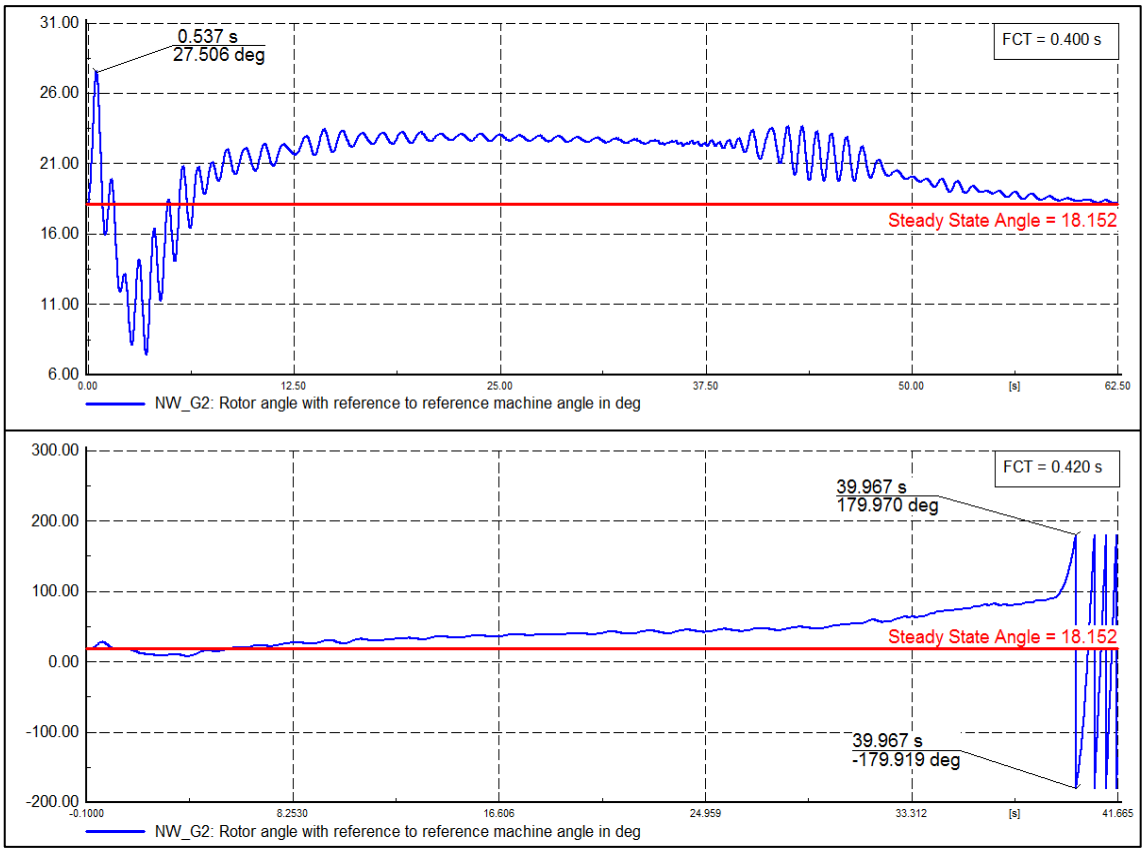

Figure 5.23: NW_G2 Rotor Angle

The graphs shown in figures 5.22 and 5.23 illustrate the response of the rotor angle and rotor speed of generator NW_G2 for different fault clearing times. From figure 5.22 it can be observed that when the fault is cleared at 400 ms, the rotor speed increases rapidly until it reaches a maximum value of 1.034 p.u., after which it begins to decrease until it returns to its steady state value. When the fault is cleared at 420 ms, the rotor speed increases rapidly until it reaches a peak value of 1.036 p.u. after which it decreases slightly and then continues to maintain the same value for approximately 25 seconds. The rotor speed then begins to increase indefinitely, which is a sign of loss of synchronism due to pole slip. From figure 5.23, it can be seen that when the fault is cleared at 400 ms, the rotor angle eventually returns to its steady state value. This is an indication of stable operation of the machine. When the fault is cleared at 420 ms, the rotor angle gradually increases until it begins to oscillate between the maximum and minim angle values. This is an indication that the machine has gone out of step due to pole slip. From this observation it can be concluded that the CCT for NW_G2 is 400 ms.

5.2.5.4 CCT of Generator SW_G3

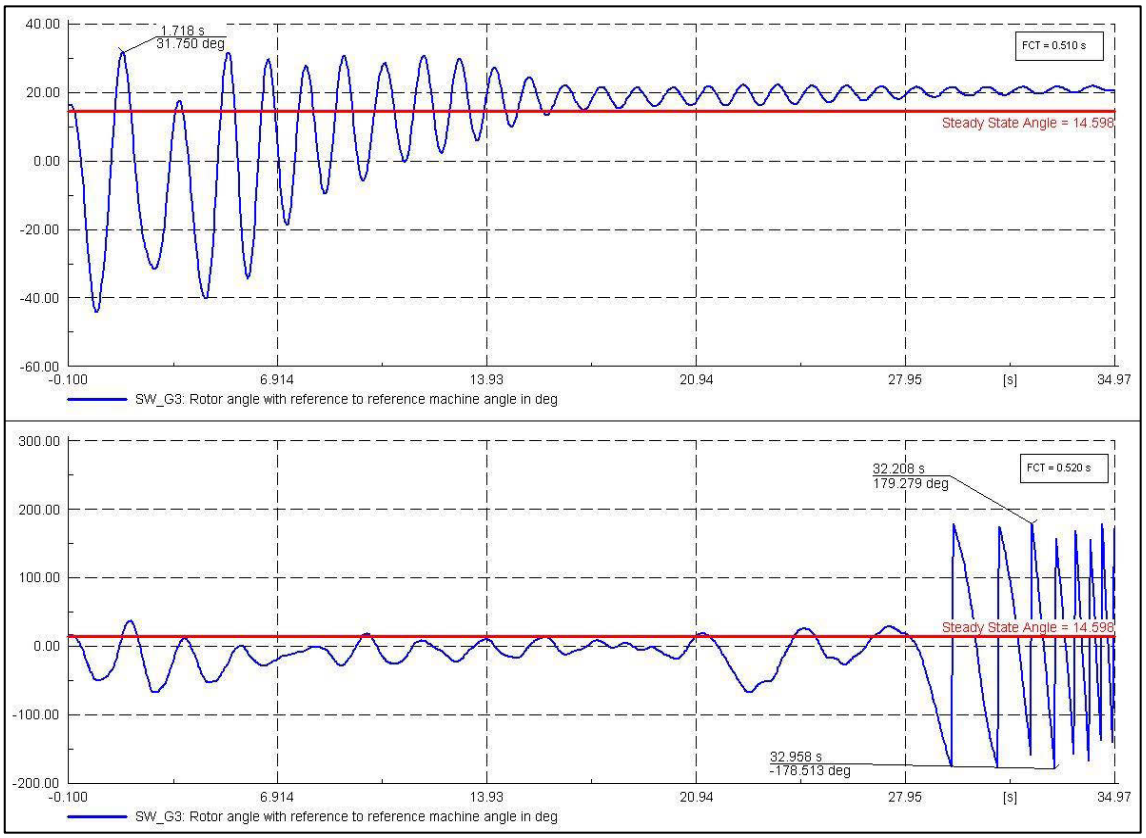

Figure 5.24: SW_G3 Rotor Angle

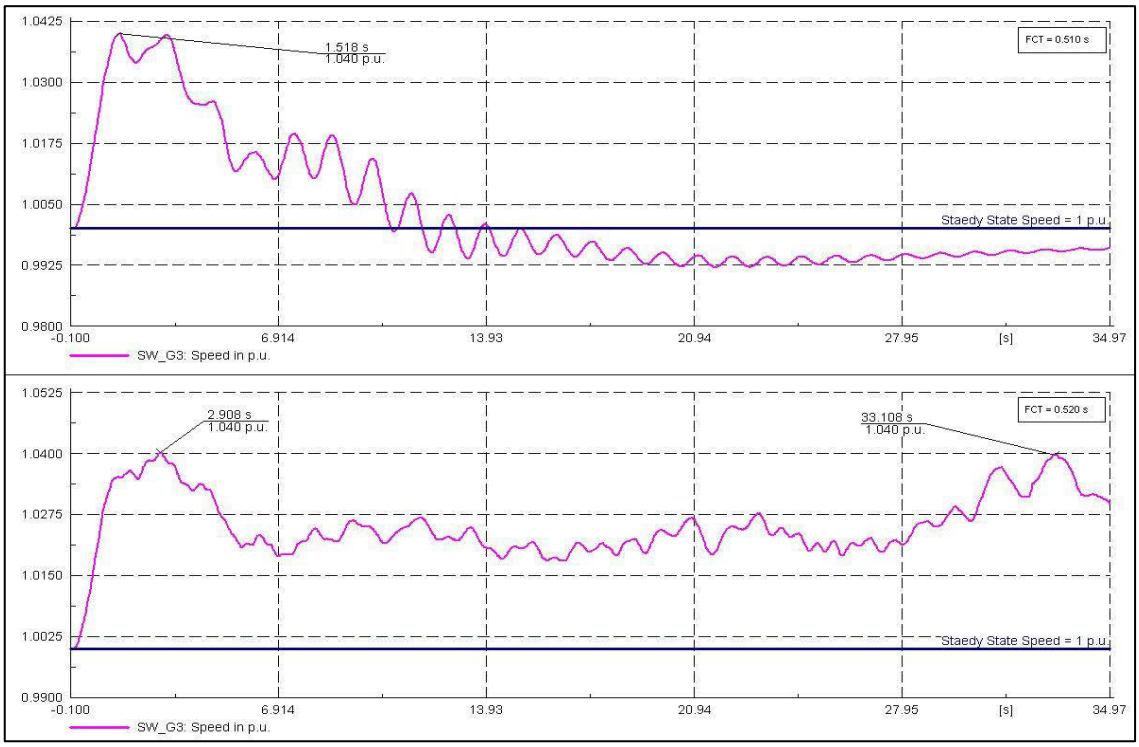

Figure 5.25: SW_G3 Rotor Speed

Figures 5.24 and 5.25 depict the response of the rotor angle and rotor speed of generator SW_G5. It can be observed that when the fault is cleared at 510 ms, SW_G3 remains transiently stable. However, when the fault is cleared at 520 ms SW_G3 loses synchronism with the rest of the generators in the system. It can therefore be concluded that the CCT for SW_G3 is 510 ms.

5.2.5.5 CCT of Generator SE_G6

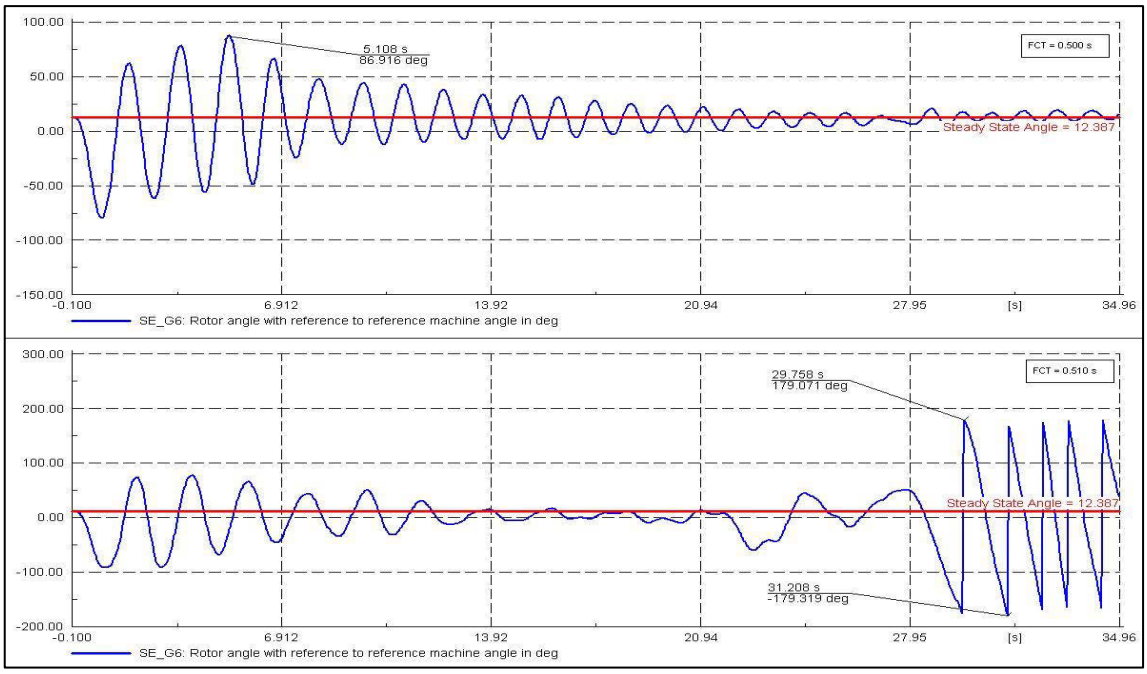

Figure 5.26: SE_G6 Rotor Angle

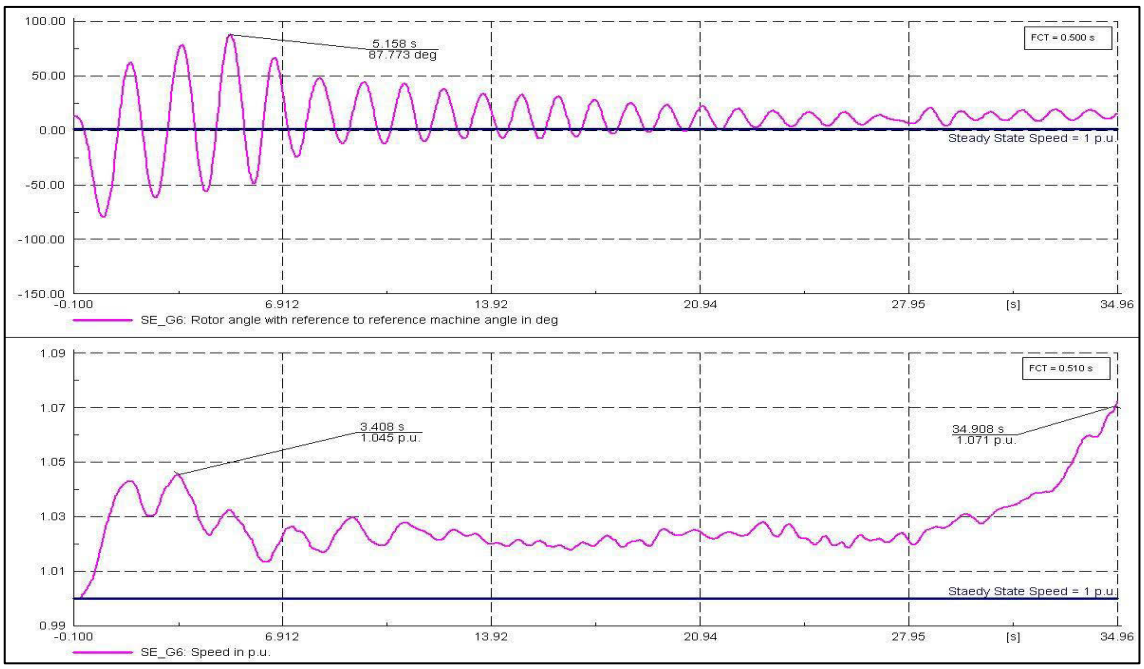

Figure 5.27: SE_G6 Rotor Speed

Figures 5.26 and 5.27 show the response of the rotor angle and rotor speed of generator SE_G6. It can be seen that when the fault is cleared at 500 ms, SE_G6 remains transiently stable. However when the fault is cleared at 510 ms SE_G6 goes out of step due to pole slip. It can therefore be concluded that the CCT for SE_G6 is 500 ms.

From the analysis done on the obtained results it was found that generator NE_G8 has the shortest CCT of 380 ms, and generator SW_G3 has the longest CCT of 510 ms. It can therefore be concluded that the critical machine of network 2 is generator NE_G8 and the most stable machine of the four machines analysed is SW_G5. The mean CCT of the four generators that where analysed is 448 ms. This value is close to the system CCT of 406 ms which was obtained by using the critical fault screening script (CFSS), taking into consideration that only the CCT times of four generators were used to calculate the mean system CCT time.

The South African Grid Code-The System Operation Code [64] stipulates that: fault clearing times, including breaker operation time, shall not exceed 120 ms plus an additional 30 ms for DC offset decay. This means that the system protection devices should be set such that, the total fault clearing time does not exceed 150 ms. The normal fault clearing time on high voltage (HV) transmission systems is considered to be 5 cycles (100 ms), which is the total fault clearing time inclusive of the relay time and breaker-interruption time. It is therefore desirable that the CCT of the generators be greater than the normal fault clearing times. This means that the fault is cleared successfully without the generators in the network losing synchronism.

The South African Grid Code-The Network Code [65], stipulates that: Transient stability shall be retained for a three-phase line or busbar fault, cleared in normal protection times, with the system healthy and the most onerous power station loading condition. Since the CCT for the critical machine of Network 2 is 380 ms, it can be concluded that in terms of network transient stability, the generators in Network 2, meets requirements for transient stability as stipulated in the grid code. Network 2 can therefore be considered to be rotor angle transiently stable.

5.2.6 Effects of LCC-HVDC Scheme on Network 2 Transient Stability

In order to analyse how an HVDC transmission scheme would affect the transient rotor angle stability of the machines in Network 2, transmission lines 5 and 6 were taken out of services and replaced with a mono-polar LCC-HVDC scheme. The HVDC scheme

transmits 500 MW to area South East, over a distance of 200 km. The same fault condition as in the previous cases was then simulated and the response of the rotor angle and rotor speed of NE_G8, which is the critical machine of the network, was observed. The network CCT was then determined. The obtained results are shown in figures 5.28 and 5.29.

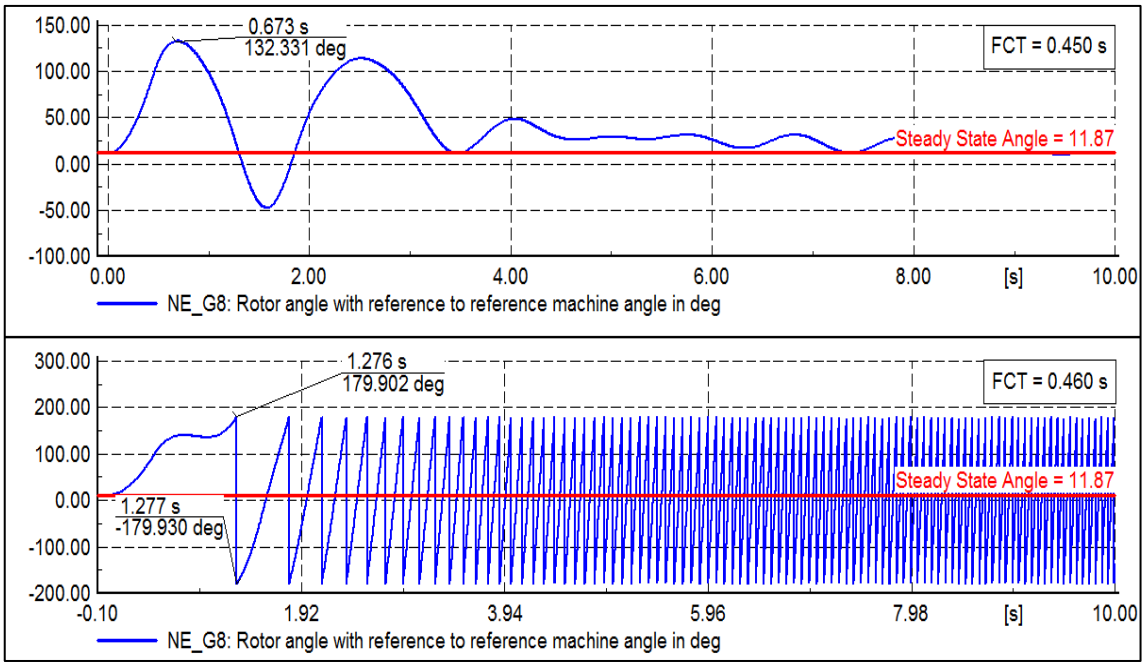

Figure 5.28: Rotor Angle of NE_G8

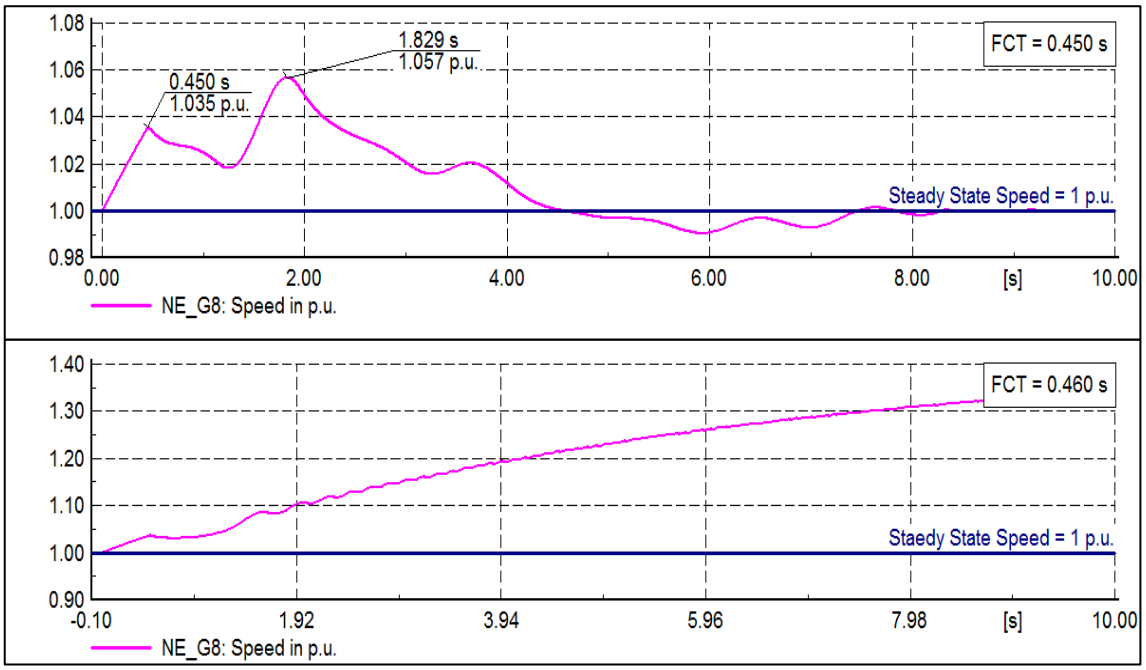

Figure 5.29: Rotor Speed of NE_G8

From figures 5.28 and 5.29 it can be seen that when the fault is cleared at 450 ms, the machine rotor angle and rotor speed have a stable response. On the contrary, when the fault is cleared at 460 ms, the rotor speed increases indefinitely and the rotor angle continuously oscillates between minimum and maximum values of 178 degrees and -178 degrees. This is an indication that NE_G8 went out of step due to pole slip. The results presented in figures 5.19 to 5.21 showed that the CCT of NE_G8 when no HVDC scheme is imbedded into the network is 380 ms. After the integration of the LCC-HVDC scheme into the network, the CCT of NE_G8 increased from 380 ms to 450 ms. It can therefore be concluded that the integration of the LCC-HVDC scheme caused an improvement in the CCT of the network by 70 ms, and thus improved the transient rotor angle stability of Network 2.

5.2.7 Summary

The research methodology as described in chapter 3 has been successfully applied to test Network 2 to determine the CCT and the transient stability state of the network. It was found that the CCT of a particular generator can be determined by either analysing the response of the rotor angle, rotor speed or the power-angle characteristics of that particular machine. From the obtained results, it was found that Network 2 meets the transient stability requirements as stipulated in the SAGC. In this chapter, it was demonstrated that an HVDC scheme can be used to enhance the transient rotor angle stability of a large multi-machine AC network. The methodology presented in chapter 3 and demonstrated in this chapter will therefore also be applied to Eskom's MTS network to determine the CCT of the network and to investigate the impacts that the proposed LCC-HVDC scheme might have on the transient rotor angle and voltage stability of Network 3.

CHAPTER 6: NETWORK 3 ANALYSIS

6.1 Eskom MTS Network Model

The methodology developed in chapter 3 and demonstrated in chapter 5 is applied to Eskom's MTS network for machine rotor angle and busbar voltage transient stability analysis. The impact of HVDC transmission schemes on the power system dynamics is analysed by introducing HVDC transmission schemes at strategic locations in the network.

Network 3 consists of four base load coal fired power stations located in the Limpopo province, which forms part of the Northern transmission grid of South Africa's power grid. The power stations included in this study are: Matimba, Medupi, Coal 2, and Coal 3 power stations. The focus area includes a number of transmission substations and transmission lines that make up the Limpopo-West power transmission corridor. These lines interconnect the substations and load centres in the Limpopo, North-West and Gauteng provinces. The focus area of the network is based on Eskom's 2015-2024 TDP and it represents the envisioned 2021 Northern transmission grid. The network consists of both existing and planned power stations, substations and HV transmission lines.

A detailed network model of Eskom's MTS was used to carry out this study. Power stations under construction and planned power stations, substations, transmission lines and system loads were modelled onto the network. The load estimates are based on the 2015-2024 TDP [1]. Figure 6.1 illustrates the overview diagram of Network 3. The rectifier station is located at Masa substation. The inverter stations are located at Etna and Jupiter substations which form part of the central grid and they are shown in the overview diagram of the central grid, which is presented in figure C1 of appendix C. All the main power stations and substations forming part of the focus area of the network are listed in table 6.1. The updated Eskom's power plant portfolio is shown in appendix E. It should be noted that simulations were run for the entire Eskom MTS network, however, the analysis is only carried out for the network elements in the focus area. This was done to ensure that the effects of all the other generators, HV transmission lines, loads and FACTS devices in the MTS network are taken into consideration in the study and thus making the study more realistic. The letters E and P are designated to each station to distinguish between the Existing and Planned stations.

Table 6.1: Network 3 Stations

Power Stations	765 kV Substations	400 kV Substations	275 kV Substations
Medupi (E)	Ngwedi (P)	Midas (E)	Pelly (E)
Matimba (E)	Selemo (P)	Spitskop (E)	Carmel (E)
Coal 3 (P)	Masa (P)	Pluto (E)	Spencer (E)
Coal 2 (P)		Dinaledi (E)	Watershed (E)
		Bighorn (E)	Warmbad (E)
		Marang (E)	Trident (E)
		Witkop (E)	Ararat (E)
		Borutho (P)	Etna (E)
		Apollo(E)	Jupiter (E)

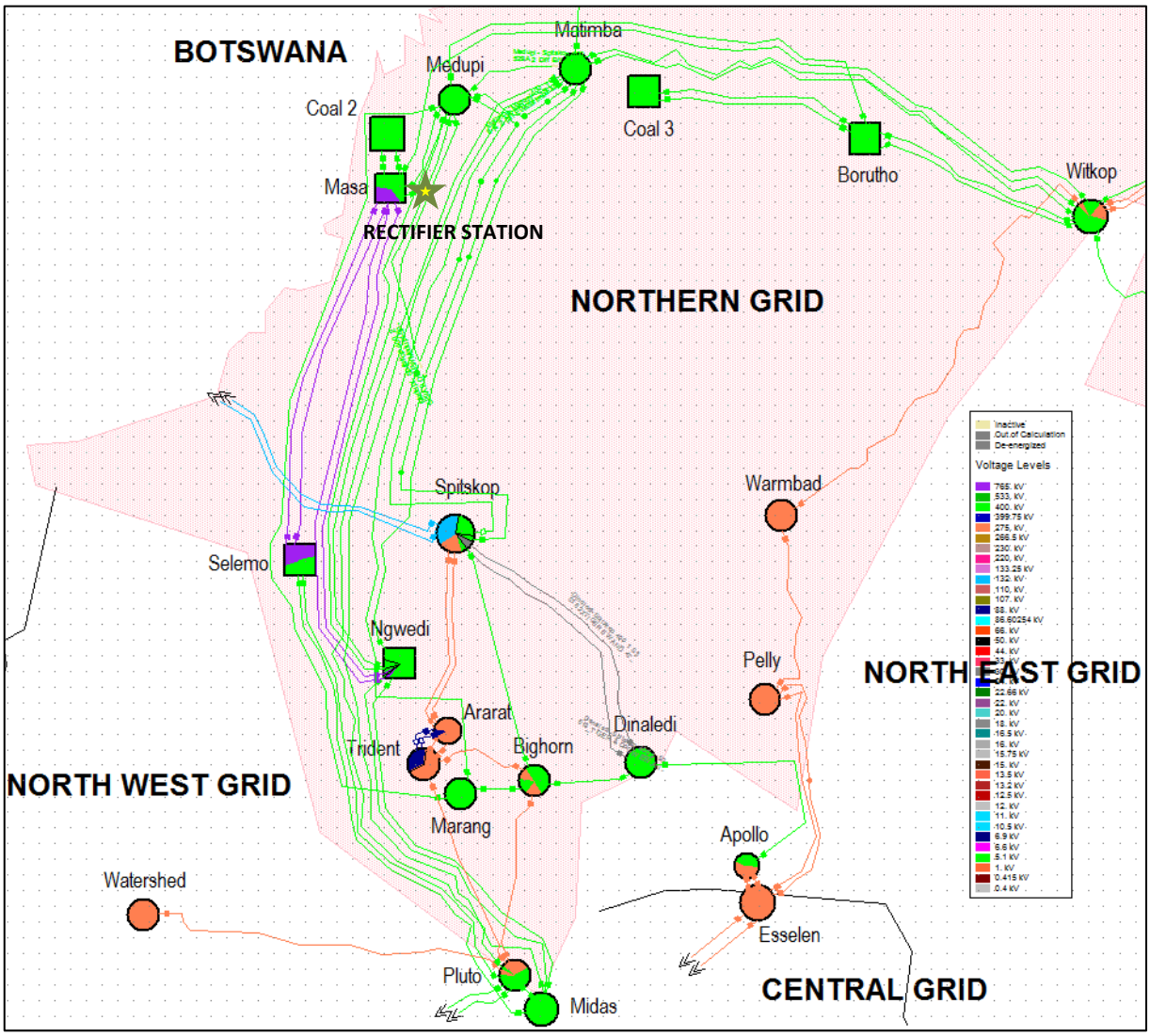

Figure 6.1: Network 3 Overview Diagram

6.2 Network Security Guidelines and Grid Code Requirements

In this research, the integration of the HVDC schemes at different locations of the network will be assessed against the System Operation and Security Guidelines and the requirements as stipulated by the South African Grid Code (SAGC)-The Network Code [65]. Network steady state conditions or system healthy conditions are referred to as (N) contingencies, while system transient state conditions caused by a disturbance on one element of the network, such as the loss of one transmission line or a transformer, are referred to as single contingencies or (N-1) contingencies. This research focuses on analysing (N) and (N-1) contingencies of the network only. Clauses 7.6.1 and 7.6.5 of the Network Code relating to the voltage limits and targets, and integration of power stations into the network stipulates the following:

a) **Voltage Limits:** The minimum and maximum busbar voltages during (N) or worst (N-1) condition should be in the range of 0.95 p.u. to 1.05 p.u.

b) **Thermal Limits:** No transmission line or transformer may exceed its normal rating during system healthy (N) or single contingency (N-1) conditions.

c) **Power Transfer:** With one connecting line out of service (N-1), it shall be possible to transmit the total output of the power station to the system for any system load condition.

d) **Transient Stability:** Transient stability shall be retained for a three-phase line or busbar fault, cleared in normal protection times (100ms), with the system healthy and the most onerous power station loading condition.

These conditions apply to integration of an HVDC scheme into the network because an HVDC scheme is regarded as a bulk power source. The aim of this research is to investigate whether conditions A to D, as mentioned above are satisfied or violated when an HVDC scheme is integrated into Network 3, with the focus of the research being on conditions A and D. In addition to satisfying the grid code requirements, the CCT will be determined to determine the level of rotor angle transient stability of the network, which will allow for a conclusion to be drawn on the magnitude of the impact of the HVDC schemes on the system's transient rotor angle stability.

6.3 Steady State Conditions Analysis of Network 3 without HVDC

Steady state analysis of the network is carried out to establish a base case of the network and to come up with a suitable critical case list of Network 3. This case list will then be used as a guide to carry out the transient state analysis of the worst case scenarios of the network.

6.3.1 Variables of Interest

The variables to be analysed in this study are:

- Generator rotor angle with reference to reference machine angle in degrees
- Generator speed in p.u.
- Generator and busbar active power in MW
- Busbar voltage in p.u.

6.3.2 Thermal Limits

Load Flow Results

The loading of a network element such as a transmission line, transformer, busbar or a generator gives an indication on how great the impact on system stability will be if that particular element is faulted, tripped and taken out of service by the protection equipment. It is important to ensure that the thermal limits of the network elements are not violated during system healthy conditions and worst when the system is subjected to (N-1) contingencies, to avoid damage to equipment. Table 6.2 presents the load flow results for loading of the generators in Network 3. Table 6.3 presents load flow results for MW loading and the line lengths of the main transmission lines in the network. Only the transmission lines rated 765 kV and 400 kV are considered in this study.

Table 6.2: Generator Loading

Matimba Generators	**MW Loading**	**MVAr Loading**	**% Loading**
Gen 1	610	97.8	77
Gen 2	610	97.8	77
Gen 3	610	97.8	77
Gen 4	610	97.8	77
Gen 5	610	-86	77
Gen 6	610	97.8	77
Medupi Generators	**MW Loading**	**MVAr Loading**	**% Loading**
Gen 1	738	249	83
Gen 2	738	249	83
Gen 3	738	249	83

Gen 4	738	249	83
Gen 5	738	249	83
Gen 6	738	249	83
Coal 3 Generators	**MW Loading**	**MVAr Loading**	**% Loading**
Gen 1	188	16.6	85.2
Gen 2	188	16.6	85.2
Gen 3	188	16.6	85.2
Gen 4	188	16.6	85.2
Coal 2 Generators	**MW Loading**	**MVAr Loading**	**% Loading**
Gen 1	188	72.8	91
Gen 2	188	72.8	91
Gen 3	188	72.8	91

Table 6.3: Main Transmission Line Lengths and Loading

Line Name	Rated Voltage (kV)	MW Loading	Length (km)
Matimba-Spitskop_1	400	661	145
Matimba-Pluto_1	**400**	**413**	**342**
Matimba-Witkop_S3	400	203	168
Matimba-Midas_1	**400**	**441**	**367**
Marang-Matimba	400	442	194
Matimba-Ngwedi_1	400	477	156
Matimba-Phokoj_1	400	327	166
Medupi-Marang_1	400	442	270
Medupi-Masa	400	816	20
Medupi-Ngwedi_1	**400**	**1054**	**200**
Medupi-Borutho	400	100	124
Medupi-Spitskop_1	400	612	200
Coal 2-Masa	400	282	40
Coal 3-Borutho	400	376	100
Midas-Selemo	400	500	60
Midas-Ngwedi_2	400	447	200
Marang-Midas_1	400	247	137
Pluto-Midas_1	400	803	22.8
Masa-Witkop	400	74	350
Borutho-Witkop_2	400	422	65
Selemo-Pluto	400	152	80
Masa-Selemo_1	**765**	**571**	**350**
Masa-Ngwedi_1	765	488	180

From table 6.2 it can be observed that the generators in Medupi power station have the highest apparent power loading and the generators in Coal 2 and Coal 3 power stations have the lowest apparent power loadings. The generators at Coal 2 power station have the highest percentage loading, this means that they are close to the overload limit of 100%. It can further be observed that the generators in each of the four power stations are identical. It is a preferred practice in industry to have identical generating units in a power station. Having identical generators in a power station allows the maintenance team of that particular power station to develop great skills and expertise and gain good experience in operating, maintaining and repairing of that particular type of generator.

Table 6.3 presents load flow results for the MW loading of the main transmission lines in the network, as well as the line lengths. System transient instability is caused by a lack of synchronizing power to counter balance the difference between the input mechanical power and output electrical power. It is therefore expected that the most server line fault in the system would be a fault that occurs on a highly loaded transmission line transporting power over a long distance. The four transmission lines with high MW loading and long line lengths are bolded in table 6.3. Because the impact of a line fault on the generator transient stability does not only depend on the line loading and line length but also on the location of the line, such as how close the line is to the power stations under study, how low the fault impedance is and how the line is interconnecting the networks, a solid three-phase fault was simulated on each of the four lines to determine their impacts on system transient stability. A solid three-phase fault was also simulated on each of the generation station busbars to determine the most critical generator busbar fault in the system. The obtained results are presented in appendix B. From the obtained results, it was found that the most critical line fault is the three-phase fault on line Matimba-Midas 400_1, and the most critical generator busbar fault is a three-phase fault on Medupi 400 BB1.

6.3.3 Voltage Limits

Load Flow Results

The load flow results for the main substation busbar voltages during system healthy (N) conditions are shown in table 6.4. It can be seen that except for the Ngwedi 400 BB1 voltage, the voltage levels at all the other substation busbars are within the limits as stipulated in the network code.

Table 6.4: Substation Busbar Voltage Levels

Busbar Voltage Levels			
Busbar Name	**Voltage Level (p.u.)**	**Busbar Name**	**Voltage Level (p.u.)**
Medupi 400 BB1	1.01	Spitskop 400 BB	0.96
Matimba 400 BB1	1.01	Midas 400 BB2	0.97
I Coal 3 400 BB	1.05	Pluto 400 BB1	0.99
I Coal 2 400 BB1	1.01	Borutho 400 BB2	1.04
Bighorn 400 BB1	0.98	Leseding 400 BB	1.03
Dinaledi 400 BB1	0.98	Witkop 400 BB1	1.04
Marang 400 BB1A	1.01	Ngwedi 765 BB1	1.03
Masa 400 BB1	1.00	Selemo 765 BB1	1.02
Ngwedi 400 BB1	0.91	Masa 765 BB1	1.04
Selemo 400 BB1	1.01	Etna 275 BB1	1.00
Medupi 400 BB1	1.01	Jupiter 275 BB1	1.03

6.3.4 Busbar Fault Levels

The busbar fault levels indicate the strength of a busbar. A busbar with a high fault level (MVA and kA) is considered to be a strong busbar. A strong busbar has the ability to maintain its voltage levels close to the steady state value after being subjected to a transient condition in the system. Maintaining the voltage levels after a contingency in the system allows for a reduction in power swings at the busbar. The reference machine of a power system should therefore be connected to the strongest busbar (with highest fault level) in the system.

When connecting a new element to the network, it is important to make sure that the network fault levels are limited within the fault current ratings of the installed network equipment. Using the IEC 60909 method of short circuit calculation for a three-phase short circuit with a short circuit duration of 0.1 s break time and 1.0 s fault clearing time, a short circuit calculation simulation was run in DIgSILENT PowerFactory to determine the short circuit current levels (fault levels) at the generator busbars of all the power stations in Network 3. The obtained results are presented in table 6.5.

Table 6.5: Generator Busbar Fault Levels

Busbar Name	**Fault Level (MVA)**	**Fault Current (kA)**
Drakensberg 400 BB	4 566	6.59
Majuba 400 BB	28 206	40.7
Arnot 400 BB	23 697	33.3
Duvha 400 BB1	**36 697**	**53**
Hendrina 400 BB1	24 759	35.7
Kendal 400 BB1	30 858	45
Komati 275 BB1	10 297	21.6
Kriel 400 BB1	30 222	43.6
Kusile 400 BB1A	10 816	15.6
Matla 400 BB1S	26 421	38.1
Sasol 132 BB1	5 365	23.5
Tutuka 400 BB2	**36 690**	**53**
Matimba 400 BB	34 221	49.4
Coal 2 400 BB1	15 866	23
Coal 3 400 BB1	8 090	11
Medupi 400 BB1	36 056	52
Koeberg 400 BB1	15 788	22.8

Table 6.5 shows that Duvha power station 400 kV BB1 and Tukuta power station 400 kV BB1 have the highest fault levels, with Duvha 400 kV BB1 having fault levels of 36 697 MVA and 53 kA. Duvha Gen 1 was therefore chosen as the reference machine of the entire Eskom network. The rotor angles of all the generators in Network 3 are measured with reference to the rotor angle of Duvha Gen. 1. The reference machine is also used for electric power balance in the network.

6.3.5 Steady State Generator Rotor Angle and Rotor Speed

The rotor angle transient stability level of a network is determined by analysing the response of the generator rotor angles with reference to a rotating reference. For the purpose of network model validation, and to ensure that the network generators are in a stable operation mode during steady state conditions of the network, a simulation was run to determine the steady state rotor angle values of all the generators in the power stations of Network 3. The obtained results are presented in figures 6.2 and 6.3.

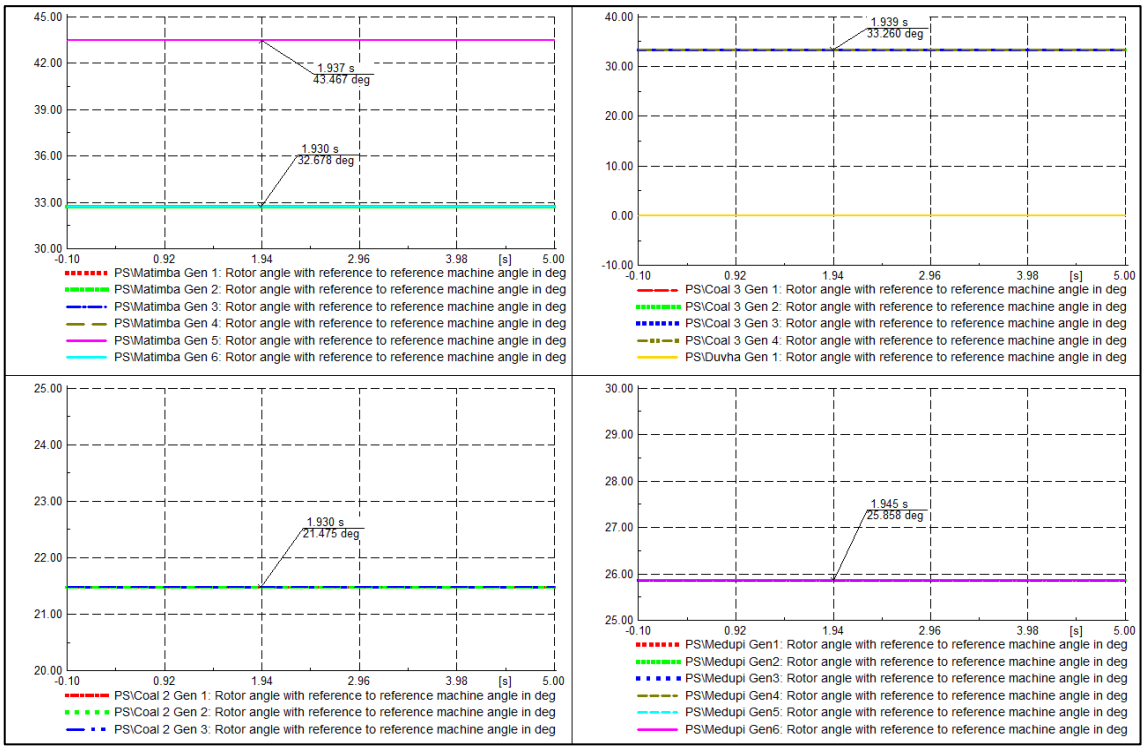

Figure 6.2: Machine Rotor Angle Response

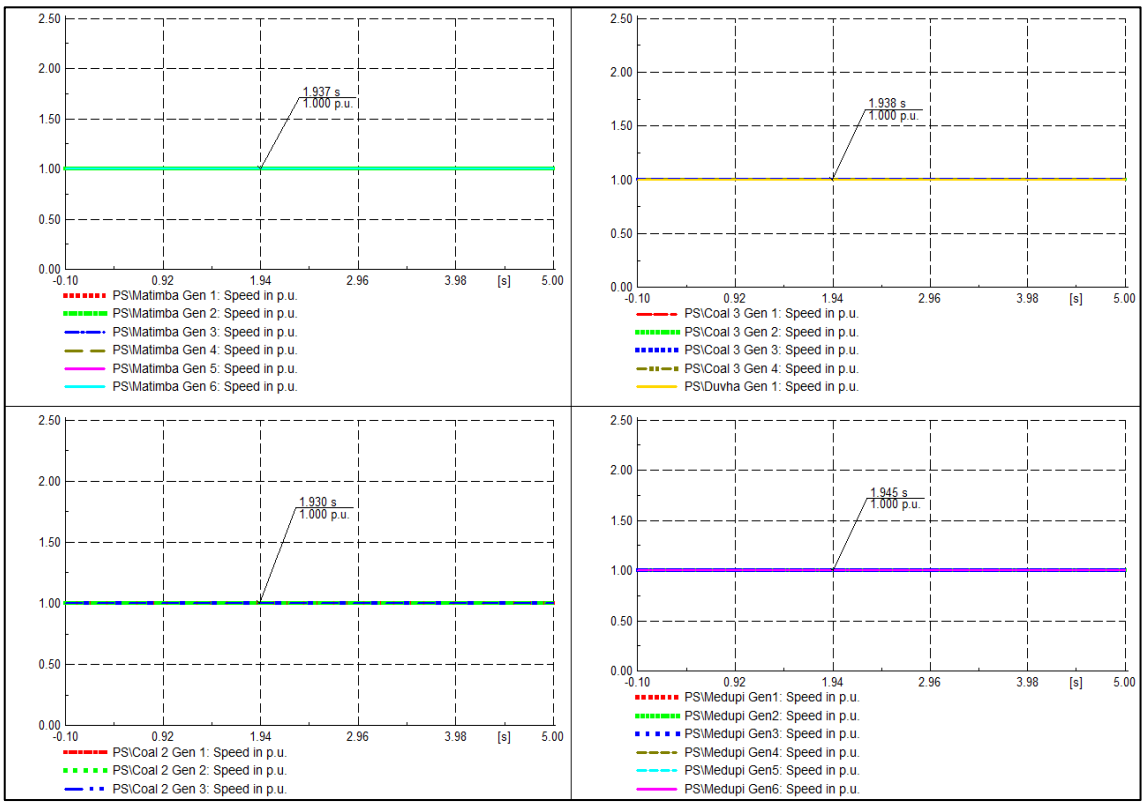

Figure 6.3: Machine Rotor Speed Response

From figure 6.2, on the graph showing the rotor angles of Coal 3 generators and Duvha Gen 1, it can be seen that the rotor angle value of the reference machine (Duvha Gen1)

is zero degrees as expected. From the obtained results it can further be observed that during steady state conditions, all the generators in the system maintain their steady state rotor angle and rotor speed values over the simulated time period as expected. It can further be seen that the rotor angles and rotor speed curves for the various machines in each of the power stations overlap each other. This is an indication that each power station consists of identical generating units.

6.3.6 Critical Case List and Switching Events

The critical case list of Network 3 is presented in table 6.6.

Table 6.6: Network 3 Critical Case List and Switching Events

Pre-Fault System Conditions	
Generator Controls	PSS and AVR in service
System Loading	Peak load
System Generation	All generators in service
Reactive Power Compensation	TX line reactors and SVCs in service
Lines out of Service	All lines in service
Load Models	Constant current, voltage dependent
Fault Condition 1	
Fault Type	Solid three-phase short circuit
Initial Fault Duration	100 milliseconds
Fault Location	End (98%) of Matimba-Midas TX line
Fault Impedance	0 ohms
Fault Condition 2	
Fault Type	Solid three-phase short circuit
Initial Fault Duration	100 milliseconds
Fault Location	Medupi 400 kV BB1
Fault Impedance	0 ohms
Switching Events	
Fault Occurring Time	0 seconds
Fault Clearing Time	100 milliseconds
Switching Type	Fault clearing event or opening and closing of the line circuit breakers

6.4 Transient Analysis of Network 3 without LCC-HVDC Integrated

Using the critical case list presented in table 6.6 as a guide, the single contingency conditions (N-1) identified as the most severe were induced into the system and simulated to analyse the transient rotor angle stability, transient voltage stability as well as the thermal limits of the network elements when no HVDC scheme is integrated into the network. Fault condition 1 (line fault) was used to analyse the thermal and voltage limits of the network. The thermal and voltage limits of the network elements were analysed by using the contingency analysis method of analysing abnormal system conditions. In electrical network planning, contingency analysis is used to examine the performance of a power system and the need for new transmission expansion due to load growth or generation expansion [66]. Contingency analysis is the evaluation of violations in the system operating states (if any) that certain contingencies can pose to the electrical power system. In system operation therefore, contingency analysis assists power systems engineers to operate the system at a secure operating point at which equipment are loaded within their safe limits and power is delivered to consumers at acceptable quality standards [66, 67]. Contingency analysis is carried out by executing an outage (fault) of a network element or groups of elements, and then evaluating the post-fault load flow results to check for voltage and loading (thermal) limits violations of the network elements. The contingency analysis tool bar in DIgSILENT PowerFactory was used to carry out the analysis of the network equipment thermal and voltage limits. Based on the SAGC requirements, the voltage and thermal limits were set in the contingency analysis tab for the defined contingency. The equipment voltage and loading levels were designated with various colours as shown in figure 6.4. The contingency analysis report was set as shown in figure 6.5.

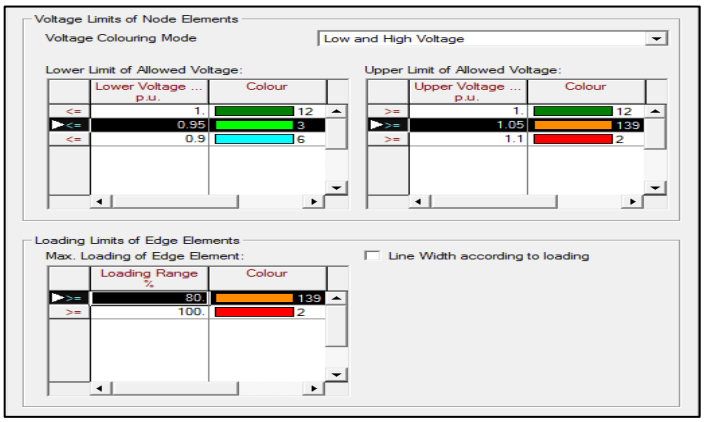

Figure 6.4: Voltage and Thermal Limits Colour Coding

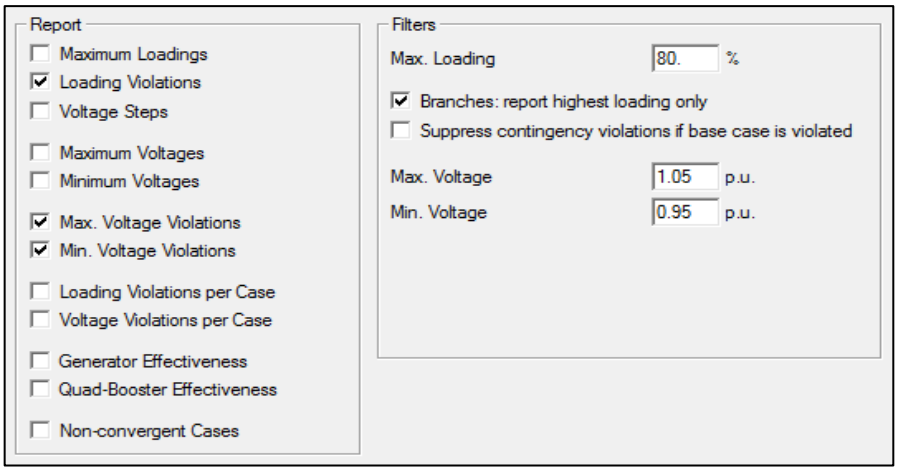

Figure 6.5: Contingency Analysis Report Settings

From figure 6.5 it can be seen that the maximum loading limit was set to 80% loading of the elements. The maximum overloading limit is 100%. Any network element with loading greater than 80% is considered to have violated the loading limit. However, only elements that exceed the 100% overloading limit are considered to be critical cases and requires immediate attention. The voltage limits were set are as shown in figure 6.5.

The load flow results obtained in section 6.3 are considered to be the base case results of the study. The contingency analysis tool bar in DIgSILENT power factory compares the post-fault load flow results to the base case results to quantify the step change in the variables being analysed (voltage or loading) and to determine whether the pre-defined limits have been violated, either during the base case (N) or during the post-fault (N-1) conditions.

Both fault conditions 1 and 2 were used to analyse the transient rotor angle stability of the network. This was done to determine the CCT of the system under these single contingency conditions when no HVDC transmission scheme is integrated into the system.

6.4.1 Thermal Limits

The (N-1) contingency analysis results for evaluation of the network elements thermal limits is presented in figure 6.6. It is important to mention that the contingency analysis for the outage of transmission line Matimba-Midas 1 was performed for the entire Eskom MTS network, however, due to the large number of network elements, only the network elements in the focus area (Network 3) are analysed and discussed in this study.

Contingency Analysis Report: Loading Violations

Study Case: Matimba-Midas
Result File: Contingency Analysis AC

Loading Limit: 80.0
Overloading Limit: 100

	Component	Branch, Substation or Site	Loading Continuous [%]	Loading Short-Term [%]	Loading Base Case [%]	Contingency Number	Contingency Name	Base Case and Continuous Loading [0.0 % - 171.7 %]
1	Midas 400/132/22 T1	Midas	166.72	166.72	166.72	-1	Base Case	
2	Coal 2 Gen TRF 2	Coal 2 Power Station	91.69	91.69	90.85	1	Matimba-Midas 400_1	
3	Coal 2 Gen TRF 2	Coal 2 Power Station	90.85	90.85	90.85	-1	Base Case	
4	Medupi-Ngwedi 400_1		91.57	91.57	87.62	1	Matimba-Midas 400_1	
5	Medupi-Ngwedi 400_1		87.62	87.62	87.62	-1	Base Case	
6	Midas-Pluto 400_1		86.12	86.12	74.11	1	Matimba-Midas 400_1	
7	Coal 3 Gen TRF 3	Coal 3 Power Station	85.84	85.84	85.70	1	Matimba-Midas 400_1	
8	Coal 3 Gen TRF 3	Coal 3 Power Station	85.70	85.70	85.70	-1	Base Case	

Figure 6.6: Loading Violations

The elements that violate the 80% loading limit after the network has been subjected to fault condition 1 are shown in figure 6.6. The three-winding transformer, Midas 400/132/22 T1 is overloaded to 167%. In order to avoid possible thermal damage to this transformer, its nominal apparent power rating needs to be upgraded. The other 7 elements violate the 80% limit but they do not exceed the 100% overloading limit, and therefore, they are not considered to be critical cases.

6.4.2 Voltage Limits

Contingency Analysis Report: Minimum Voltage Violations

Study Case: Matimba-Midas
Result File: Contingency Analysis AC

Min. Voltage 0.950
Min.Voltage Limit: 0.95

	Component	Branch, Substation or Site	Voltage Min. [p.u.]	Voltage Step [p.u.]	Voltage Base [p.u.]	Contingency Number	Contingency Name	Base Case and Post Voltage [0.865 p.u. - 0.971 p.u.]
1	Ngwedi 400 BB2A	Ngwedi	0.89	-0.02	0.91	1	Matimba-Midas 400_1	
2	Ngwedi 400 BB2A	Ngwedi	0.91	0.00	0.91	-1	Base Case	
3	Midas 400 BB B2	Midas	0.94	-0.03	0.97	1	Matimba-Midas 400_1	
4	Midas 400 BB B1	Midas	0.94	-0.03	0.97	1	Matimba-Midas 400_1	
5	Spitskop 400 BB1A	Spitskop	0.95	-0.01	0.96	1	Matimba-Midas 400_1	
6	Spitskop 400 BB2A	Spitskop	0.95	-0.01	0.96	1	Matimba-Midas 400_1	

Figure 6.7: Minimum Voltage Violations

The minimum voltage limit violations are shown in figure 6.7. The 400 kV busbar at Ngwedi substation violates the minimum voltage limit during both the base case (N) and during (N-1) contingency conditions. During (N) conditions, the voltage at Ngwedi

400 BB2A is 0.91 p.u. during (N) conditions and during (N-1) conditions it drops to 0.89 p.u. During (N) contingency conditions, the voltage at Midas 400 kV BB1 and BB2 is 0.97 p.u., during (N-1) conditions, the voltage drops to 0.94 p.u. Reactive power compensation devices such as shunt capacitors need to be installed at these busbars, for voltage support during (N-1) conditions.

Contingency Analysis Report: Maximum Voltage Violations

Study Case: Matimba-Midas
Result File: Contingency Analysis AC

Max. Voltage 1.050
Max. Voltage Limit: 1.05

	Component	Branch, Substation or Site	Voltage Max. [p.u.]	Voltage Step [p.u.]	Voltage Base [p.u.]	Contingency Number	Contingency Name	Base Case and Post Voltage [1.051 p.u. - 1.082 p.u.]
1	Witkop 275 BB1	Witkop	1.08	0.00	1.08	-1	Base Case	
2	Witkop 275 BB1	Witkop	1.07	0.00	1.08	1	Matimba-Midas 400_1	
3	Warmbad-Witkop 275_1 SP2	Warmbad-Witkop 275_1	1.07	0.00	1.07	1	Matimba-Midas 400_1	
4	Tabor 275 BB2	Tabor	1.07	0.00	1.07	-1	Base Case	
5	Apollo 275 DS BB1	Apollo	1.06	0.00	1.06	-1	Base Case	
6	Masa 765 BB1	Masa	1.06	0.00	1.06	-1	Base Case	
7	Matimba 20 Gen 5	Matimba Power Station	1.05	-0.01	1.06	1	Matimba-Midas 400_1	

Figure 6.8: Maximum Voltage Violations

The maximum voltage violations are shown in figure 6.8. In total, seven elements violate the maximum limit of 1.05 p.u. From the report, it can be seen that apart from the 20 kV generator busbar of Matimba Gen 5, the other six elements violate the maximum voltage limit during both the base case and the post-fault system operation conditions. The voltage levels at these busbars are not affected by the simulated contingency. This is evident because the voltage step values for these busbar voltages are zero. The voltage level at Matimba 20 kV Gen 5 BB decreases from 1.06 p.u. to 1.05 p.u. after the simulated contingency. This amounts to a voltage step value of -0.01 p.u.

It is important to note that most of the elements (busbars) that violated the maximum voltage limit have voltage ratings below 400 kV. This research focuses on voltage levels greater than or equal to 400 kV.

6.4.3 Transient Rotor Angle Stability

Fault Condition 1 Results

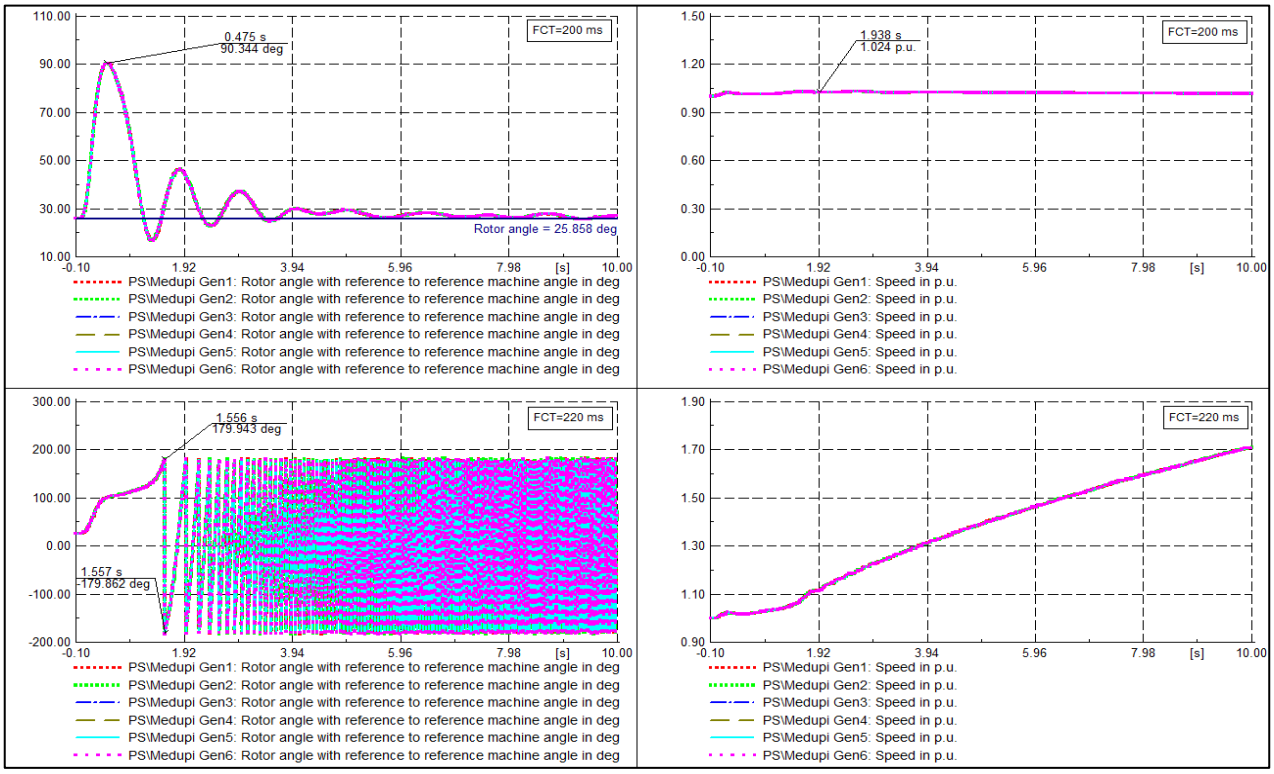

Figure 6.9: Medupi Angle and Speed

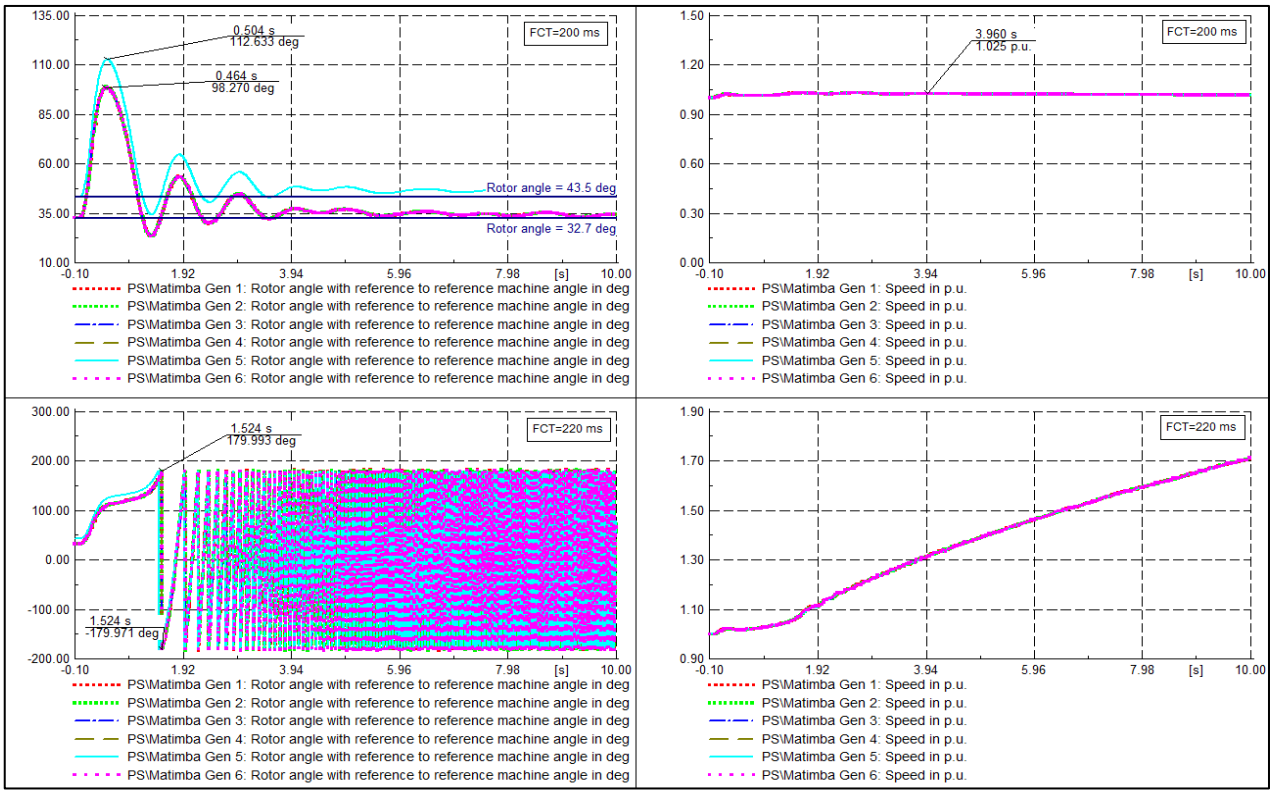

Figure 6.10: Matimba Angle and Speed

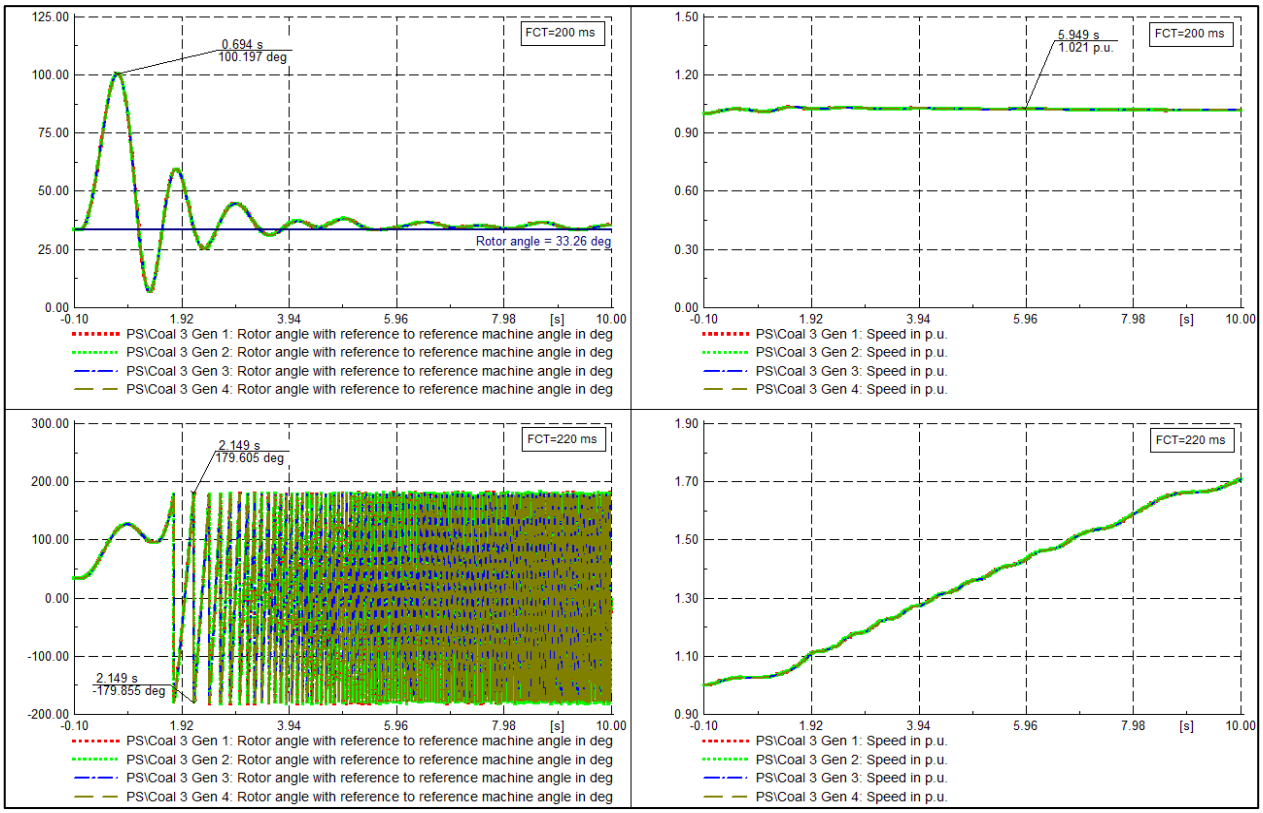

Figure 6.11: Coal 3 Angle and Speed

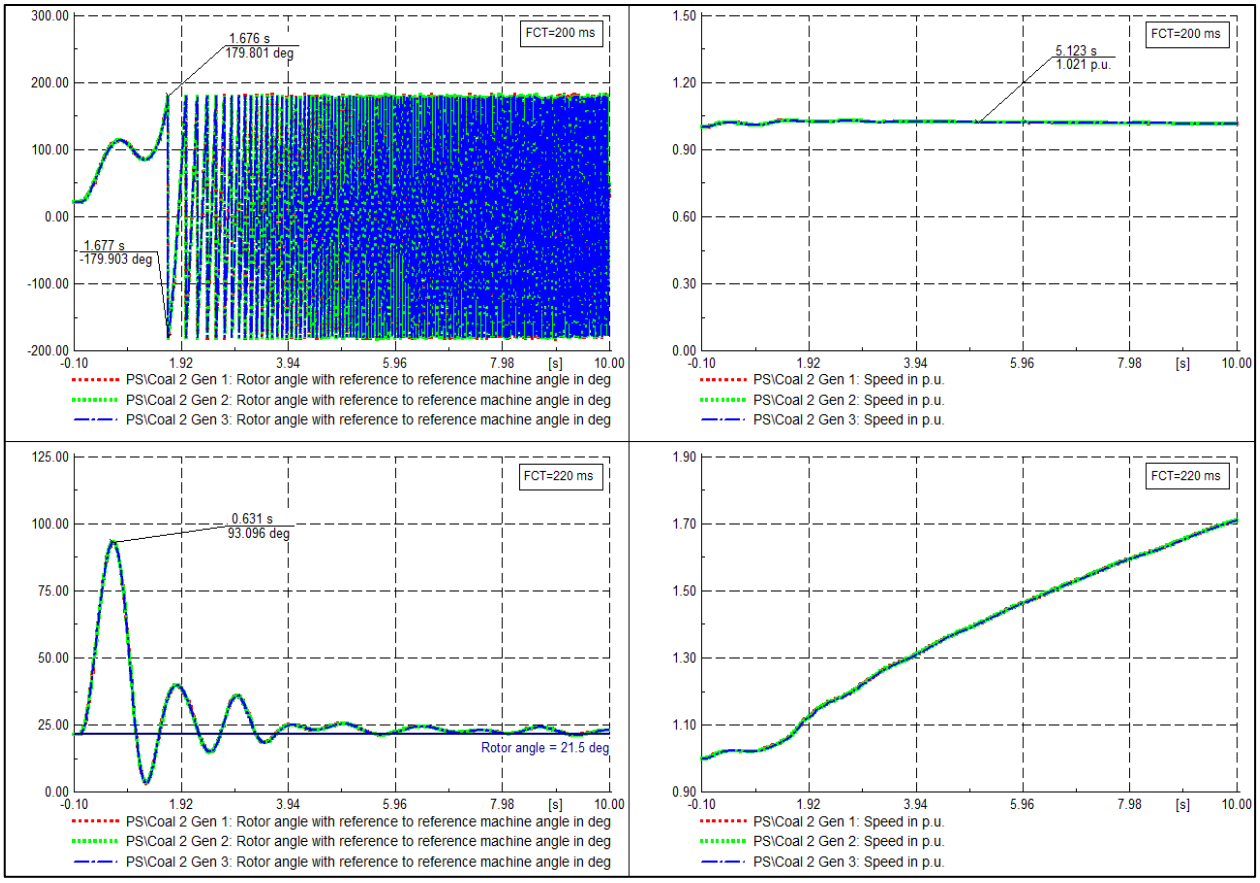

Figure 6.12: Coal 2 Angle and Speed

The graphs shown in figures 6.9 to 6.12 presents the response of the rotor angles and rotor speeds of all the machines in the four power stations, when subjected to fault condition 1 (Matimba-Midas 400kV line fault). The simulated fault was cleared at different FCTs in order to determine the CCTs of all the machine in the power system. From the results, it can be seen that when the fault is cleared at 200 ms, all the machines in Network 3 remain transiently stable. When the FCT is increased to 220 ms, it was observed that the machine rotor speed increases indefinitely after the fault has been cleared. The rotor angles of all the machines in the network oscillate indefinitely between the maximum and minimum values of approximately 180 degrees and -180 degrees. This is an indication that the generators in the network have gone out of step due to pole slip. It can therefore be concluded that the CCT of the machines in Network 3, for fault condition 1 is 200 ms.

Fault Condition 2 Results

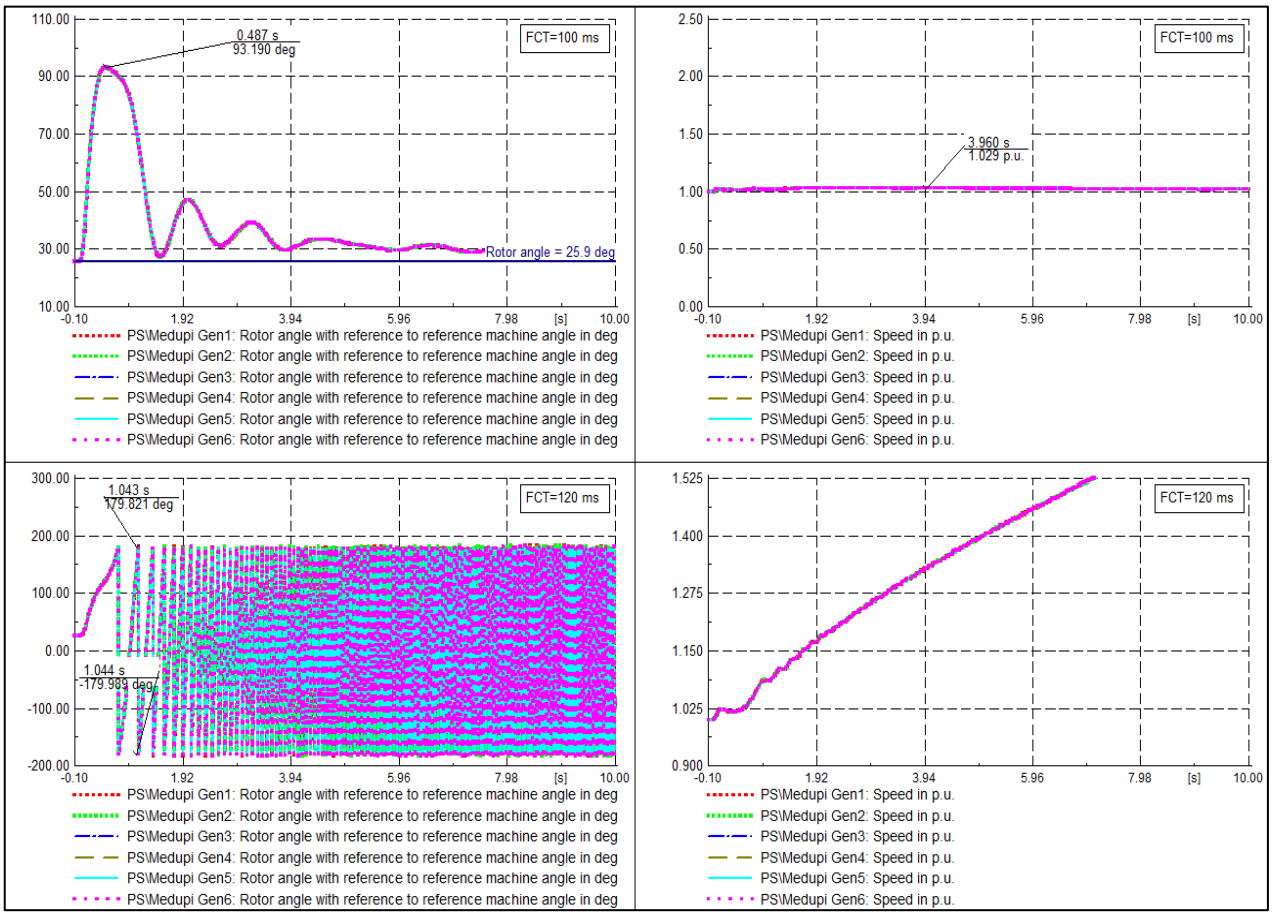

Figure 6.13: Medupi Angle and Speed

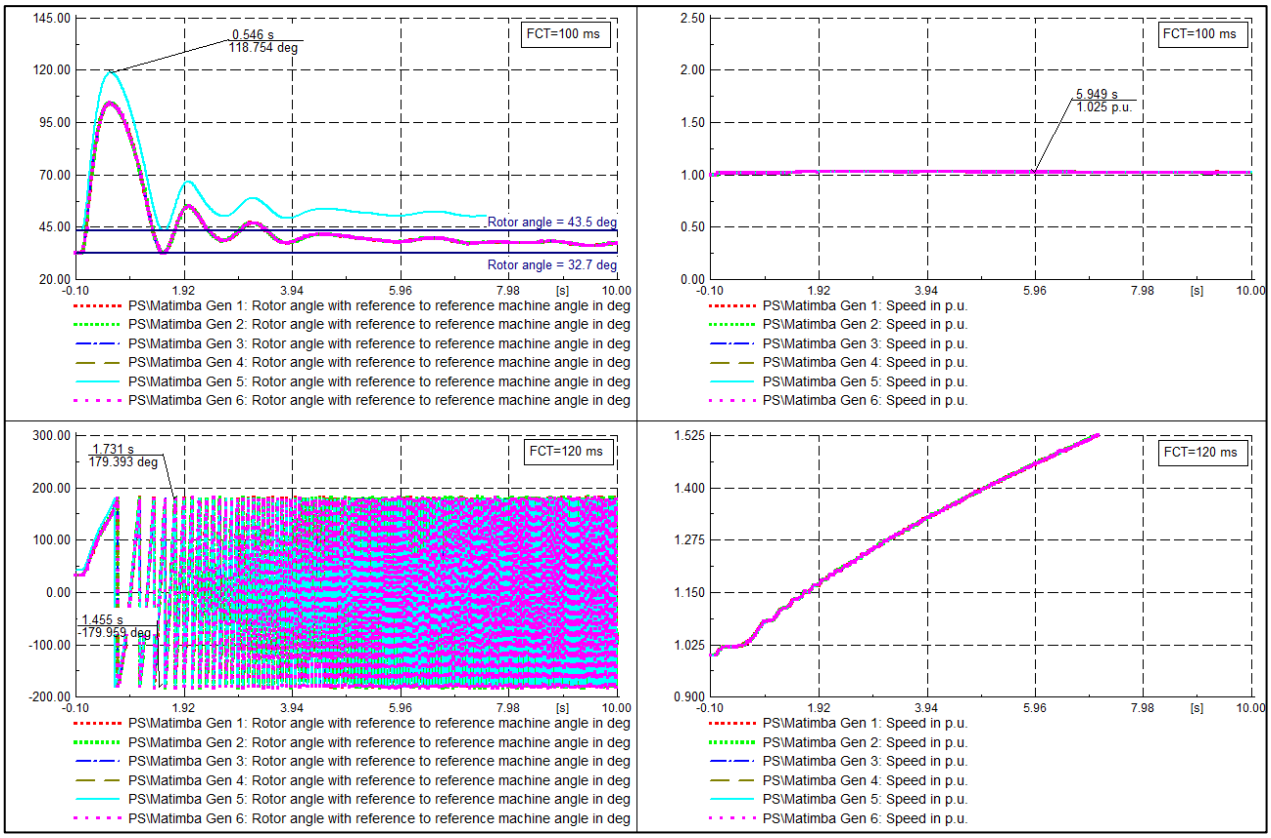

Figure 6.14: Matimba Angle and Speed

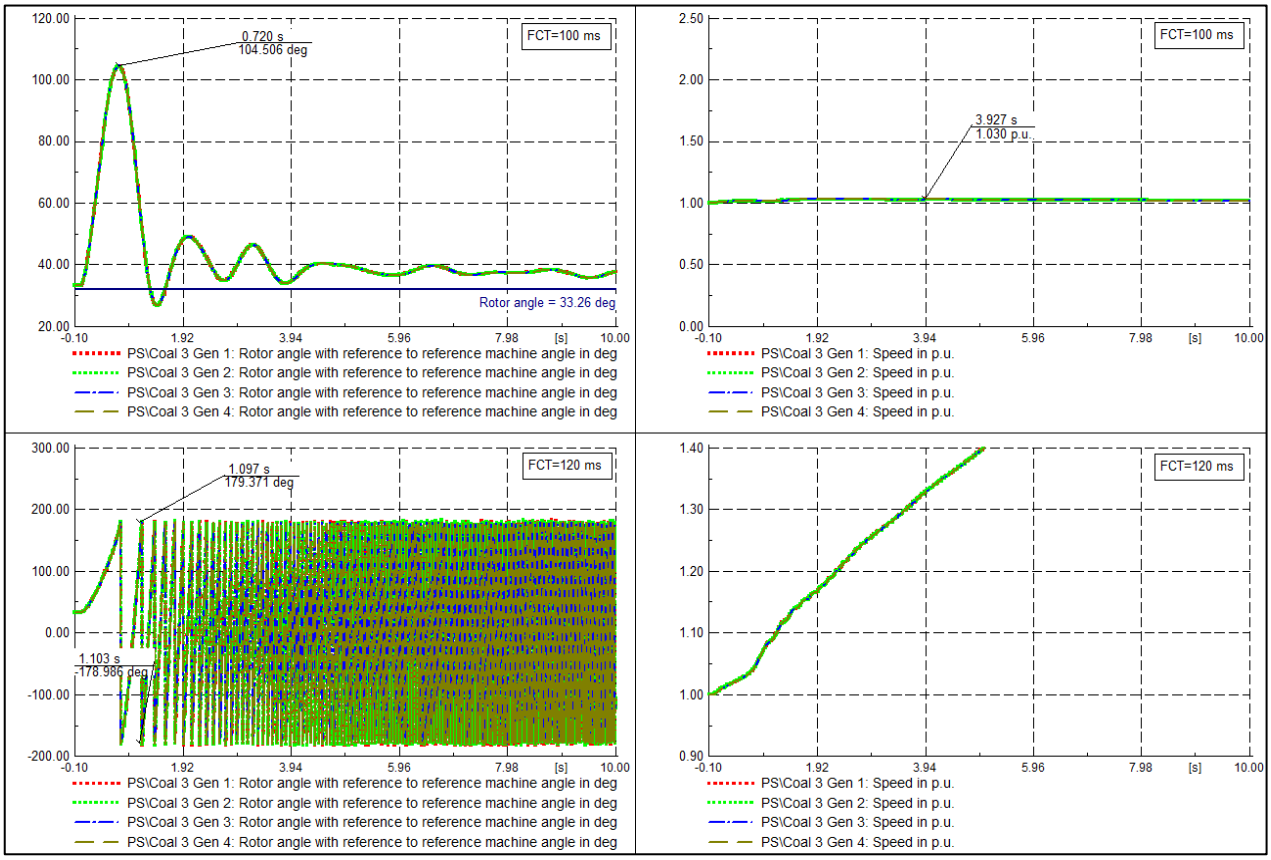

Figure 6.15: Coal 3 Angle and Speed

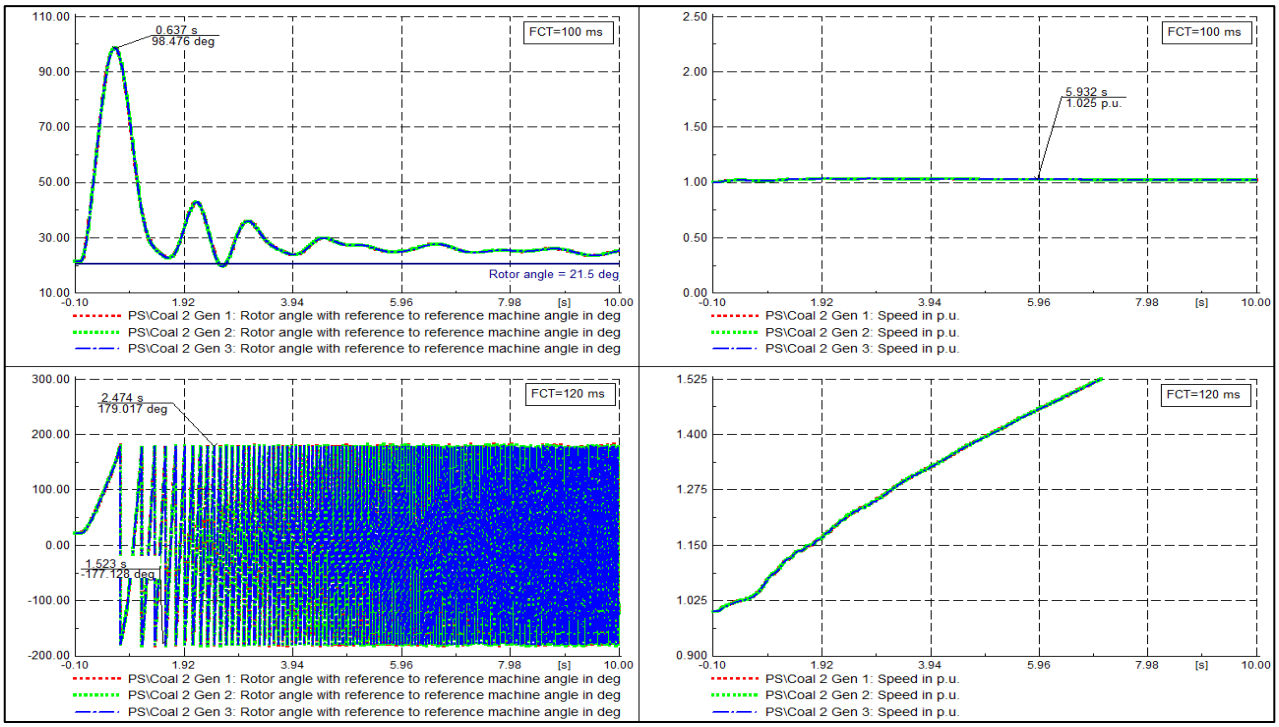

Figure 6.16: Coal 2 Angle and Speed

The graphs shown in figures 6.13 to 6.16 present the response of the rotor angle and rotor speed of the machines when a solid three-phase short circuit is simulated at Medupi 400 BB1. It can be observed that when the FCT is set to 100 ms, all the machines remain transiently stable. When the FCT is increased to 120 ms, the machines go out of step due to pole slip. It can therefore be concluded that when a solid three-phase short circuit is simulated on the 400 kV BB1 at Medupi power station, the CCT is 100 ms. The three-phase fault at Medupi 400 kV BB1 drastically reduces the system CCT, and therefore, it can be said that it has a more severe impact on the machines transient rotor angle stability compared to a solid three-phase fault on line Matimba-Midas 400_1. From the results presented in sub-sections 6.3.2 and 6.3.5, as well as the results obtained from the results output window which is presented in figure B1 of appendix B, it can be observed that for the simulated system faults, all the generators have a similar response, such that, the four power stations loose synchronism almost at the same time. This means that the simulated faults have a similar impact on all the generators in the four power stations. This was expected because the power stations being studied are in very close proximity to each other and therefore a severe fault in the system would have a similar impact on the machines. It has therefore been decided that for the subsequent analysis to be done in this study, only the response of generators in one power station (Medupi) will be analysed. Since the generators at Medupi power

station are all identical, only one generator in the power station needs to be analysed and studied for transient rotor angle stability.

6.5 Transient Analysis of Network 3 with LCC-HVDC Integrated

Different system operation scenarios of Network 3 with LCC-HVDC schemes integrated into the network were studied. The variations done on the HVDC scheme included: change of line length, change of the value of the steady state power transmitted by the LCC-HVDC scheme and change of the location of the HVDC scheme. It is important to note that because the presented HVDC schemes uses the earth as a return path of the current, the location of the converter stations is highly dependent on the suitability of installation of earth electrodes in the area where the converter stations are to be located. It was therefore assumed that all the locations chosen for placement of converters in this study are suitable for installation of earth electrodes. It is important to note that the LCC-HVDC line lengths and DC power transmitted is dependent on the network topology and steady state conditions of the network. The details of the different LCC-HVDC scenarios studied are as follows:

a) **New long LCC-HVDC with low steady state power**

   A new monopole LCC-HVDC scheme was imbedded into the network to transmit power from Medupi power station to Midas substation, in parallel with the existing HVAC lines. Line length is 368 km, and the DC power transmitted is 800 MW.

b) **New medium length LCC-HVD with low steady state power**

   A new monopole LCC-HVDC scheme was imbedded in the network to transmit power from Medupi power station to Ngwedi substation, in parallel with the existing HVAC lines. Line length is 200 km, and the DC power transmitted is 800 MW

c) **Replacing HVAC with long LCC-HVDC with very low steady state power**

   HVAC transmission line Matimba-Pluto_1 was replaced with a monopole LCC-HVDC scheme. Line length is 342 km, transmitted power is 450 MW.

d) **Replacing HVAC with medium length LCC-HVDC with medium steady state power**

   HVAC transmission line Medupi-Ngwedi_1 was replaced with a bi-polar LCC-HVDC scheme. Line length is 200 km, transmitted power is 1040 MW.

e) **New long LCC-HVDC with high steady state power**

In this scenario, a bi-polar LCC-HVDC scheme was used to transmit power from Medupi power station to Apollo substation. Line length is 500 km, transmitted power is 1400 MW.

f) **New long LCC-HVDC with very high steady state power**

This is the proposed LCC-HVDC scheme that was described in detail in chapter 3, in which two bi-polar LCC-HVDC schemes are used to transmit power from Masa substation to Etna and Jupiter substations in the central grid. Each bi-polar LCC-HVDC scheme transmits 2000 MW over a distance of approximately 600 km. Total power transmitted by the scheme during system healthy conditions is 4000 MW.

It should be noted that the two fault conditions, except for the fault duration, were left unchanged during the different network operation scenarios.

6.5.1 Fault Levels

In order to observe the effect of the integrated LCC-HVDC schemes on the network fault levels, the fault levels of Network 3 were calculated, with the system having a network configuration as described in scenario F. The results are presented in table 6.7.

Table 6.7: Generator Busbar Fault Levels

Busbar Name	**Fault Level (MVA)**	**Fault Current (kA)**
Drakensberg 400 BB	4 566	6.59
Majuba 400 BB	28 205	40.7
Arnot 400 BB	23 106	33.4
Duvha 400 BB1	**36 692**	**53**
Hendrina 400 BB1	24 763	35.7
Kendal 400 BB1	30 865	45
Komati 275 BB1	10 295	21.6
Kriel 400 BB1	30 222	43.6
Kusile 400 BB1A	10 816	15.6
Matla 400 BB1S	26 421	38.1
Tutuka 400 BB2	**36 683**	**53**
Matimba 400 BB	34 111	50
Coal 2 400 BB1	15 839	23
Coal 3 400 BB1	8 070	12
Medupi 400 BB1	35 259	52
Koeberg 400 BB1	15 788	22.8

Comparing tables 6.7 and 6.5, it can be seen that the busbar fault level values remain very close to the values obtained when there was no HVDC scheme integrated into the network. This is an indication that the integrated LCC-HVDC scheme do not have a significant effect on the busbar fault levels of the network.

6.5.2 Thermal Limits

The impact of integrating the LCC-HVDC schemes into Network 3, as described in scenario F, on the thermal limits of the various elements in the network was analysed. The (N) and (N-1) contingency analysis report is shown in figure 6.17.

Contingency Analysis Report: Loading Violations

Study Case: Matimba-Midas
Result File: Contingency Analysis AC

Loading Limit: 80.0
Overloading Limit: 100

	Component	Branch, Substation or Site	Loading Continuous [%]	Loading Short-Term [%]	Loading Base Case [%]	Contingency Number	Contingency Name	Base Case and Continuous Loading [0.0 % - 487.6 %]
1	Midas 400/132/22 T1	Midas	253.21	253.21	253.21	-1	Base Case	
2	Midas 400/132/22 T2	Midas	251.33	251.33	251.33	-1	Base Case	
3	Medupi-Masa 400_1		127.09	127.09	126.04	1	Matimba-Midas 400_1	
4	Medupi-Masa 2		127.09	127.09	126.04	1	Matimba-Midas 400_1	
5	Apollo 275/107 T5	Apollo	86.37	86.37	86.34	1	Matimba-Midas 400_1	
6	Medupi Gen T1	Medupi Power Station	86.37	86.37	85.90	1	Matimba-Midas 400_1	
7	Coal 3 Gen TRF 3	Coal 3 Power Station	85.99	85.99	85.92	1	Matimba-Midas 400_1	
8	Matimba 420/20 Gen4 T4	Matimba Power Station	85.31	85.31	84.90	1	Matimba-Midas 400_1	
9	Apollo-Pluto 400_1 S1		82.08	82.08	81.62	1	Matimba-Midas 400_1	

Figure 6.17: Loading Violations

From the report it can be seen that, in total nine elements violate the set thermal limit. Six of the elements are within the acceptable loading margin of 80%-100%. The two transformers, Midas 400/132/22 T1 and T2 and the two transmission lines that transmit power from Medupi power station to Masa substation violates the overloading limit of 100%. The worst case reported is that of the parallel transformers Midas 400/132/22 T1 and T2 which have a loading of 243%, both for the system healthy (N) contingency and the line outage contingency (N-1). The transmission lines have a percentage loading of 127%. For successful integration of the HVDC schemes into the network, the overloaded elements need to be upgraded. Comparing figure 6.17 to figure 6.6 it can be observed that there is a general increase in the network element loadings during system healthy conditions. The HVDC scheme allows for a higher power transfer before, during and post-fault, and this causes higher loading of the elements in the vicinity of the inverters.

6.5.3 Voltage Limits

Contingency Analysis Report: Minimum Voltage Violations

Study Case: Matimba-Midas
Result File: Contingency Analysis AC

Min. Voltage: 0.950
Min.Voltage Limit: 0.95

	Component	Branch, Substation or Site	Voltage Min. [p.u.]	Voltage Step [p.u.]	Voltage Base [p.u.]	Contingency Number	Contingency Name	Base Case and Post Voltage [-1.021 p.u. - 0.956 p.u.]
1	Ngwedi 400 BB2A	Ngwedi	0.89	-0.01	0.91	1	Matimba-Midas 400_1	
2	Midas 400 BB B3	Midas	0.93	-0.02	0.95	1	Matimba-Midas 400_1	
3	Spitskop 400 BB1C	Spitskop	0.95	-0.01	0.96	1	Matimba-Midas 400_1	

Figure 6.18: Minimum Voltage Violations

Figure 6.18 shows the minimum voltage limit violations of the elements in Network 3 when the LCC-HVDC scheme as described in scenario F is integrated into the network. Comparing figure 6.18 to figure 6.7, it can be observed that there is a decrease in the number of elements that violate the minimum voltage limit. Ngwedi 400 BB2A violates the minimum voltage limit both during the base case (N) contingency and during (N-1) contingency operation. Midas 400 BB B3 violates the minimum voltage limit during (N-1) contingency only. The shunt capacitors at Ngwedi and Midas substations need to be adjusted to a higher step in order to provide adequate reactive power compensation that will allow the busbar voltages to increase to acceptable values.

Contingency Analysis Report: Maximum Voltage Violations

Study Case: Matimba-Midas
Result File: Contingency Analysis AC

Max. Voltage: 1.050
Max. Voltage Limit: 1.05

	Component	Branch, Substation or Site	Voltage Max. [p.u.]	Voltage Step [p.u.]	Voltage Base [p.u.]	Contingency Number	Contingency Name	Base Case and Post Voltage [1.049 p.u. - 1.337 p.u.]
1	Witkop 275 BB1	Witkop	1.07	0.00	1.07	-1	Base Case	
2	Tabor 275 BB2	Tabor	1.06	0.00	1.06	1	Matimba-Midas 400_1	

Figure 6.19: Maximum Voltage Violations

Figure 6.19 shows the maximum voltage violations report after integration of the LCC-HVDC schemes. Comparing figure 6.19 to figure 6.8 which shows the maximum voltage violations when there is no HVDC scheme integrated into the system, it can be seen that there is a drastic decrease in the number of elements that violates the maximum voltage limits. From figure 6.19, it can be seen that Witkop 275 BB1 and Tabor 275 BB2 violates the maximum voltage limit, both during (N) and (N-1) contingencies. Reactors at these stations need to be adjusted to decrease the busbar voltages to acceptable values.

6.5.4 Transient Rotor Angle Stability

Transient rotor angle stability analysis was carried out to determine how the different operation scenarios of the network with integrated LCC-HVDC schemes affects the CCT of the network generators. The analysis was done for both fault conditions 1 and 2. The simulated fault clearing time (FCT), which is used to determine the CCT for each scenario is shown in the legends of the graphs.

Fault Condition 1 Results

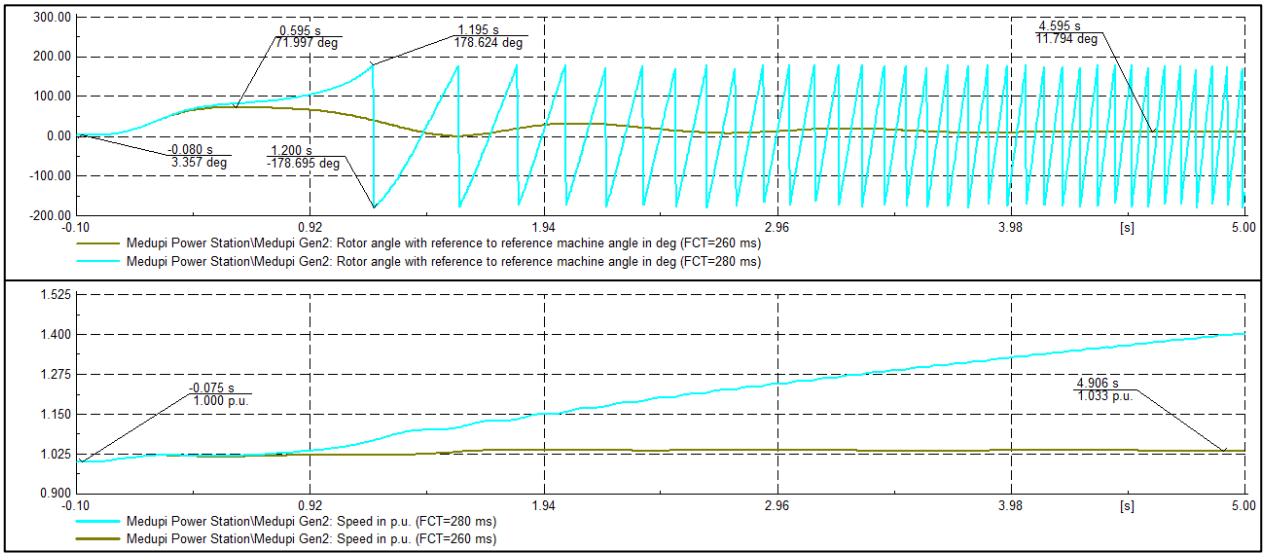

Figure 6.20: Scenario A

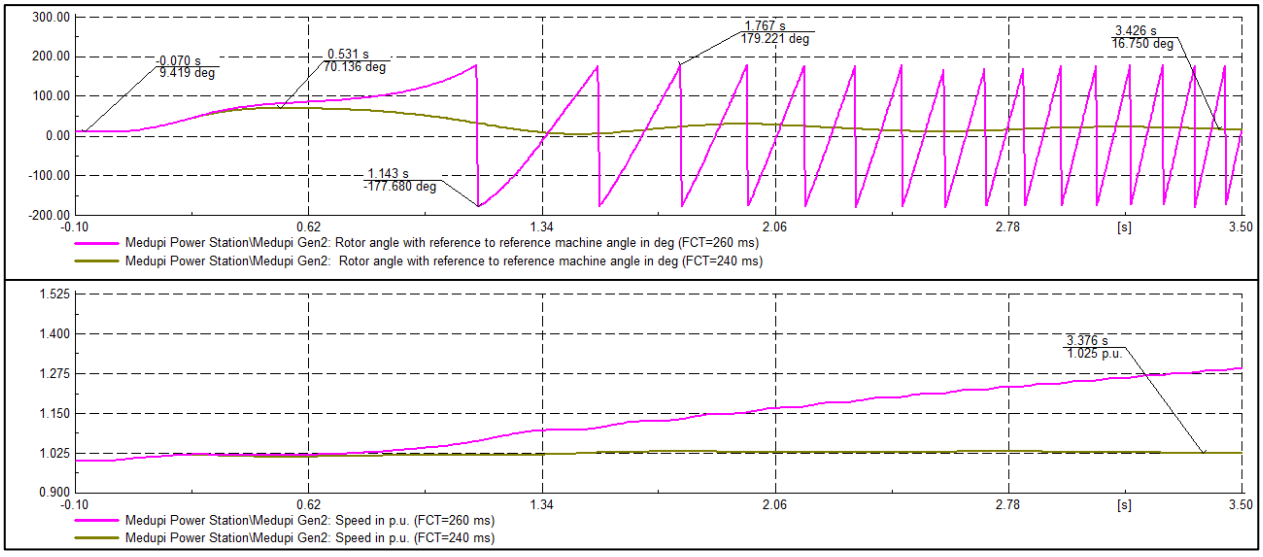

Figure 6.21: Scenario B

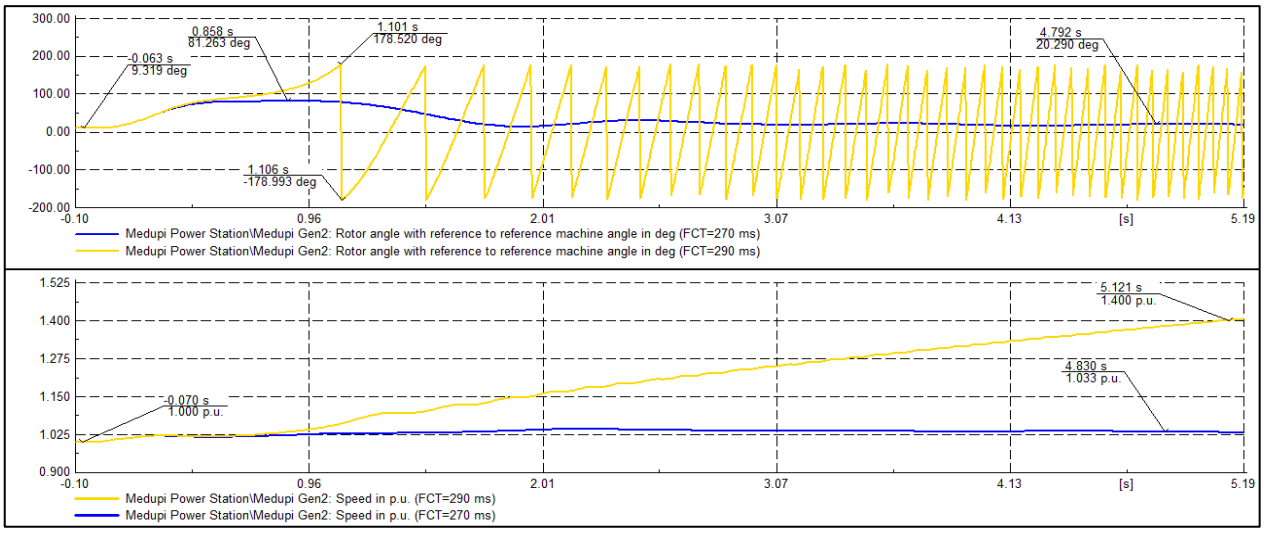

Figure 6.22: Scenario C

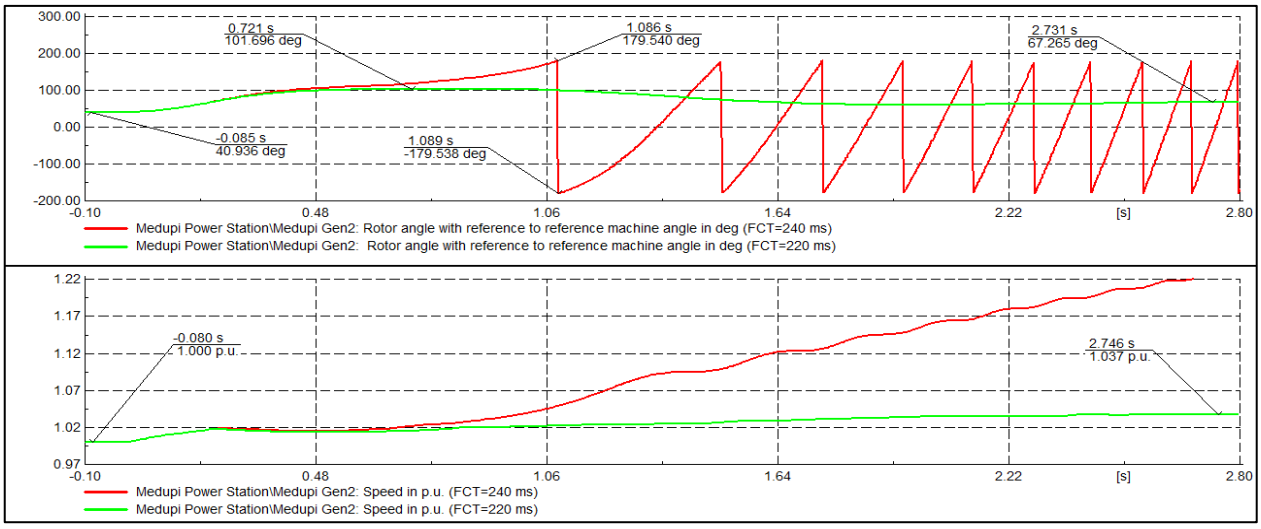

Figure 6.23: Scenario D

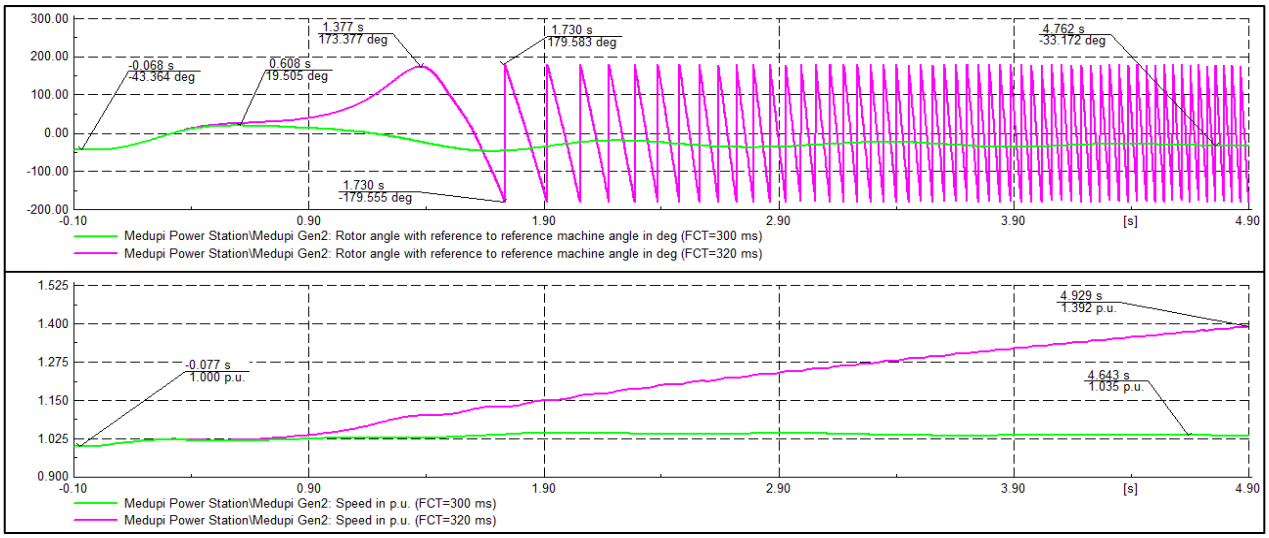

Figure 6.24: Scenario E

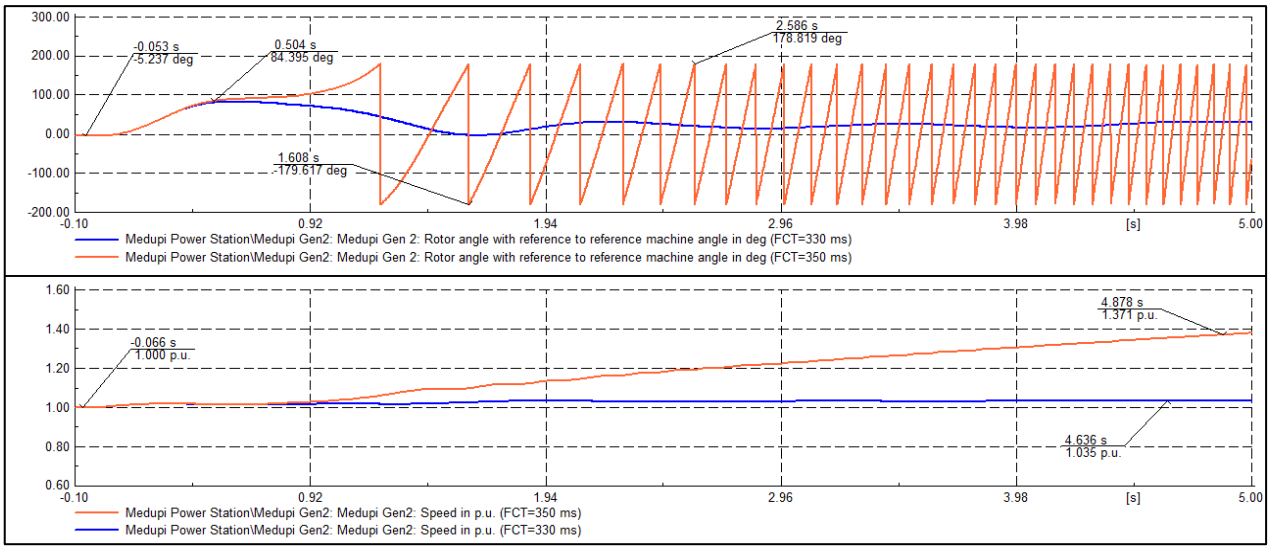

Figure 6.25: Scenario F

Table 6.8: Summary of CCTs for Fault Condition 1

Scenario	**Critical Clearing Time (CCT)**
No HVDC	200 ms
Scenario A	260 ms
Scenario B	240 ms
Scenario C	270 ms
Scenario D	220 ms
Scenario E	300 ms
Scenario F	330 ms

The results presented in figures 6.20 to 6.25 shows the response of the rotor angle and rotor speed of Medupi Gen 2, when different scenarios of LCC-HVDC schemes parallel to HVAC lines in the Limpopo-West corridor are used to transmit power in the network. The CCT is an indicator of how each of the HVDC schemes affects the transient rotor angle stability of the network generators. The points of operation shown on the graphs indicates: the steady state rotor angle value, highest value of rotor angle swing during stable operation, the new stable equilibrium point (SEP) after fault clearance, the maximum and minimum rotor angle values during unstable operation, and the rotor speed during stable operation. From the obtained results it can be seen that the different HVDC scenarios have an effect on the steady state value of the rotor angle. The CCTs are summarized in table 6.8. From the results presented in table 6.8 it can be seen that for fault condition 1, the CCT of the system is 200 ms when there is no HVDC scheme integrated into the network. The CCT is improved to 260 ms when a new long LCC-HVDC scheme is imbedded into the system to transmit low power from Medupi power

station to Midas substation (scenario A). When a new medium length LCC-HVDC scheme is used to transmit low DC power from Medupi power station to Ngwedi substation (scenario B), the CCT time is 240 ms. When an existing long HVAC line is converted or replaced with a new long LCC-HVDC scheme transmitting low power (scenario C), the CCT improves to 270 ms. When an existing medium length HVAC line is converted or replaced with a HVDC scheme transmitting medium DC power (scenario D), the CCT is to 220 ms. The CCT is improved to 300 ms when the steady state DC power being transmitted by the new long HVDC scheme is high (scenario E). The scenario that caused the biggest improvement in CCT is when two bi-polar LCC-HVDC schemes transmit a total of 4000 MW over a distance of 600 km is integrated into the network, the CCT improves to 330 ms.

For the network under study and for fault condition 1, and taking normal protection times to be 100 ms, the following conclusions have been drawn from the obtained results:

- The SAGC requirements for system rotor angle transient stability are satisfied for all scenarios studied under the simulated fault condition 1.
- The HVDC scheme de-loads some of the parallel HVAC lines and overloads the lines transmitting power from Medupi power station to Masa substation.
- A long HVDC scheme improves the system transient stability more, compared to a medium length HVDC scheme.
- Placing a new HVDC scheme into the network running parallel to the existing HVAC lines improves the network rotor angle transient stability more compared to replacing or converting an existing HVAC line to HVDC.
- Converting a medium length HVAC line into a HVDC scheme has a negative impact on rotor angle transient stability, contrary to converting a long HVAC line to HVDC.
- An HVDC scheme transmitting high DC power during steady state improves the rotor angle transient stability more compared to an HVDC scheme transmitting low steady state DC power.

Fault Condition 2 Results

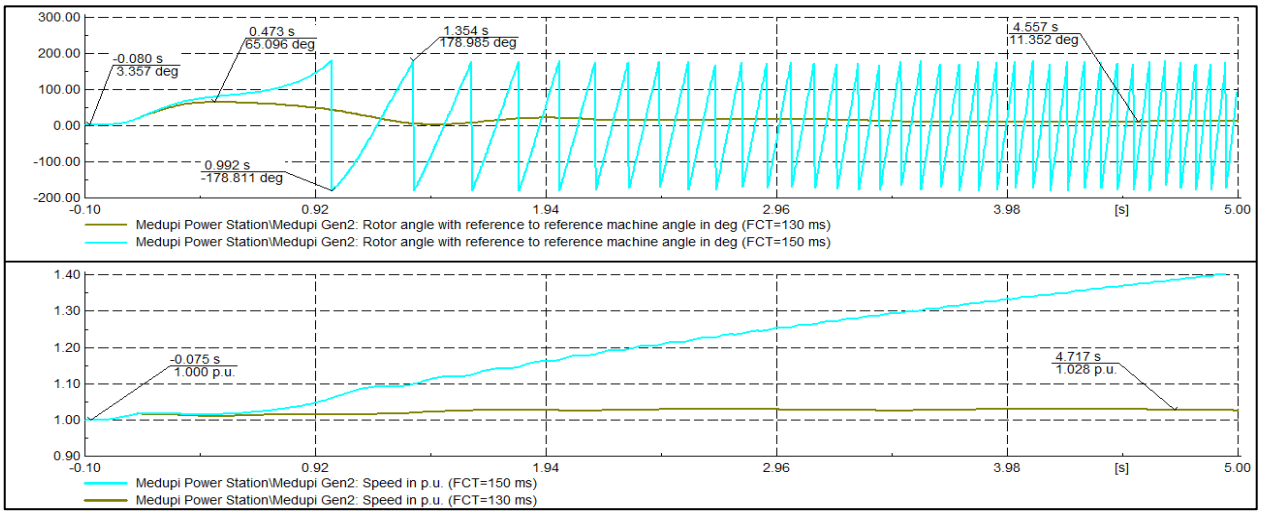

Figure 6.26: Scenario A

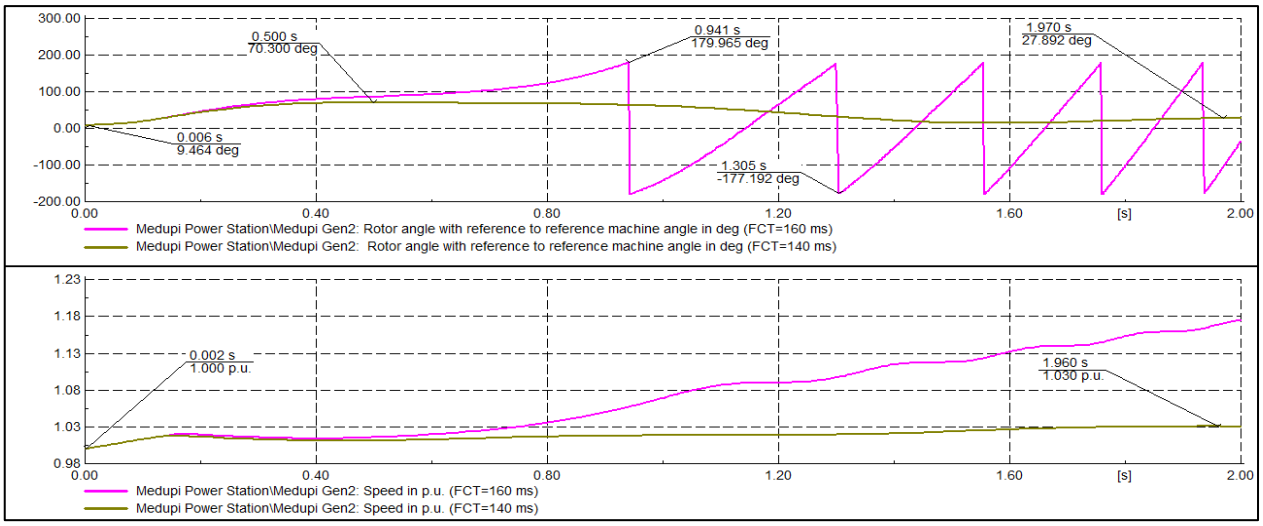

Figure 6.27: Scenario B

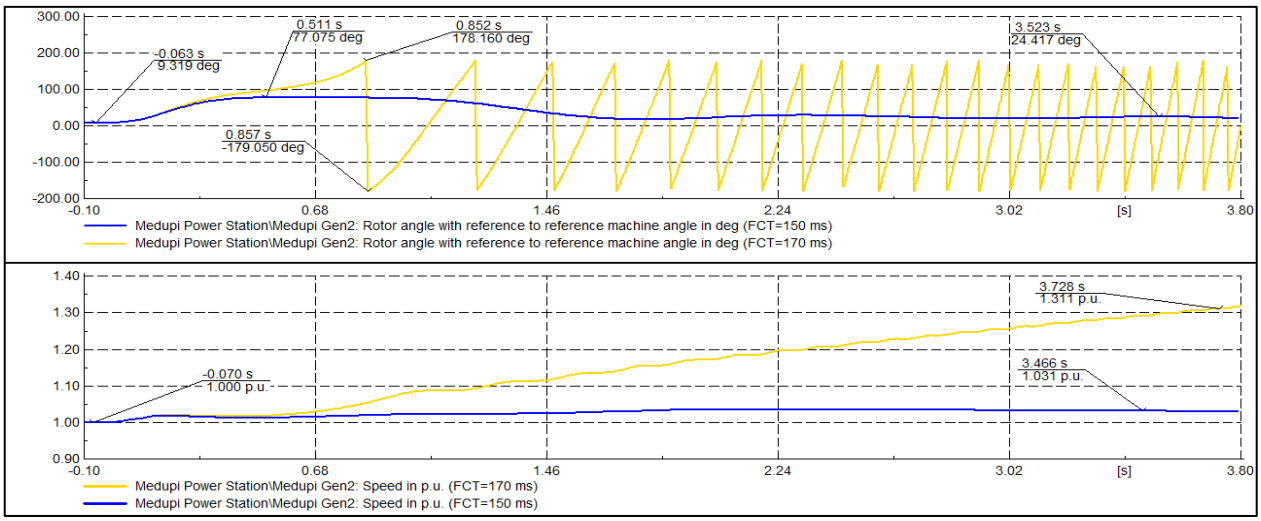

Figure 6.28: Scenario C

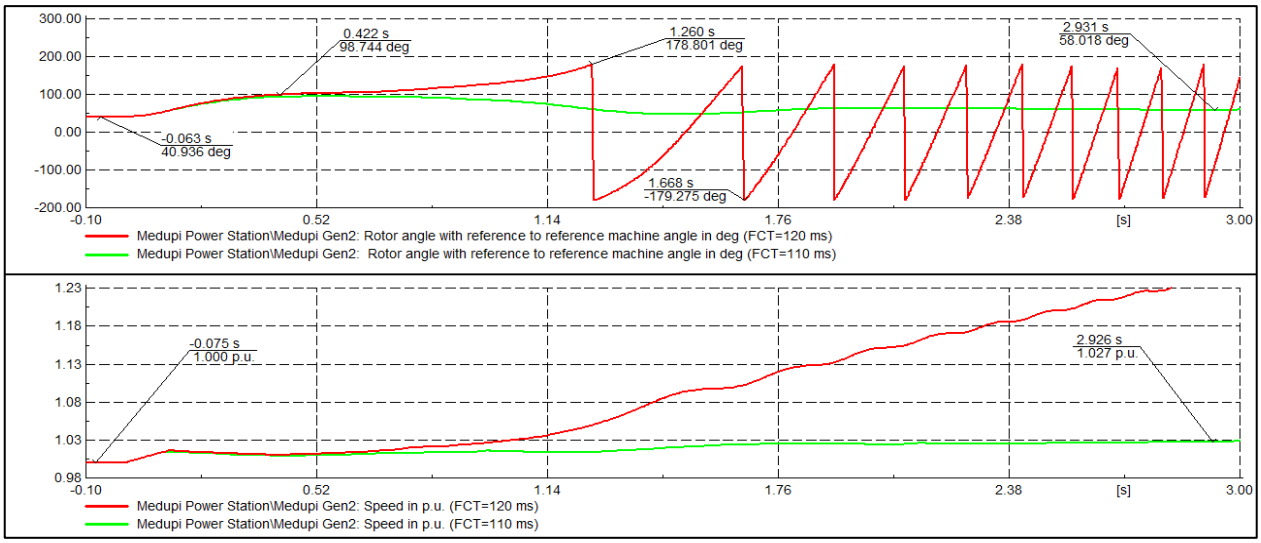

Figure 6.29: Scenario D

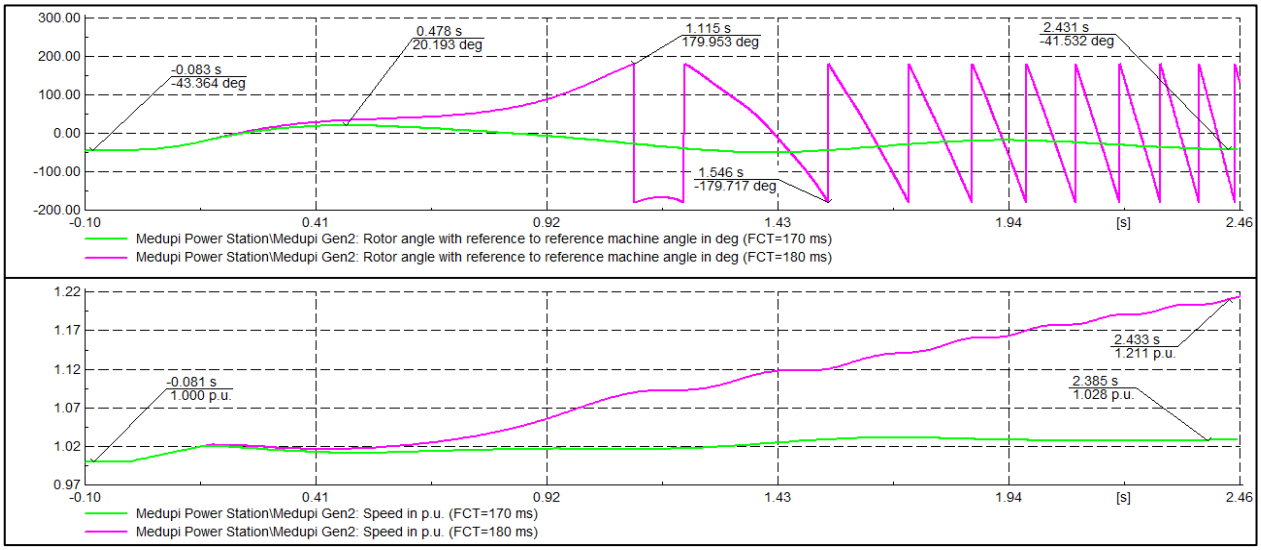

Figure 6.30: Scenario E

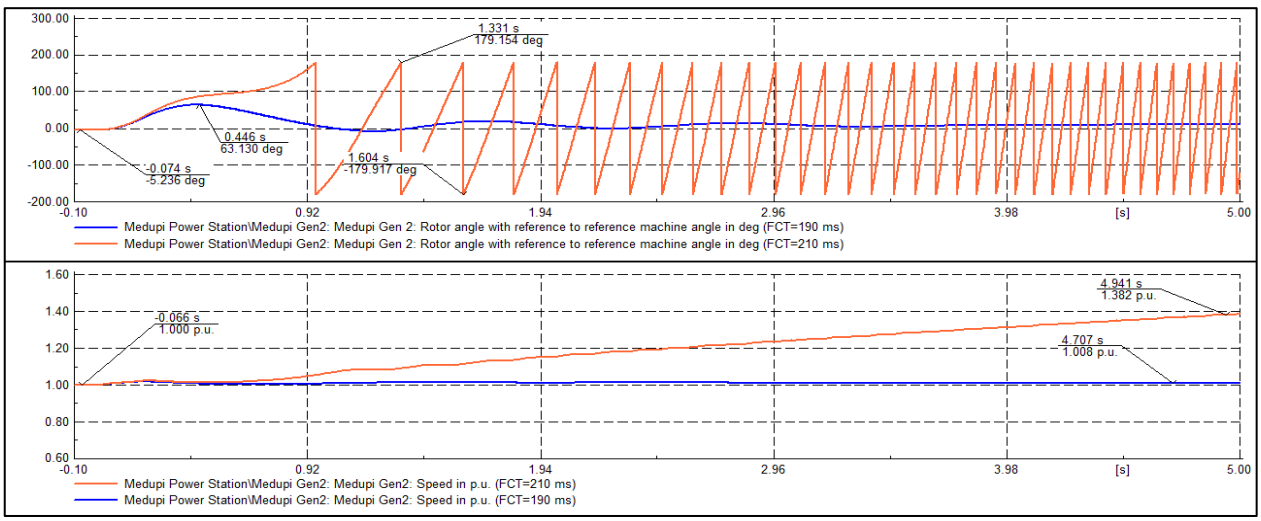

Figure 6.31: Scenario F

Table 6.9: Summary of CCTs for Fault Condition 2

Scenario	CCT
No HVDC	100 ms
Scenario A	130 ms
Scenario B	140 ms
Scenario C	150 ms
Scenario D	110 ms
Scenario E	170 ms
Scenario F	190 ms

Figures 6.26 to 6.31 illustrate the response of the machine rotor angle and rotor speed when fault condition 2 is simulated for the different system operation scenarios, when the LCC-HVDC scheme is integrated into the network. The CCT for each scenario was determined from the obtained graphs. A summary of the obtained CCTs is presented in table 6.9. From the results it can be seen that when fault condition 2 is simulated, the CCT of the machine improves from 100 ms to 130 ms, when the LCC-HVDC scheme of scenario A is integrated into the network. For scenarios B and C, the CCT is further improved to 140 ms and 150 ms. Like in the case of fault condition 1, the CCT is relatively low at 110 ms, when scenario D is simulated. For scenarios E and F the CCT is improved to 170 ms and 190 ms. Taking the normal protection times to be 100 ms, the following conclusions and observations have been drawn from the results obtained for the simulated fault condition 2:

- The grid code requirement for system rotor angle transient stability is satisfied for all scenarios studied under the simulated fault condition 2.
- Integrating a new HVDC scheme into the network running parallel to the existing HVAC lines, improves the machine rotor angle transient stability.
- Converting a medium length HVAC line to HVDC has a negative impact on rotor angle transient stability, contrary to converting a long HVAC line to HVDC.
- An HVDC scheme transmitting high DC power during the steady state, improves the rotor angle transient stability more compared to an HVDC scheme transmitting low DC power during steady state.

6.6 Summary

In this chapter, an analysis was done on how an LCC-HVDC scheme affects the transient rotor angle and transient voltage stability of Eskom's MTS network. A detailed

network model of Eskom's MTS was used to carry out this study. The simulations were run for the entire MTS network. The research focused on voltage levels equal to or greater than 400 kV. A focus area that consists of four power stations, transmission stations and transmission lines was chosen as the network on which the study is carried out. The study aimed at determining the system healthy and transient state conditions of the network when there is no HVDC scheme integrated into the network and when LCC-HVDC schemes of different configurations are integrated into the network. The system fault levels, busbar voltage violations, thermal limit violations and machine transient rotor angle stability was analysed and assessed against the grid code requirements. The steady state results were used to identify the critical elements in the network, which allowed for a critical case list to be developed for Network 3. From the steady state results it was found that the network conditions meet the SAGC requirements. The steady state results further shows that the machines in each power station are identical. The transient state conditions analysis of the network was carried out by making use of both the RMS and contingency analysis tool bars in DIgSILENT PowerFactory. By comparing the results for the case when there is no HVDC scheme integrated into the network with the case when an LCC-HVDC scheme is integrated into the system, the following observations where made:

- The LCC-HVDC scheme does not have a significant impact on the busbar fault levels of the network.
- The imbedded LCC-HVDC scheme causes a post-fault increase in the loading of the generator transformers and some network elements in the vicinity of the HVDC converter stations. Elements that exceed their maximum overloading limit of 100% need to be upgraded.
- Integration of the LCC-HVDC scheme causes a general decrease in the number of elements which violate their lower and upper voltage limits.
- The LCC-HVDC scheme causes a general increase in the network generator's CCTs, with the longest CCT observed when the LCC-HVDC scheme as described in scenario F, is integrated into the network. The lowest CCT is observed when a medium length HVAC line is replaced or converted into a LCC-HVDC scheme. The increase in CCT was observed for both simulated fault conditions. The increase in the network generator's CCTs is an indication of an improvement in the machine transient rotor angle stability of the network.

CHAPTER 7: DISCUSSIONS OF RESULTS

7.1 HVDC Scheme Model Test Results

This chapter summarizes and explains the findings of this research project. The research work was broken down into different sections which were presented in the various chapters of this dissertation. A research methodology was developed and presented in chapter 3. From the reviewed literature done in chapter 2, it was found that because each power system is unique in structure and system operation conditions, the ability of parallel HVDC schemes to successfully enhance the transient stability of a network largely depends on the pre-disturbance conditions of that particular network, as well as the operation and robustness of the controllers of the HVDC scheme being implemented. It was further found that HVDC schemes may have a negative impact on the system synchronising torque, therefore increasing the risk of system instability, if slow and outdated ineffective methods of HVDC converter DC power control are used. Modern, fast, state of the art control techniques that make use of very good measurement and communication systems are therefore required to allow the HVDC scheme to effectively and optimally contribute large amounts of system synchronizing and damping torque.

Two HVDC schemes utilising two different types of HVDC technologies, namely; LCC-HVDC and VSC-HVDC, were modelled and tested. The results for the HVDC system response tests were presented in chapter 4. The HVDC schemes were tested for their response to a step change in the reference parameters, as well as their response to faults in the AC system. For the step change test carried out on both the LCC-HVDC and VSC-HVDC schemes, the obtained results shows that the measured variables follows the step response of the reference parameter, and they are regulated to the new values of the reference parameters. This is an indication of stable operation of the HVDC systems. From the results showing the measured DC voltage response to a step change in the DC voltage reference, for both the VSC-HVDC and LCC-HVDC (figure 4.4 and 4.18) schemes, it can be observed that the DC voltage of the VSC has a faster response to the step change compared to that of the LCC. This shows that the VSC-HVDC scheme is more stable and will therefore have a faster response to faults on the DC and AC systems.

For faults in the AC grid, the results obtained for the LCC-HVDC scheme test shows that all the measured voltages and currents are regulated back to their steady state values by the reference voltage and current, at both the inverter and rectifier sides, after the system has been subjected to a fault. The firing and extinction angles of the converters are also regulated back to their nominal values after successful clearance of a fault. It was observed that the AC fault on the inverter side had a greater impact and causes temporary commutation failure at the inverter. For the AC grid fault test carried out on the VSC-HVDC scheme, the obtained results shows that the effect of the AC fault on the VSC-HVDC scheme is very minimal and negligible. The results further shows that the measured variables are regulated back to their steady state values by the reference parameters, after successful clearance of a fault.

From the overall analysis done on the results, it can be concluded that both the LCC-HVDC and VSC-HVDC schemes have been modelled correctly. The converter controllers are operating correctly as expected and the overall operation of the HVDC systems is stable.

7.2 Test Networks Results

In order to observe how parallel HVDC schemes impacts the transient rotor angle and busbar voltage stability of an AC grid, three test networks were used to carry out the study.

From the results presented in section 5.1.2, it was observed that the VSC-HVDC link has a shorter fault recovery time (FRC) compared to that of the LCC-HVDC scheme. A short FRC means that the DC power transmitted through the HVDC link is restored back to its steady state value in a short period of time, after the fault has been cleared. This allows for an increase in the power transmitted during the transient period, and therefore increases the post fault synchronizing torque of the system. This means that the VSC-HVDC scheme improves the transient rotor angle stability of the generator more compared to the LCC-HVDC scheme. The results presented in section 5.1.2 for the two machine infinite bus system (Network 1), the obtained results further show that placing a LCC-HVDC scheme in parallel to HVAC lines improves the machine CCT from 80 ms to 250 ms. Placing a VSC-HVDC scheme in parallel to HVAC lines improves the machine CCT from 80 ms to 310 ms. This is an indication that the VSC-HVDC scheme improves the machine transient rotor angle stability more compared to

the LCC-HVDC scheme. This can be attributed to the more robust and faster controllers that the VSC-HVDC scheme employs for DC power modulation.

In the study done on Network 2, a LCC-HVDC scheme was placed in parallel with long HVAC lines transporting electric power from area North-East to area South-East. The obtained results shows that the integration of the LCC-HVDC scheme into the network causes an improvement in the CCT of the critical machine from 380 ms to 450 ms. The 70 ms improvement in CCT is considered a significant improvement in the machine transient rotor angle stability.

In the study done on Network 3, in terms of transient rotor angle stability, for both fault conditions simulated, the results obtained shows that: Generally, the integration of the LCC-HVDC schemes causes the CCTs of the network generators to increase, with the longest CCT observed when two bi-pole HVDC schemes are transmitting high DC power (4000 MW) over a long distance of 600 km. The lowest CCT was observed when a medium length HVAC transmission line is replaced with a mono-pole LCC-HVDC scheme. It was found that for faults condition 1, the CCT improved from 200 ms to 330 ms when the LCC-HVDC scheme described in scenario F was integrated into the system. The increase in the CCTs is an indicator of the enhancement of the machine transient rotor angle stability.

Comparing the results obtained for the three test networks it can be seen that, the smaller network (test network 1) has the highest improvement in CCT of 170 ms, followed by the largest network (test network 3) with an improvement in CCT of 110 ms. The medium sized network, test network 2 has an improvement in CCT of 70 ms. The high improvement in CCT in the small network can be attributed to the fact that apart from the overload capability and fast controlled power modulation of the HVDC scheme helping to improve system synchronising torque, the effect of the HVDC scheme impedance on the total effective system impedance is much greater and significant in the smaller network and this adds to the improvement of system synchronising torque by improving the post-fault power transfer capabilities of the transmission lines. It was expected that the HVDC scheme would have a more positive impact on the CCT of the medium sized network (Network 2) compared to the larger Eskom network. However, this was not the case. The reason for this may be that, in the medium sized network, due to the network topology and system steady state conditions,

the HVDC scheme was not connected in parallel with the faulted HVAC line, but was rather used to replace two parallel tie-lines which interconnect two distant areas in Network 2. And thus, the HVDC scheme did not have much effect on the synchronising torque applied to the critical machine in Network 2.

The results obtained for voltage limit violations shows that the integration of the LCC-HVDC scheme into Network 3 causes a general decrease in the number of elements that violate their voltage limits. The HVDC scheme causes an increase in loadings of the elements via which power is transmitted to and from the converter stations. An increase in MW loading of these elements causes a voltage drop at the busbars that these elements are connected to, which may lead to minimum voltage violations. Similarly, the integration of the HVDC scheme into the system causes some busbars to be de-loaded, which in turn causes an increase in busbar voltages and this may lead to maximum voltage violations.

CHAPTER 8: CONCLUSIONS AND RECOMMENDATIONS

8.1 Conclusions

By comparing the obtained results to the objectives of this study, it can be concluded that the main and sub-objectives of the research have been met. Based on the discussion of the results done in chapter 7, the following conclusions have been drawn:

1. A research methodology for analysing the transient rotor angle stability of a large multi-machine AC network has been developed and successfully applied to the test networks.
2. The LCC-HVDC and VSC-HVDC schemes have been modelled correctly. The operation of the HVDC schemes is stable and the converter controller models are operating correctly, as expected.
3. The planned power stations, substations and transmission lines have been successfully modelled onto Eskom's MTS network.
4. Integration of an HVDC scheme in parallel with HVAC transmission lines, in a large multi-machine AC network, improves the CCTs of the network generators, which is an indication that the HVDC scheme helps to improve the network transient rotor angle stability by improving on the system synchronizing torque.
5. For Network 3, the longest CCT is observed when two bi-pole LCC-HVDC schemes transmitting high DC power over a long distance is integrated into the network, and the lowest CCT is observed when a medium length HVAC transmission line is replaced/converted into a LCC-HVDC scheme.
6. The general trend in the results obtained from transient rotor angle stability analysis of Network 3 shows that the machine transient rotor angle stability is improved more with an increase in the power being transmitted by the LCC-HVDC scheme during steady state operation. Based on this, it can be concluded that increasing the steady state power of the LCC-HVDC scheme described in scenario F, from 2000 MW per bi-pole to 4000 MW per bi-pole, as originally planned for the 2030 envisioned network, will have a positive impact on the machine transient rotor angle stability.

7. From the analysis done on test network 1, it was found that due to faster operation of the VSC-HVDC controllers for power modulation during and after fault conditions, the VCS-HVDC scheme improves the generator CCT more compared to the LCC-HVDC scheme.
8. After the integration of the LCC-HVDC scheme into Eskom's MTS network, the system generators meet the SAGC requirements, in terms of transient rotor angle stability.
9. Generally, the integration of the LCC-HVDC scheme into Eskom's MTS Network causes a decrease in the number of elements that violate their voltage limits.
10. The integration of the LCC-HVDC scheme into Eskom's MTS Network causes transformers Midas 400/132/22 T1 and Midas 400/132/22 T2 and transmission lines Medupi-Masa 400_1 and Medupi-Masa 400_2 to violate their overloading limits. For successful integration of the HVDC schemes into the network, the overloaded elements would need to be upgraded.
11. The LCC-HVDC scheme does not have a significant impact on the system busbar fault levels.

The findings of this investigation gives the network planner and system operators of large power utilities such as Eskom a broader knowledge and good understanding on how HVDC transmission schemes may impact the transient rotor angle and voltage stability of the network. And thus, giving the network planner a good idea on the expected modifications and improvements that would need to be done on the existing network, in terms of elements that will need to be upgraded before the proposed LCC-HVDC scheme can be integrated into the network. This also makes it less challenging to assess the possible cost implications of implementing the proposed LCC-HVDC scheme project.

8.2 Recommendations and Future Research

The obtained results shows that the proposed LCC-HVDC scheme improves the Eskom MTS network conditions most when it is integrated into the network as described in scenario F, which is presented in chapter 6. For future research, it is thus recommended that a thorough investigation be carried out on the cost implications of installing the proposed HVDC scheme as described in scenario F.

For future research, it is further recommended that by making use of P-V and Q-V curves, an in-depth investigation be carried out to analyse the impact of the HVDC scheme on the static voltage stability of the weak busbars in the network that violates their voltage limits after being subjected to a system fault. The analysis should be carried out for different loading levels and loads of different power factors at these busbars. The outcome of such an investigation will provide an improved understanding on how the HVDC scheme affects the voltage stability of the network.

It is further recommended that an investigation be carried out to determine the magnitude of the impact that wide area measurement systems (WAMS) may have on improving the network transient stability, when used in conjunction with the HVDC control system. In this type of study, it is recommended that a WAMS which utilises Phasor Measurement Units (PMUs) which continuously monitors the network conditions in real time and sends this information to a control centre for processing, be used to continuously send the network conditions to the HVDC control system. The PMUs should be deployed at the weak busbars which violates their voltage limits after being subjected to a system fault. The information collected by the PMUs will then be synchronized with the HVDC converter controllers such that the active and reactive power modulation of the converters is based on the real time network information collected by the PMUs.

REFERENCES

[1] G. Pervelan, C. Jafta, E. Roy, and S. Kabir, "Transmission development plan 2015," EskomOctober 2014 2014.

[2] S. Panda and R. N. Patel, "Improving power system transient stability with an off-centre location of shunt FACTS devices," *JOURNAL OF ELECTRICAL ENGINEERING-BRATISLAVA-,* vol. 57, p. 365, 2006.

[3] H. Wang and F. Swift, "A unified model for the analysis of FACTS devices in damping power system oscillations. I. Single-machine infinite-bus power systems," *Power Delivery, IEEE Transactions on,* vol. 12, pp. 941-946, 1997.

[4] J. Arrillaga, Y. H. Liu, and N. R. Watson, *Flexible power transmission: the HVDC options*. England: John Wiley & Sons, 2007.

[5] A. Hammad, "Stability and control of HVDC and AC transmissions in parallel," *Power Delivery, IEEE Transactions on,* vol. 14, pp. 1545-1554, 1999.

[6] P. Kundur, *Power system stability and control*. New York: McGraw-Hill, 1994.

[7] S. A. Nasar and F. C. Trutt, *Electric power systems*. Florida: CRC Press, 1998.

[8] P. Anderson and A. Fouad, *Power system control and stability*. Hoboken: John Wiley & Sons, 2003.

[9] P. Kundur, J. Paserba, V. Ajjarapu, G. Andersson, A. Bose, C. Canizares*, et al.*, "Definition and classification of power system stability IEEE/CIGRE joint task force on stability terms and definitions," *Power Systems, IEEE Transactions on,* vol. 19, pp. 1387-1401, 2004.

[10] C. A. Gross, *Power system analysis*, 2 ed. vol. 1. London: John Wiley & Sons, 1986.

[11] "Proposed Terms & Definitions for Power System Stability," *Power Apparatus and Systems, IEEE Transactions on,* vol. PAS-101, pp. 1894-1898, 1982.

[12] M. E. El-Hawary, *Electrical energy systems*: Crc Press, 2007.

[13] C. Cecati and H. Latafat, "Time domain approach compared with direct method of Lyapunov for transient stability analysis of controlled power system," in *Power Electronics, Electrical Drives, Automation and Motion (SPEEDAM), 2012 International Symposium on*, 2012, pp. 695-699.

[14] G. Maria, C. Tang, and J. Kim, "Hybrid transient stability analysis [power systems]," *Power Systems, IEEE Transactions on,* vol. 5, pp. 384-393, 1990.

[15] H.-D. Chiang, F. F. Wu, and P. P. Varaiya, "A BCU method for direct analysis of power system transient stability," *Power Systems, IEEE Transactions on,* vol. 9, pp. 1194-1208, 1994.

[16] A. Kumar and G. Priya, "Power system stability enhancement using FACTS controllers," in *Emerging Trends in Electrical Engineering and Energy Management (ICETEEEM), 2012 International Conference on*, 2012, pp. 84-87.

[17] K. Meah and S. Ula, "Comparative evaluation of HVDC and HVAC transmission systems," in *Power Engineering Society General Meeting, 2007. IEEE*, 2007, pp. 1-5.

[18] B. Andersen, S. Bisnath, A. C. Britten, and A. R. Williamson, *HVDC Power Transmission (Basic Principles, Planning and Converter Technology)*. Johannesburg Crown Publications cc, 2012.

[19] N. Mohan, T. M. Underland, and W. P. Robbins, *Power Electronics* 2003.

[20] M. Bahrman and B. Johnson, "The ABCs of HVDC transmission technologies," *IEEE Power and Energy Magazine,* vol. 2, pp. 32-44, 2007.

[21] G. P. Adam, *Voltage Source converter: modulation, modelling, control and applications in power systems*. Glasgow: CreateSpace Independent Publishing Patform 2014.

[22] Y. Ma, Y. Yang, Y. Tao, L. Qian, and Q. Zhong, "Model development of HVDC control system for real time digital simulation," in *Power and Energy Engineering Conference, 2009. APPEEC 2009. Asia-Pacific*, 2009, pp. 1-4.

[23] S. Li, T. Haskew, and L. Xu, "Control of HVDC light system using conventional and direct current vector control approaches," *Power Electronics, IEEE Transactions on,* vol. 25, pp. 3106-3118, 2010.

[24] Z. Yuan and H. Wang, "The Research on the VSC-HVDC Control System Structure," in *Power and Energy Engineering Conference (APPEEC), 2012 Asia-Pacific*, 2012, pp. 1-4.

[25] J. Pan, R. Nuqui, K. Srivastava, T. Jonsson, P. Holmberg, and Y.-J. Hafner, "AC grid with embedded VSC-HVDC for secure and efficient power delivery," in *Energy 2030 Conference, 2008. ENERGY 2008. IEEE*, 2008, pp. 1-6.

[26] M. Abido, "Power system stability enhancement using FACTS controllers: A review," *The Arabian Journal for Science and Engineering,* vol. 34, pp. 153-172, 2009.

[27] A. Hammad, "Analysis of power system stability enhancement by static var compensators," *Power Systems, IEEE Transactions on,* vol. 1, pp. 222-227, 1986.

[28] S. R. Kumar and S. S. Nagaraju, "Transient stability improvement using UPFC and SVC," *ARPN Journal of Engineering and Applied Sciences,* vol. 2, pp. 38-45, 2007.

[29] M. Haque, "Improvement of first swing stability limit by utilizing full benefit of shunt FACTS devices," *Power Systems, IEEE Transactions on,* vol. 19, pp. 1894-1902, 2004.

[30] T. Machida, "Improving transient stability of AC system by joint usage of DC System," *Power Apparatus and Systems, IEEE Transactions on,* pp. 226-232, 1966.

[31] C. Taylor and S. Lefebvre, "HVDC controls for system dynamic performance," *Power Systems, IEEE Transactions on,* vol. 6, pp. 743-752, 1991.

[32] K. To, A. K. David, and A. Hammad, "A robust co-ordinated control scheme for HVDC transmission with parallel AC systems," *Power Delivery, IEEE Transactions on,* vol. 9, pp. 1710-1716, 1994.

[33] L. A. S. Pilotto, M. Szechtman, A. Wey, W. F. Long, and S. L. Nilsson, "Synchronizing and damping torque modulation controllers for multi-infeed HVDC systems," *Power Delivery, IEEE Transactions on,* vol. 10, pp. 1505-1513, 1995.

[34] J. Fu and J. Zhao, "Nonlinear robust control for parallel AC/DC transmission systems: A new adaptive back-stepping approach," *Cybernetics and Systems: An International Journal,* vol. 37, pp. 347-359, 2006.

[35] J. Hazra, Y. Phulpin, and D. Ernst, "HVDC control strategies to improve transient stability in interconnected power systems," in *PowerTech, 2009 IEEE Bucharest*, 2009, pp. 1-6.

[36] Y. Peng, S. Yuqiu, Y. Yinghua, L. Xiaoming, and T. Jiaqi, "Transient Stability Analysis of Hu-Liao HVDC and AC Parallel Transmission System," *Smart Grid and Renewable Energy,* vol.1 No. 2, pp. 74-80, 2010.

[37] R. Aouini, K. Ben Kilani, B. Marinescu, and M. Elleuch, "Improvement of fault critical time by HVDC transmission," in *Systems, Signals and Devices (SSD), 2011 8th International Multi-Conference on*, 2011, pp. 1-6.

[38] M. Benasla, T. Allaoui, Y. Chedni, and A. Boudali, "Enhancement of the Transient Stability of AC/DC Power System by Controlling HVDC Power Flow," 2013.

[39] K. P. Basu, "Stability enhancement of power system by controlling HVDC power flow through the same AC transmission line," in *Industrial Electronics & Applications, 2009. ISIEA 2009. IEEE Symposium on*, 2009, pp. 663-668.

[40] T. V. Muni, T. Vinoditha, and D. K. Swamy, "Improvement of power system stability by simultaneous AC-DC power transmission," *International Journal of Scientific & Engineering Research,* vol. 2, pp. 1-6, 2011.

[41] H. Rahman and B. Khan, "Stability improvement of power system by simultaneous AC–DC power transmission," *Electric Power Systems Research,* vol. 78, pp. 756-764, 2008.

[42] A. Fuchs, M. Imhof, T. Demiray, and M. Morari, "Stabilization of Large Power Systems Using VSC–HVDC and Model Predictive Control," *Power Delivery, IEEE Transactions on,* vol. 29, pp. 480-488, 2014.

[43] Y. Phulpin, J. Hazra, and D. Ernst, "Model predictive control of HVDC power flow to improve transient stability in power systems," in *Smart Grid Communications (SmartGridComm), 2011 IEEE International Conference on*, 2011, pp. 593-598.

[44] M. M. Alamuti, R. Rabbani, S. K. Kerahroudi, and G. Taylor, "System stability improvement through HVDC supplementary Model Predictive Control," in *Power Engineering Conference (UPEC), 2014 49th International Universities*, 2014, pp. 1-5.

[45] J. Machowski, P. Kacejko, Ł. Nogal, and M. Wancerz, "Power system stability enhancement by WAMS-based supplementary control of multi-terminal HVDC networks," *Control Engineering Practice,* vol. 21, pp. 583-592, 2013.

[46] G. M. Huang and V. Krishnaswamy, "HVDC controls for power system stability," in *Power Engineering Society Summer Meeting, 2002 IEEE*, 2002, pp. 597-602.

[47] L. Wang, K.-H. Wang, W.-J. Lee, and Z. Chen, "Power-flow control and stability enhancement of four parallel-operated offshore wind farms using a line-commutated HVDC link," *Power Delivery, IEEE Transactions on,* vol. 25, pp. 1190-1202, 2010.

[48] Y. Liu and Z. Chen, "Transient voltage stability analysis and improvement of a network with different HVDC systems," in *Power and Energy Society General Meeting, 2011 IEEE*, 2011, pp. 1-8.

[49] H. F. Latorre and M. Ghandhari, "Improvement of voltage stability by using VSC-HVdc," in *Transmission & Distribution Conference & Exposition: Asia and Pacific, 2009*, 2009, pp. 1-4.

[50] X. Tang and D. D.-C. Lu, "Enhancement of voltage quality in a passive network supplied by a VSC-HVDC transmission under disturbances," *International Journal of Electrical Power & Energy Systems,* vol. 54, pp. 45-54, 2014.

[51] C. Zhao and Y. Sun, "Study on control strategies to improve the stability of multi-infeed HVDC systems applying VSC-HVDC," in *Electrical and Computer Engineering, 2006. CCECE'06. Canadian Conference on*, 2006, pp. 2253-2257.

[52] A. Fuchs and M. Morari, "Placement of HVDC links for power grid stabilization during transients," in *PowerTech (POWERTECH), 2013 IEEE Grenoble*, 2013, pp. 1-6.

[53] R. Y. J. Hammons, CL Gwee, PA Kacejko, T, "Enhancement of power system transient response by control of HVDC converter power," *Electric Machines &Power Systems,* vol. 28, pp. 219-241, 2000.

[54] J. Dorn, M. Pohl, D. Retzmann, and F. Schettler, "Transformation of the Energy System in Germany-Enhancement of System Stability by Integration of innovative Multilevel HVDC in the AC Grid," in *Security in Critical Infrastructures Today, Proceedings of International ETG-Congress 2013; Symposium 1:*, 2013, pp. 1-6.

[55] V. Burtnyk, E. Neudorf, D. Povh, E. Starr, C. Taylor, and R. Walling, "AC-DC economics and alternatives-1987 panel session report," *Power Delivery, IEEE Transactions on,* vol. 5, pp. 1956-1979, 1990.

[56] A. Clerici, L. Paris, and P. Danfors, "HVDC conversion of HVAC lines to provide substantial power upgrading," *Power Delivery, IEEE Transactions on,* vol. 6, pp. 324-333, 1991.

[57] P. Naidoo, D. Muftic, and N. Ijumba, "Investigations into the upgrading of existing HVAC power transmission circuits for higher power transfers using HVDC technology," in *Power Engineering Society Inaugural Conference and Exposition in Africa, 2005 IEEE*, 2005, pp. 139-142.

[58] H. Rahman and B. Khan, "Power upgrading of transmission line by combining AC–DC transmission," *Power Systems, IEEE Transactions on,* vol. 22, pp. 459-466, 2007.

[59] O. Ozerdem, "Converting a three-phase AC line to a three-wire DC line by a modified converter," *Electrical Engineering,* vol. 92, pp. 185-192, 2010.

[60] B. Singh and G. Sharma, "Power upgrading of Transmission Line by converting EHVAC into EHVDC," *International Journal for Science and Emerging Technologies with Latest Trends, ISSN,* pp. 2250-3641, 2012.

[61] M. Szechtman, T. Wess, and C. Thio, "A benchmark model for HVDC system studies," in *AC and DC Power Transmission, 1991., International Conference on*, 1991, pp. 374-378.

[62] M. O. Faruque, Z. Yuyan, and V. Dinavahi, "Detailed modeling of CIGRE HVDC benchmark system using PSCAD/EMTDC and PSB/SIMULINK," *Power Delivery, IEEE Transactions on,* vol. 21, pp. 378-387, 2006.

[63] R. N. Nayak, Y. K. Sehgal, and S. Sen, "EHV Transmission Line Capacity Enhancement Through Increase in Surge Impedence Loading Level " in *Power India Conference, 2006 IEEE*, New Delhi, 2006.

[64] NERSA, "The South African Grid Code- The System Operation Code," ed, 2008.

[65] NERSA, "The South African Grid Code-The Network Code," ed, 2010.

[66] J. A. Refaee, M. Mohandes, and H. Maghrabi, "Radial basis function networks for contingency analysis of bulk power systems," *Power Systems, IEEE Transactions on,* vol. 14, pp. 772-778, 1999.

[67] Q. Morante, N. Ranaldo, A. Vaccaro, and E. Zimeo, "Pervasive grid for large-scale power systems contingency analysis," *Industrial Informatics, IEEE Transactions on,* vol. 2, pp. 165-175, 2006.

[68] A. Gole and V. Sood, "A static compensator model for use with electromagnetic simulation programs " *IEEE Transactions on Power Delivery,* vol. 5, pp. 1398-1407, 1990.

[69] S. J. T. Mwale and I. E. Davidson, "Power deficits and outage planning in South Africa," in *2nd International Symposium on Energy Challenges and Mechanics*, Aberdeen, Scotland, 2014.

APPENDICES

Appendix A: Equipment Ratings and Generator Models

Test Network 1 Equipment

Table A1: Generator Ratings

Parameter	Value
Nominal Apparent Power	950 MVA
Nominal Voltage	24 kV
Power Factor	0.9
Connection	YN
Xd	1.81 p.u.
Xq	1.71 p.u.
Inertia Acceleration Time Constant	6.3
Stator Resistance (rstr)	0.003
Leakage Reactance (Xl)	0.15

Table A2: Transformer Ratings

Parameter	Value
Rated Power	1000 MVA
Nominal Frequency	50 Hz
Rated Voltage (LV)	24 kV
Rated Voltage (HV)	400 kV
Vector Group and Phase Shift	YNd1
Positive Sequence Impedance	0.15 p.u.
Zero Sequence Impedance	0.15 p.u.

Table A3: HVAC Transmission Line Parameters

Parameter	Value
Rated Voltage	400 kV
Rated Current	2 kA
Type	Overhead line
Positive and Negative Sequence Impedance	R=0.05 Ω/km X=0.25 Ω/km

Zero Sequence Impedance	R=0.2 Ω/km X=1 Ω/km

Test Network 2 Equipment

Table A4: Generator Parameters

Parameter	**Value**
Nominal Apparent Power	592 MVA
Nominal Voltage	18 kV
Power Factor	0.9
Connection	YN
Xd	2.3 p.u.
Xq	2 p.u.
Inertia Time Constant (H)	3.5
Stator Resistance (rstr)	0.001
Leakage Reactance (Xl)	0.15

Table A5: Transformer Parameters

Parameter	**T1**	**T2**	**T3**
Rated Power	600 MVA	600 MVA	1000 MVA
Nominal Frequency	50 Hz	50 Hz	50 Hz
Rated Voltage (LV)	16.5 kV	18 kV	345 kV
Rated Voltage (HV)	400 kV	400 kV	400 kV
Vector Group and Phase Shift	YNd1	YNd1	YNd1
Positive Sequence Impedance	0.144 p.u.	0.125 p.u.	0.07 p.u.
Zero Sequence Impedance	0.144 p.u.	0.125 p.u.	0.07 p.u.

Table A6: HVAC Transmission Line Parameters

Parameter	**Line Type 1**	**Line Type 2**
Rated Voltage	230 kV	400 kV
Rated Current	2 kA	1 kA
Type	Overhead line	Overhead line
Pos. and Neg. Sequence Impedance	R=0.023 Ω/km X=0.2 Ω/km	R=0.023 Ω/km X=0.2 Ω/km
Zero Sequence Impedance	R=0.2 Ω/km X=1 Ω/km	R=0.2 Ω/km X=1 Ω/km

Generator Model

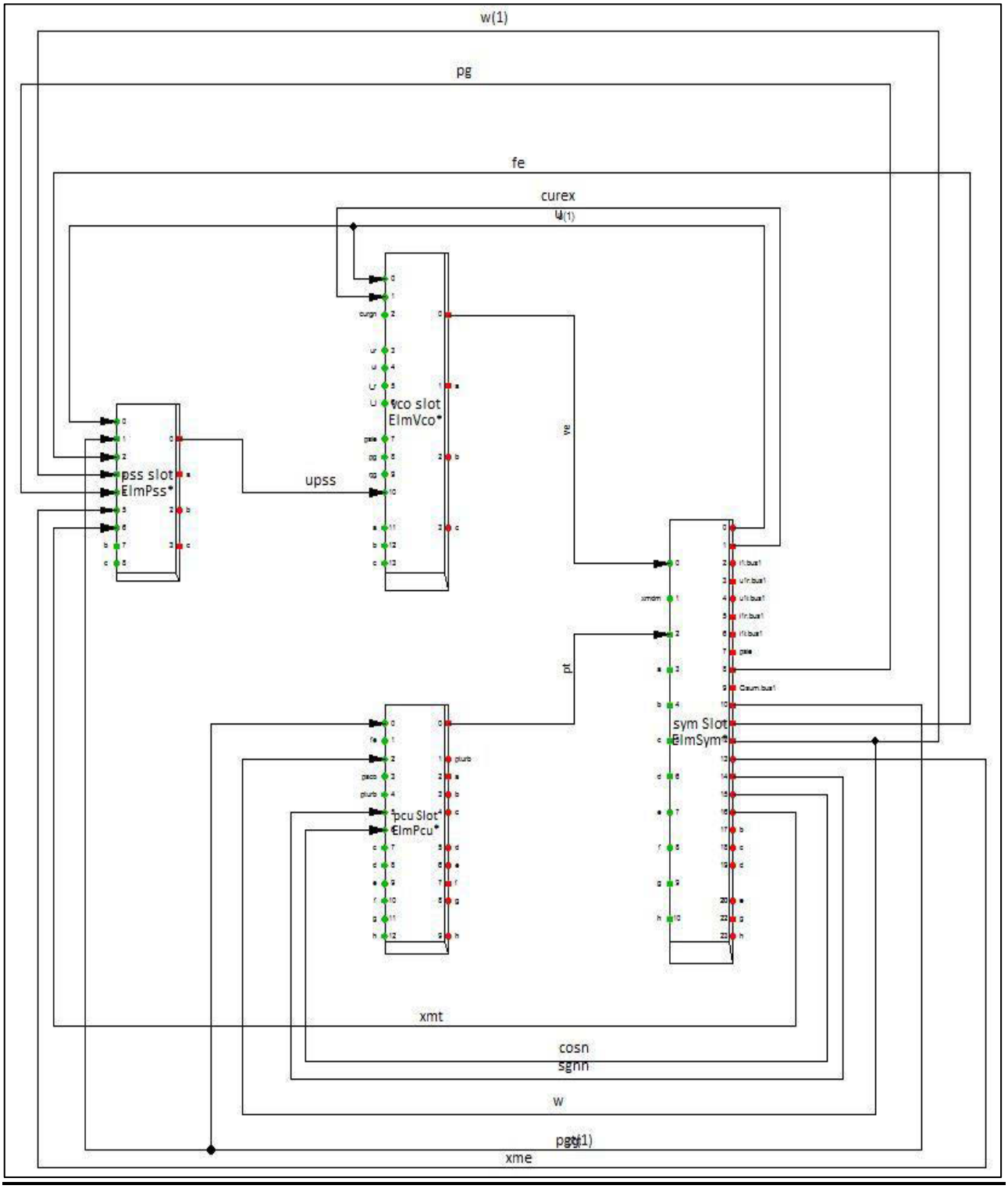

Figure A1: Generator Composite Model Block Diagram

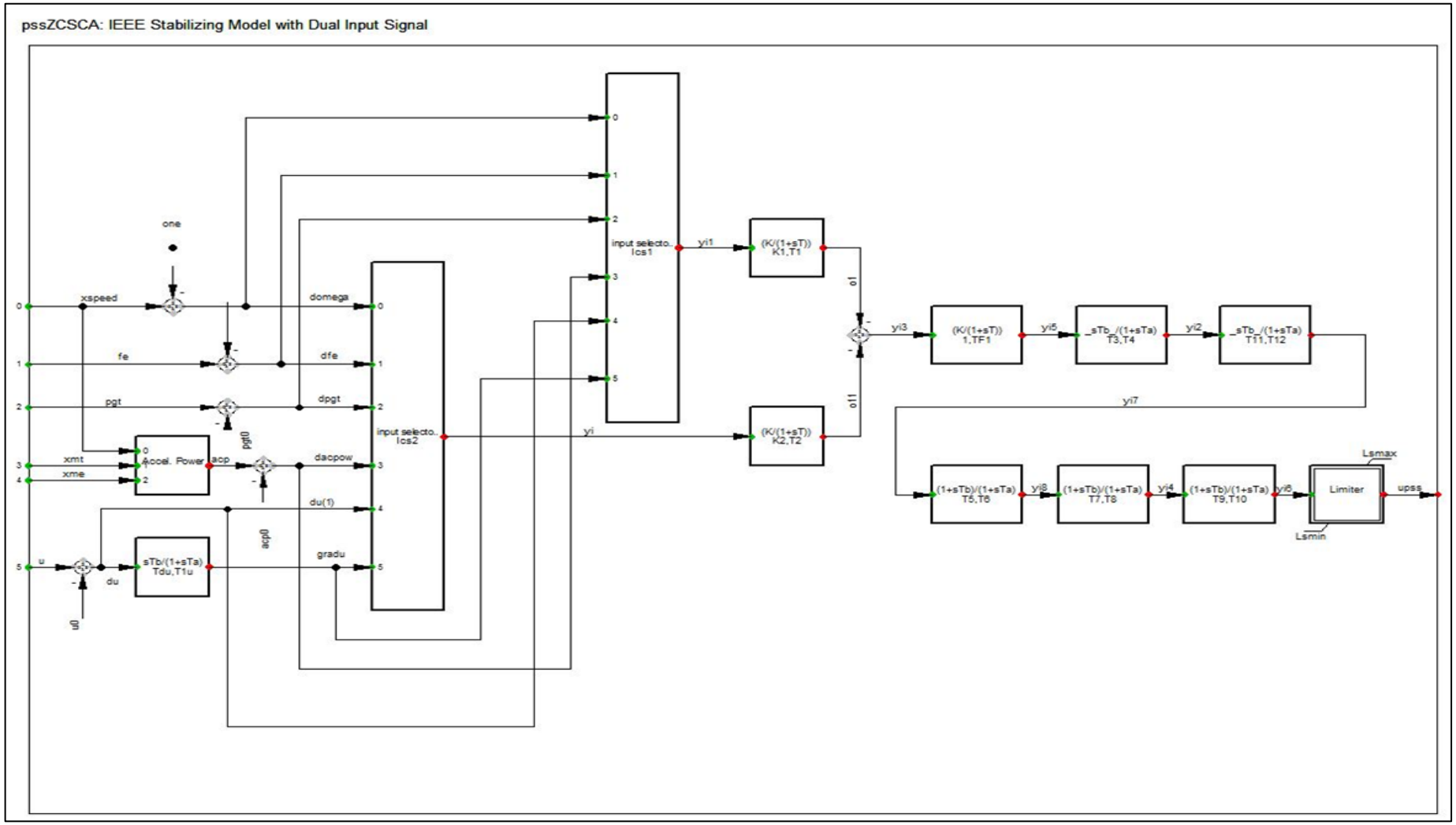

Figure A2: pss_ZCSCA IEEE Power System Stabilizing Model Block Diagram

Table A7: PSS Parameters

Parameter	**Value**
TF1 Time Constant [s]	0.017
Ics1 1th Input Selector [1-6]	3
Ics2 2th Input Selector [1-6]	0
K1 1th Path Stabilizer Gain [p.u.]	1.265
T1 1th Path Time Constant [s]	0.0135
K2 2th Path Stabilizer Gain [p.u.]	0
T2 2th Path Time Constant [s]	10
T3 Washout 1th Time Constant [s]	1.6
T4 Washout 2th Time Constant [s]	1.6
T5 Filter 1th Time Constant [s]	0.63
T6 Filter 2th Time Constant [s]	0.92
T7 Filter 3th Time Constant [s]	0.15
T8 Filter 4th Time Constant [s]	0.92
T9 Filter 5th Time Constant [s]	0.15
T10 Filter 6th Time Constant [s]	0.04
Tdu Time Constant for Gradient Calculation [s]	1
T1u Delay Time Constant for Gradient Calculation [s]	0.1
T11 Washout 3th Time Constant [s]	1000
T12 Washout 4th Time Constant [s]	1000
Lsmin Controller Minimum Output [p.u.]	-0.05
Lsmax Controller Maximum Output [p.u.]	0.05

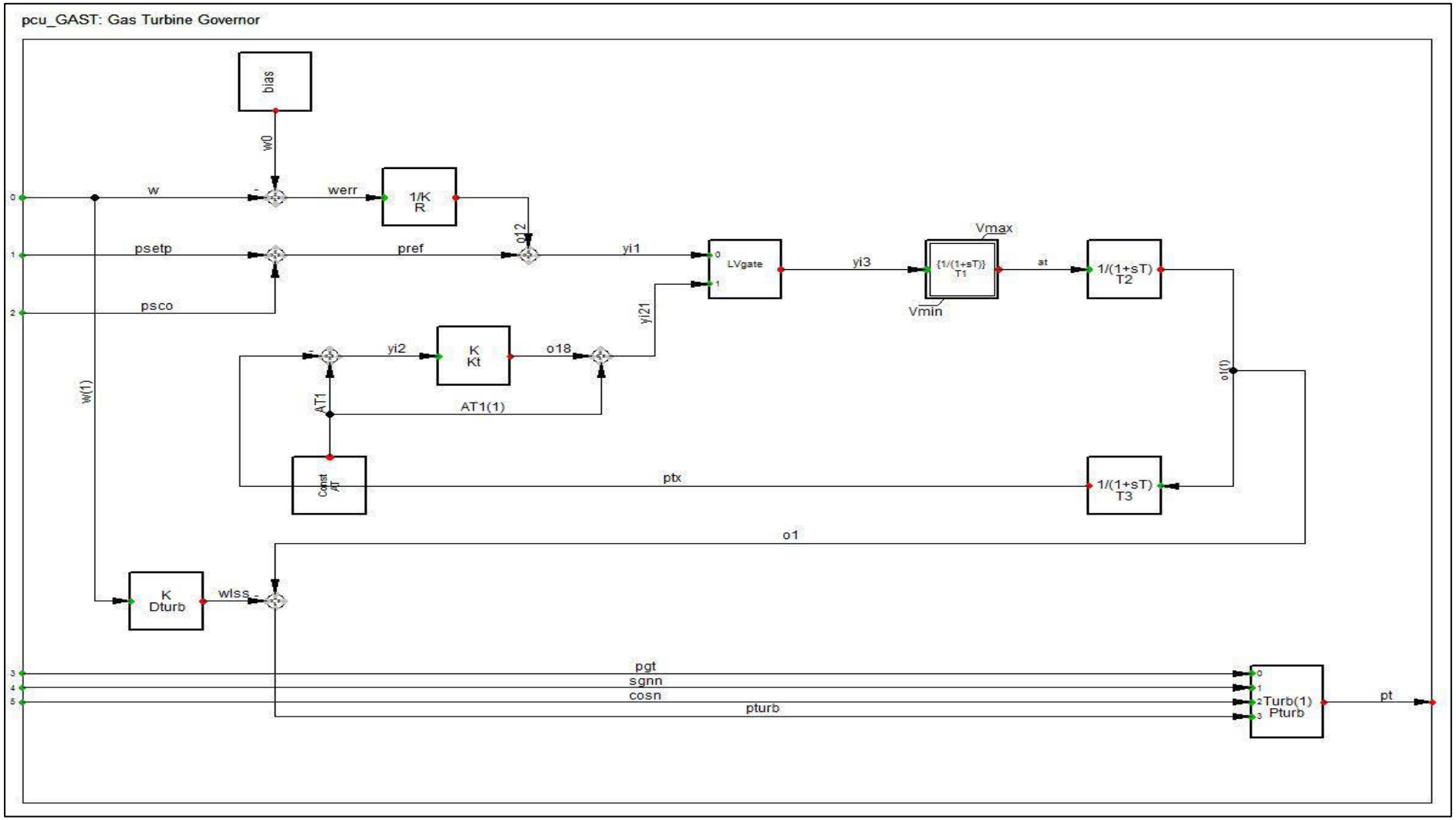

Figure A3: pcu_GAS Turbine Governor

Table A8: Turbine Governor Parameters

Parameter	**Value**
R Speed Droop [p.u.]	0.05
T1 Controller Time Constant [s]	0.4
T2 Actuator Time Constant [s]	1
T3 Compressor Time Constant [s]	3
AT Ambient Temperature Load Limit [p.u]	1
Kt Turbine Factor [p.u.]	2
Dturb Frictional Losses Factor [p.u.]	0
Pturb Turbine Rated Power (0=pturb=pgen) [MW}	0
Vmin Controller Minimum Output [p.u.]	0
Vmax Controller Maximum Output [p.u.]	1

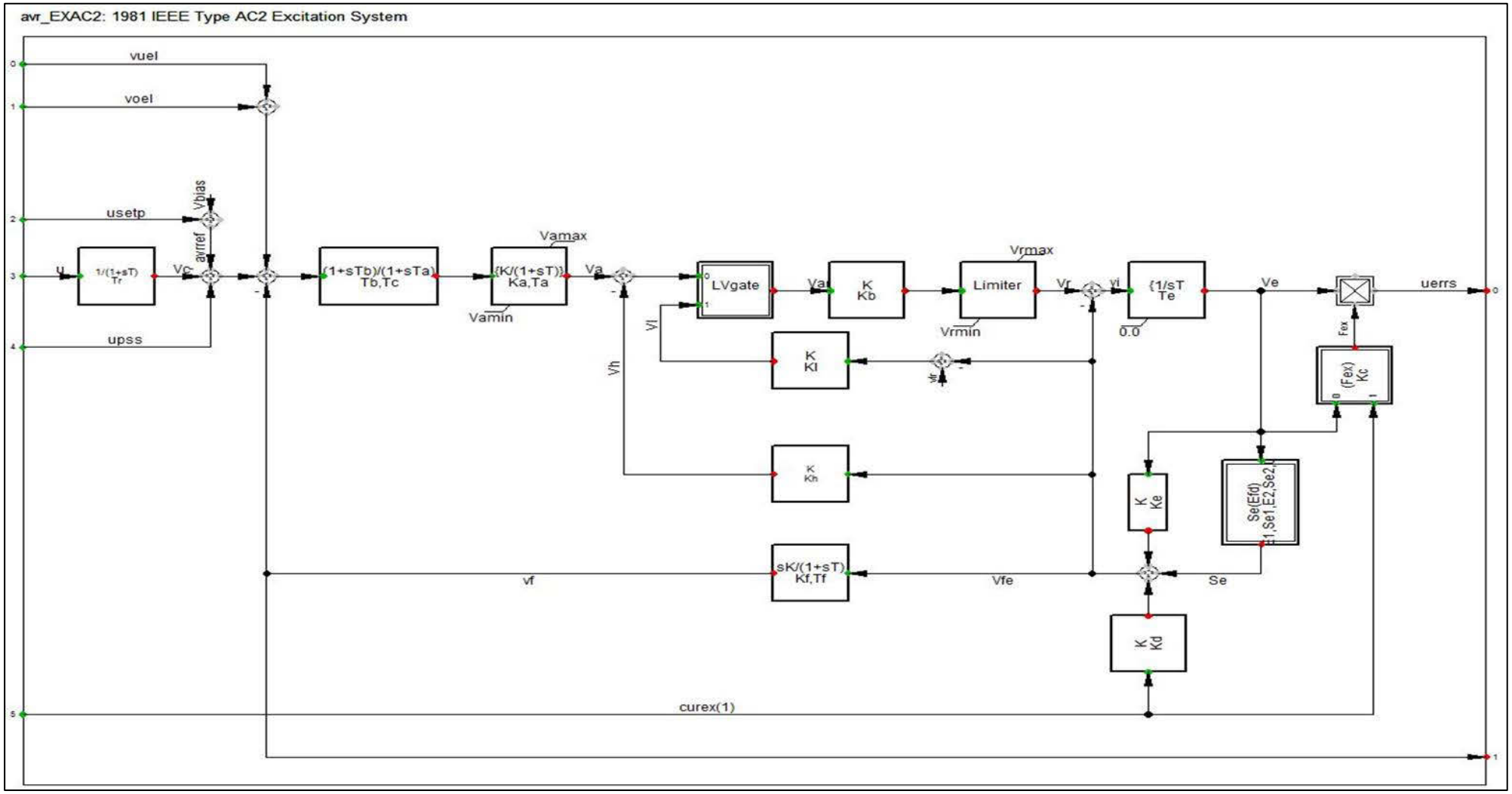

Figure A4: avr_EXAC2 IEEE Type AC2 Excitation System Block Diagram

Table A9: AVR Parameters

Parameter	**Value**
Tr Measurement Delay [s]	0.025
Tb Filter Delay time [s]	1
Tc Filter Derivative Time Constant [s]	1
Ka Controller Gain [p.u.]	400
Ta Controller Time Constant [s]	0.02
Kb Excitation System Factor [p.u.]	10
Te Exciter Time Constant [s]	0.8
Kl Excitation System Factor [p.u.]	1
Kh Excitation System Factor [p.u.]	1
Kf Stabilization Path Gain [p.u.]	0.008
Tf Stabilization Path Delay Time [s]	1
Kc Rectifier Regulation Constant [p.u.]	0.65
Kd Exciter Armature Reaction Factor [p.u.]	1
E1 Saturation Factor 1 [p.u.]	3.9
Se1 Saturation Factor 2 [p.u.]	0.1
E2 Saturation Factor 3 [p.u.]	5.2
Se2 Saturation Factor 4 [p.u.]	0.5
Vlr Excitation System Factor [p.u.]	14.29
Ke Excitation Constant [p.u.]	1
Vamin Controller Minimum Output [p.u.]	-10
Vmin Excitation System Minimum Output [p.u.]	-6.6
Vamax Controller Maximum Output [p.u.]	10
Vmax Excitation System Maximum Output [p.u.]	7.3

Appendix B: Simulation Results

Output Window Results for Network 3

```
DIgSI/pcl  - (t=000:000 ms) -----------------------------------------------------------
DIgSI/pcl  - (t=000:000 ms) 'Northern TX\Medupi Power Station\Medupi 400 BB1.ElmTerm':
DIgSI/pcl  - (t=000:000 ms) 3-Phase Short-Circuit.
DIgSI/pcl  - (t=000:000 ms) with Fault Impedance Rf = 0.000000 Ohm Xf = 0.000000 Ohm
DIgSI/pcl  - (t=120:000 ms) -----------------------------------------------------------
DIgSI/pcl  - (t=120:000 ms) 'Northern TX\Medupi Power Station\Medupi 400 BB1.ElmTerm':
DIgSI/pcl  - (t=120:000 ms) Clear Short Circuit.
DIgSI/wrng - (t=01:000 s) Real time out of synchronization
DIgSI/pcl  - (t=01:234 s) -------------------------------------------------------------
DIgSI/pcl  - (t=01:234 s) 'Northern TX\Matimba Power Station\Matimba Gen 5.ElmSym':
DIgSI/pcl  - (t=01:234 s) Generator out of step (pole slip).
DIgSI/pcl  - (t=01:236 s) -------------------------------------------------------------
DIgSI/pcl  - (t=01:236 s) 'Northern TX\Medupi Power Station\Medupi Gen6.ElmSym':
DIgSI/pcl  - (t=01:236 s) Generator out of step (pole slip).
DIgSI/pcl  - (t=01:236 s) -------------------------------------------------------------
DIgSI/pcl  - (t=01:236 s) 'Northern TX\Medupi Power Station\Medupi Gen4.ElmSym':
DIgSI/pcl  - (t=01:236 s) Generator out of step (pole slip).
DIgSI/pcl  - (t=01:236 s) -------------------------------------------------------------
DIgSI/pcl  - (t=01:236 s) 'Northern TX\Medupi Power Station\Medupi Gen3.ElmSym':
DIgSI/pcl  - (t=01:236 s) Generator out of step (pole slip).
DIgSI/pcl  - (t=01:236 s) -------------------------------------------------------------
DIgSI/pcl  - (t=01:236 s) 'Northern TX\Medupi Power Station\Medupi Gen2.ElmSym':
DIgSI/pcl  - (t=01:236 s) Generator out of step (pole slip).
DIgSI/pcl  - (t=01:236 s) -------------------------------------------------------------
DIgSI/pcl  - (t=01:236 s) 'Northern TX\Medupi Power Station\Medupi Gen1.ElmSym':
DIgSI/pcl  - (t=01:236 s) Generator out of step (pole slip).
DIgSI/pcl  - (t=01:236 s) -------------------------------------------------------------
DIgSI/pcl  - (t=01:236 s) 'Northern TX\Medupi Power Station\Medupi Gen5.ElmSym':
DIgSI/pcl  - (t=01:236 s) Generator out of step (pole slip).
DIgSI/pcl  - (t=01:239 s) -------------------------------------------------------------
DIgSI/pcl  - (t=01:239 s) 'Northern TX\Matimba Power Station\Matimba Gen 3.ElmSym':
DIgSI/pcl  - (t=01:239 s) Generator out of step (pole slip).
DIgSI/pcl  - (t=01:239 s) -------------------------------------------------------------
DIgSI/pcl  - (t=01:239 s) 'Northern TX\Matimba Power Station\Matimba Gen 6.ElmSym':
DIgSI/pcl  - (t=01:239 s) Generator out of step (pole slip).
DIgSI/pcl  - (t=01:239 s) -------------------------------------------------------------
DIgSI/pcl  - (t=01:239 s) 'Northern TX\Matimba Power Station\Matimba Gen 2.ElmSym':
DIgSI/pcl  - (t=01:239 s) Generator out of step (pole slip).
DIgSI/pcl  - (t=01:239 s) -------------------------------------------------------------
DIgSI/pcl  - (t=01:239 s) 'Northern TX\Matimba Power Station\Matimba Gen 4.ElmSym':
DIgSI/pcl  - (t=01:239 s) Generator out of step (pole slip).
DIgSI/pcl  - (t=01:239 s) -------------------------------------------------------------
DIgSI/pcl  - (t=01:239 s) 'Northern TX\Matimba Power Station\Matimba Gen 1.ElmSym':
DIgSI/pcl  - (t=01:239 s) Generator out of step (pole slip).
DIgSI/pcl  - (t=01:272 s) -------------------------------------------------------------
DIgSI/pcl  - (t=01:272 s) 'Northern TX\Coal 2 Power Station\Coal 2 Gen 1.ElmSym':
DIgSI/pcl  - (t=01:272 s) Generator out of step (pole slip).
DIgSI/pcl  - (t=01:272 s) -------------------------------------------------------------
DIgSI/pcl  - (t=01:272 s) 'Northern TX\Coal 2 Power Station\Coal 2 Gen 2.ElmSym':
DIgSI/pcl  - (t=01:272 s) Generator out of step (pole slip).
DIgSI/pcl  - (t=01:272 s) -------------------------------------------------------------
DIgSI/pcl  - (t=01:272 s) 'Northern TX\Coal 2 Power Station\Coal 2 Gen 3.ElmSym':
DIgSI/pcl  - (t=01:272 s) Generator out of step (pole slip).
DIgSI/pcl  - (t=01:283 s) -------------------------------------------------------------
DIgSI/pcl  - (t=01:283 s) 'Northern TX\Coal 3 Power Station\Coal 3 Gen 1.ElmSym':
DIgSI/pcl  - (t=01:283 s) Generator out of step (pole slip).
```

Figure B1: Output Window Results of Network 3

Network 1 Results

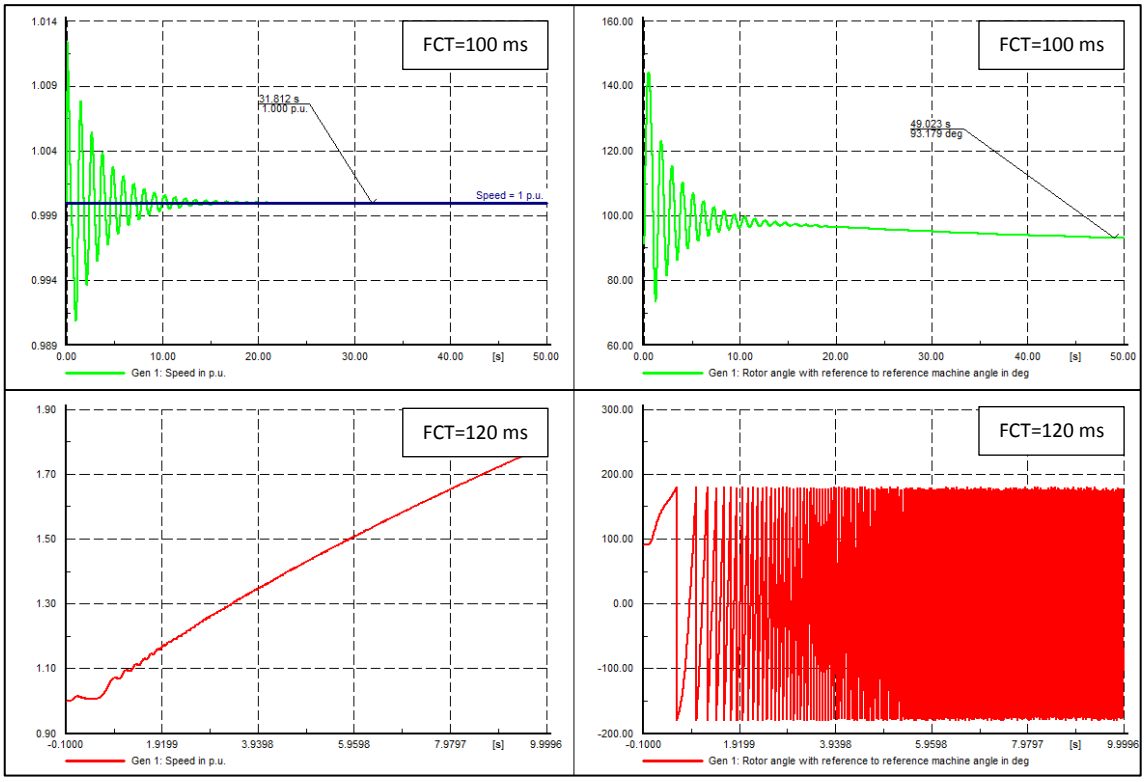

Figure B2: TMIB System Result for 50 seconds Simulation Time

Network 3 Transmission Line Fault Results

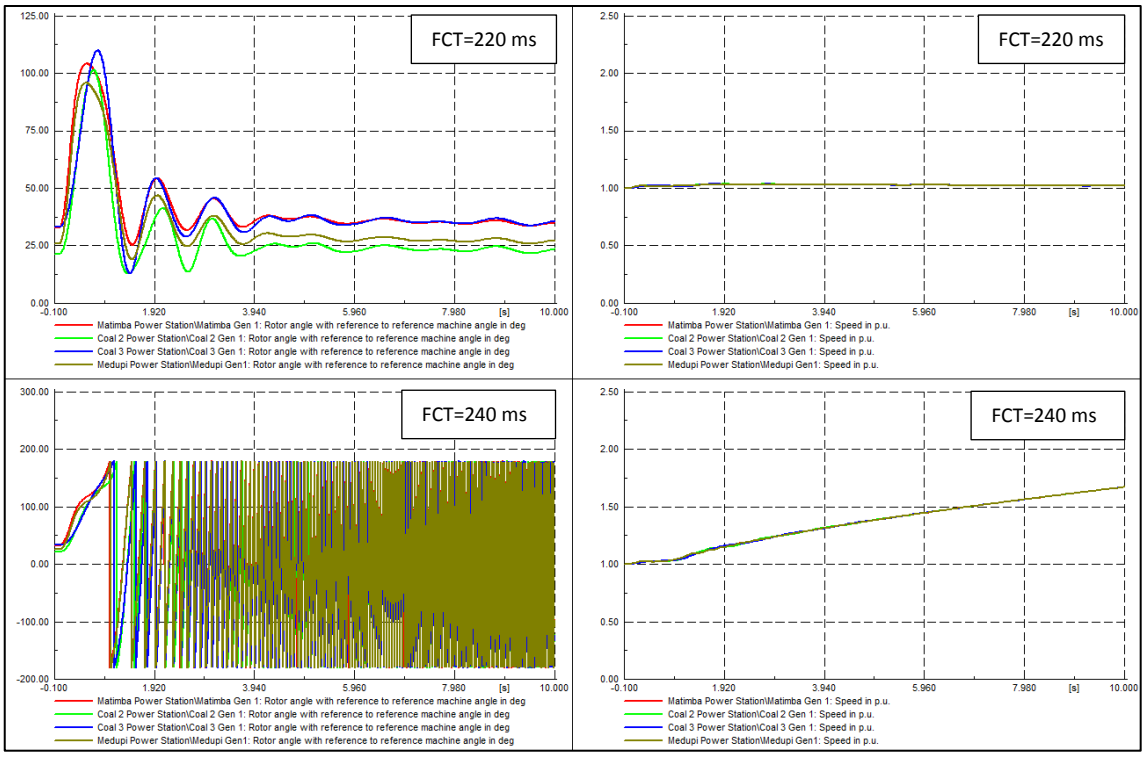

Figure B3: Results for Fault on Line Matimba-Pluto

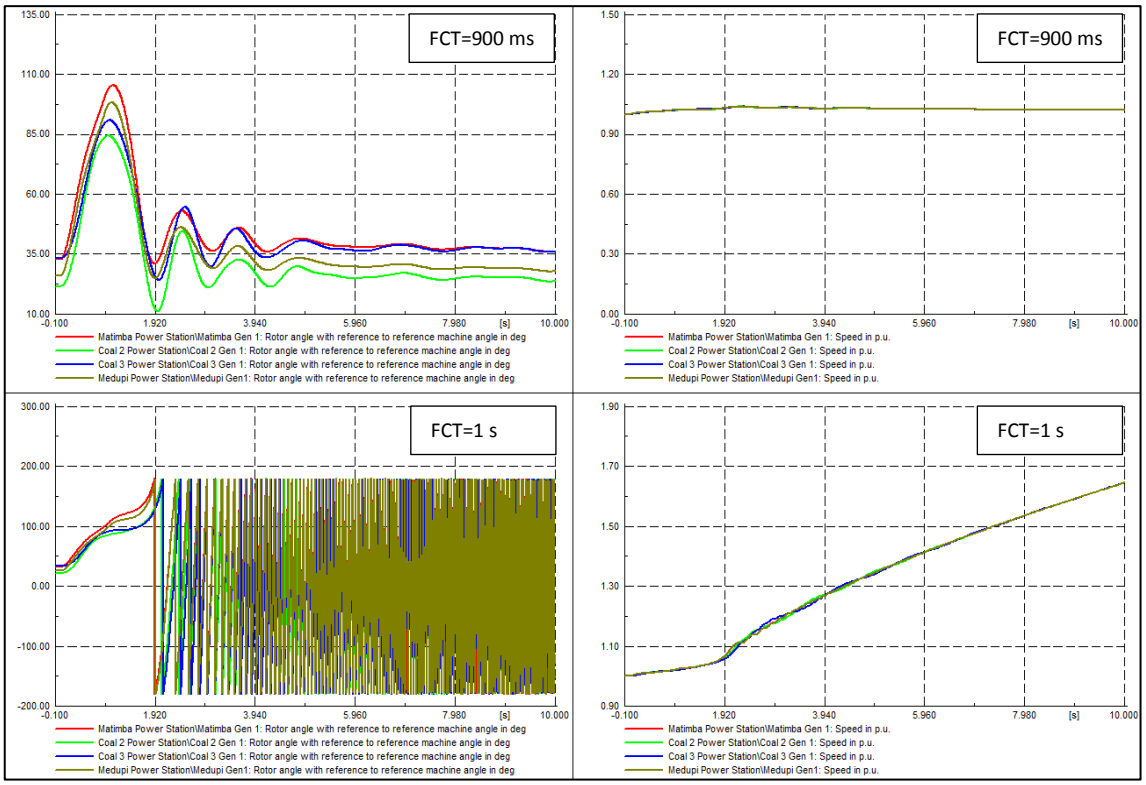

Figure B4: Results for Fault on Line Medupi-Ngwedi

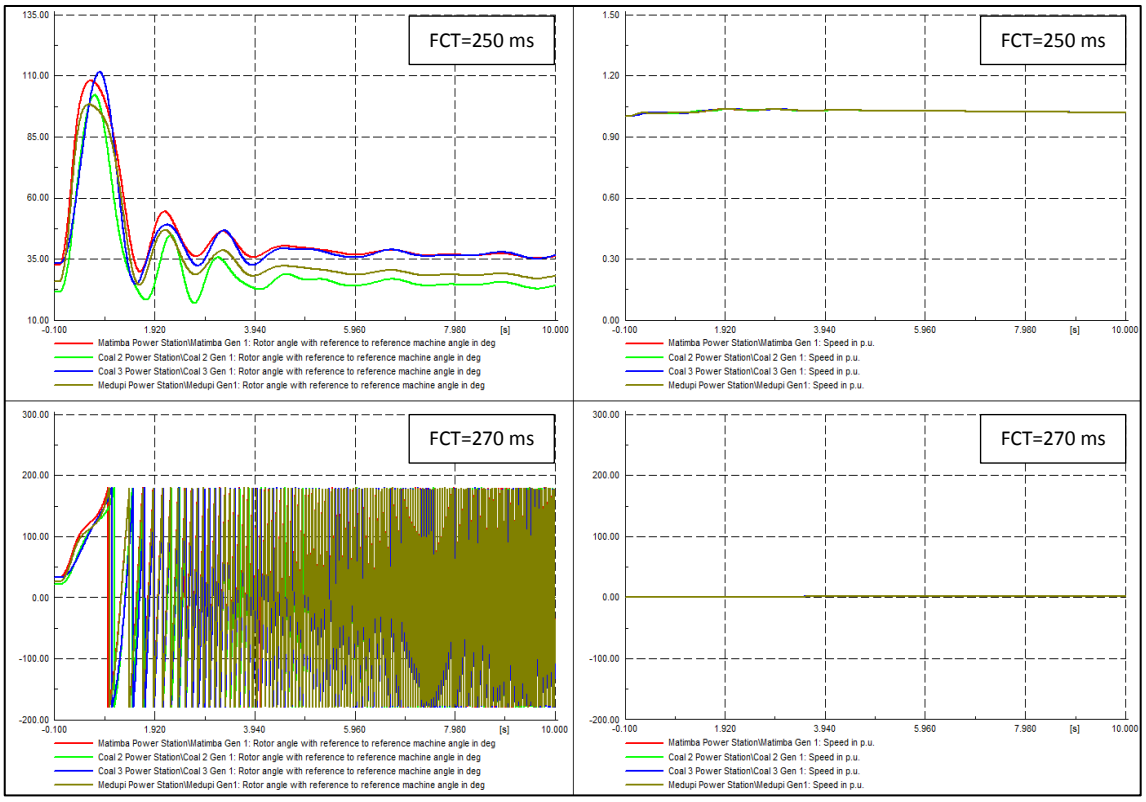

Figure B5: Results for Fault on Line Selemo-Masa

Network 3 Generator Busbar Fault Results

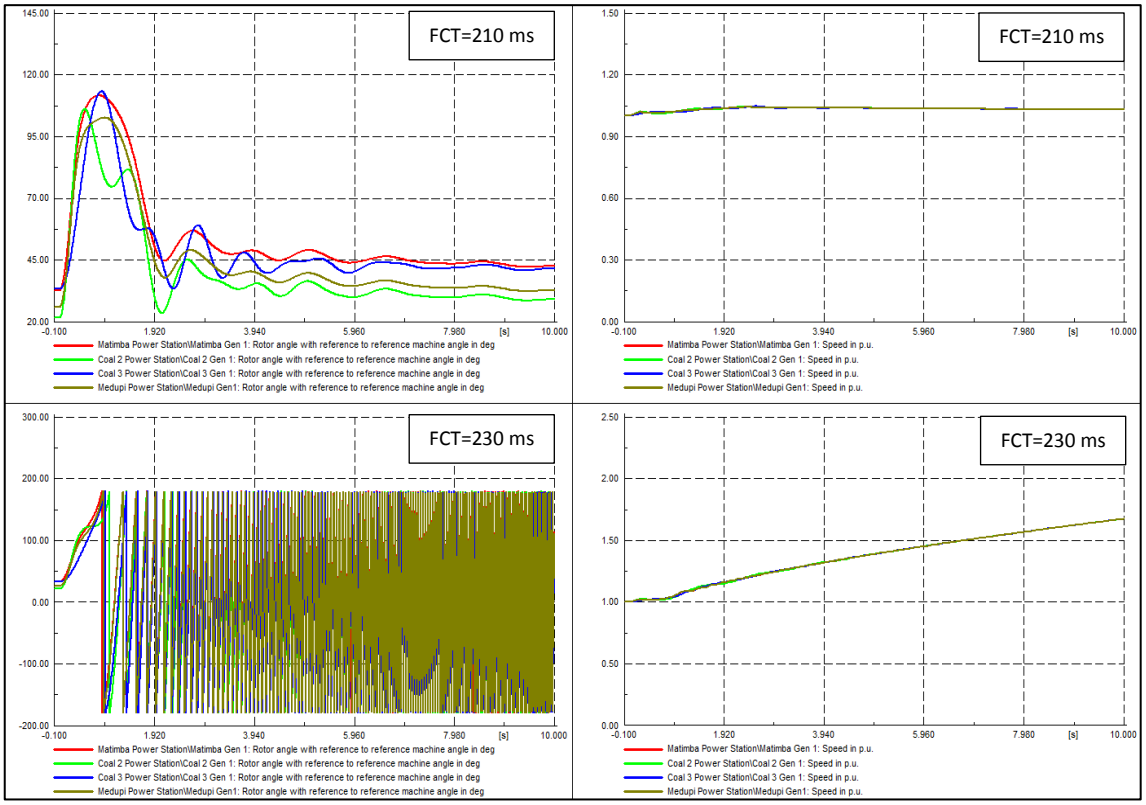

Figure B6: Results for Fault on Coal 2 400 kV BB1

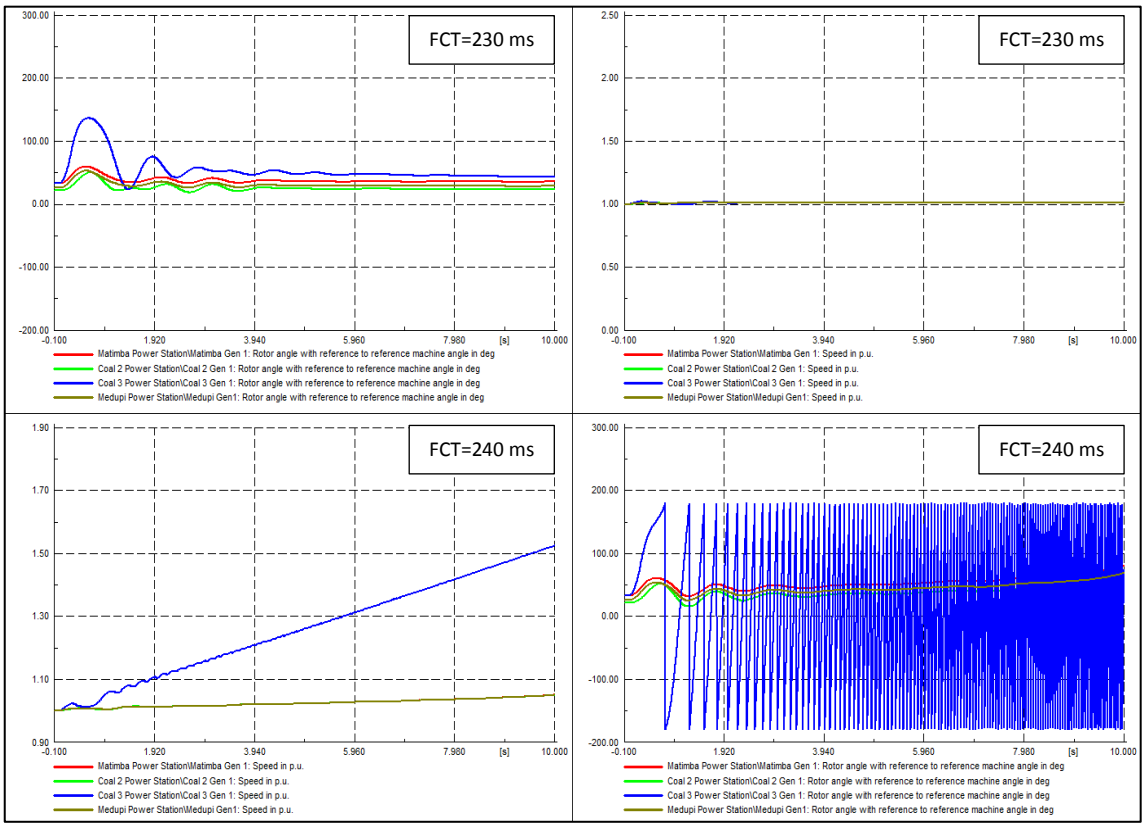

Figure B7: Results for Fault on Coal 3 400 kV BB1

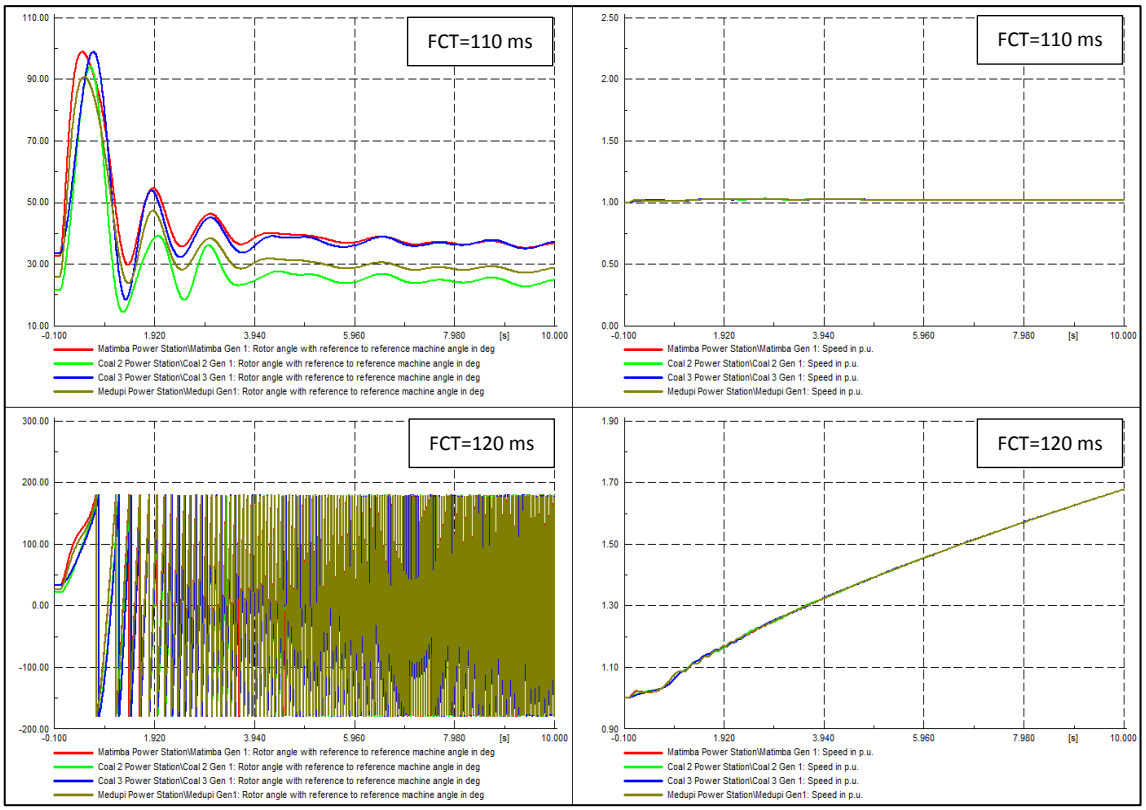

Figure B8: Results for Fault on Matimba 400 kV BB1

Appendix C: Schematic Diagrams

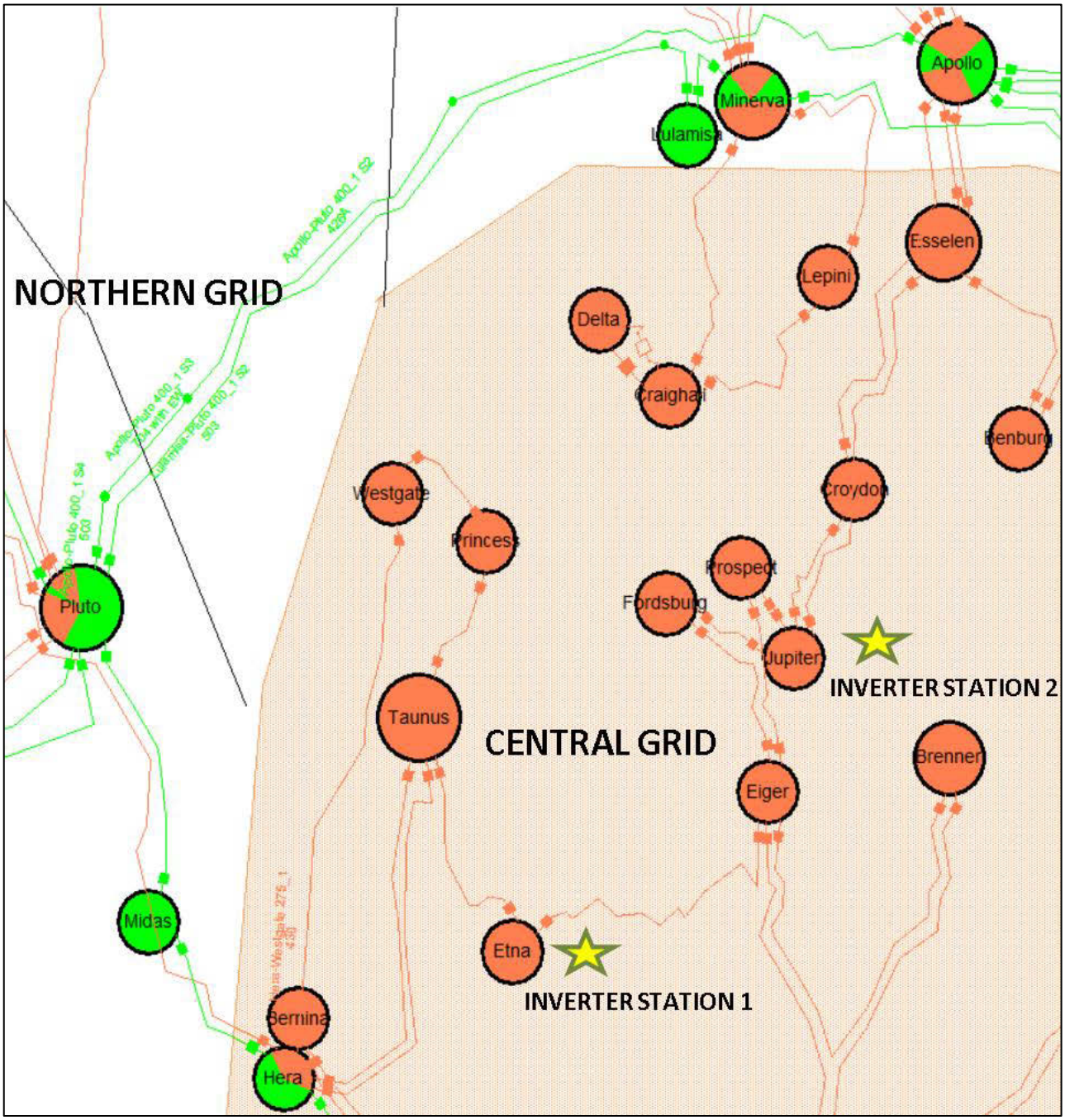

Figure C1: Central Grid Overview Diagram

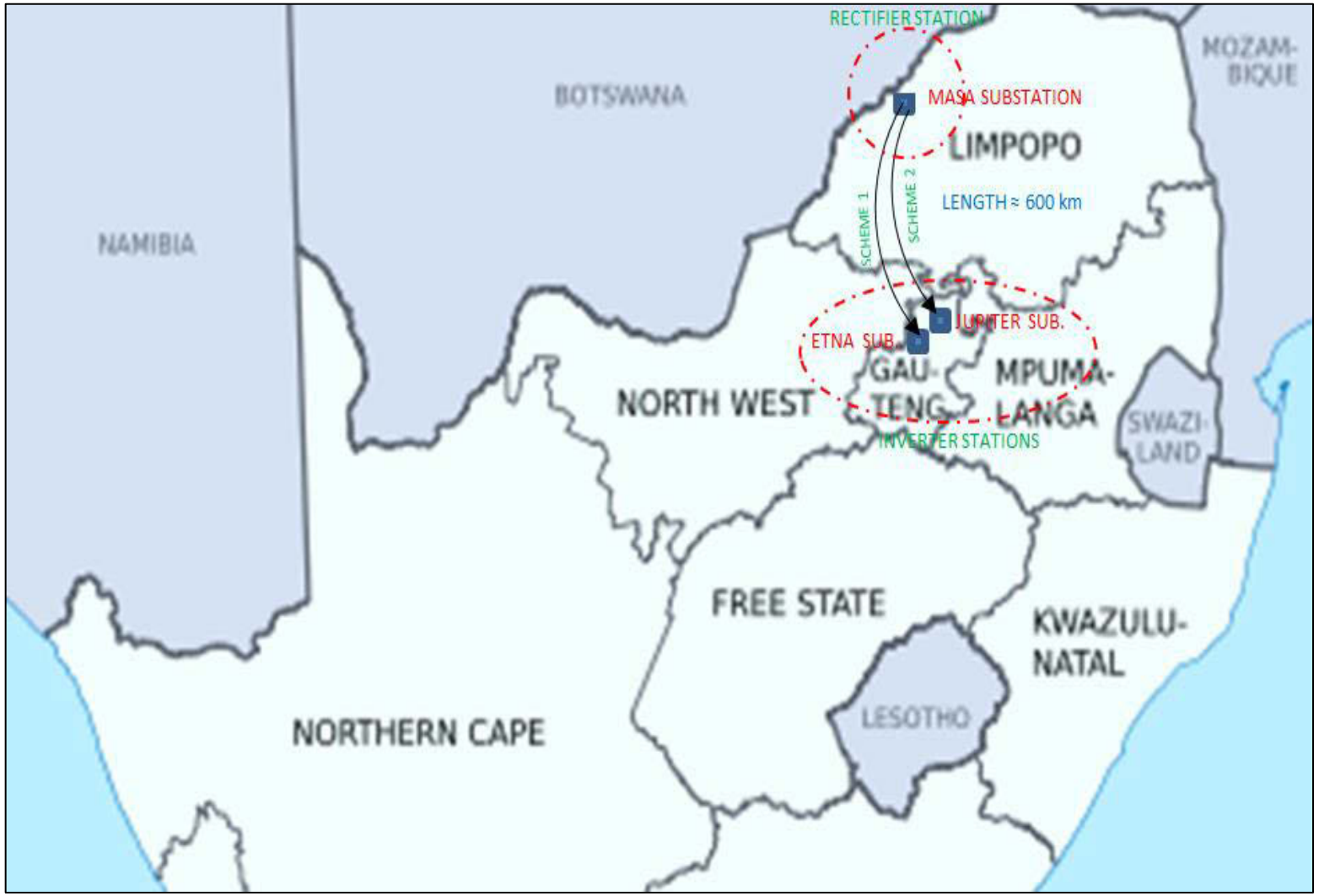

Figure C2: Limpopo-West LCC-HVDC Scheme Overview

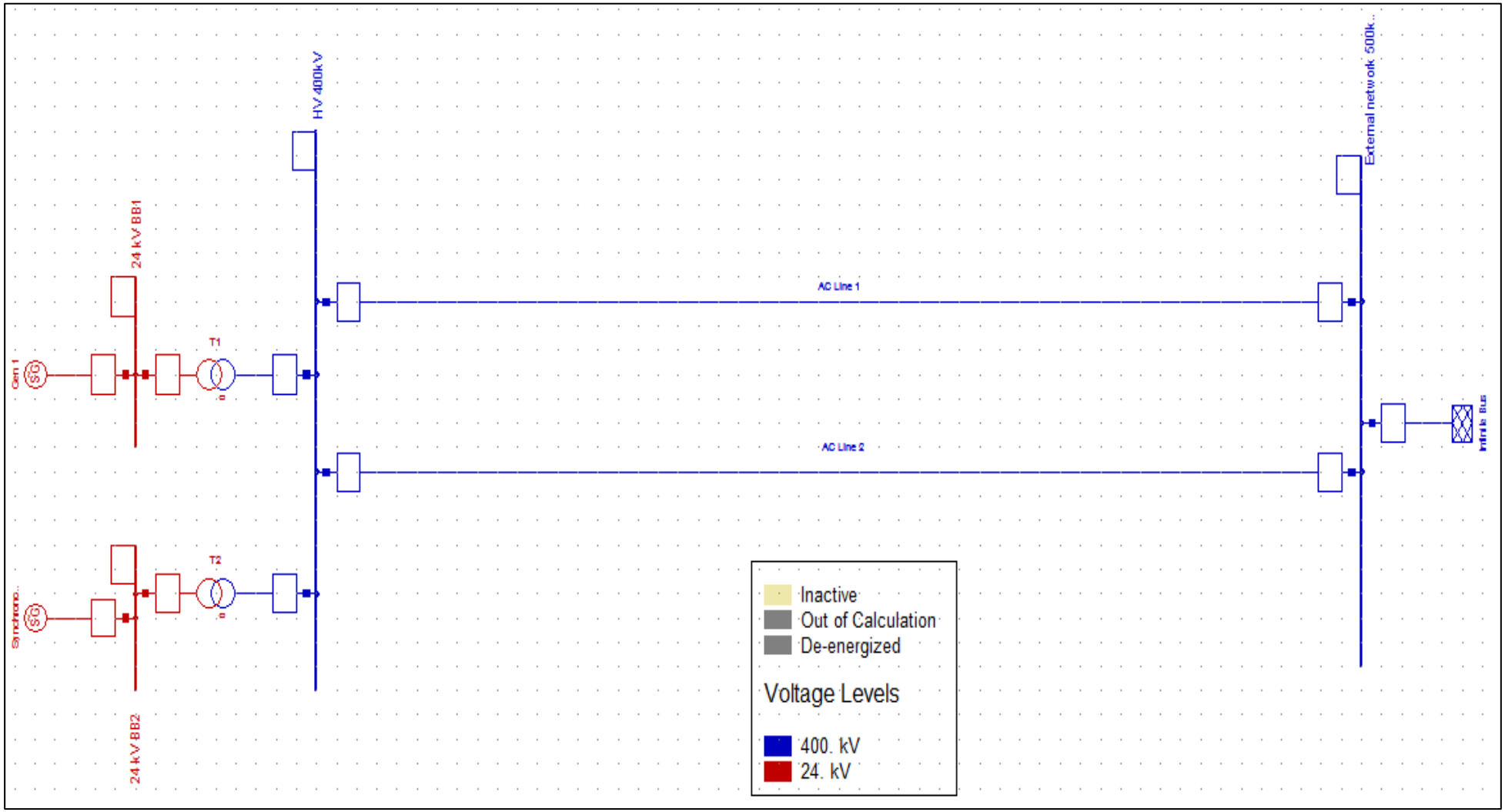

Figure C3: Two Machine Infinite Bus System (TMIB)

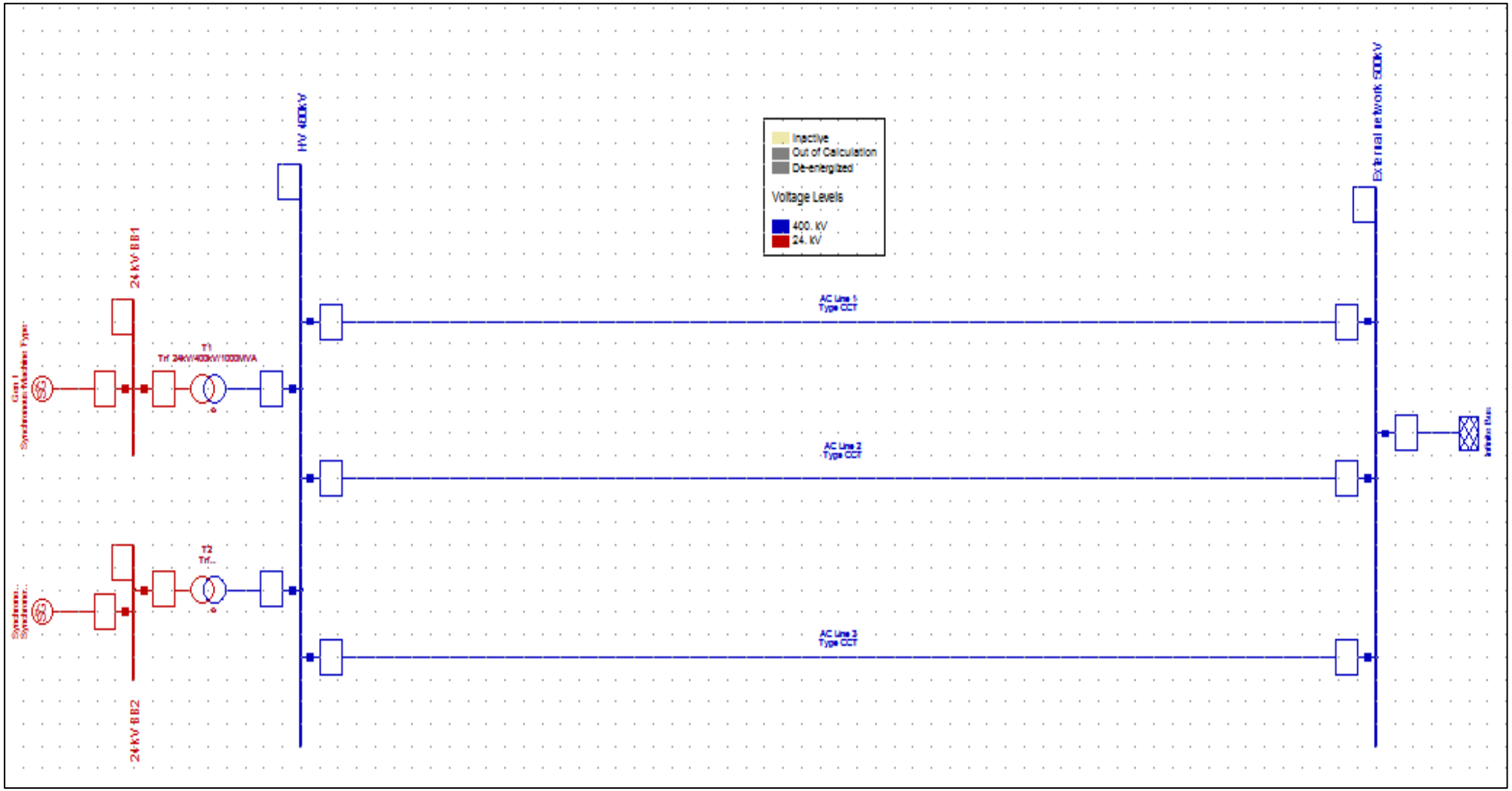

Figure C4: TMIB with an Additional HVAC Line in Parallel

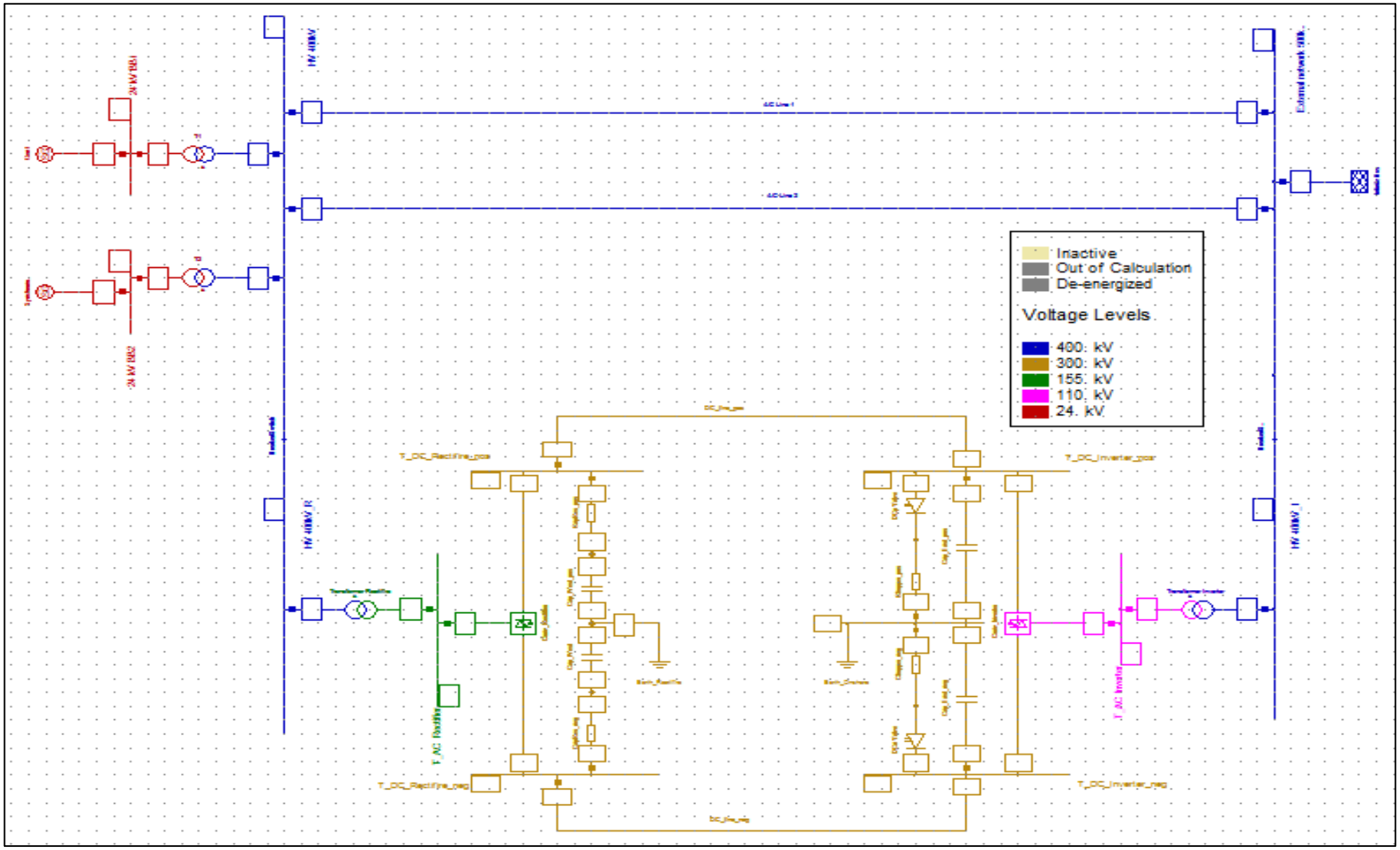

Figure C5: TMIB with a VSC-HVDC Scheme in Parallel

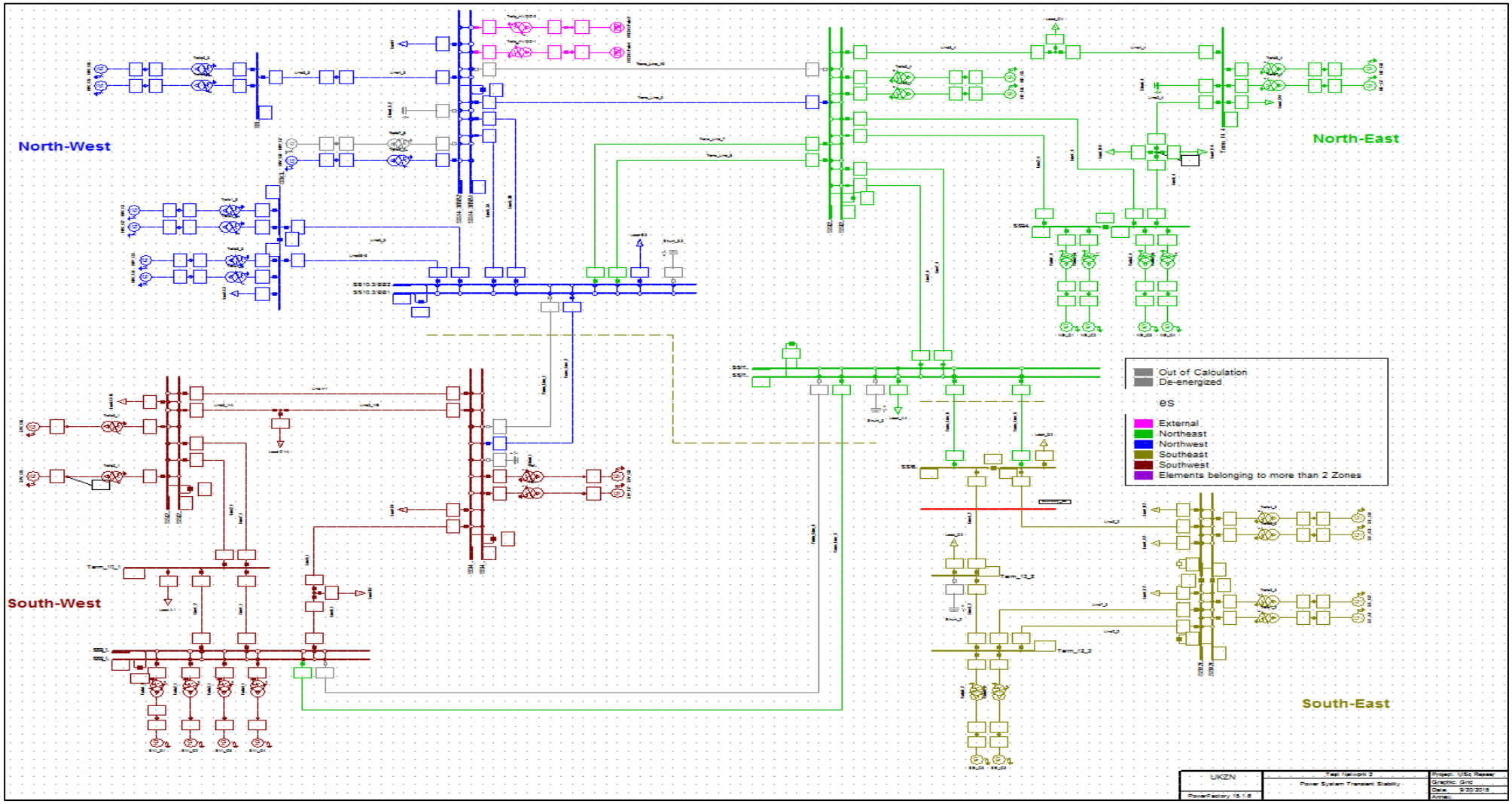

Figure C6: Network 2 Schematic Diagram

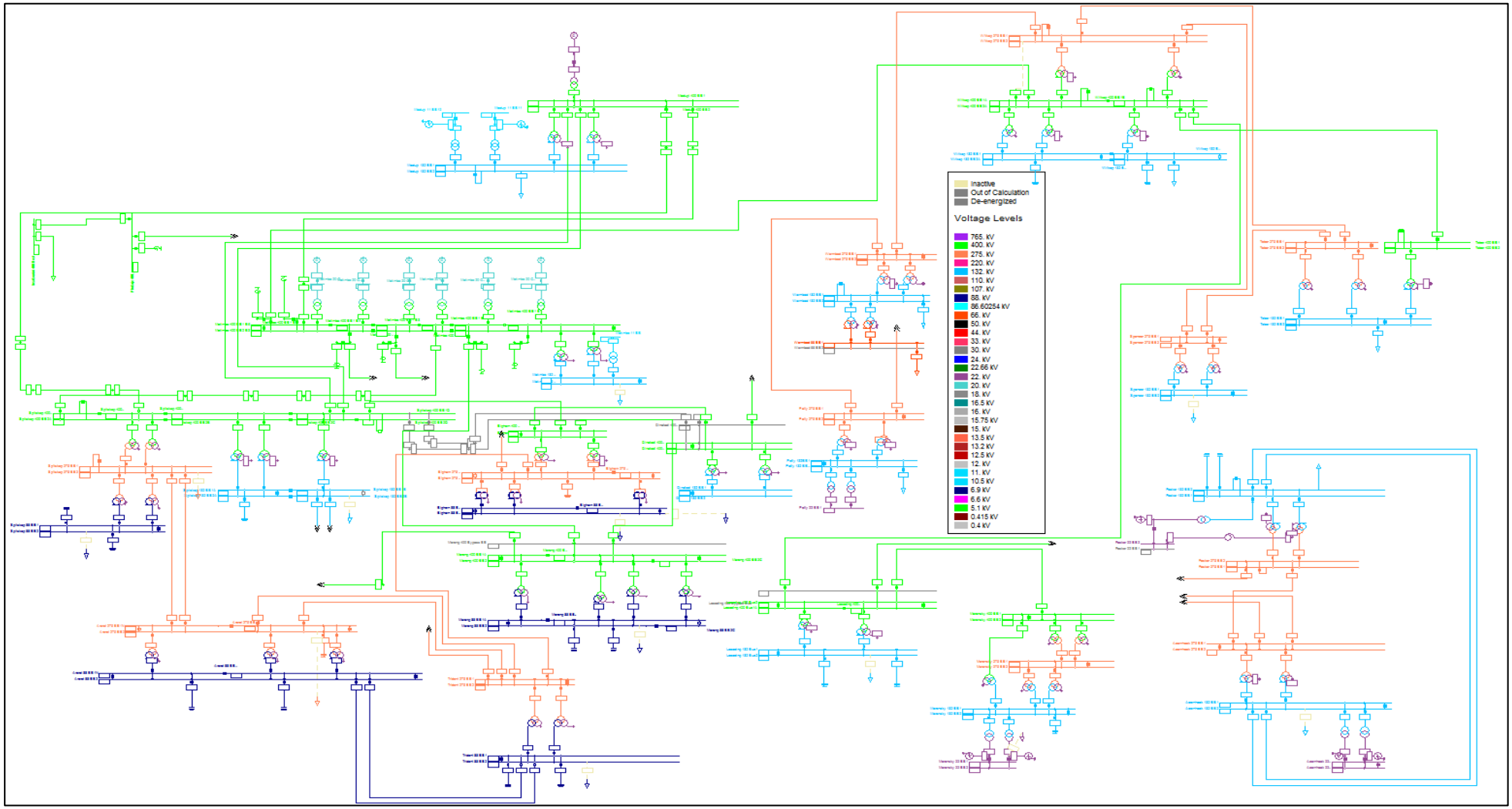

Figure C7: Network 3 Schematic Diagram

Appendix D: LCC-HVDC Control Theory

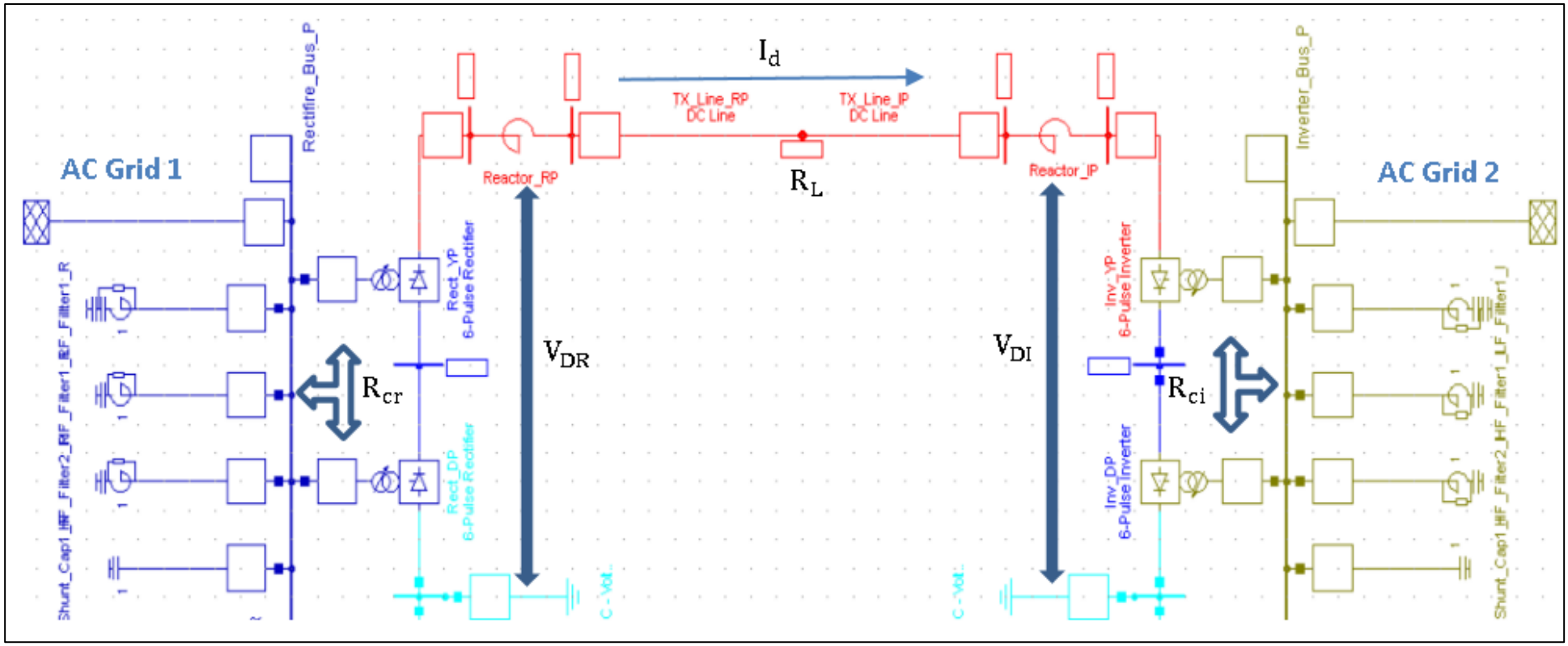

Figure D1: Mono-polar LCC-HVDC Link

Figure D1 shows a mono-polar LCC-HVDC link. The transmission line parameters, direction of the line current and transformer resistances are shown.

The DC transmission line current (I_d) and voltage (V_d), relative to the system parameters is given by [6]:

$$I_d = \frac{V_{dor}.cos\alpha_r - V_{doi}.cos\gamma_i}{R_{cr}+R_L-R_{ci}} \quad \text{(D-1)}$$

$$V_d = V_{do}.cos\alpha - R_c I_d \quad \text{(D-2)}$$

Where:

I_d = DC current flowing from the rectifier to the inverter

V_{dor} = Internal rectifier voltage

V_{doi} = Internal inverter voltage

R_{cr} = Rectifier transformer resistance

R_{ci} = Inverter transformer resistance

R_L = DC line resistance

α_r = Rectifier firing angle

γ_i = Inverter extinction angle

By using the control system for the control of the gate firing angle, the DC voltage is continuously controlled by controlling the converter's internal voltages ($V_{dor}.cos\alpha_r$ and $V_{doi}.cos\gamma_i$) [6]. Consequently, the DC current and DC power is controlled to the desired magnitude. In HVDC systems, it is essential to prevent large DC current fluctuations. This is achieved by continuously controlling the converter internal voltages by continuously manipulating the converter firing and extinction angles. During system healthy conditions, the rectifier is assigned the responsibility of constant DC current control and the inverter is assigned the responsibility of DC voltage control [6].

If there is a reduction in the rectifier internal voltage, the inverter takes over DC current control and the rectifier switches to DC voltage control. Under low AC voltage operation conditions, it is desirable to limit the maximum allowable DC current to a pre-

determined value, thus limiting the transferable DC power. The voltage dependent current order limiter is used to perform this function [6]. The various LCC-HVDC control system functions are shown in figure D2.

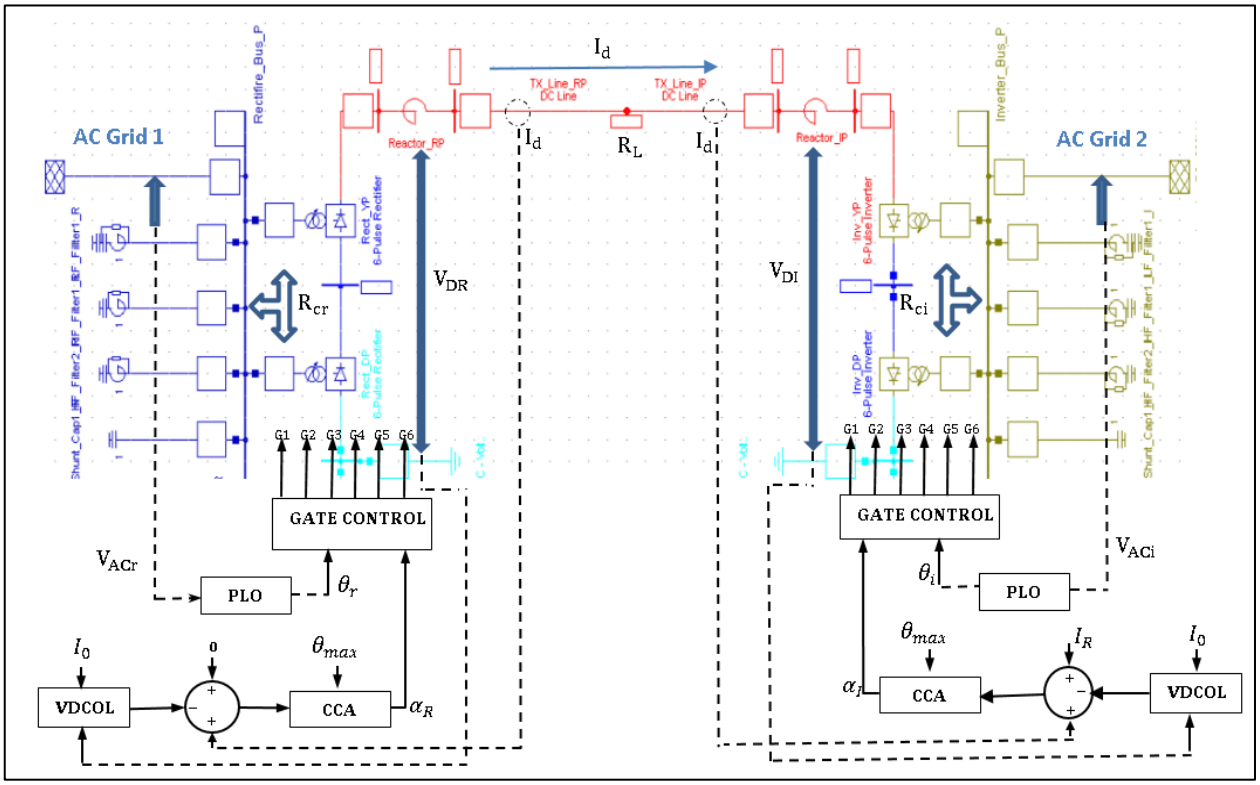

Figure D2: Mono-polar LCC-HVDC Control System

The main LCC-HVDC control system functions are [6]:

- Voltage dependent current order limiter (VDCOL)
- Phase locked oscillator (PLO)
- Current control amplifier (CCA)
- Gate controller (GC)

The implementation of each of these control functions is explained in detail as follows:

VDCOL

The VDCOL function is used to reduce the current order for a reduction in the measured DC voltage. The static characteristics of the VDCOL function are shown in figure D3 [6].

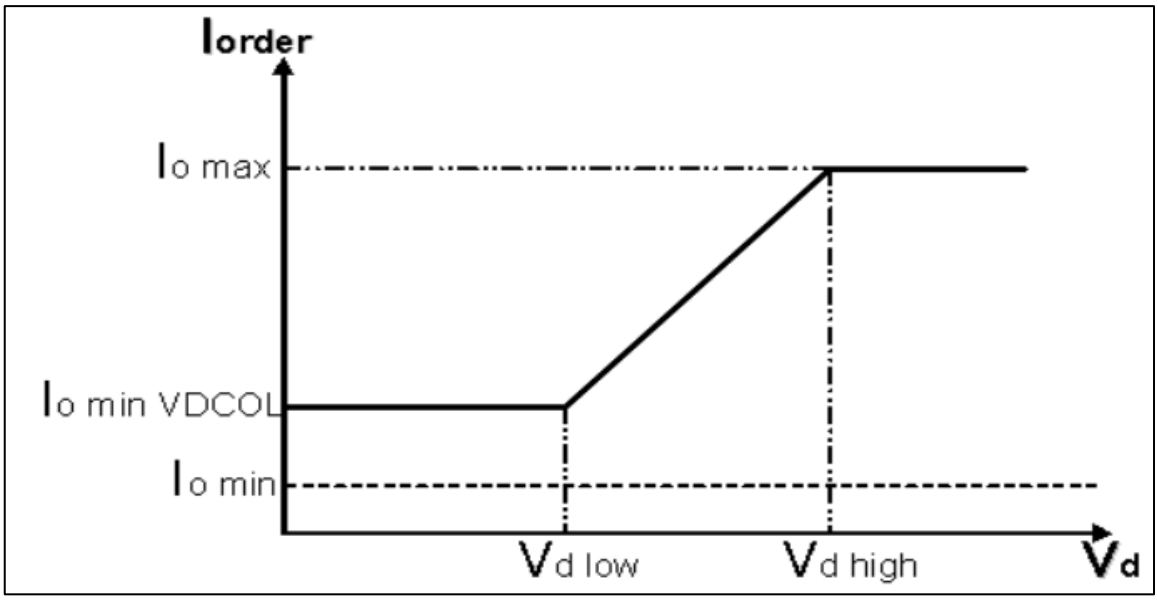

Figure D3: VDCOL Function Characteristics

More information on the implementation of the VDCOL function is presented in [6].

CCA

The CCA function is used to improve the dynamic operation of the current control loop. The current control loop is used to ensure stable current control, fast step response and to minimize the current error during steady-state operation [6].

PLO

In this function, the phase vector technique is used to exploit trigonometric multiplication identities to form an error signal; this error signal is then used to either speeds up or to slow down the PLO in order to match the phase. More detailed information on the operation of PLO is found in [68].

GC

The gate control compares the firing order α_{order} to the phase locked ramp signal $\boldsymbol{\theta}$ and produces the gate firing pulses [6].

More information on the implementation of the HVDC control system functions and the block diagrams of the functions can be found in [6].

Appendix E: Eskom Power Plant Portfolio

Table E1: Eskom's Power Stations [69]

Station Name	Type of Station	Total Gen. Capacity (MW)	Year Commissioned
Arnot	Coal	2100	1975
Candem	Coal	1600	1967
Duvha	Coal	3600	1980
Grootvlei	Coal	1200	1969
Hendrina	Coal	2000	1970
Kendal	Coal	4116	1988
Komati	Coal	1000	1961
Kriel	Coal	3000	1976
Lethabo	Coal	3708	1985
Majuba	Coal	4110	1996
Matimba	Coal	3990	1987
Matla	Coal	3600	1983
Tutuka	Coal	3654	1985
Koeberg	Nuclear	1920	1984
Gariep	Hydro	360	1971
Vanderkloof	Hydro	240	1977
Drakensberg	Pumped Storage	1000	1981
Palmiet	Pumped Storage	400	1988
Darling	Wind	5.2	2008
Klipheuwel	Wind	3.2	2002
Acacia	OCGT	171	1976
Port Rex	OCGT	171	1976
Ankerlig	OCGT	1338	2007
Gourikwa	OCGT	746	2007
Medupi	Coal	4764 (794 installed)	2015
Total Installed Generation Capacity		**44 826.4 MW**	

Appendix E: HVDC Control Algorithm Code

VSC-HVDC Control Algorithm Code

Rectifier controller

```
!Rectifier VSC-Controller, controlls the Rectifier Voltage and Frequ.
! Use of Feedforward: Pm=uac/(sqrt(3/2)*udc))
!Changes the frequ. in case of overvoltage in the DC-line as a signal
! for the wind turbines to reduce the power output
!In case of a Rectifier short circuit, the converter current will exceed
! the limit, thus, the Rectifier voltage have to be limited
inc0(u) = 1
inc0(udcp) = 1
inc0(udcm) = 1

inc(x1)=-iq
inc(x2)=Pm*sqrt(3/2)*udc*1.5/1.55
inc(xu)=u
inc(Uacref)=ufilter
inc(udc0)=udcp-udcm



vardef(Kiac)='pu';'Proportional Gain for Current Controller'
vardef(Tiac)='s';'Integrator Time Const. for Cur. Controller'
vardef(i_min)='pu';'Min Limit Value for Current Limitation'
vardef(i_max)='pu';'Max Limit Value for Current Limitation'
vardef(Tfilter_U)='s';'Time constant for PT1-Filter'
vardef(Kuac)='pu';'Proportional Gain for Voltage Controller'
vardef(Tuac)='s';'Integrator Time Const. for Volt. Controller'
vardef(Uac_max)='pu';'Max Limit for Rectifier Voltage'
vardef(Uac_min)='pu';'Min Limit for Rectifier Voltage'
!
```

vardef(F_ref)='pu';'Reference Frequency'

!

vardef(UdcHigh)='pu';'Upper Udc Limit for Frequ. Lifting'

vardef(UdcLow)='pu';'Lower Udc Limit for Frequ. Lifting'

vardef(Frequ_Grad)='1/s';'Gradient for Frequ. Lifting'

vardef(plusFrequ)='pu';'Value of Frequ. Lifting'

Inverter current controller

!Simple current controller for Inverter VSC-converter without decoupling

inc(xPd)=Pmd

inc(xPq)=Pmq

inc(id_ref)=id

inc(iq_ref)=iq

vardef(Kpm)='pu';'Proportional Gain for d&q-axis'

vardef(Tpm)='s';'Integral Time for d&q-axis'

vardef(P_max)='pu';'max limit Pm for d&q-axis'

vardef(P_min)='pu';'min limit Pm for d&q-axis'

Inverter chopper controller

inc0(udcp) = 1

inc0(udcm) = 1

inc(udc0)=udc

inc(choptime)=0

vardef(UdcUpper)='pu';'Threshold for Chopper Connection'

vardef(UdcLower)='pu';'Threshold for Chopper Disconnection'

Inverter control

inc(udcref)=(udcp-udcm)/2-udc_offset

inc(uac_ref) = select(MODE=0,uac,select(MODE=1,uac+Qin*Droop,uac))

inc(Qref) = Qin

inc(xrudc)= udc

```
inc(xruac)= uac

inc(xqm)  = Qin

inc(xd)   = id_ref


inc0(id_ref) = 0.852

inc0(iq_ref) = -0.1269


inc(iqref) = iq_ref


vardef(K_flt) = '-';'Reactive current flt gain'

vardef(fltMODE)='0/1';'0=ctrl acc MODE, 1=ctrl acc TC2007'

vardef(MODE) ='0/1/2';'0=voltg. ctrl. 1=droop 2=Q ctrl.'

vardef(array_iqlim)='pu';'Current Limit Curve'

vardef(iqfmax)='pu';'Max. reactive current in fault case'

vardef(Trudc)='s';'DC Voltage Filter Time Constant'

vardef(i_max)='pu';'Current Limit'

vardef(Droop)='pu';'Gain for Droop Control'

vardef(Kd)   ='-';'Gain of DC PI-Controller'

vardef(Td)   ='s';'Integral Time Constant of DC PI-Controller'

vardef(Ku)   ='-';'Gain of PID Droop-Controller (Q and Vac)'

vardef(Kiu)  ='1/s';'Integral Constant of PID Droop Controller (Q and Vac)'

vardef(Kdu)  ='1/s';'Derivative Constant of PID Droop Controller (Q and Vac)'

vardef(Ut)   ='pu';'Voltage Deviation to enable Fault-Mode'

vardef(umax) ='pu';'Max. internal voltage allowed'

vardef(x)    ='pu';'Series reactor impedance'
```

LCC-HVDC Control Algorithm Code

Hvdc or alpha control

inc(REC_INT)=select(alpha>pi()/2,-1,1)

inc(du0)=VORD0-VMEAS-CEC

inc(dg0)=GMEAS-0.01745329*GORD0

inc(mode)=select(REC_INT=1,1,select(du0<dg0,2,3))

inc(xpi)=alpha

inc(xamax)=Grad*select(REC_INT=1,amax_rec,amax_inv)

inc(xamin)=Grad*select(REC_INT=1,amin_rec,amin_inv)

inc(xgpg)=select(mode=1,GID,select(mode=2,GUD,GGAM))

inc(xI)=GI*IDC

inc(xV)=GV*VDC

inc(IMARG)=select(REC_INT=1,0,IMARG0)

inc(IORD)=select(REC_INT=1,GI*IDC,GI*IDC+IMARG0)

inc(VORD)=select(mode=2,VMEAS-CEC,VORD0)

inc(GORD)=select(mode=3,GMEAS/0.01745329,GORD0)

inc0(VDC)=VORD0/GV

inc(INV)=VDC/abs(VDC)/REC_INT

alpha_deg=alpha/pi()*180

GAMMA control

inc(gamma)=min(gamma_Y,gamma_D+0.000001)

Power control

inc(DIR)=DIR_OUT

inc(xV)=abs(GV*VAC)

inc(POD)=0

inc(PMEAS)=Iorder*abs(GV*VAC)

inc(Porder_pu)=PMEAS/GP

inc(xP)=PMEAS

VDCOL

inc(REC_INT)=REC_INT_OUT

inc(DIR)=POLE*select(VDC>0,1,-1)

inc(Iorder)=select(REC_INT,IORD,IORD-IMARG0)

inc(xV)=GV*abs(VDC)